BIBLIOTECA D ENTO
FISICA E AS. OMIA
Viale A. Doria, 6 - CATANIA

STRUCTURE of the NUCLEUS

by

M. A. PRESTON
and
R. K. BHADURI
McMaster University

Westview Press
A Member of the Perseus Books Group

1st printing, 1975
2nd printing, 1982

Library of Congress Cataloging in Publication Data

Preston, Melvin Alexander.
Structure of the nucleus.

Includes bibliographical references.
1. Nuclear physics. I. Bhaduri, R. K., joint author. II. Title.
QC776.P74 539.7 74-13242

Copyright © 1975 by Westview Press, A Member of the Perseus Books Group
Published simultaneously in Canada

All rights reserved. No part of this publication may be reproduced, stored in a retrieval system, or transmitted, in any form or by any means, electronic, mechanical, photocopying, recording or otherwise, without the prior written permission of the publisher, Addison-Wesley Publishing Company, Inc., Advanced Book Program, Reading, Massachusetts 01867, U.S.A.

Printed in the United States of America

ISBN 0-201-62729-9 (pbk)

10 9 8 7 6 5 4

Structure of the Nucleus

Contents

Preface xi

Part I Fundamental Properties of Nuclei

Chapter 1 The Constituents of Nuclei 3

1–1 Nucleons and Nuclei 3
1–2 Isospin 7
1–3 Mesons and Excited Nucleons 10
1–4 Mesonic Effects in Nuclei 14
References 18
Problems 18

Chapter 2 Internucleon Forces: I 19

2–1 Introduction 19
2–2 Possible Nucleon Forces 21
2–3 Scattering Experiments 27
2–4 Bound State 35
2–5 Experimental Results 36
2–6 Proton-Proton Forces 39
2–7 Low-Energy Neutron-Neutron (n-n) Interaction 45
2–8 Charge Independence of Nuclear Forces 50
2–9 Experimental Evidence for Charge Independence and Charge Symmetry 53

References 60
Problems 61

Chapter 3 Nuclear Moments and Nuclear Shapes 64

3–1 Electromagnetic Multipoles 64
3–2 Angular Momentum 66
3–3 Electric Moments 68
3–4 Magnetic Moments 75
References 80
Problems 80

Chapter 4 Sizes of Nuclei 82

4–1 Introduction 82
4–2 Electron Scattering 85
4–3 Form Factor of Nucleons 103
4–4 Muonic Atoms 111
References 116
Problems 118

Chapter 5 Internucleon Forces: II 123

5–1 Electromagnetic Moments of the Deuteron and Tensor Forces 123
5–2 The *D*-State Admixture in the Deuteron and Meson-Exchange Currents 130
5–3 The Nuclear Force and General Features of High-Energy Scattering 134
5–4 Polarization 137
5–5 The Scattering Matrix for Coupled Waves 141
5–6 Experimental Results and Preliminary Interpretations . 145
5–7 More Precise Analysis of Experimental Data 154
5–8 Phenomenological Nucleon-Nucleon Potentials 158
5–9 Definition of a Potential from Meson Theory 166
5–10 Boson Resonances 170
5–11 Derivation of the OBEP 173
5–12 Main Features of the OBEP 177
References 180
Problems 182

Chapter 6 Nuclear Binding Energies 188

6–1 Introduction 188
6–2 Fermi Gas Model of the Nucleus 191
6–3 Shell Effects and Refinements in the Mass Formula . . 204
References 208
Problems 209

Part II Nuclear Models

Chapter 7 Single-Particle Model 217

7–1 Introduction 217
7–2 Single-Particle Orbits 218
7–3 Extreme Single-Particle Model and Spin 223
7–4 Single-Particle Model 233
7–5 Configuration Mixing 239
References 241
Problems 242

Chapter 8 Correlations in Nuclear Matter 244

8–1 Introduction 244
8–2 Exclusion Principle Correlations 248
8–3 Bethe-Goldstone Equation and *G*-Matrix 252
8–4 Results in Nuclear Matter and Finite Nuclei 275
8–5 Pairing Correlations and the Ground State 309
References 328
Problems 330

Chapter 9 Collective Nuclear Motion 340

9–1 Introduction 340
9–2 The Vibrational Modes of a Spherical Nucleus 343
9–3 Collective Modes of a Deformed Even-Even Nucleus . . 355
9–4 Symmetries of the Collective Wave Function for Well-Deformed, Even-Even Nuclei 362
9–5 Collective Spectra of Even-Even Nuclei 368
9–6 Even-Even Transition Nuclei 390
9–7 Strong Coupling of Particle and Collective Motions . . . 403
9–8 Particle States in Distorted Nuclei 410

9–9 Calculation of Equilibrium Shape 420
9–10 Levels of Distorted Odd-A Nuclei 429
References 434
Problems 435

Chapter 10 Hartree-Fock and Particle-Hole Calculations . . . 441

10–1 Refinements on the Spherical-Shell Model 441
10–2 The Shell-Model Approach to Calculating Nuclear Spectra 442
10–3 The Hartree-Fock (H-F) Equations 449
10–4 Binding Energies of Closed-Shell Nuclei in the Hartree-Fock Approximation 456
10–5 Deformed Hartree-Fock Orbitals 463
10–6 Projection of Angular-Momentum States from the Intrinsic State 474
10–7 Particle-Hole (Tamm-Dancoff) Calculations 482
10–8 Calculation of Inertial Parameters 493
References 499
Problems 502

Part III Alpha Disintegration and Fission of Nuclei

Chapter 11 Alpha Radioactivity 509

11–1 Introduction 509
11–2 Basic Theory 512
11–3 One-Body Theory 516
11–4 Higher Electric Moments 523
11–5 Formation Factors 531
References 539
Problems 539

Chapter 12 Fission 541

12–1 The Phenomenon of Fission 541
12–2 Fission-Fragment Characteristics 553
12–3 The Liquid-Drop Model 567
12–4 Shell Correction to the Liquid-Drop Mass Formula . . . 576
12–5 The Triumph of the Double Hump 589
References 602
Problems 604

Appendixes

A Angular Momentum, Spherical Tensors, Dirac Matrices 611

A–1 Angular Momentum 611
A–2 Spherical Tensors 620
A–3 Dirac Equation 628
A–4 Strong, Electromagnetic, and Weak Interaction Hamiltonians 635
References 638

B Some Results Used in Scattering Theory 639

B–1 Radial Wave Functions 639
B–2 Effective-Range Formula 642
B–3 Proton-Proton Scattering Cross Section 644
B–4 Coherent-Scattering Length 647
References 650

C The Notation of Second Quantization 651

C–1 The Wave Function of a Many-Fermion System 651
C–2 The Operators 654
C–3 Evaluation of Matrix Elements 657

D The WKB Approximation 660

E Electromagnetic Transitions 668

E–1 Multipole Expansion of the Electromagnetic Field . . . 668
E–2 Single-Particle Transition Rates 674

Author Index 677

Subject Index 685

Preface

This book is the result of activity generated by the publisher's request for a revision of M. A. Preston's 1962 book, *Physics of the Nucleus*. As we worked at that task, we gradually realized that the intervening decade had seen such a substantial increase of knowledge of the atomic nucleus that a book at this level would perforce have to be much more voluminous or, alternatively, more concentrated in its emphasis. The result is this essentially new book, emphasizing nuclear structure. Some parts of it are unchanged or are revisions of material in the earlier book, but most of it is new.

In the preface to the earlier work, the view was expressed that nuclear physics had advanced almost far enough that one could attempt to write a book on a deductive basis, stating first the fundamental laws determining the interaction of nucleons and then deducing the properties of nuclei. If that hope were realistic in 1960, it should be even more capable of fulfilment at the present time. But physicists now have a more precise appreciation of the extent of the difficulties encountered in completing some of the links in this chain of deductive reasoning. If a fairly satisfying structure exists for calculating some properties of many-body systems, we also know that there are gaps in our current ability to perform some steps in the calculation. If our knowledge of the two-nucleon force is much better than it was fifteen years ago, we also realize more clearly the importance of the gaps in our current knowledge about the nature and role of many-body forces and the structure of the nucleons themselves. It is still true that many fascinating aspects of the behavior of nuclei are best discussed in terms of models whose limits of validity are not fully understood in terms of a more fundamental

theory. Thus, although in this book we tend to emphasize the fundamental approach which should unify the concepts used in describing nuclei, this work, like its predecessor, remains semideductive.

Although we intend the book to be useful as a reference volume for research physicists, while writing most parts of it we pictured the reader as a graduate student engaged in his first detailed examination of nuclear physics. We make essential use of the material normally covered in a first course in quantum mechanics. The pace of the text also assumes that a reader has had a prior introduction to nuclear phenomenology, but in fact the discussion of each topic proceeds *ab initio* and makes no essential use of-unstated facts of nuclear physics.

The book is intended to be neither "experimental" nor "theoretical"; it deals with the structure and physics of the nucleus, and not primarily with either laboratory or mathematical techniques. Although there is more discussion of theories than of experiments, we have tried to restrict the presentation of theoretical technique to that necessary for physical understanding.

The book falls into three parts. The first part, entitled "Fundamental Properties of Nuclei," contains a detailed discussion of the two-nucleon interaction and of basic model-independent nuclear properties. The description of nuclear force at a simple level begins in Chapter 2. A detailed discussion of its noncentral character, however, can be appreciated only after acquiring a background knowledge of electromagnetic moments and form factors. It is therefore natural to continue the discussion of nuclear force at a more sophisticated level in Chapter 5 after the topics of moments and sizes have been covered in Chapters 3 and 4.

The first part of the book prepares the way for the second, in which we discuss nuclear models and their agreement with experimental results and then explain their bases in fundamental theory. Chapter 7 describes the simple single-particle model, while Chapter 8 attempts to justify the independent-particle picture by developing the theory of nuclear matter and finite nuclei in a unified manner, and making a connection between the free two-nucleon force obtained from scattering experiments and the effective two-nucleon force used in nuclear structure calculations. Ordinarily, one would expect the description of microscopic calculations in finite nuclei, which is the content of Chapter 10, to immediately follow Chapter 8. We believe, however, that topics like deformed Hartree-Fock orbitals can be much better appreciated after a thorough exposition of the phenomenological collective model, which is so successful in correlating experimental data. That

is why Chapter 9 intercepts the logical continuation of the materials in Chapters 8 and 10.

The third part of the book deals in some detail with two processes that cast considerable light on nuclear structure, alpha decay and fission. Our understanding of the phenomenon of fission has improved tremendously in the last six years with the advent of the double hump in fission barriers, and we have attempted to incorporate these exciting developments in Chapter 12 without cluttering up the material with too much detail.

Throughout this book, the underlying emphasis is on how a nucleus is constituted through the interaction between the nucleons. This emphasis and limitations on the size of the book have led us to exclude explicit accounts of the theory of reactions and of weak interactions and beta decay, although we do refer to results from the whole range of nuclear physics experiments which elucidate features of structure. When we use a reaction or decay experiment, we give sufficient theoretical background to make the reference understandable. We hope this choice of topics makes possible a one-volume work that not only fits the requirements of many current graduate courses but also is of some use to research physicists. In giving a course, certain sections of the book may be omitted without loss of coherence. In our opinion these are Sections 5–9, 5–11, 10–4, more detailed parts of 8–3 and 8–4, and possibly Chapter 11.

Problems for the student should be an integral part of a course in nuclear physics. Most instructors like to design their own problems, but, as in the earlier book, we include some fairly instructive problems in the text. Although most are original, over the years we have collected problems from friends and now we are not always sure of their sources.

An important function of a graduate course is to introduce the student to the periodical literature. For this reason numerous references are given to original and review articles. No attempt has been made at historical completeness; rather we have referred to an article whenever it seemed natural to do so in our presentation of a subject. The result should be a representative sampling of the literature of nuclear structure.

The preface to *Physics of the Nucleus* acknowledged indebtedness to Dr. L. G. Elliott and to Professor Sir Rudolf Peierls for their indirect but very significant influence on the book. We reiterate that sentiment now. One of the authors (R. K. B.) is grateful to Dr. Kailash Kumar for initiating him into nuclear physics. We also wish to express appreciation to our colleagues Yuki Nogami and Don Sprung for useful discussions on certain sections of the book, to Subal Das Gupta and Carl Ross for reading parts

of the manuscript and giving us the benefit of their suggestions, and to Hazel Coxall and Erie Long for their patience in typing the manuscript. Finally, our thanks go to our wives and families for cheerfully tolerating our excessive allocation of time to this task.

M. A. Preston
R. K. Bhaduri

Part I

Fundamental Properties of Nuclei

Chapter 1

The Constituents of Nuclei

1-1 NUCLEONS AND NUCLEI

The basic aim of any fundamental science is the understanding of observed phenomena in terms of general underlying concepts and laws. Scientific progress is made in two ways. One is the gradual reduction of the number of fundamental hypotheses needed to explain all the results of observation and experiment. In physics this is achieved by the formulation of theories and the performing of experiments intended to confirm or reject them. The other method of progress is the discovery, often not motivated by a theory, of unexpected phenomena. Existing theories must then be revised to include these newly found facts in the structure of the science. The interplay of these two facets of development is quite evident in the history of nuclear and atomic physics.

We can begin our account with what was one of the most important unifying steps in the advance of our knowledge of matter, the recognition that all material substances are composed of "atoms" of the chemical "elements," and that the number of elements is limited. We now have knowledge of about 100 elements. At the time of these early developments, individual atoms were thought of as indivisible and the atoms of any one element were indistinguishable; in effect, there were about 100 "elementary particles." The observation that the atomic weights of the different elements are roughly integral multiples of the atomic weight of hydrogen led Prout, in about 1815, to suggest that all heavier atoms were in fact combinations of hydrogen atoms. If this hypothesis had been correct—and we now know that it was a step in the right direction—it would have brought about a great

simplification in basic concepts. There would have been only one type of primary particle, from which all matter was constructed. However, Prout's hypothesis was discarded, largely because accurate determinations of atomic weights showed that the ratios differ from integers by amounts which, although usually small, are definitely not zero. Nevertheless, the pronounced regularities in the properties of the elements, as exemplified in the periodic table, led to continued speculation that atoms were indeed structures composed of some more fundamental particles.

The next unifying discovery, largely due to the work of J. J. Thomson, was that all atoms can be made to emit identical electrons. Since electrons are very much lighter than atoms, and since atoms are electrically neutral whereas electrons are negatively charged, the suggestion arises that the bulk of the mass of the atom is made up of particles with a net positive charge. One might imagine a sphere of positively charged material, the size of the atom, in which the electrons are embedded. Alternatively, the positively charged mass might be concentrated in a small region at the center of the atom, with the electrons moving about it, the extreme excursions of their paths defining the atomic radius ($\sim 10^{-8}$ cm). The decision between these two atomic models was made by a famous experiment by Rutherford in 1911 [1],† which showed that the positive charge is confined to a region with radius of about 10^{-11} cm or less. This constituted the first experimental demonstration of the existence of the nucleus.

An atom, then, consists of a nucleus of small volume containing almost all the mass of the atom and bearing a positive charge, Ze, surrounded by a cloud of Z electrons moving in the much larger atomic volume. The number Z is called the charge number or atomic number. We have since learned that all atomic and chemical properties of the elements are determined essentially by the motions of the extranuclear electrons, so that all atoms with the same atomic number have the same chemical properties. However, there exist nuclei with the same Z but different masses. (One can estimate the mass of the nucleus by subtracting the mass of Z electrons from the mass of the atom.) The existence of atoms of the same element differing in mass could be inferred from the different atomic weights of the lead (and other elements) produced in the natural radioactive chains. More directly, by the deflection of ionized atoms, J. J. Thomson [2] demonstrated in 1913 the existence of chemically identical atoms with different masses. These atoms are called isotopes, from Greek words meaning "same place," a reference

† Numbers enclosed in brackets refer to the references listed at the end of each chapter.

to the fact that all the isotopes of an element appear in the same place in the periodic table. It was soon found that the masses of all nuclei are very nearly, but not precisely, integral multiples of a mass very close to that of a proton, the hydrogen nucleus. For a given nucleus, this integer is called its mass number and is denoted by A. It is easy to understand why Prout's law failed so long as it was interpreted in terms of chemically determined atomic weights; in a quantity of chlorine, for example, 75% of the atoms have $A = 35$, 25% have $A = 37$, and standard chemical procedures suggest an effective A of 35.5.

Because of the nearly integral masses, it would seem tempting to assume that nuclei are made up of protons. Strong direct evidence that protons do exist in nuclei was forthcoming in 1919 when Rutherford [3] found that nitrogen, bombarded by sufficiently energetic α-particles, emitted hydrogen nuclei. It is clear, however, that a nucleus cannot be composed solely of protons, for this would imply $Z = A$. In fact, Z is less than A; for most stable nuclei Z is not far from $\frac{1}{2}A$. For example, the common isotope of oxygen has $Z = 8$, $A = 16$; the two stable isotopes of chlorine have $Z = 17$, $A = 35$ and 37; and the stable isotopes of lead are $Z = 82$, $A = 204, 206, 207, 208$. A natural assumption, particularly in view of the emission of electrons in β-radioactivity, is that there are also electrons in a nucleus, in just sufficient number, namely, $A - Z$, to produce the observed charge. For example, the ^{37}Cl nucleus would consist of 37 protons and 20 electrons. This hypothesis involves a number of difficulties, and in 1931 it was shown to be in disagreement with the observed spectrum of the nitrogen molecule, which reveals information about the statistics of the ^{14}N nucleus [4, 5, 6].† An alternative hypothesis which had been advanced from time to time suggests that the nucleus consists of Z protons and $A - Z$ particles which approximate the proton mass but are electrically neutral. This was merely speculation until such a particle, the neutron, was found in 1932 by Chadwick [7] in England and by Curie and Joliot [8] in France. Specifically, they found that beryllium, bombarded by α-particles from radium, emitted an electrically neutral radiation which in turn imparted considerable energy to nuclei with which it collided. It was shown that these recoils could not be explained on the assumption that the radiation was electromagnetic, but were consistent with the hypothesis that it consisted of neutral particles of proton mass.

† An odd number of particles of spin $\frac{1}{2}$, such as 14 protons plus 7 electrons, has a total angular momentum of half an odd integer and has Fermi-Dirac statistics, whereas an even number, 7 protons plus 7 neutrons, has integral angular momentum and Bose-Einstein statistics.

A nucleus, then, is specified by two numbers: A, the total number of nucleons, and Z, the number of protons, or $N = A - Z$, the number of neutrons.

The same reasoning which shows that there could not be electrons in the nucleus shows that a neutron must not be thought of as a composite particle, say a proton and an electron tightly bound, but must be treated as a fundamental particle on the same footing as a proton. Indeed, it is useful to consider the neutron and the proton as simply two different states of a single particle, the nucleon. If a nucleon changes from one of its states to another, it of course changes its electrical charge. Charge can be conserved if the nucleon's change of state is always accompanied by the creation of an electron, positively or negatively charged, as may be required. This provides an explanation of β-radioactivity without necessitating the presence of electrons in the nucleus.

The properties of individual nucleons have been carefully measured. Determination of the masses of the proton and neutron is based on energy measurements of certain nuclear reactions and requires a knowledge of other fundamental numbers such as the electron mass, Avogadro's number, and the fine-structure constant. The preferred values [9, 10] are as follows:

$$\begin{aligned} M_p &= 938.2592 \pm 0.0052 \text{ MeV}/c^2 \\ &= 1836.109 \pm 0.011m \\ &= (1.672614 \pm 0.000011) \times 10^{-24}\text{g} \\ &= 1.00727661 \pm 0.00000008u \quad \text{(atomic mass units)} \\ M_n &= 939.5527 \pm 0.0052 \text{ MeV}/c^2 \\ &= 1837.64 \pm 0.01m \\ &= (1.674920 \pm 0.000011) \times 10^{-24}\text{g} \\ &= 1.00866520 \pm 0.00000010u \end{aligned}$$

where m is the mass of the electron. An accurate measurement of the mass difference yields

$$M_n - M_p = 1.29344 \pm 0.00007 \text{ MeV}/c^2 = 2.531m$$

so that sufficient energy is available for a free neutron to change to a proton, creating an electron and still providing 0.7825 MeV of kinetic energy. This makes feasible the explanation of β-decay suggested in the preceding paragraph. The half-life of the free neutron is 10.8 min [11], but to change a neutron bound

in a nucleus (A, Z) into a proton bound in $(A, Z + 1)$ may require more energy than is available because of the differing binding energies of different nuclear species.

Both neutron and proton are fermions, that is, they have intrinsic spin angular momentum $\frac{1}{2}\hbar$ and obey Fermi-Dirac statistics and the exclusion principle. This means that a wave function must change sign if we interchange all the coordinates of two protons or of two neutrons. For this purpose we must think of four coordinates: the three coordinates of ordinary space and the spin component along some fixed direction. The latter can take only two values, $\pm \frac{1}{2}$.

1-2 ISOSPIN

We have suggested that the neutron and the proton are two different quantum states of a single entity, the nucleon. To give mathematical expression to this idea we must assign an additional quantum number. This quantum number can take only two values since there are only two states, and it follows that the associated variable has the same algebra as spin-$\frac{1}{2}$ operators. For this reason, it is customary to call the observable associated with this degree of freedom by the rather inept name "isotopic spin," now usually shortened to "isospin" or i-spin. In particular, we say that the nucleon has i-spin $\frac{1}{2}$ and that, just as the values $+\frac{1}{2}$ and $-\frac{1}{2}$ for s_z tell us the actual spin directions of the nucleon, there is a variable t_3 with two possible values, $+\frac{1}{2}$ and $-\frac{1}{2}$, which tell us the charge state of the nucleon. We take $t_3 = +\frac{1}{2}$ for the proton state and $t_3 = -\frac{1}{2}$ for the neutron state.† In complete analogy with angular momentum, we introduce $\tau_3 = 2t_3$ (corresponding to $\sigma_z = 2s_z$) and write

$$\tau_3|p\rangle = |p\rangle, \qquad \tau_3|n\rangle = -|n\rangle. \tag{1-1}$$

It is sometimes convenient to use the abbreviations $\gamma \equiv |p\rangle$ and $\delta \equiv |n\rangle$:

$$\tau_3\gamma = \gamma, \qquad \tau_3\delta = -\delta. \tag{1-2}$$

As with spin, it is possible to introduce a two-dimensional matrix representation, as described in Appendix A.

It is tempting to complete this formalism by introducing the other two components τ_1 and τ_2, with properties analogous to those of σ_x and σ_y. We

† The opposite sign convention (making T_3 positive for nuclei with neutron excess) is used by some nuclear physicists, but the convention given here is always used in elementary particle work and relates i-spin to charge and hypercharge in the same way for nucleons as for other particles. We recommend this usage for all purposes; the continued existence of two conventions causes confusion.

would then have a vector $\boldsymbol{\tau}$ in a three-dimensional "i-spin space." This mathematical exercise would seem pointless unless some physical significance could be attached to the additional two dimensions. In fact, τ_1 and τ_2 can be connected with operators which transform a nucleon from its neutron state into its proton state, and vice versa. Thus they may be useful to describe β-decay. To see this, we recall (Appendix A) that $\sigma_x \pm i\sigma_y$ is the operator that increases (decreases) the z-component of spin by 1 unit. Similarly, if we define $\tau_\pm = \tau_1 \pm i\tau_2$, we have

$$\tau_+|p\rangle = \tau_+\gamma = 0, \qquad \tau_+|n\rangle = \tau_+\delta = 2\gamma = 2|p\rangle, \tag{1-3}$$

$$\tau_-|p\rangle = \tau_-\gamma = 2\delta = 2|n\rangle, \qquad \tau_-|n\rangle = \tau_-\delta = 0. \tag{1-4}$$

Thus τ_+ annihilates a proton state and converts a neutron into a proton, while τ_- has the complementary effect.

The nucleon is a particle obeying Fermi-Dirac statistics and requiring five "coordinates" to specify its position and state—the space coordinates, the component of $\boldsymbol{\sigma}$ in a specified direction, and the value of τ_3. Any nuclear state must have a wave function which is antisymmetric for the exchange of all coordinates of any two nucleons. Consequently, if the space and spin part of the wave function is symmetric, the i-spin part must be antisymmetric, and vice versa.

When dealing with a two-nucleon system, it is of course convenient to introduce the singlet and triplet spin states, which are, respectively, $S = 0$ and antisymmetric and $S = 0$ and symmetric. The possible i-spin states are as follows:

Symmetric i-spin triplet:

$$^3(\tau)_1 = \gamma(1)\gamma(2), \quad \text{the proton-proton state,}$$
$$^3(\tau)_{-1} = \delta(1)\delta(2), \quad \text{the neutron-neutron state,}$$
$$^3(\tau)_0 = 2^{-1/2}[\gamma(1)\delta(2) + \gamma(2)\delta(1)], \quad \text{a neutron-proton state;}$$

Antisymmetric i-spin singlet:

$$^1(\tau)_0 = 2^{-1/2}[\gamma(1)\delta(2) - \gamma(2)\delta(1)], \quad \text{a neutron-proton state.}$$

This shows explicitly that the need to have specified symmetry against two-particle interchange has led us to a formalism in which the i-spins of two nucleons (and hence of any number) are added by the same rules as are angular momenta. In the two-nucleon case, if we define $\mathbf{T} = \mathbf{t}(1) + \mathbf{t}(2)$, we denote that $^3(\tau)_m$ is the state with $T = 1$, $T_3 = m$, and $^1(\tau)_0$ has $T = T_3 = 0$.

In so far as one works only with nucleons, the use of i-spin is simply a formalism which does not introduce any physical consequences different from

the results of the treatment of neutrons and protons as distinct particles. Sometimes one method is more convenient, sometimes the other.

If the i-spin concept were simply a mathematical convenience, it would not be so important as it is. But in fact i-spin appears to be a physical observable of wide applicability. We introduced it in connection with the nucleon, which can be called a charge doublet; it has two charge states, and we described these by analogy with the two-component state vectors of spin $\frac{1}{2}$ and the operators $\boldsymbol{\sigma}$. Now, there are other particles that have more than one charge state. For example, the π-meson or pion can have charges $+e$, $-e$, and zero, and its other properties, like those of the nucleon, depend only slightly on its charge. Can it be assigned an i-spin analogous to angular momentum of 1 unit, writing $t_\pi = 1$, $t_{3,\pi} = +1, -1, 0$ for the three states? Clearly we can do this as a mathematical device, but it turns out to be much more than that. In studying the scattering of pions from nucleons, one finds that i-spin is conserved if one adds the i-spins of the pion and nucleon vectorially, analogous to addition of two angular momenta of magnitudes 1 and $\frac{1}{2}$. The π^+-proton system has the resultant $T_3 = \frac{3}{2}$, and therefore $T = \frac{3}{2}$, whereas π^--proton and π^+-neutron systems are mixtures of $T = \frac{1}{2}$ and $\frac{3}{2}$, with $T_3 = \pm\frac{1}{2}$, and the π^--neutron system is $T_3 = -\frac{3}{2}$, $T = \frac{3}{2}$. The interaction at low energies is greater in the $T = \frac{3}{2}$ state than in the $T = \frac{1}{2}$ state and does not depend (except for electromagnetic forces) on the value of T_3. Hence the scattering cross sections of (π^+, p), (π^-, p), (π^+, n) and (π^-, n) are all connected by certain relationships, permitting some to be predicted if others are known. These expectations are confirmed by experiment.† There are many other examples of particles that constitute charge multiplets, and there is ample confirmation that i-spin is one of the important physical observables associated with a conservation law.

Actually i-spin is not a precise constant of motion in any situation where electromagnetic forces act, since the magnitude of this force depends on the third component of the i-spin. For example, the charge Q_N of a nucleon is given by

$$Q_N = \tfrac{1}{2} + t_3, \tag{1-5}$$

and the Coulomb force between two nucleons is

$$\frac{e^2}{r_{12}}[\tfrac{1}{2} + t_3(1)][\tfrac{1}{2} + t_3(2)].$$

† Further details are given in a number of books. In, for example, G. Källén, *Elementary Particle Physics*, Addison-Wesley, Reading, Mass., 1964, pp. 71–79.

The algebra of i-spin being that of angular momentum, t_3 does not commute with the magnitude T of the total i-spin of a system of more than two nucleons; therefore, when the Hamiltonian contains the Coulomb force, T cannot be a constant. However, if the electromagnetic force is weak compared to other forces present, the total i-spin may well have a nearly fixed value with only small components of other values in the wave function. Of course T_3 is always conserved, because it is related to total charge.

For pions the charge

$$Q_\pi = t_3. \tag{1-6}$$

This and the expression for Q_N are special cases of a general relationship,

$$Q = t_3 + \tfrac{1}{2}Y, \tag{1-7}$$

where Y is a quantity, called the hypercharge, which must be assigned to each elementary particle.

1-3 MESONS AND EXCITED NUCLEONS

The most important force acting between nucleons is the strong nuclear interaction. Not only is this interaction associated with nucleons, but also it is the principal force applied to mesons. The meson most significant for low-energy phenomena is the lightest strongly interacting particle, the pion.

Pions are produced in nucleon-nucleon collisions:

$$N + N \rightarrow N + N + \pi. \tag{1-8}$$

There must be sufficient bombarding energy (about 290 MeV) to supply the rest-mass of the pion. Charge must be conserved, so that, although the collision of two protons will permit creation of π^+ and π^0, one of the initial nucleons must be a neutron in order to produce π^-.

Pions have zero spin and negative intrinsic parity. They have masses $m_\pm = 139.6$ MeV, $m_0 = 135.0$ MeV. In the free state they decay, the charged pions predominantly to muons and neutrinos with a mean life of 2.6×10^{-8} sec, the neutral pions electromagnetically and mainly to two γ-rays with a mean life of 0.84×10^{-16} sec. Both these lifetimes are very long compared with typical times for periods of motions of nucleons bound in nuclei (10^{-22} sec), and elementary-particle physicists refer to pions as stable particles.

Pions can also be absorbed by nucleons:

$$\pi + N \rightarrow N. \tag{1-9}$$

It will be seen that pions are created and destroyed by the strong interaction of nucleons, much as photons are created and destroyed by the electromagnetic interaction of charged particles. In the same sense that the electromagnetic force is attributed to the exchange of photons, the nuclear force is attributed to the exchange of mesons. This is discussed in considerable detail in Chapter 5, but some preliminary remarks here will be useful.

A reaction in which one particle absorbs another and does not change its mass is in fact impossible, since the conservation of momentum demands that the initial state have greater energy than the final state. But there can be short-lived fluctuations in the energy of a system, a fluctuation of amount ΔE lasting for a time

$$\Delta t \sim \frac{\hbar}{\Delta E}. \tag{1-10}$$

Hence a nucleon can emit or absorb a pion (or an electron, a photon) provided there is a mechanism for rapidly readjusting the energy of the total system of interacting particles. Let us consider a nucleon that emits a pion with momentum q. Then the energy of the system will have increased by the rest-mass of the pion and the change in the kinetic energy. If q is small ($q \ll m_\pi c$), then the fluctuation in energy is about $m_\pi c^2$, which corresponds to $\Delta t \sim 5 \times 10^{-24}$ sec. If a mechanism exists to reduce the energy to its original value in this time, such "virtual" mesons will exist. In fact, the emitting nucleon can itself reabsorb the pion, and since this process can occur *in vacuo* it is always present and its effects are a part of the properties of the "physical" nucleon. When we use this phrase, we are contrasting the "physical" nucleon with an idealized nucleon which is "undressed," that is, is not accompanied by the cloud of virtual pions we have just described. It is of course only the "dressed" nucleon which can be observed. The physical and undressed nucleons have different masses; the difference is the self-energy contribution of the meson cloud (and also the similar electromagnetic self-energy).

The emitted meson could also be absorbed if another nucleon were sufficiently close that the emitted meson could reach it within the time Δt. It would need to be within a distance $c\,\Delta t \sim 1.5$ fm.† Then the second nucleon would acquire the extra momentum q carried by the meson. The net effect

† The International Union of Pure and Applied Physics authorizes the abbreviation f for femto, signifying 10^{-15}. Thus a femtometer (fm) is 10^{-13} cm. (The full recommendations on symbols, units and nomenclature may be found in *Nucl. Phys.* 81, 677 (1966).) There is a widespread unofficial usage which refers to the length 10^{-13} cm as a Fermi.

is that two nucleons are seen to have scattered off each other, with conservation of momentum and energy. In experiments that do not examine times as short as 10^{-24} sec, the whole interaction process appears as a nucleon-nucleon force, and, if the particles are moving at nonrelativistic speeds, the force can be ascribed to a potential. We see that the nucleon-nucleon potential will be expected to have a range of the order of 1–2 fm.

There is, however, a circumstance in which one particle can absorb another. Photons can be absorbed by a single atom, but of course the atom is raised to an excited state, to conserve both momentum and energy, and only photons of suitable energy can be absorbed. Similarly, a nucleon can absorb a pion if there are excited states of nucleons:

$$\pi + N \rightarrow N^*. \tag{1-11}$$

Photons are elastically scattered from atoms by a process that can be described as absorption and re-emission:

$$\gamma + A \rightarrow A^* \rightarrow A + \gamma.$$

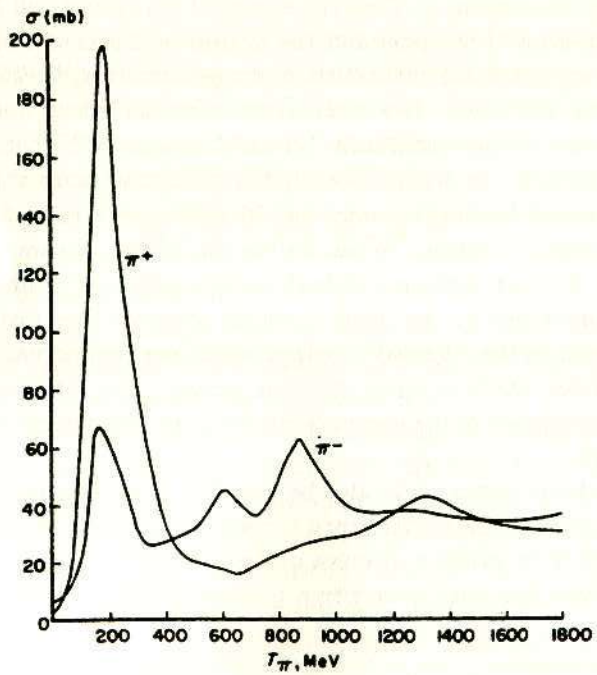

Fig. 1-1 Total cross section for π^+ and π^- scattering from protons from 0- to 1800-MeV pion kinetic energy.

In this case, photons of any energy may be scattered, since the excited state of the atom lives for only a short time and hence some energy fluctuations occur. The maximum scattering occurs for an energy-conserving photon—one with energy near $E(A^*) - E(A)$—and the lifetime of the state A^* determines for how wide a region of energy around this value photons will experience appreciable scattering. In other words, the scattering cross section has a "resonance" for a certain value of the photon energy corresponding to the excited state of the atom.

The total cross section for pions incident on protons is shown in Fig. 1–1. A number of peaks appear in the figure and are highly suggestive of resonances due to excited states of the nucleon. Thorough analysis bears out this interpretation. Some resonances are obvious on visual inspection, and the bumpy shape of the curves implies others that are wide and relatively weak. The lowest few excited states are listed in Table 1–1. The state π^+ with proton has $T_3 = \frac{3}{2}$ and hence has only $T = \frac{3}{2}$ states, whereas π^- with proton has both $T = \frac{1}{2}$ and $T = \frac{3}{2}$ components. The symbol Δ is used for $t = \frac{3}{2}$, and N for $t = \frac{1}{2}$, states.

TABLE 1-1 Resonances of the Pion-Nucleon System: Excited State of the Nucleon. These resonances are well established. The recommended mass is that shown in the name, but the possible experimental range is also indicated. Corresponding ranges are shown for the width. A width of 100 MeV corresponds to $\Delta t = 6.6 \times 10^{-24}$ sec.

Name	T_π MeV	Mass	Width Γ MeV	J^P	t
$\Delta(1236)$	195	1230–1236	110–122	$\frac{3}{2}^+$	$\frac{3}{2}$
$\Delta(1650)$	830	1615–1685	130–200	$\frac{1}{2}^-$	$\frac{3}{2}$
$\Delta(1670)$	870	1650–1720	175–300	$\frac{3}{2}^-$	$\frac{3}{2}$
$\Delta(1890)$	1280	1840–1920	135–350	$\frac{5}{2}^+$	$\frac{3}{2}$
$\Delta(1910)$	1330	1780–1935	230–420	$\frac{1}{2}^+$	$\frac{3}{2}$
$\Delta(1950)$	1410	1930–1980	140–220	$\frac{7}{2}^+$	$\frac{3}{2}$
$N(1470)$	530	1435–1505	165–400	$\frac{1}{2}^+$	$\frac{1}{2}$
$N(1520)$	610	1510–1540	105–150	$\frac{3}{2}^-$	$\frac{1}{2}$
$N(1535)$	640	1500–1600	50–160	$\frac{1}{2}^-$	$\frac{1}{2}$
$N(1670)$	870	1655–1680	105–175	$\frac{5}{2}^-$	$\frac{1}{2}$
$N(1688)$	900	1680–1692	105–180	$\frac{5}{2}^+$	$\frac{1}{2}$
$N(1700)$	920	1665–1765	100–400	$\frac{1}{2}^-$	$\frac{1}{2}$
$N(1780)$	1070	1650–1860	50–450	$\frac{1}{2}^+$	$\frac{1}{2}$
$N(1860)$	1220	1770–1900	180–330	$\frac{3}{2}^+$	$\frac{1}{2}$

The lowest state, the $\Delta(1236)$, is also by far the most readily excited. It is a $t = \frac{3}{2}$ state, can be found with charge -1, 0, 1, or 2, and has spin $j = \frac{3}{2}$,

parity positive. Because of the j- and t-values it is often called the (3, 3) resonance. Its energy lies just 300 MeV above the proton mass. The shape of the $\pi^- - p$ scattering cross section above 350 MeV is seen to be consistent with a weak peak at 530 MeV due to $N(1470)$, which is lost in the rise to the $N(1520)$ and $N(1535)$ peaks.

A nucleon-nucleon collision at an energy of around 300 MeV can produce a $\Delta(1236)$. Over 500 MeV is needed before the next state, $N(1470)$, can be formed, and it has a much lower formation cross section because of certain angular-momentum considerations, which we shall not discuss here. As we shall suggest in a moment, this energy difference makes the $\Delta(1236)$ about the only excited nucleon state important for nuclear structure.†

1-4 MESONIC EFFECTS IN NUCLEI

We began this chapter with the early concept of the indivisible atom and gradually introduced successive levels of complication which brought us to the picture of atomic electrons moving outside a small nucleus composed of massive, but structureless, neutrons and protons, interacting with each other through a nuclear potential, undergoing β-decay, and subject to electromagnetic interactions. This model has been the main conceptual framework for the remarkable progress of nuclear physics from 1930 to the present. But in Section 1-3 we mentioned the virtual meson clouds which give a nucleon structure and the existence of excited states of nucleons. Are we about to enter an era in which still a further level of complication of our model will be needed? Does the nucleus contain some $\Delta(1236)$'s some of the time? Are the nucleons of the nucleus "dressed" with mesons differently than in free space, because of the presence of the other nucleons? Should we think of a nucleus as nucleon kernels in a meson soup?

Nuclear physics has made immense strides in the experimental examination of fine details of the structure and of the dynamics of the nucleus. In Fig. 1-2 we show the spectrum produced by 70-MeV oxygen ions on ^{188}Os as determined in two experiments, representative of the best techniques available at two times about 10 years apart. This dramatically illustrates the attainment of a new level of detail. But the experimental refinements of recent years have not required any basic change in our theoretical nuclear model; on

† The baryons Λ and Σ lie at 175 and 250 MeV above the nucleons; however, because strange particles must be produced in pairs, the energy required to have them as virtual particles in the nucleus is greater than these values by the mass of the K-meson (i.e., 500 MeV).

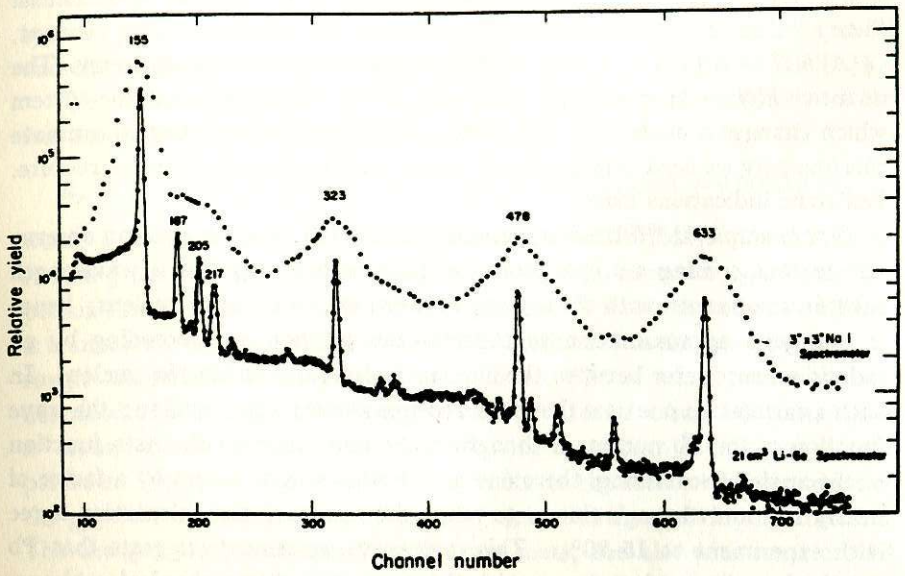

Fig. 1-2 Comparison of the γ-radiation spectra, from Coulomb excitation of ^{188}Os nuclei by a 70-MeV beam of oxygen ions, as measured with a sodium iodide spectrometer and with a lithium-germanium semiconductor spectrometer. (From *Physics in Perspective*, Vol. I, National Academy of Science, Washington, D.C., 1972.)

the contrary, confidence in it has grown as increasingly precise experiment has been understood in terms of increasingly precise calculations.

Have we now, however, reached the point at which a new model should be introduced? The answer depends on the facts to be understood. Clearly, if one contemplates some types of experiment at several hundred MeV, where very short times are important, the structure of the nucleons and the mesonic "components" of the nucleus will be important, as will other aspects of high-energy elementary particle physics. But if one wishes to examine the structure of nuclei in their ground states and other low-lying states and processes up to 100 MeV or so, what model should be used?

There is no single answer to this question. The $\Delta(1236)$ clearly is present in every nucleus for some fraction of the time—how large a fraction? If we think of the wave function of a nucleus as

$$\psi = \psi(A) + \psi(A - 1, \Delta) \tag{1-12}$$

with $\psi(A)$ representing the wave function of an A-nucleon system and

$\psi(A-1,\Delta)$ a system with one $\Delta(1236)$ present, we know, from perturbation theory,† that the amplitude of $\psi(A-1,\Delta)$ is a transition matrix element, $\langle\psi(A)|h(N\to\Delta)|\psi(A-1,\Delta)\rangle$, divided by an average excitation energy. The quantity $h(N\to\Delta)$ symbolizes that part of the Hamiltonian of the system which changes a nucleon to a $\Delta(1236)$. It is clear that in order to estimate this quantity we need details of both meson field theory and nuclear structure. But some indications exist.

For example, if ^{208}Pb is bombarded with 24-GeV protons, one can observe the protons coming out. A proton of such high energy has a wavelength short in comparison with the spacing between nucleons in the nucleus; hence it is a good approximation to consider the reaction as proceeding by an individual encounter between the incident proton and one in the nucleus. In such a calculation one uses the measured free nucleon cross section; the wave function of the Pb nucleus is thought to be well understood. As a function of the angle of scattering, the value of the cross section alters by a factor of nearly 10^6, and through this large range the results of the calculation agree with experiment to 15–20%. This impressive agreement suggests that Pb is indeed made up of nucleons, with the properties of free physical nucleons, to at least 85% of its contents. But there is presumably some fraction of $\Delta(1236)$, and the ground-state wave function presumably also contains a component consisting of a pion moving in an "orbit" in the nucleus, since the lowest state of the pionic Pb atom is only about 100 MeV above the ground state. Since the Pb nucleus has 1600-MeV binding energy, it is easy to realize that the continual random allocation of the kinetic energy among the nucleons could lead to the creation for short times of a state 100 MeV up. Experiments involving pions (e.g., pion production) would be sensitive to a pionic component in the wave function.

At the other end of the periodic table, calculations have been made of the amount of $\Delta(1236)$ in the wave functions of ^{3}H and ^{3}He [12, 13]. It is found that the probability of the presence of a Δ is a few per cent; more exactly, if we write

$$\psi = a\psi(N^3) + b\psi(N^2\Delta) + c\psi(N\Delta^2),$$

where we allow for the presence of either one or two Δ's, it is found that $|b|^2$ is 0.04–0.06 and $|c|^2$ is 0.02–0.03. These small percentages may, however, have important consequences, particularly in any effect which would involve b or c linearly. (These small terms are of the same order as the important

† Or from a generalized Bethe-Goldstone equation (Chapter 8).

inclusion of the D-state in the deuteron.) Such percentages in three-body systems permit the otherwise difficult explanation of the β-decay rate of ^{3}H and the magnetic moments of ^{3}He and ^{3}H.

We shall briefly describe the latter point. The magnetic moments of the free neutron and proton are [9, 14] as follows:

$$\mu_p = (2.792782 \pm 0.000017)\mu_0, \qquad \mu_n = -(1.913148 \pm 0.000066)\mu_0,$$

where $\mu_0 = \hbar e/2M_pc$ is the nuclear magneton $= 3.152526 \times 10^{-18}$ MeV/G. A spin-$\frac{1}{2}$ particle of charge e would have magnetic moment μ_0. Hence the proton has an anomaly, $1.79\mu_0$, and the neutron's whole moment, $-1.91\mu_0$, is anomalous. The contributions are to be attributed to the meson clouds. A rough calculation would proceed as follows. The physical proton can be described as a mixture of a bare proton, a π^+ around a bare neutron, and a π^0 around a bare proton, and terms involving more than one pion and other particles. However, the first few terms indicate the idea. All three terms of the physical proton state contribute magnetic moments of varying amounts. The charged pion, with spin 1, with lower mass, and also with some orbital angular momentum, makes a much greater contribution than μ_0; hence a bare neutron with a π^+ will have almost the same moment (except for sign) as a bare proton with a π^-, and each will be much greater than the moment of the bare proton alone. If these two states are about equally admixed in a small amount into the physical proton and neutron, respectively, the magnetic-moment values will be understood.

But if the magnetic moment is so importantly determined by the pionic cloud, we can expect significant meson effects when we put nucleons together to form a nucleus. The first effect will be that some virtual pions are reabsorbed, not by the nucleon that emitted them, but by another. This gives "exchange" currents of charged mesons and therefore leads to "exchange magnetic moments." Also we note that the excited nucleon states, the Δ's and N's, will each have a magnetic moment different from that of the proton or neutron, since they have different spins and different internal structures. Given some model of nucleon structure, we can calculate these values and find to what extent the presence of a $\Delta(1236)$ in the nucleus will alter the magnetic moment. Such a calculation [13] substantiates the wave function of Eq. 1–12.

In the rest of this book, there will be only a few references to mesons or Δ's as constituents of the nucleus. This reflects the current state of knowledge (or, rather, of ignorance) concerning their role but is not a serious defect, since, as we have seen, these particles are not expected to be present with

high probability. Nevertheless, this hitherto largely unexplored aspect of nuclear structure does make it clear that the best parameters for the "pure nucleon" model of the nucleus may sometimes differ somewhat from those derived from the properties of free nucleons. This may have particular significance in connection with "effective" forces between nucleons in nuclei.

REFERENCES

1. E. Rutherford, *Phil. Mag.* **21**, 669 (1911).
2. J. J. Thomson, *Rays of Positive Electricity*, Longmans Green, London, 1913.
3. E. Rutherford, *Phil. Mag.* **37**, 537 (1919).
4. P. Ehrenfest and J. R. Oppenheimer, *Phys. Rev.* **37**, 333 (1931).
5. H. Heitler and G. Herzberg, *Naturwissenschaften* **17**, 673 (1929).
6. F. Rasetti, *Z. Phys.* **61**, 598 (1930).
7. J. Chadwick, *Nature* **129**, 312, and *Proc. Roy. Soc. (London)* **A136**, 692 (1932).
8. M. Curie and F. Joliot, *C. R. Acad. Sci.* **194**, 273, 708, 876, 2208 (1932).
9. B. N. Taylor, W. H. Parker, and D. N. Langenberg, *Rev. Mod. Phys.* **41**, 375 (1969).
10. J. H. E. Mattauch, W. Thiele, and A. H. Wapstra, *Nucl. Phys.* **67**, 1 (1965).
11. C. J. Christenson, A. Nielsen, A. Bahnsen, W. K. Brown, and B. M. Rustad, *Phys. Lett.* **26B**, 11 (1967).
12. A. M. Green and T. H. Shucan, *Nucl. Phys.* **A188**, 289 (1972).
13. M. Ichimura, H. Hyuga, and G. E. Brown, *Nucl. Phys.* **A196**, 17 (1972).
14. V. W. Cohen, N. R. Corngold, and N. F. Ramsey, *Phys. Rev.* **104**, 283 (1956).

PROBLEMS

1–1. Consider $N + N \rightarrow N + N + \pi$. Let the initial state be $p + p$, that is, $T = 1$, $T_3 = 1$. The final state must also have $T = 1$. Therefore the final state is

$$A[(1110|11)|pp\pi^0\rangle + (1101|11)|(pn)^3\pi^+\rangle] + B|(pn)^1\pi^+\rangle$$

where the superscripts on (pn) refer to i-spin triplet and singlet. The quantity A is related to a triplet-triplet production amplitude; B, to a triplet-singlet amplitude. What angular-momentum states are possible for the two final nucleons?

1–2. Calculate the connection between the masses in column 1 and the kinetic energies in column 2 of Table 1–1.

1–3. Calculate the $t = \frac{1}{2}$, $t_3 = \frac{1}{2}$ state of the pion and bare nucleon and find its magnetic moment. Assume the pion to be in an $l = 1$ state. You will need to use an arbitrary value for pion-nucleon distance.

Chapter 2

Internucleon Forces: I

2-1 INTRODUCTION

In order to investigate the forces which act between nucleons, it would seem advisable to study first the simplest systems, namely, those in which only two nucleons are interacting. Actually, only the main features of these systems are necessary background for a discussion of heavier nuclei. Indeed, the finer details of the two-nucleon force are to some extent irrelevant in such discussions because there is no reason to suppose that the force between two nucleons is unaffected by the presence of other nucleons. In other words, the force on a nucleon need not be the simple vector sum of the elementary two-body forces due to the other nucleons in its neighborhood, but may involve terms that arise only when third, fourth, etc., particles are present and that are typical of groups of three, four, etc., nucleons. Such forces are referred to as "many-body forces." Meson theories predict these forces. In spite of many theoretical attempts, however, little is known definitively about many-body forces, except the long-range part of the three-body force. Furthermore, experimentally it is not possible to isolate the effects of these from the effects of two-body forces. Indeed much progress has been made in understanding features of nuclear behavior in terms of two-body forces alone. Nevertheless, we certainly cannot expect the force between two isolated protons to be precisely the same as that between two protons the same distance apart in a nucleus (see Chapter 8).

The two-nucleon systems are, of course, the proton-proton, neutron-neutron, and neutron-proton systems. The last of these, the neutron-proton

system, can exist in a stable bound state, the deuteron. The deuteron is a quite simple nuclide in that no excited bound states are known, that is, it exists only in its ground state. Apart from the deuteron, we can study the neutron-proton system also in a state of positive energy in which the particles are free. Such experiments are normally performed by letting a beam of neutrons from a nuclear pile or an accelerator impinge on a substance containing many essentially free protons. The simplest substance is hydrogen gas, but in many experiments it is advantageous to use other substances that contain many hydrogen nuclei, such as thin nylon sheets or paraffin. Corrections must be made for scattering from the other nuclei in these substances, and hence their scattering cross sections must be known. When such a beam of neutrons impinges on protons, a few will be captured to form deuterons, with the extra energy emitted as a γ-ray, but the great majority will be scattered elastically (i.e., without any change in the total kinetic energy of neutron and proton). Of course, the neutron and proton "feel" each other's presence through the nuclear forces which change the magnitude and direction of their velocities. Hence the angle through which a neutron is scattered is determined by nuclear forces, or, conversely, experimental determination of the angular distribution of scattered neutrons and protons gives evidence concerning the nuclear force. In addition to the various properties of the stable state of the deuteron and the observations on nuclear scattering, there is one more source of information on the neutron-proton system, namely, a study of the photodisintegration of the deuteron; since the properties of the electromagnetic field are well known, these experimental results allow us to draw certain conclusions about the nuclear force.

When we turn to the system of two protons, we see an immediate difference in that there are no bound states: ^{2}He does not exist. This means that the nuclear force between two protons is not sufficiently strong to bind the protons in the face of the Coulomb repulsion, e^2/r^2. As we shall see, an analysis of the proton-proton scattering data reveals that the system would be unbound even if there were no electrostatic repulsion. In any case, the experimental evidence on the two-proton system comes entirely from scattering experiments.

There is no direct experimental evidence on the neutron-neutron system. Since neutrons decay to protons in a few minutes, and since it would, in any event, be difficult to devise a suitable box for neutrons, direct neutron-neutron scattering would seem of necessity to involve the intersection of two neutron beams. The intensity of scattered particles would be low. Such experiments have not been performed. There is considerable indirect evidence, however, on the neutron-neutron force, which will be described in this chapter, and which leads to the general conclusion that it is very similar to the force between two protons, excluding the electrostatic interaction. The question of a possible bound state, the dineutron, has been raised from time to time. Experiments have been performed in which it might be a possible product, but have met with negative results. If the *n-n* force were exactly the same as the *nuclear p-p* force, the bound state would not exist. The evidence favors the conclusion that there is no dineutron. An excellent review of the historical development of the subject is given in Brink's book [1].

2-2 POSSIBLE NUCLEON FORCES

Before examining in detail the possible form of the nucleon interaction, one might find it worth while to recall the conservation and invariance laws. The physical behavior of a system is not affected by one's arbitrary choice of coordinate systems. If the energy is independent of the choice of origin or, in other words, if the system behaves identically wherever it is located in space, then the total momentum of the system is a constant of motion. Similarly, if there are no physically preferred directions in space or if the energy is independent of the orientation of the coordinate axes, then the total angular momentum of the system is conserved. There is apparently no "center of the universe" and no preferred direction, or, as is sometimes said, space is homogeneous and isotropic. We therefore expect the two momentum-conservation laws to hold for any isolated system.

A third conservation law, that of parity, is connected with physical invariance under the change from a right-handed to a left-handed coordinate system or, equivalently, under a reflection of axis. In this case the wave function is either odd or even when all coordinates x, y, and z are replaced by $-x$, $-y$, and $-z$. However, if there should be a fundamental process in nature which distinguishes between left- and right-handedness, the wave function describing systems subject to such processes need not have definite parity.

It will be assumed that all nuclei are in states of definite parity and that in all reactions involving only nuclear or electromagnetic forces the total parity of the system is conserved. Strictly, nuclear states are not of definite parity because there is a force between nucleons associated with the β-decay interaction which does possess left-right asymmetry. However, these forces are approximately 10^{-20} of nuclear forces, and it has been estimated that they should produce a term of opposite parity with a relative amplitude of order 10^{-7} in the wave function [2]. Experimentally, the effect of such

admixtures in the wave function has been detected, for example, in the α-decay of the 8.8-MeV 2^- state of ^{16}O to the 0^+ ground state of ^{12}C [3] and in the observed left-right asymmetry in the angular distribution of γ-radiation from polarized ^{180m}Hf [4].

We shall begin our discussion with the neutron-proton system, in which there are no electrostatic forces. There is a force due to the two magnetic moments, but this is small enough to be treated as a slight correction to the nuclear forces. As Rutherford's experiment in 1911 on α-particle scattering showed, the nuclear forces must be of very short range, certainly less than 10^{-12} cm. We therefore consider a situation in which no appreciable force acts on the nucleons so long as they are far enough apart, but a reasonably strong force is effective when the distance between them falls below a certain value. Such a situation could be represented, for example, by postulating a potential energy between neutron and proton, given by

$$V = -V_0 \exp(-r/r_n), \tag{2-1}$$

where r is the distance between the nucleons, r_n is a fixed (short) length, and V_0 is a fixed positive energy. This potential, of course, leads to a force

$$F = -\frac{\partial V}{\partial r} = -\frac{V_0}{r_n}\exp(-r/r_n).$$

The minus sign indicates that the force is attractive, and this is associated with the fact that the potential is negative. This form of potential satisfies our condition that both the potential and the force be essentially zero for sufficiently large r—in this case, for r greater than a few times r_n. Of course, many other potentials are also *a priori* admissible. Forms commonly used are

$$V = -V_0 \exp(-r^2/r_n^2) \quad \text{(Gaussian)}, \tag{2-2}$$

$$V = -V_0 \frac{\exp(-r/r_n)}{r/r_n} \quad \text{(Yukawa)}, \tag{2-3}$$

$$\begin{aligned} V &= -V_0, \quad r < r_n \\ &= 0, \quad r > r_n \end{aligned} \quad \text{(square well)}. \tag{2-4}$$

The exponential, Gaussian, and square-well potentials are employed because they offer mathematical simplicity and because they represent a range of different shapes. In particular, they have different cutoffs at the larger distances: the square-well potential represents an extremely strong force just at $r = r_n$ with zero force elsewhere, while the Gaussian potential, although

falling fairly abruptly in a short distance, nevertheless has a tail outside this region. The exponential has a still longer tail (see Fig. 2–1). The Yukawa potential has some theoretical significance and was predicted by the earliest form of meson theory. It provides an example of a potential that is strongly attractive at very small distances of separation.

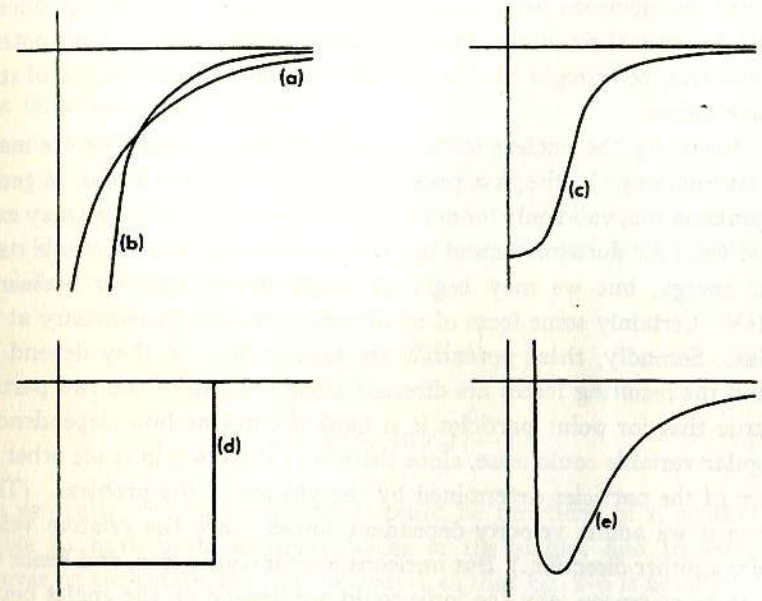

Fig. 2-1 Various proposed nuclear potentials. The shapes shown are (a) exponential, (b) Yukawa, (c) Gaussian, (d) square-well, and (e) repulsive core followed by exponential.

We shall use the expression "shape" of the potential in the following sense. If the constants, such as V_0 and r_n, in the potential are varied but the functional form remains unchanged, we say that the shape is unchanged. It will be realized that a potential shape must have at least two constants: one, V_0, determining the strength of the potential, and the other, r_n, fixing its range. It could, however, have more than two parameters. An example is the so-called repulsive core potential, which we shall have to consider later. This is shown in Fig. 2–1e and is defined by

$$V = \infty, \qquad r < r_c,$$

$$= -V_0 f\left(\frac{r}{r_n}\right), \quad r > r_c, \tag{2–5}$$

where $f(r/r_n)$ is any short-range function, such as one of the four shapes already considered. This potential implies a very strong (strictly infinite) repulsive force at $r = r_c$, with an attractive force outside. In effect, it is as though the nucleons were impenetrable spheres of diameter r_c, since the distance between their centers cannot become smaller than r_c. This potential may, however, be thought of as a simplified description of a region of strong repulsive forces.

In describing the nuclear force by such simple potentials we are making great assumptions. In the first place, the concept of potentials is, in general, an approximation, valid only for nonrelativistic particles. Thus we may expect it to be valid for nucleons bound in nuclei or moving with reasonably small kinetic energy, but we may begin to doubt its validity for nucleons of 300 MeV. Certainly some form of relativistic correction is necessary at such energies. Secondly, these potentials are central, that is, they depend only on r and the resulting forces are directed along the join of the two particles. It is true that for point particles it is hard to imagine how dependence on an angular variable could arise, since there is no direction in space other than the join of the particles determined by the physics of the problem. (This is not true if we admit velocity-dependent forces, since the relative velocity provides another direction.) But nucleons have intrinsic spin, and hence there seems to be no reason why the force could not depend on the angles between the two spin directions, or on the angles between the spin directions and the join $\mathbf{r}$. Indeed, we shall see that it depends on all these angles.

Let us examine the dependence on the angle between the two spin vectors. Since the energy of the system is assumed to be invariant under translation, rotation, and reflection of the coordinate system, all terms in the energy must be scalars. Consequently, the vectors $\boldsymbol{\sigma}_1$ and $\boldsymbol{\sigma}_2$ must appear in the potential in the form of the scalar product $\boldsymbol{\sigma}_1 \cdot \boldsymbol{\sigma}_2$. This, then, is the nature of the spin dependence. Now $\boldsymbol{\sigma}_1 \cdot \boldsymbol{\sigma}_2$ is an operator with definite eigenvalues for the singlet and triplet spin states. Indeed,

$$\boldsymbol{\sigma}_1 \cdot \boldsymbol{\sigma}_2\, {}^1(\sigma)_0 = -3\,{}^1(\sigma)_0,$$

$$\boldsymbol{\sigma}_1 \cdot \boldsymbol{\sigma}_2\, {}^3(\sigma)_m = {}^3(\sigma)_m.$$

Hence, if we write

$$V = -V_0 f\left(\frac{r}{r_n}, \boldsymbol{\sigma}_1 \cdot \boldsymbol{\sigma}_2\right), \tag{2–6}$$

we have defined two potentials, one for the singlet state and the other for the triplet state:

$$V_s = -V_0 f\left(\frac{r}{r_n}, -3\right), \tag{2–7a}$$

$$V_t = -V_0 f\left(\frac{r}{r_n}, 1\right). \tag{2–7b}$$

As an important example, take

$$V = -V_0(A + B\boldsymbol{\sigma}_1 \cdot \boldsymbol{\sigma}_2) f\left(\frac{r}{r_n}\right). \tag{2–8}$$

This gives potentials of the same shape in singlet and triplet states, but with different strengths, namely,

$$V_s = -(A - 3B)V_0 f\left(\frac{r}{r_n}\right), \tag{2–9a}$$

$$V_t = -(A + B)V_0 f\left(\frac{r}{r_n}\right). \tag{2–9b}$$

More generally, of course, A and B could be functions of r, so that it is possible to have quite different forces in the singlet and triplet states. However, in each state, the force is central, so that Eq. 2–6 is usually referred to as a central potential.

A case of particular interest is Eq. 2–8 with $A = B = \frac{1}{2}$, that is,

$$V = -V_0(\tfrac{1}{2} + \tfrac{1}{2}\boldsymbol{\sigma}_1 \cdot \boldsymbol{\sigma}_2) f\left(\frac{r}{r_n}\right), \tag{2–10}$$

$$V_s = V_0 f\left(\frac{r}{r_n}\right), \tag{2–11a}$$

$$V_t = -V_0 f\left(\frac{r}{r_n}\right). \tag{2–11b}$$

The singlet and triplet potentials are equal but have opposite signs, the singlet corresponding to a repulsive force. As explained in Appendix A, $P_\sigma = \frac{1}{2}(1 + \boldsymbol{\sigma}_1 \cdot \boldsymbol{\sigma}_2)$ is called the spin-exchange operator, since it exchanges the spins of the two particles in the wave functions. Consequently Eq. 2–10

describes a "spin-exchange force." For historical reasons, this is often called a Bartlett force [5].

In addition to the angles discussed above, there is another variable on which the potential might depend. This is the *parity* of the state. We can best see how to introduce this dependence by considering another exchange operator. We define P_x as the operator that exchanges the position coordinates of the two particles:

$$P_x\psi(\mathbf{r}_1, \mathbf{r}_2) = \psi(\mathbf{r}_2, \mathbf{r}_1). \tag{2–12}$$

For a two-particle system, this is the same as changing the sign of the relative coordinates. If the parity of the state is even, the interchange of space coordinates leaves the wave function unaltered, whereas if the parity is odd, the sign of the wave function is changed. For a two-particle system, in a state of definite orbital angular momentum, the parity is even or odd, according as the quantum number l is even or odd. Hence

$$P_x \equiv 1 \qquad (l \text{ even}), \tag{2–13a}$$

$$P_x \equiv -1 \quad (l \text{ odd}). \tag{2–13b}$$

A potential

$$V = -V_0 f\left(\frac{r}{r_n}\right)P_x \tag{2–14}$$

is called a "space-exchange" potential or a Majorana potential [6]. We can also introduce a Heisenberg exchange force [7] defining the operator

$$P_H = P_\sigma P_x, \tag{2–15}$$

and write

$$V = -V_0 f\left(\frac{r}{r_n}\right)P_H. \tag{2–16}$$

It will be realized that the Heisenberg operator, which exchanges both spin and space coordinates, is equivalent to an exchange of the charges of the nucleons. Indeed, $P_H = -P_\tau$, where P_τ is a charge-exchange operator analogous to P_σ but based on i-spin.

To complete the assignment of physicists' names to types of forces and to commemorate one of the early workers in this field, it is customary to refer to an ordinary force derived from $V = -V_0 f(r/r_n)$ as a Wigner force [8]. Originally this name was applied to any short-range force, but it has now come to be used exclusively for exchange-independent forces.

To summarize this discussion, we see that it is possible to write a potential which, while still essentially central, displays spin and parity dependence in the form

$$V = -V_0[W(r) + B(r)P_\sigma + M(r)P_x + H(r)P_H], \tag{2–17}$$

where the various functions of r are arbitrary. Since Eq. 2–17 implies different potentials for (a) triplet and singlet states, and (b) states of even and odd parity, we can equally well speak of four different potentials: one for triplet even states (such as $^3S_1$, $^3D_1$); one for triplet odd states ($^3P_0$, $^3P_1$, $^3P_2$, ...); one for singlet even states ($^1S_0$, $^1D_2$, ...); and one for singlet odd states ($^1P_1$, $^1F_3$, ...). This last method of description corresponds more closely to the experimental situation (at least at low energies), where individual states may be studied with the hope of finding the form of the potential acting. Of course, if we knew the potentials in the four types of states, we could easily calculate the functions in Eq. 2–17 (see Problem 2–5).

2-3 SCATTERING EXPERIMENTS

Consider a neutron beam incident on a target. As suggested in Fig. 2–2, many of the neutrons may not come close enough to any nucleus to interact with it and therefore pass straight through the target. Some, however, do come within nuclear force range of a nucleus and are scattered. We must be a little more precise. The de Broglie wavelength of a neutron is determined by its momentum through the formula $\lambda\!\!\!^{-} = \hbar/p$. The position of a neutron cannot be considered to be fixed more closely than $\lambda\!\!\!^{-}$. Hence, if $\lambda\!\!\!^{-}$ is of the order of magnitude of the distance between nuclei in the target, a neutron cannot avoid a collision. There will still be some probability of its continuing undeflected, but a large number of unscattered neutrons (as in Fig. 2–2)

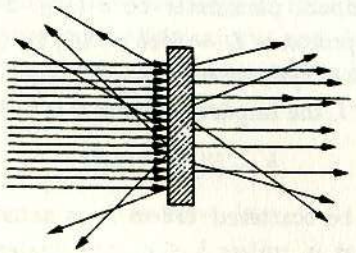

Fig. 2-2 Scattering of a neutron beam incident from the left.

implies that $\lambda\!\!\!^{-}$ is small in comparison with internuclear distances. In such a case, we can consider each neutron in interaction with at most one nucleus, the one that it approaches most closely. Then the neutron is well localized so far as the target nuclei are concerned. However, since the distance between two nuclei, even in a molecule, is never much less than 1 Å, $\lambda\!\!\!^{-}$ can be much smaller than internuclear distance, but at the same time considerably greater than the range of nuclear forces. This is the situation for neutrons of energy up to about 10 MeV.

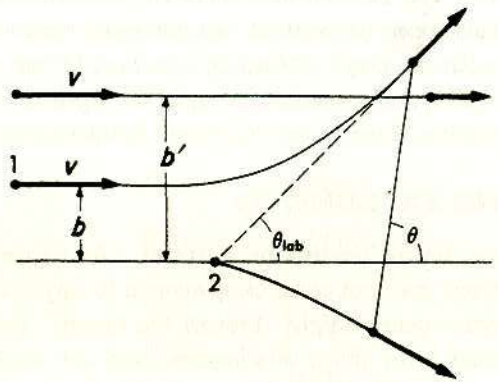

Fig. 2-3 Various parameters in a scattering experiment.

Let such a neutron approach a proton with energy $E = \frac{1}{2}M_n v^2$. Since it is fairly well localized, let us apply a mixture of classical and quantum mechanics. Let its impact parameter be b (Fig. 2-3). Then its angular momentum about the proton is $L = Mvb = \hbar(b/\lambda\!\!\!^{-})$. Quantum-mechanically, we know that $L^2 = l(l+1)\hbar^2$, where l is an integer. Hence, for a neutron with quantum number l, the impact parameter is

$$b \sim [l(l+1)]^{1/2}\lambda\!\!\!^{-}. \tag{2-18}$$

The neutron will not be scattered unless it is acted upon by the nuclear field of the proton, that is, unless $b \lesssim r_n$, the nuclear force range. Hence, for a given neutron energy and therefore $\lambda\!\!\!^{-}$, only those neutrons are scattered whose quantum number l is given by

$$l(l+1)\lambda\!\!\!^{-2} < r_n^2. \tag{2-19}$$

Thus, so long as $\lambda\!\!\!^{-}/r_n$ is greater than about $2^{-1/2}$, only neutrons of zero angular momentum will be scattered. For sufficiently low energies ($\lesssim$ 10 MeV), only the S-state potential need be considered; as the energy increases, the P-, D-, etc., states progressively become of importance. (This is, of course, a semiclassical argument, and the result is not exact.)

We set our problem up in the coordinate system in which the center of mass is at rest. Figure 2-3 shows the situation in the laboratory coordinate system in which particle 2 (the proton) is initially at rest. The center of mass G is moving, and θ_{lab} is the laboratory scattering angle. Particle 1 has initial velocity v in the laboratory system. Figure 2-4 shows the same scattering process in the system in which G is at rest. Particles 1 and 2 have initial (and final) speeds v_1 and v_2, and θ is the scattering angle. The following relationships hold:†

$$\tan\theta_{\text{lab}} = \frac{\sin\theta}{\cos\theta + M_1/M_2}, \tag{2-20a}$$

$$v_1 = \frac{M_2}{M_1+M_2}v, \tag{2-20b}$$

$$v_2 = \frac{M_1}{M_1+M_2}v, \tag{2-20c}$$

$$E = \tfrac{1}{2}M_1v_1^2 + \tfrac{1}{2}M_2v_2^2 = \frac{1}{2}\frac{M_1M_2}{M_1+M_2}v^2 = \frac{1}{2}\frac{M}{M_1}E_{\text{lab}}, \tag{2-20d}$$

where

$$M = \frac{2M_1M_2}{M_1+M_2}. \tag{2-20e}$$

The quantity E is the center-of-mass energy or the kinetic energy of relative motion, E_{lab} is the energy in the laboratory, and M is twice the reduced mass of the system. If we ignore the difference between proton and neutron masses, M is the "mass of a nucleon," and

$$\theta_{\text{lab}} = \tfrac{1}{2}\theta, \tag{2-21a}$$

$$v_1 = v_2 = \tfrac{1}{2}v, \tag{2-21b}$$

$$E = \tfrac{1}{2}E_{\text{lab}}. \tag{2-21c}$$

† For example, ref. [26], p. 86.

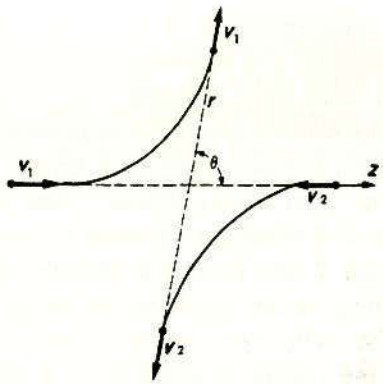

Fig. 2-4 The scattering in the center-of-mass system.

The momentum of relative motion is $\frac{1}{2}Mv$, and we shall define

$$k = \frac{1}{2}\frac{Mv}{\hbar} = \left(\frac{ME}{\hbar^2}\right)^{1/2}. \tag{2-22}$$

It is clear, of course, that a uniform beam of neutrons incident on a proton contains neutrons of many angular momenta; if the beam could be considered of infinite cross section, it would contain all angular momenta. This means that the wave function which represents a beam of particles of momentum $k\hbar$ traveling in the z-direction, that is, e^{ikz}, can be expanded in a series of the wave functions appropriate to all angular momenta. Mathematically,

$$e^{ikz} = \sum_{l=0}^{\infty} (2l+1)i^l j_l(kr)P_l(\cos\theta). \tag{2-23}$$

The geometry is indicated in Fig. 2-4: P_l is the Legendre polynomial (the angular-momentum wave function), and $j_l(kr)$ is a Bessel function, whose properties are summarized in Appendix B. Roughly speaking, we can interpret $|(2l+1)i^l j_l(kr)|^2$ as the probability that a neutron of angular momentum l will be found at a distance r. If $\lambda\!\!\!^{-} > r_n$, the motion of particles with $l > 0$ is undisturbed; they are not scattered, and the terms of Eq. 2-23 for $l > 0$ are the appropriate wave functions for the complete problem. To examine the scattering, we must study the wave equation for $l = 0$.

For the S-state, we can take as function $(1/r)u(r)$, since for $l = 0$ there is no angular dependence. The Schrödinger equation in the center-of-mass system gives

$$\frac{d^2u}{dr^2} + [k^2 - V(r)]u = 0, \tag{2-24}$$

where $V(r)$ is the neutron-proton potential in the S-state in question, which can be either singlet or triplet, depending on the spin orientations of the incident and target nucleons. For very large values of r, the nuclear potential is zero, and Eq. 2-24 becomes

$$\frac{d^2u}{dr^2} + k^2u = 0, \qquad r \gg r_n. \tag{2-25}$$

Since the two independent solutions of this equation are e^{ikr} and e^{-ikr}, the wave function at large r has the form†

$$u \sim A\sin(kr+\delta) = \frac{Ae^{-i\delta}}{2i}(e^{2i\delta}e^{ikr} - e^{-ikr}). \tag{2-26}$$

The first term in the parentheses represents particles traveling outward from the scattering center; the second term, incoming particles. But in a scattering experiment the only incoming particles are those in the incident beam. Therefore we must adjust the value of A so that the incoming particles of Eq. 2-26 are just those of the ($l = 0$) part of the plane wave (of Eq. 2-23), namely, $j_0(kr)$:

$$j_0(kr) = \frac{\sin kr}{kr} = \frac{1}{2ikr}(e^{ikr} - e^{-ikr}). \tag{2-27}$$

Thus, if we take $A = e^{i\delta}/k$, $u(r)/r$ will contain as incoming particles only the particles in the incident beam. Then $u \sim (e^{ikr}e^{2i\delta} - e^{-ikr})/2ik$. Comparing this with Eq. 2-27, we see that the effect of scattering on the asymptotic wave function is to modify the outgoing part of the wave by a factor $e^{2i\delta(k)}$, which is denoted by the symbol

$$S(k) = e^{2i\delta(k)}. \tag{2-28}$$

† The symbol $\sim$ means "equal for large r." The constant δ is real. If it were not, the amplitudes of the outgoing and incoming waves would be different; this would mean that inelastic collisions were occurring, effectively removing particles of wave number k. The only inelastic n-p process is radiative capture, which has a very small cross section.

In this simple example, $S(k)$ is just a k-dependent number. In more complicated cases with noncentral forces present, the Schrödinger equation has two channels which are coupled (see Chapter 5), and then $S(k)$ is a 2×2 matrix. It is for this reason that $S(k)$ is generally called the S-matrix. Writing

$$u \sim \frac{1}{2ik}(e^{ikr} - e^{-ikr}) + \frac{1}{2ik}(e^{2i\delta} - 1)e^{ikr}$$
$$\sim u_{\text{inc}} + u_{\text{sc}},$$

where u_{inc} is the incident and u_{sc} is the scattered wave, we see that the scattered particles are represented by

$$u_{\text{sc}} \sim \frac{1}{2ik}(e^{2i\delta} - 1)e^{ikr} = \frac{e^{i\delta}}{k}\sin\delta\, e^{ikr}. \tag{2–29}$$

Hence we can write

$$u \sim u_{\text{inc}} + f_k e^{ikr}, \tag{2–30}$$

where

$$f_k = \frac{e^{i\delta(k)}}{k}\sin\delta(k). \tag{2–31}$$

The quantity f_k is called the scattering amplitude. For S-waves, as we see, f_k is independent of θ, but for higher partial waves it is θ dependent.

Consider a sphere S of large radius R. In one second the scattered particles which were on the surface of S will be on a sphere of radius $R + v$, and during this second all particles that lie between R and $R + v$ will have passed through the surface of S. From Eq. 2–29, we see that there are $\sin^2\delta/k^2r^2$ scattered particles per unit volume. Hence the number of scattered particles that pass through the sphere per second is $(\sin^2\delta/k^2R^2)4\pi R^2 v = (4\pi v/k^2)\sin^2\delta$. This is the number of particles scattered per second.

By similar arguments, the wave function e^{ikz} represents a beam of v incident particles per unit area per second. Since the cross section for any event is defined as the number of desired events per second divided by the number of particles incident per unit area per second, we see that the cross section for scattering in the S-state is

$$\sigma_S(E) = \frac{4\pi}{k^2}\sin^2\delta = 4\pi\lambda\!\!\!^{-2}\sin^2\delta. \tag{2–32}$$

We remark that S-wave scattering is isotropic, since u has no angular

dependence. The scattering in states of higher angular momentum is not isotropic; this makes it possible, by measuring the angular distribution experimentally, to decide at what energy the effects of higher angular momenta are becoming important.

Let us consider very low velocities, indeed the limit of zero energy. Since

$$u \sim e^{i\delta}\frac{\sin(kr + \delta)}{k},$$

it is clear that, if u is to remain finite at large but finite values of r (as it must), δ must approach zero at least as fast as k does. Thus $\sin\delta/k$ must be finite. This can also be seen from Eq. 2–29 for the scattered amplitude u_{sc}. If we define the *scattering length* a by the equation

$$\lim_{k\to 0}\left(-\frac{\sin\delta}{k}\right) = a, \tag{2–33}$$

we have

$$\sigma_S(0) = 4\pi a^2 \tag{2–34}$$

and

$$u \sim \frac{e^{i\delta}}{k}(\sin kr\cos\delta + \cos kr\sin\delta) \to r - a. \tag{2–35}$$

Equations 2–32 and 2–34 show that the phase shifts δ (or, for very low energy, the scattering length a) are the quantities that may be found by measuring the scattering cross section. The quantities δ and a are in turn related to the potential causing the scattering by asymptotic expressions for u. This is seen as follows.

The Schrödinger equation (Eq. 2–24) must be satisfied by a quantity $u(r)$ with the boundary condition

$$u(0) = 0. \tag{2–36}$$

[Otherwise the wave function $u(r)/r$ would be infinite.] This initial condition fixes $u(r)$ except for an arbitrary multiplication constant, A, which was determined by consideration of the incoming wave in u. Hence, if we solve the Schrödinger equation subject to $u(0) = 0$, we shall be able to establish the asymptotic form of u and therefore find δ. Similarly, for $E = 0$, the equations

$$\frac{d^2u_0}{dr^2} - V(r)u_0 = 0 \tag{2–37}$$

and

$$u_0(0) = 0 \tag{2-38}$$

will yield a solution which asymptotically is proportional to $r - a$. Hence a can be found if V is known.

It is clear, then, that if a potential $V(r)$ is suggested as the nuclear potential, its agreement with experiment (at least so far as low-energy scattering is concerned) can be checked by solving Eq. 2–24 subject to 2–36 and thus determining δ at various energies. The converse procedure, that is, deducing $V(r)$ from a knowledge of δ at various energies, is not as straightforward; indeed, it can be shown that the values of δ define a unique potential function only under certain restrictive assumptions. In particular, low-energy scattering does not reveal very much about the shape of the potential, as we shall now proceed to show.

Let us introduce the symbol $\psi(r)$ for the asymptotic form of u. The quantity ψ is determined by solving Eq. 2–24. Thus, for a fixed nuclear potential V, ψ depends only on r and k^2, apart from a normalizing constant; this means that $(1/\psi)(d\psi/dr)$ depends only on r and k^2. Therefore, since $\psi = A \sin(kr + \delta)$, we have, setting $r = 0$,

$$k \cot \delta = \left(\frac{1}{\psi}\frac{d\psi}{dr}\right)_{r=0}. \tag{2-39}$$

However, if we are concerned only with low energies, we may expand this function in powers of k^2. Hence we see that, in general,

$$k \cot \delta = \alpha + \beta k^2 + \cdots. \tag{2-40}$$

We can fix α by considering zero energy, for by Eq. 2–33 $\lim_{k\to 0}(k \cot \delta) = -1/a$. Also, it is clear that β must have the dimension of length. We set $\beta = \frac{1}{2}r_0$ and write

$$k \cot \delta = \frac{-1}{a} + \tfrac{1}{2}r_0 k^2, \tag{2-41}$$

which is valid, provided k is sufficiently small so that higher powers may be neglected. To a good approximation, this condition allows energies up to about 10 MeV. It is shown in Appendix B that the length r_0 is given by

$$r_0 = 2\int_0^\infty \left[\left(\frac{\psi_0}{a}\right)^2 - \left(\frac{u_0}{a}\right)^2\right] dr, \tag{2-42}$$

where u_0 is the zero-energy wave function and ψ_0 is its asymptotic form.

From Eq. 2–35 we have

$$r_0 = 2\int_0^\infty \left[\left(1 - \frac{r}{a}\right)^2 - \left(\frac{u_0}{a}\right)^2\right] dr. \tag{2-43}$$

Since $\psi_0(r) = u_0(r)$ when r is appreciably outside the range of nuclear forces, we see that r_0 is a length of the same order as the range of the nuclear potential. It is called the *effective range*. Since the result of a scattering experiment is simply the determination of the phase shifts, it follows that, as long as Eq. 2–41 is valid, the only data available from scattering are the values of a and r_0. We are entitled, then, to think of these two lengths as experimentally determined quantities.

We may summarize this discussion by saying that the low-energy ($\lesssim 10$ MeV) scattering of the neutron-proton system is determined by two quantities: the scattering length a and the effective range r_0. Consequently, experiments at these energies cannot distinguish between potentials that yield the same values of a and r_0 upon solution of Eqs. 2–37 and 2–42. As the expression $V_0 f(r/r_n)$ makes clear, any potential function contains at least two constants which can, in general, be adjusted to give the experimental values of a and r_0, whatever the form of $f(r/r_n)$ may be. This shows that low-energy scattering experiments cannot determine the shape of the potential; or, alternatively, the low-energy properties of the neutron-proton system are insensitive to the shape of the potential.

2-4 BOUND STATE

We can see that not only scattering, but also the properties of a bound state, may be expressed in terms of a and r_0. For a bound state, the energy is negative, say $-\epsilon$, and

$$k = i\gamma = i\left(\frac{M\epsilon}{\hbar^2}\right)^{1/2}. \tag{2-44}$$

Then Eqs. 2–24 and 2–25 still hold, and the asymptotic form of u given by 2–26 is

$$u \sim \frac{A}{2i}(e^{i\delta}e^{-\gamma r} - e^{-i\delta}e^{\gamma r}). \tag{2-45}$$

For a bound state, the probability of a large separation of the particles must be small, that is, u must behave like $e^{-\gamma r}$. Hence $e^{-i\delta} = 0$, and consequently $i\delta$ is a large positive real number. Also A must be small so that the product $Ae^{i\delta}$ remains finite and is the normalizing factor. These conditions replace

the restriction to outgoing waves required in the scattering problem to determine A. However, the argument that leads to $k \cot \delta = -1/a + \frac{1}{2}r_0k^2$ remains valid. Now $\cot \delta = i \coth i\delta = i$ as $i\delta$ approaches infinity. Thus $k \cot \delta = ik = -\gamma$, and we find

$$\gamma = \frac{1}{a} + \tfrac{1}{2}r_0\gamma^2. \tag{2–46}$$

This means that the binding energy of the deuteron can be determined from a knowledge of the scattering length and effective range of the force acting between the nucleons.† It will be realized that Eq. 2–46 is valid only for sufficiently small γ. Otherwise, higher powers should appear on the right-hand side of the equation. Fortunately, the binding energy of the deuteron turns out to be small enough (2.226 MeV) so that the approximation is good.

2-5 EXPERIMENTAL RESULTS

The preceding discussion of scattering has been carried out without regard to spin dependence of the forces. In a situation in which each neutron can be considered as interacting with just one proton, the encounter will be either a singlet or a triplet one, and if there is no spin polarization (i.e., no preferred direction of spin), the total cross section will be

$$\sigma(E) = 4\pi\lambda^2(\tfrac{1}{4}\sin^2\delta_s + \tfrac{3}{4}\sin^2\delta_t). \tag{2–47}$$

This expression arises since there are three triplet states and one singlet state and hence a three-to-one probability that the nucleons will collide in the triplet state. At very low energies, therefore, we have

$$\sigma(0) = \pi(a_s^2 + 3a_t^2). \tag{2–48}$$

The subscripts refer to the singlet and triplet states.

If, however, the neutron is sufficiently slow so that it is in effective interaction with more than one proton, there will be interference of the waves from the two scatterers. In this case, as in all such wave phenomena, it becomes necessary to add the amplitudes of the waves. This effect is significant for the so-called thermal neutrons, which have energy of a few one-hundredths of an electron volt. Experiments with these neutrons provide information

† This is true only if the range of the force is much smaller than the extent of the deuteron wave function. For examples of potentials for which Eq. 2–46 is not valid, see K. F. Chong and Y. Nogami, *Am. J. Phys.* 39, 182 (1971).

about the *coherent-scattering amplitude* a_H for the hydrogen molecule, which is given by

$$a_H = \tfrac{1}{2}(a_s + 3a_t). \tag{2–49}$$

Such experiments are discussed further in Appendix B.

The most accurate determinations of the total cross section for slow neutrons and of the coherent-scattering amplitude are as follows:

$$\sigma(0) = 20.442 \pm 0.23 \text{ b} \quad [9],^{\dagger}$$

$$a_H = -3.707 \pm 0.008 \text{ fm} \quad [10].$$

Substitution of the weighted means of these values into Eqs. 2–48 and 2–49 yields

$$a_s = -23.710 \pm 0.030 \text{ fm},$$

$$a_t = 5.432 \pm 0.005 \text{ fm}.$$

The signs of a_s and a_t are in themselves instructive. A negative scattering length indicates that the corresponding potential does not have a bound state, at least not for any reasonably small value of binding energy. This can be seen immediately from Eq. 2–46, which shows that, if a bound state were assumed and we used this equation to calculate its binding energy ϵ, the essentially positive quantity γ would turn out to be negative. It can also be seen from a consideration of the graphs of the zero-energy wave function. Writing

$$\frac{d^2u}{dr^2} = -V_0 f\left(\frac{r}{r_n}\right)u - \frac{2mE}{\hbar^2}u, \tag{2–50}$$

we notice that at zero energy d^2u/dr^2 is negative until the potential vanishes when it is zero. If the scattering length is negative, we have the result for u_0 shown in Fig. 2–5a. If we now consider the effect of the last term in Eq. 2–50 for small negative E, we see that d^2u/dr^2 is increased so that u slopes upward more rapidly than u_0 and continues to rise after the potential has vanished, giving a wave function that is infinite at large values of r. The case $a > 0$ is illustrated in Fig. 2–5b. Here the effect of the increase in the second derivative is, in general, the same, that is, an unbounded wave function, but it is possible that for certain energies the wave function will decay exponentially as illustrated by the curve u_B, giving a bound state. We deduce, then, that the singlet S-state is unbound. However, the large value of a_s means

† The measure 1 barn = 10^{-24} cm^2 is a useful unit for nuclear cross sections.

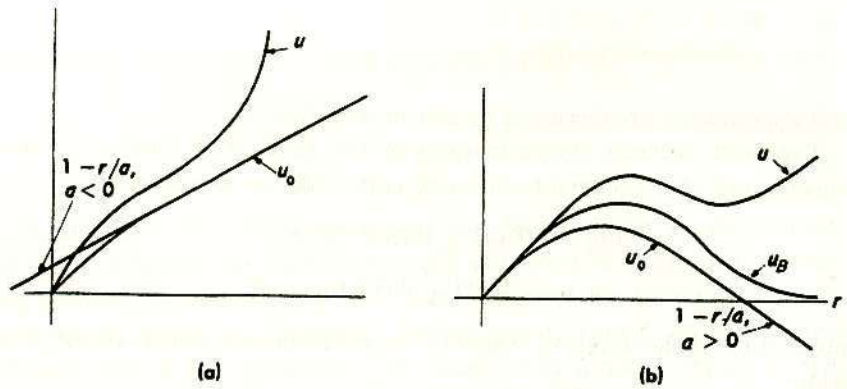

Fig. 2-5 Wave function u_0 for $E = 0$ and u for nonzero E. In (a) the scattering length a is negative, and in (b) it is positive; u_B is the wave function for a bound state.

that it is "only just" unbound, that is, the line $1 - r/a$ is not rising extremely rapidly. This result also suggests very strongly that the deuteron might be in the triplet S-state, an assumption which receives experimental support from measurement of the total angular momentum J, which is 1. Although this would not rule out P- and D-states, as we shall see in Chapter 5 the electromagnetic properties show that the wave function of the deuteron is more than 90% that of the ^3S-state. For many purposes, including those of this section, it is sufficiently accurate to treat the deuteron as a ^3S-state.

Because of these facts, Eq. 2–46 provides us with a good value of the triplet effective range r_{0t}, since ϵ and a are accurately known. The result is

$$r_{0t} = 1.749 \pm 0.008 \text{ fm}.$$

To determine r_{0s} we have to use the results of scattering at small energies in the form of Eq. 2–47, which can be written as

$$\begin{aligned}\sigma(E) &= \pi[(k^2 \operatorname{cosec}^2\delta_s)^{-1} + 3(k^2 \operatorname{cosec}^2\delta_t)^{-1}] \\ &= \pi\left\{\left[k^2 + \left(\frac{1}{a_s} - \tfrac{1}{2}r_{0s}k^2\right)^2\right]^{-1} + 3\left[k^2 + \left(\frac{1}{a_t} - \tfrac{1}{2}r_{0t}k^2\right)^2\right]^{-1}\right\}. \qquad (2\text{–}51)\end{aligned}$$

The term in r_{0s} is a small part of the cross section, so that great accuracy in measurements of $\sigma(E)$ is required to obtain a good value of r_{0s}. The available data [11] yield

$$r_{0s} = 2.73 \pm 0.03 \text{ fm}.$$

As we have remarked, the scattering length and effective range are sufficient to fix the constants in any potentials with two parameters. These potentials may be chosen to be of square, Gaussian, exponential, or Yukawa shape.

It is clear that the expressions "range of nuclear forces" and "strength of nuclear potential" are not precise, unless the shape of the potential is specified. Nevertheless, they are frequently used, and it is customary to think of the range of forces as being 1.5–2 fm and the average depth as being 20–35 MeV, depending on the spin state.

2-6 PROTON-PROTON FORCES

Experimentally, the p-p scattering data have been measured with very high precision. The theoretical analysis of the data, however, is not so clear as in the n-p case, because it is difficult to isolate the nuclear and electromagnetic effects. This would be simple if the only electromagnetic effect were a Coulomb potential e^2/r between the two protons. For the present, we naively assume this to be so, in order to understand how the scattering formalism is modified in the presence of a long-range force. At the end of this section we indicate what corrections should be made to this simple analysis.

Irrespective of the electromagnetic effects, some modifications are necessary in the theoretical framework because the two protons are identical particles and are indistinguishable from each other. Experimentally, this means that either one of the two protons is detected at an angle θ (in the center-of-mass frame) from the incident direction. The two protons are scattered back to back in the CM frame. This implies that a proton is detected when the scattering angle is either θ or $\pi - \theta$. Quantum-mechanically, this situation requires the addition of the corresponding scattering amplitudes in order to calculate the proton flux. In Section B–3 the details are given, and it is shown that interference terms appear in the formula for the cross section.

Two protons in the S-state can interact only in the singlet spin state because of the exclusion principle. First, let us suppose that only the Coulomb potential e^2/r is operating between the two protons, and that the nuclear interaction has been switched off. Because the Coulomb interaction has an infinite range, all the partial waves are affected even at low relative energies, unlike the nuclear case in which only the S-state is modified. Let us still concentrate on the S-state. On solving the radial Schrödinger equation with the Coulomb potential in the S-state, we obtain two independent solutions, $F_0(r)$ and $G_0(r)$, which are given in Section B–1. The regular solution is $F_0(r)$, which, for large r, takes the form

$$F_0 \sim \sin(kr - \eta \ln 2kr + \sigma_0), \tag{2-52}$$

where $\eta = \frac{1}{2}kR$, R being the characteristic Coulomb length for protons, given by

$$R = \frac{\hbar^2}{M_p e^2} = 28.8(15) \text{ fm}, \tag{2-53}$$

and σ_0 is a function of k alone. This should be compared with the asymptotic form of the radial wave function in the presence of a short-range nuclear potential $V(r)$ alone (see Eq. 2-26):

$$u \sim \sin(kr + \delta_0). \tag{2-26}$$

In Eq. 2-26, all that the short-range potential did to the unperturbed form $\sin kr$ was to change its phase by $\delta_0(k)$, and this was called the phase shift. In Eq. 2-52, however, we see that the Coulomb potential not only changes the phase by σ_0 but also continually distorts the wave through the factor $\eta \ln 2kr$. This occurs because the Coulomb potential has an infinite range and its presence is felt for all values of r. We still call σ_0 the Coulomb phase shift.

Now consider the case in which both the Coulomb potential and the short-range nuclear potential $V(r)$ are present. Outside the range of $V(r)$, only the Coulomb potential is present, so that for large r the wave function has the same form as Eq. 2-52:

$$u_C \sim \sin(kr - \eta \ln 2kr + \sigma_0 + \delta_0{}^C), \tag{2-54}$$

where $\delta_0{}^C$ is now the nuclear phase shift with respect to the Coulomb wave function (see Section B-3 for details). If there were no Coulomb potential but only $V(r)$, the asymptotic wave function would be written as

$$u \approx \cos \delta_0 \sin kr + \sin \delta_0 \cos kr. \tag{2-6}$$

Similarly, in the presence of the Coulomb and the nuclear potential,

$$u_C \approx \cos \delta_0{}^C F_0(kr) + \sin \delta_0{}^C G_0(kr), \tag{2-55}$$

where the above form is valid for $r > r_n$, the range of the nuclear potential. In this sense, when the Coulomb potential is present in addition to $V(r)$, it is necessary to replace $\sin kr$ by $F_0(kr)$ and $\cos kr$ by $G_0(kr)$. Since the higher partial waves remain unaffected by $V(r)$ at low energies, $\delta_l{}^C \approx 0$ for $l > 0$. We note that, although $V(r)$ alone gives a phase shift δ_0, and e^2/r gives a phase shift σ_0, the combined form $V(r) + (e^2/r)$ does not yield a phase shift $\sigma_0 + \delta_0$, but gives $\sigma_0 + \delta_0{}^C$, where $\delta_0{}^C \neq \delta_0$. This is so because the phase shift is not linearly related to the potential.

In p-p scattering, information about the nuclear phase shifts is obtained from study of the angular distribution of the protons, rather than from measurement of the total cross section. Indeed, the total cross section for pure Coulomb scattering is infinite. The differential scattering cross section† of two identical particles of charge e due only to the Coulomb force is (Section B-3)

$$\sigma_{\text{Mott}}(\theta) = \left(\frac{e^2}{4E}\right)^2 \left[\operatorname{cosec}^4 \frac{\theta}{2} + \sec^4 \frac{\theta}{2} - \operatorname{cosec}^2 \frac{\theta}{2} \sec^2 \frac{\theta}{2} \cos\left(\eta \ln \tan \frac{\theta}{2}\right)\right], \tag{2-56}$$

where all quantities are measured in the CM system. The infinite peak for $\theta = 0$ is associated with the assumption of point changes. The infinity vanishes when the protons are taken to be of finite size. In the presence of $(e^2/r) + V(r)$, the differential cross section has the form (see Section B-3)

$$\sigma(\theta) = \sigma_{\text{Mott}}(\theta) + \sigma_N(\theta) + \sigma_{NC}(\theta).$$

Note that $\sigma_{\text{Mott}}(\theta)$ is calculated by taking all partial waves into account, whereas at sufficiently low energies σ_N involves only the S-wave nuclear-force scattering, that is, $\sigma_N = (1/k^2) \sin^2 \delta_0{}^C$ and is isotropic. The third term $\sigma_{NC}(\theta)$ is due to interference and consequently is linearly dependent on $\sin \delta_0{}^C$. This allows us to fix the sign of $\delta_0{}^C$ by observing $\sigma(\theta)$.

Typical low-energy angular distributions are shown in Fig. 2-6. An important feature of these curves is the existence of the minimum due to the nuclear-Coulomb interference term. As the energy increases, the minimum moves to smaller angles. The Coulomb effect produces very little scattering near 90°, and the flat part of $\sigma(\theta)$ in this region is due almost entirely to the nuclear forces. Note that it is only necessary to plot p-p data from 0° to 90°, since the scattering is the same at θ and at $180° - \theta$, that is, symmetrical about 90°.

Even though the scattering formalism has been modified in the presence of a Coulomb force, it is still possible to write an effective-range expansion like Eq. 2-41. The formula now reads as follows:

$$C^2 k \cot \delta_0{}^C + \frac{1}{R} h(\eta) = -\frac{1}{a_p} + \tfrac{1}{2} r_{0p} k^2 - P r_{0p}{}^3 k^4 + Q r_{0p}{}^5 k^6 + \cdots. \tag{2-57}$$

The quantity C^2, often called the Coulomb penetration factor, is given by

$$C^2 = \frac{2\pi\eta}{e^{2\pi\eta} - 1}. \tag{2-58}$$

† The differential scattering cross section is defined at the beginning of Chapter 4.

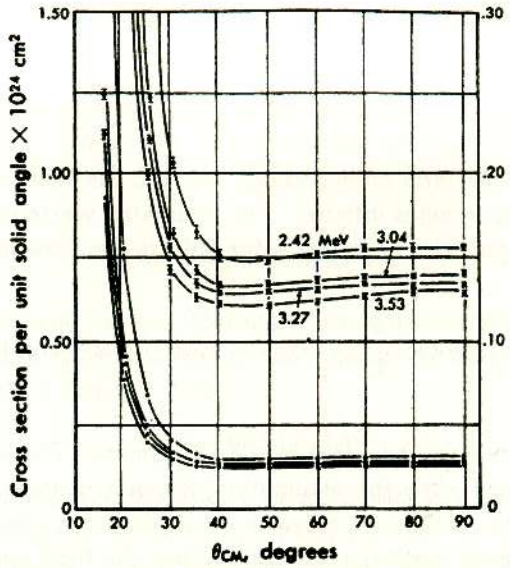

Fig. 2-6 $\sigma(\theta)$ for p-p scattering for energies of 2.42, 3.04, 3.27, and 3.53 MeV in the laboratory system. The lower curves are plotted to the vertical scale on the left; the higher curves, to that on the right. (After Blair et al. [32].)

This is essentially the ratio of the probability of finding the two protons close together to that of finding two uncharged particles there, all other factors being identical. Since the Coulomb force is repulsive, C^2 is always less than 1. It is so small below $E_{\text{lab}} = 200$ keV that there is practically no nuclear scattering, while for $E_{\text{lab}} = 800$ keV, $C^2 \approx 0.5$. The function $h(\eta)$ in Eq. 2–57 is a slowly varying function of η and is defined explicitly by Eq. B–8b. Note that, as $e \to 0$, $R \to \infty$, $C^2 \to 1$, and the left side of Eq. 2–57 becomes simply $k \cot \delta_0$. Also, a_p and r_{0p} are, as before, given by the zero-energy wave function and hence can be calculated for any given potential, just as in the n-p case. Extraction of $\delta_0{}^C$ from the experimental data allows one to plot the left side of Eq. 2–57 against k^2. At sufficiently low energies, this is a straight line, its slope being $\frac{1}{2}r_{0p}$ and its intercept at zero energy giving $-1/a_p$.

We now emphasize that experimentally one measures only various elastic-scattering data such as the differential cross section $\sigma_{pp}(\theta)$, and not the phase shifts $\delta_0{}^C$. In fact, $\delta_0{}^C$ is a model-dependent quantity, in the sense that a simple model has been taken in which the electromagnetic interactions between the two protons are replaced by a simple Coulomb potential. It follows from Eq. 2–57 that a_p, r_{0p}, and P are also, in this sense, model dependent, irrespective of the accuracy of the experiments. Actually, for energies up to about 5 MeV, experimental techniques have been developed such that $\sigma(\theta)$ can be measured to an accuracy of 0.1–0.3%. This precision

warrants a more sophisticated model, which we now outline, to isolate the electromagnetic effects from the nuclear ones.

There are several electromagnetic effects that modify the pure Coulomb interaction. A description of these, together with recent compilation of the experimental data, is given by Sher, Signell, and Heller [12]. In addition to the Coulomb potential, which arises from a single photon exchange (Fig. 2–7a), there can be the process illustrated in Fig. 2–7b, in which virtual

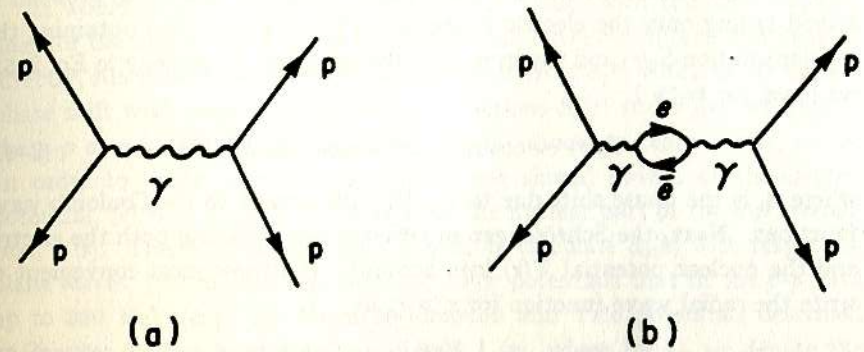

Fig. 2-7 The Coulomb force between two protons can be considered to arise from single photon exchange (a). This is modified as a result of vacuum polarization (b), in which a virtual electron-positron pair is created and annihilated during the photon-exchange process.

creation and destruction of an electron-positron pair occur. This process is called vacuum polarization (VP). The potential arising from this, to the lowest order in the fine-structure constant α $(= e^2/\hbar c)$, has been derived by Uehling [13] and is given by

$$V_{\text{VP}}(r) = \frac{2\alpha}{3\pi}\frac{e^2}{r} I(2\kappa r), \tag{2–59}$$

where $I(2\kappa r)$ is a long-range smooth function of r, which goes like $e^{-2\kappa r}/(2\kappa r)^{3/2}$ for $\kappa r \gg 1$. Here $(2\kappa)^{-1}$ corresponds to the Compton wavelength of the electron-positron pair,

$$(2\kappa)^{-1} = \frac{\hbar}{2mc} = 193.1 \text{ fm}. \tag{2–60}$$

Hence $V_{\text{VP}}(r)$ is a very long-range potential, and this in turn implies that the

effective-range formula (Eq. 2–57) should be further modified for VP correction. Had the Coulomb and VP potentials been of short-range, formula 2–41 would have remained unaltered, except that these forces would have modified the nuclear potential slightly and thereby produced different values of a and r_0.

Heller [14] has shown that one can take account correctly of both the Coulomb and the VP potential and still use Eq. 2–57, but with a more complicated left-hand side. The combination of the Coulomb and VP potentials is often called the electric potential. First, the scattering problem is solved taking only the electric potential, $(e^2/r) + V_{\mathrm{VP}}(r)$, and obtaining the regular solution $S_0(r)$ and the irregular solution $T_0(r)$. In analogy to Eq. 2–55, we have, for $kr \gg 1$,

$$S_0(r) \sim \cos \tau_0 F_0(kr) + \sin \tau_0 G_0(kr), \tag{2–61}$$

where τ_0 is the phase shift due to $V_{\mathrm{VP}}(r)$ with respect to the Coulomb wave functions. Next, the Schrödinger equation is solved taking both the electric and the nuclear potential $V(r)$ into account. It is now most convenient to write the radial wave function for $r > r_n$ as

$$u_E(r) \sim \cos \delta_0{}^E S_0(r) + \sin \delta_0{}^E T_0(r), \tag{2–62}$$

where the subscript E on u denotes that the nuclear problem is being solved in the presence of the electric potential. Here $\delta_0{}^E$ is the nuclear phase shift in the electric potential. When the effective-range formula (Eq. 2–57) is modified to take $V_{\mathrm{VP}}(r)$ into account, its left side becomes somewhat more complicated and also $\delta_0{}^C$ is replaced by $\delta_0{}^E$. The values of a_p, r_{0p}, and P will depend on whether one is using Eq. 2–57 and ignoring VP altogether or using the more general effective-range formula involving $\delta_0{}^E$. Heller [14] has shown that a_p and r_{0p} change only very slightly (less than 1% change in a_p) when the VP correction is incorporated. Omission of VP from the analysis, however, results in a value of P, the shape-dependent parameter, that is about 0.02 smaller than the value obtained with VP included in the analysis. This is a big change, since it is of the same order as P itself.

The other main electromagnetic effects are the interaction between the magnetic moments of the protons and the finite-size effect of the protons. The interaction of two magnetic dipoles gives rise to a potential of noncentral character which goes as r^{-3}. Since the potential is fairly long ranged, it should, in principle, be treated on the same footing as the Coulomb and VP potentials, but this has not been done. Rather, its effect is calculated by perturbation theory. Because of the finite size of the proton, both the

Coulomb potential and the magnetic interaction will be modified at short distances. These can be calculated using the charge and magnetic form factors of the proton (see Chapter 3). Details of these corrections are given by Sher et al. [12].

Using the data available for p-p scattering from 1 to 10 MeV, and including all these electromagnetic corrections, Sher et al. find for the singlet S-state

$$a_p = -7.821 \pm 0.004 \text{ fm}, \qquad r_{0p} = 2.830 \pm 0.017 \text{ fm}.$$

It would be interesting to compare these values with the corresponding ones for the singlet-S n-p and n-n interactions. However, this cannot be done directly, since the above numbers are obtained from $\delta_0{}^E$, which is the nuclear phase shift with respect to the electric functions $S_0(r)$ and $T_0(r)$, whereas in the n-p or n-n case the phase shifts are with respect to plane waves, $\sin kr$. In order to make a valid comparison, one should switch off the electric potential, $(e^2/r) + V_{\mathrm{VP}}(r)$, retaining only the nuclear part of the p-p interaction, $V(r)$. This $V(r)$ should then be used to calculate $\delta_0(k)$ with respect to plane waves, just as in n-p or n-n case. For potentials that fit the p-p data up to 350 MeV (e.g., the Hamada-Johnston and Yale potentials described in Chapter 5), this leads to $a_N = 16.8$–17.1 fm, where by a_N we denote the scattering length of two protons in the absence of the electric potential [15]. The corresponding effective range r_N changes by only about 1% from the r_{0p} value.

2-7 LOW-ENERGY NEUTRON-NEUTRON (n-n) INTERACTION

Direct n-n scattering experiments by two colliding neutron beams are extremely difficult to perform, although they are becoming feasible [16].

In the absence of direct methods, indirect means are used to get information about the n-n force. The standard method is to study nuclear reactions that produce three particles in the final state, two of which are neutrons. The spectra of the emitted particles are sensitive to the final-state interactions, and in some suitable reactions the scattering length a_n of the n-n interaction can be extracted with reasonable accuracy, although the experimental results are generally rather insensitive to the effective-range parameter.

To illustrate the method, we shall take the following reaction: $\pi^- + d \rightarrow n + n + \gamma$, which was originally suggested by Watson and Stuart [17] to study the n-n scattering length. This reaction will be discussed in some detail because it brings out clearly the physical principles involved and has been the subject of considerable work. Note that in the final state only the

two neutrons interact strongly; the third particle is a photon, whose interaction with the two neutrons is very small, being of electromagnetic character. In this sense, the reaction is a "clean" one. The major features of the experimental results are that the γ-ray yield peaks near 131 MeV (the high end of the spectrum) and the neutron yield is peaked around 2.4 MeV. The shapes of the spectra near these peaks are sensitively dependent on the n-n interaction, in particular on the n-n scattering length a_n. The peaks, both in the neutron and in the γ-ray spectrum, have a width of about 2 MeV, which must be measured accurately. We focus our attention on the neutron spectrum, since it is experimentally simpler to study 3-MeV neutrons than 130-MeV γ-rays [18].

In order to understand why these peaks are caused by the n-n interaction, consider what would happen if the two neutrons in the final state formed a bound state, which may be called a dineutron. The π^- is captured by the deuteron in its lowest Bohr orbit, so that it is essentially at rest in the laboratory frame. The π^- rest-mass is 139.58 MeV, of which 136.07 MeV is available for reaction (see Problem 2–8). Although so much energy is released, since the capture takes place at rest the initial total momentum is zero. If the dineutron could exist as a bound state, the final state would involve only two bodies, the dineutron and the photon. By applying the conservation laws of energy and linear momentum, one sees that these particles would be emitted back to back in opposite directions and, furthermore, that their energies would be unique. The dineutron would be emitted with about 4.8 MeV, and the rest of the energy would be carried by the γ-ray. However, if the two neutrons do not form a bound state, there are three particles in the final state, and the available reaction energy can be shared among them in a variety of ways, causing a spectrum in energy in the yield of the detected particle. If these three particles were noninteracting, the spectrum could be obtained from kinematical considerations alone; this is the so-called phase-space factor. However, if the two neutrons interact via a strong attractive force, there will be a tendency for them to recoil with approximately the same velocity in the same direction, causing the γ-ray to be more nearly monochromatic than if there were no n-n force. If the two neutrons were bound, the γ-ray would have been monochromatic at about 131 MeV. Now, instead, there will be a peak in the γ-ray spectrum at this energy, which is also the high-energy end point. Correspondingly, the spectrum of each neutron is peaked around 2.4 MeV. The same principle of enhancement in the cross section due to final-state interaction in three-body decays is used to detect "resonances" in elementary-particle physics [19].

To understand why these peaks should depend sensitively on the low-energy parameter a_n, we note that when the γ-ray has near-maximum energy the relative momentum of the two neutrons is very small. To show this,

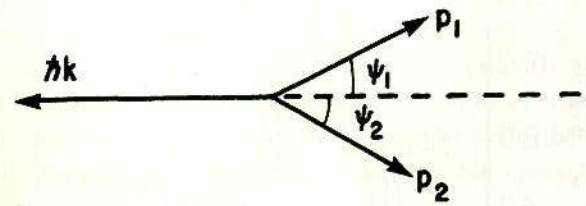

Fig. 2-8 Schematic diagram of the three-body final state in the reaction $\pi^- + d \to n + n + \gamma$. The γ-ray carries a momentum $\hbar\mathbf{k}$, while the two neutrons have momenta $\mathbf{p}_1$ and $\mathbf{p}_2$ as shown.

we denote the momenta of the two neutrons by $\mathbf{p}_1$ and $\mathbf{p}_2$ and the photon momentum by $\hbar\mathbf{k}$ (Fig. 2–8). By momentum conservation

$$\hbar\mathbf{k} = -(\mathbf{p}_1 + \mathbf{p}_2) = -\mathbf{P},$$

and by energy conservation the total energy in the final state is

$$\hbar ck + \frac{p_1^2 + p_2^2}{2M} = \hbar ck + \frac{p^2 + \frac{1}{4}\hbar^2k^2}{M} = 136.07 \text{ MeV},$$

where $\mathbf{p} = \frac{1}{2}(\mathbf{p}_1 - \mathbf{p}_2)$ is the relative momentum of the two neutrons, and $\mathbf{P} = (\mathbf{p}_1 + \mathbf{p}_2)$ is the center-of-mass momentum. Also, M is the neutron mass, and 136.07 MeV is the available reaction energy. This shows that the γ-ray energy completely determines the magnitude of the relative n-n momentum p and that k is maximum when $p = 0$. The same statement can be equivalently made for the peak of the neutron spectrum at 2.4 MeV. Consequently the neutrons near the 2.4-MeV peak have $p \approx 0$ and are recoiling in nearly the same direction, with very small scattering angles ψ_1 and ψ_2. We therefore deduce that near the neutron peak the n-n interaction can essentially be characterized by a_n alone. To show the sensitivity of the neutron spectrum to a_n, we reproduce in Fig. 2–9 the experimental histograms of Haddock et al. [20], together with the theoretical spectra for $a_n = -16$ fm and $a_n = -27$ fm.

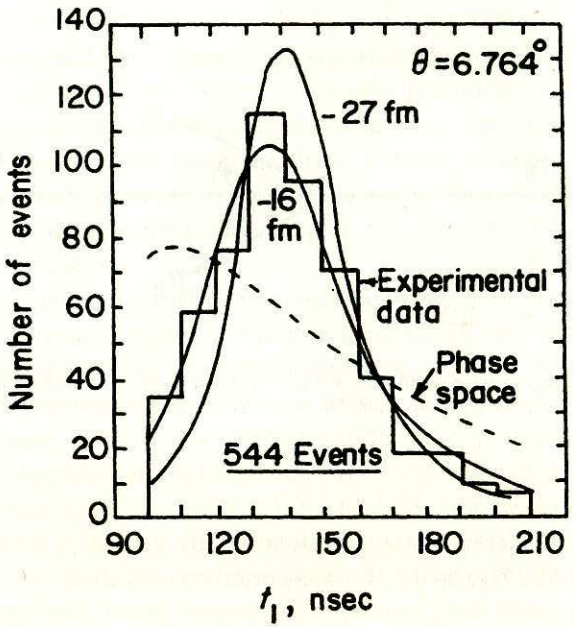

Fig. 2-9 Experimental histogram of the number of events consisting of the detection of a neutron in coincidence with another neutron at an angle of 6.764° and a γ-ray, against the time of flight (in nanoseconds) for a flight path of 118.25 in. The velocity of the neutron, and hence its energy, can be easily deduced from the flight time. Also shown are the theoretical curves for $a_n = -16$ fm and -27 fm, and the spectrum obtained from phase-space considerations alone. (After Haddock et al. [20].)

The main features of the energy dependence of the cross section of the reaction can be deduced very simply. The deuteron is a loosely bound system, the neutron and proton spending a considerable part of the time outside the range of their mutual interaction (see Section 5–1). This suggests that the rate of π^--absorption by the deuteron with subsequent γ-radiation depends essentially on the matrix element of π^--capture by a free proton, modified by the momentum distribution of the proton in the deuteron and by the final-state interaction. The transition cross section is proportional to the square of a matrix element M_s, which involves the initial-state wave functions of the pion and deuteron, the transition matrix T of π^--capture

by the proton, and the final-state wave function of the two neutrons. We are interested in finding the p-dependence of the cross section. Because the pion is essentially captured at rest by the proton (which itself has a low kinetic energy), the absorption takes place in the s-state of the π^--p system. For small relative momenta, T, the transition matrix for the capture, can be regarded as a constant. Also, since the Bohr orbit for the pion is about 50 times larger than the deuteron radius, the pionic wave function over the extent of the deuteron can be taken as a constant. Thus the p-dependence in M_s is essentially determined by the overlap of the deuteron wave function and the final-state n-n wave function in the singlet state (because $p \approx 0$, only the s-state is important, and the two neutrons can interact only in the spin singlet state). This we write as

$$M_s = \int \psi_s^*(r) r f(r)\, d^3r.$$

Here $\psi_s(r)$ is the S-state n-n wave function, and $rf(r)$ is the deuteron wave function. For simplicity, we assume zero-range n-n force. Then ψ_s is given at all values of r by its asymptotic form:

$$\psi_s(r) = \frac{\sin(pr + \delta)}{pr},$$

where $\delta(p)$ is the S-state n-n phase shift. Thus

$$M_s = \frac{\sin\delta(p)}{p}\left[\int f(r)\cos pr\, d^3r + \cot\delta \int f(r)\sin pr\, d^3r\right].$$

Note that $\cot\delta \to -(1/pa_n)$ as $p \to 0$. The spatial extent of the integrands is of the order of the deuteron radius R_d. If $pR_d \ll 1$, we can put $\sin pr \approx pr$ and $\cos pr \approx 1$. Then it is seen that the expression in the brackets is p-independent, and the p-dependence of M_s is given by $M_s = C[\sin\delta(p)/p]$, where C is independent of p. For very small p, the effective-range formula (Eq. 2–41) yields

$$\sin\delta = \frac{pa_n}{(1 + p^2a_n^2)^{1/2}}.$$

Thus the energy dependence of the cross section is given by

$$|M_s|^2\Omega(p) \propto \Omega(p)\left(\frac{1}{1 + p^2a_n^2}\right),$$

where $\Omega(p)$ is the phase-space factor and is a smooth function of p. The above

formula shows that there will be a peak in the cross section for $p = 0$, and that the character of the peak will be determined by a_n^2. The formula can be generalized to remove the approximation of zero-range n-n force, and this introduces terms linear in a_n as well as the effective range r_{0n} [21]. Actual theoretical analysis has been done in great detail by McVoy [18] and by Bander [22].

We now summarize the experimental situation. A careful study of the reaction $\pi^- + d \to n + n + \gamma$ has been made by Haddock et al. [20], who detect all three particles in coincidence. Nygren [23] has carefully analyzed their data and gives the value $a_n = -18.42 \pm 1.53$ fm, where a theoretical uncertainty of ± 1 fm is included.

The other promising method of determining a_n is the so-called comparison procedure. The idea is as follows. Reactions involving three-body final states involving two neutrons and two protons are measured and analyzed under equivalent conditions, using the same theoretical models. If one can extract a reasonable value for a_p by this indirect method, confidence can be gained in regard to the corresponding value of a_n. The α-particle spectra have been measured at small scattering angles in the reactions (1) $^3\text{He} + {}^3\text{He} \to \alpha + 2p$, (2) $^3\text{He} + {}^3\text{He} \to \alpha + n + p$, and (3) $^3\text{H} + {}^3\text{H} \to \alpha + 2n$ at a center-of-mass energy of 22.6 MeV in the final states [24]. Using a theoretical model and the known values of low-energy p-p and n-p parameters, it is possible to fit the data of reactions 1 and 2 accurately. Applying the same theoretical formalism to reaction 3, one can find values for the n-n parameters. Reference [24] gives $a_n = -17.4 \pm 1.8$ fm and the n-n effective range $r_{0n} = 2.4 \pm 1.5$ fm.

For a review of the n-n scattering length, the reader is referred to the article by Verondini [33].

2-8 CHARGE INDEPENDENCE OF NUCLEAR FORCES

Table 2–1 lists the experimentally determined low-energy parameters for n-p, p-p, and n-n forces. These data indicate that the singlet S-state nuclear forces for p-p, n-p, and n-n pairs are nearly the same, if the electric potential is removed from the p-p pair. There is a difference of about 6–7 fm between the scattering lengths a_s and a_N (or a_n), and this may seem to be a large difference. However, the scattering length is very sensitively dependent on the potential, particularly when its magnitude is large compared to the range of the nuclear force, r_n. This has been carefully investigated by Moravcsik [25]. If the scattering length changes by Δa because of a change in the potential

by ΔV, the relation between $\Delta a/a$ and $\Delta V/V$ is dependent on the shape of the potential. For a singlet-S square well of depth V (see problem 2–4),

$$\frac{\Delta a}{a} \approx -\frac{a}{r_n}\frac{\Delta V}{V}. \tag{2–63}$$

For the $^1S_0$-state, $a/r_n \approx 8$, showing that a 24% change in scattering length can be brought about by only a 3% alteration in the potential. More careful analysis by Henley [21] indicates that the n-p force is only slightly stronger (by about 2%) than the p-p force, while the n-n force is almost identical to the p-p force, all in the $^1S_0$-state. Only the n-p pair can interact in both the $^1S_0$- and the $^3S_1$-state, and no comparison of the n-p force in the $^3S_1$-state can be made.

TABLE 2-1 Low-Energy Parameters for n-p, p-p, and n-n Forces

For n-p system:

$$\left.\begin{aligned} \varepsilon &= 2.224644 \pm 0.000034 \text{ MeV} \\ a_t &= 5.425 \pm 0.0014 \text{ fm} \\ a_s &= -23.714 \pm 0.013 \text{ fm} \\ r_{0t} &= 1.749 \pm 0.008 \text{ fm} \\ r_{0s} &= 2.73 \pm 0.03 \text{ fm} \end{aligned}\right\} \quad [11]$$

For p-p system:

$$\left.\begin{aligned} a_p &= -7.821 \pm 0.004 \text{ fm} \\ r_{0p} &= 2.830 \pm 0.017 \text{ fm} \\ a_N &\approx -(16.8 - 17.1) \text{ fm} \end{aligned}\right\} \quad [12]$$

For n-n system:

$$a_n = -17.4 \pm 1.8 \text{ fm}; \quad -18.4 \pm 1.5 \text{ fm [24, 23]}$$
$$r_{0n} = 2.4 \pm 1.5 \text{ fm [24]}$$

The above observation suggests a generalized postulate of charge independence, stating that the *nuclear forces* for the p-p, n-n, and n-p pairs are identical in any given state antisymmetric in angular momentum (that is, spin-singlet, l-even, or spin-triplet, l-odd). A less general postulate is that of charge symmetry, which implies the equality of p-p and n-n nuclear forces. Before giving more experimental evidence in support of the above postulates, we shall see what charge independence means within the framework of i-spin (see the last part of Chapter 1).

Since each nucleon has i-spin $\frac{1}{2}$, a two-nucleon system can have total i-spin $T = 0$ or 1. In the notation of Chapter 1, there are four possible states, $^1(\tau)_0$, $^3(\tau)_1$, $^3(\tau)_0$, $^3(\tau)_{-1}$, where the superscript is $2T + 1$ and the

subscript is T_3. The charge-independence postulate states that the nuclear force in all three of the $T = 1$ states is the same. It turns out that the nuclear force in the $T = 0$ state is quite different from that of the $T = 1$ state. Actually, the concept of charge independence has been extended to all strong interactions and seems to hold very well. Electromagnetic forces do not obey charge independence, and therefore any test of charge independence should make corrections for this fact.

To bring out some formal aspects of charge independence, we may frame it as follows: strong interactions cannot change the total i-spin T or its third component T_3 of an interacting system, and furthermore are independent of the T_3 quantum number, that is, independent of the total charge of the system. The last part follows because, as Eq. 1–5 shows, the total charge Q of an assemblage of nucleons is given by

$$Q = \frac{A}{2} + T_3, \tag{2–64}$$

where A is the total number of nucleons. Each nucleon of course has $T = \frac{1}{2}$, and their i-spins are added vectorially to give a resultant T, T_3. If the nuclear Hamiltonian is denoted by H_N, this implies that

$$\langle T_b, T_{3b}\alpha_b|H_N|T_a, T_{3a}\alpha_a\rangle = \delta_{T_bT_a}\delta_{T_{3b}T_{3a}}M_{T_a}(\alpha_b, \alpha_a). \tag{2–65}$$

The left-hand side denotes a matrix element between two nuclear states of the various quantum numbers describing the states, T and T_3 have been shown explicitly, and α represents the set of all other quantum numbers. The important point to note is that M_{T_a} is independent of the third component of i-spin, T_3. Since the total i-spin of the system is being conserved, it follows that the total i-spin operator must be the generator of a symmetry operation under which the Hamiltonian H_N remains invariant. This is a general principle in both classical and quantum mechanics (see Goldstein [26]). For example, the conservation of orbital angular momentum implies that the Hamiltonian is invariant under rotations in configuration space, and it is the orbital-angular-momentum operator that generates these rotations. Similarly, the conservation of total i-spin T implies that H_N is invariant under rotations in a space whose axes are given by T_1, T_2, and T_3. In other words, H_N may contain only scalars in i-spin operators. For a two-nucleon system, the only possible scalar in i-spin space is $\boldsymbol{\tau}(1)\cdot\boldsymbol{\tau}(2)$. Thus the most general form of a central two-nucleon potential which is a function of the variable $r = |\boldsymbol{r}_1 - \boldsymbol{r}_2|$ only is

$$V = -[V_1(r) + V_2(r)\boldsymbol{\sigma}_1\cdot\boldsymbol{\sigma}_2 + V_3(r)\boldsymbol{\tau}_1\cdot\boldsymbol{\tau}_2 + V_4(r)(\boldsymbol{\sigma}_1\cdot\boldsymbol{\sigma}_2)(\boldsymbol{\tau}_1\cdot\boldsymbol{\tau}_2)], \tag{2–66}$$

which is actually completely equivalent to Eq. 2–17. This is so since the potential defined in Eq. 2–17 was written down without regard to the charge of the nucleons. Of course the exclusion principle requires antisymmetry under the exchange of all quantum numbers specifying two fermions, that is, $P_xP_\sigma P_\tau = -1$, and hence, as Eq. 2–15 shows, $P_H = -P_\tau$. Since $\boldsymbol{\tau}_1\cdot\boldsymbol{\tau}_2 = 2P_\tau - 1$, the formal identity of Eqs. 2–66 and 2–17 is evident.

2-9 EXPERIMENTAL EVIDENCE FOR CHARGE INDEPENDENCE AND CHARGE SYMMETRY

Charge independence manifests its consequences in a variety of areas in nuclear physics—in the nuclear spectra of complex nuclei, in nuclear reactions and their selection rules, and in radioactive transitions. The predictions of charge independence are rather clear cut, so that it is one aspect of the nuclear force which can be tested in a quantitative manner by studying light and complex nuclei. Of course it is true that in nuclei the electromagnetic forces, particularly the Coulomb force between the protons, cannot be ignored, and this violates charge independence. Since nature does not allow us to turn off the electromagnetic forces, we have to subtract their effects theoretically.

The charge-dependent effects due to the electromagnetic field are classified into two types: direct and indirect [27]. The direct effects include the n-p mass difference and the finite size of the charge and magnetic-moment distribution in the system. These involve no meson exchange between the nucleons. The indirect effects include any process in which the electromagnetic interaction modifies the nuclear force. Simple examples of these are the mass splittings between the charged and neutral mesons and the coupling-constant splitting; other examples are given in detailed accounts, for example reference [21]. Often it is possible to estimate theoretically the corrections to charge independence required by the direct electromagnetic effects in a given experiment. However, calculations of the indirect effects, violating charge independence by a few per cent, rest on the less secure theoretical basis of field theory.

The most important direct electromagnetic effect is the presence of the static Coulomb force between protons. Since the Coulomb force is of long range and varies slowly over the dimensions of a nucleus, it does not greatly alter the details of the nuclear wave function, although the Coulomb energy can be appreciable. Fortunately, this energy is not very sensitive to the wave function but is determined primarily by the nuclear radius (see Chapter 3). Thus the Coulomb energy is approximately the same for the ground state and the excited states of a nucleus, so that the relative spacings of the

energy levels are primarily determined by nuclear forces alone. This would not be true if some of the excited states were unbound, since then the wave function is so different from a bound-state one that the Coulomb energy alters appreciably.

The speculations concerning charge symmetry are confirmed when we examine nuclear spectra. First, consider a nucleus with Z protons and $Z - 1$ neutrons, and another one with $Z - 1$ protons and Z neutrons. These are called "mirror nuclei," and examples are found in the lighter varieties, for example, (^{11}B, ^{11}C), (^{13}C, ^{13}N), (^{17}O, ^{17}F). The number of n-p bonds is the same in any two mirror nuclei, but the numbers of n-n and p-p bonds in one nucleus differ from those of its mirror. Therefore, if charge symmetry is true, the spectra of mirror nuclei should be very similar. This is confirmed by Fig. 2–10, where the low-lying energy levels of ^{11}C and ^{11}B are displayed.

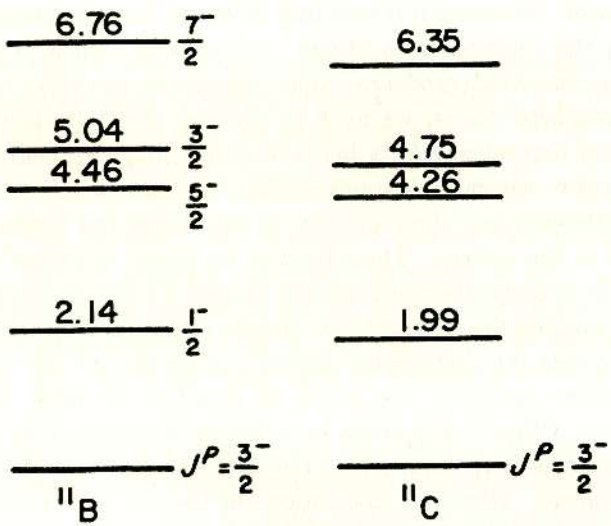

Fig. 2-10 The low-lying energy levels of mirror nuclei ^{11}B and ^{11}C (all energies in MeV). The spin and parity J^P, where known experimentally, are also shown.

A much worse example is given in Fig. 2–11, where the levels of ^{13}C and ^{13}N seem to show a large deviation from charge symmetry. The first excited states differ by more than 700 keV. Actually, the first excited state of ^{13}C is bound with respect to ^{12}C + n, whereas that of ^{13}N is unstable against proton emission, as shown in the same figure. This results in the

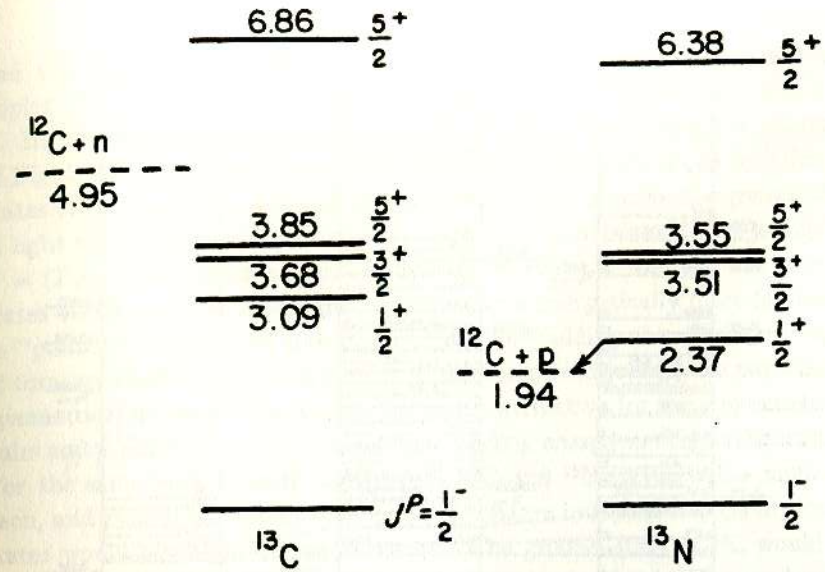

Fig. 2-11 The low-lying energy levels of mirror nuclei ^{13}C and ^{13}N (energies in MeV). The spin-parity assignments are known experimentally. Note that the 2.37-MeV state of ^{13}N is unstable against proton emission.

wave functions of the first excited states of ^{13}C and ^{13}N being vastly different, so that the respective Coulomb energy shifts with respect to the bound ground states are also very different. This type of change in the Coulomb shift due to different boundary conditions on the wave function of the nuclear surface is called the Thomas-Ehrman effect after Thomas [28] and Ehrman [29].

One consequence of i-spin conservation is the existence of the so-called isobaric multiplets. The idea arises in a simple form when strongly interacting elementary particles are considered. A meson or a baryon has a definite T, and the $2T + 1$ possible values of T_3 correspond to different charge states of the particle. These different charge states have nearly the same mass, and all quantum numbers, such as spin, parity, strangeness, and so forth are identical. The small mass differences between the members of a multiplet are believed to be of electromagnetic origin, although a fully quantitative understanding has not yet been achieved.

Similar examples are found in nuclear physics. A given nuclear state has a definite i-spin T. There are $2T + 1$ possible values of T_3 for a given T. Since the nuclear interaction is independent of T_3 (charge independent), all these $2T + 1$ states with differing T_3's but the same T, spin, and parity should be degenerate in energy. Different values of T_3 can occur only in

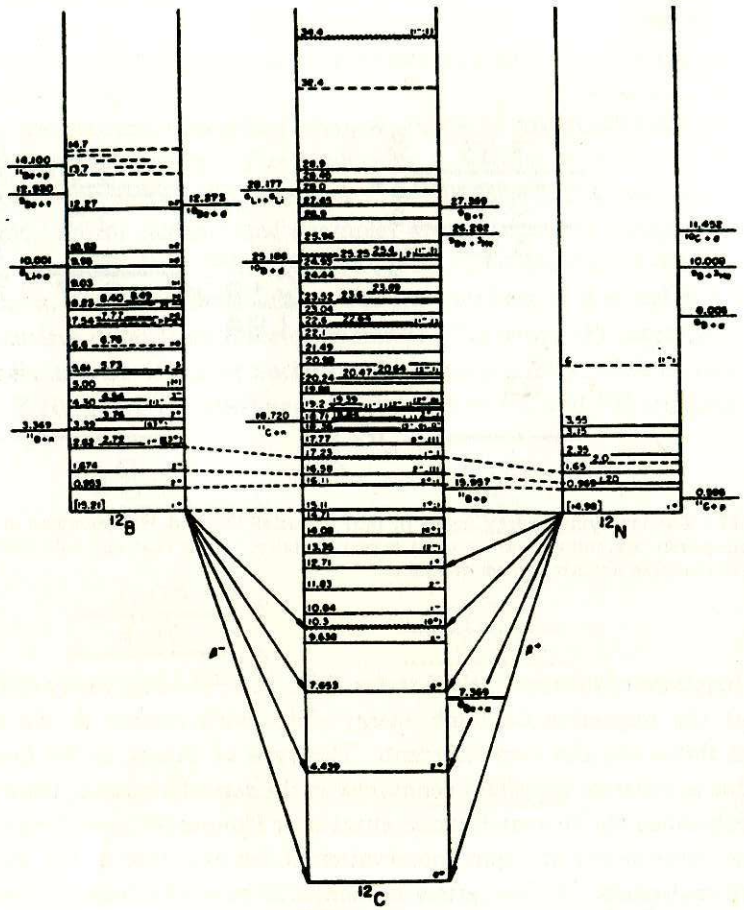

Fig. 2-12 The ground states of ^{12}B, ^{12}N, and the 1^+ excited state of ^{12}C form an i-spin triplet, while the ground state of ^{12}C is an i-spin singlet. [From F. Ajzenberg-Selove and T. Lauritsen, *Nucl. Phys.* **A114**, 1 (1968), Fig. 8.]

different nuclei, since $T_3 = \frac{1}{2}(Z - N)$. Thus each member of the degenerate multiplet comes from a different nucleus. For example, Figure 2–12 shows the ground states of ^{12}B ($T = 1, T_3 = -1$), ^{12}N ($T = 1, T_3 = 1$), and the 1^+ excited state of ^{12}C at 15.11 MeV ($T = 1, T_3 = 0$), which form an isobaric triplet. The three levels are not quite degenerate because of Coulomb effects and n-p mass differences. Another well-known example is found in ^{14}C, ^{14}N, and ^{14}O. The ground states of ^{14}C ($T = 1, T_3 = -1$) and ^{14}O ($T = 1, T_3 = 1$)

and the 2.3-MeV excited state of ^{14}N ($T = 1, T_3 = 0$) form an isobaric triplet of 0^+ states.

In passing, we shall enumerate a few general rules, using the example of Fig. 2–12. For a given nucleus, T_3 is fixed (for instance, $T_3 = -1$ for all states of ^{12}B, and $T_3 = 0$ for all states of ^{12}C). The i-spin for the *ground state* of light nuclei is generally the smallest possible T consistent with T_3, that is, $T = |T_3|$. Thus, for the ground state of ^{12}C, $T = 0$, and for the ground states of ^{12}B and ^{12}N, $T = 1$. In a nucleus, it is energetically more favorable to "pair off" nucleons to spin and i-spin zero, yielding the minimum value of total spin and i-spin. This results in the wave functions of the pairs being symmetrical in space. The nuclear forces are attractive for these symmetrical pairs and produce the state with greatest binding energy in this configuration. For the same reason, even though both ^{12}C and ^{12}B have twelve nucleons each, and even if the forces were perfectly charge independent, their ground states would not have the same energy. The ground state of ^{12}C would be lower because its i-spin, $T = 0$, is less than the i-spin of the ^{12}B ground state, which is $T = 1$.

Isobaric multiplets are found also in heavy nuclei in spite of the Coulomb effects being appreciable. These so-called isobaric analog states are best detected by nuclear reactions, and an exciting new field of research in this area has developed in the last decade.

Charge independence imposes severe selection rules on nuclear reactions, and sometimes the ratio of cross sections of two reactions can be predicted, using only this principle, and without using any dynamic knowledge. To illustrate this, we consider the reactions (1) $p + d \to {}^3\text{He} + \pi^0$ and (2) $p + d \to {}^3\text{H} + \pi^+$. The initial state in both reactions has $T = \frac{1}{2}, T_3 = \frac{1}{2}$, since the deuteron d has $T = 0$. Consequently, the final states in reactions 1 and 2 should also have $T = \frac{1}{2}, T_3 = \frac{1}{2}$. The ^{3}He nucleus has $T = \frac{1}{2}, T_3 = \frac{1}{2}$, and ^{3}H has $T = \frac{1}{2}, T_3 = -\frac{1}{2}$. The scattering amplitude (the square of which gives the cross section) depends on the overlap of the initial- and final-state wave functions with the interaction in the channel, $T = \frac{1}{2}$. To construct final-state wave functions with $T = \frac{1}{2}, T_3 = \frac{1}{2}$, we can use the vector-addition coefficients (see Eq. A–29), which couple two angular momenta. For reaction 1 this coefficient is $(\frac{1}{2}\ \ 1\ \ \frac{1}{2}\ \ 0|\frac{1}{2}\ \ \frac{1}{2})$, and for reaction 2 it is $(\frac{1}{2}\ \ 1\ \ -\frac{1}{2}\ \ 1|\frac{1}{2}\ \ \frac{1}{2})$, using the notation of Appendix A. The ratio of the cross sections of reactions 1 and 2 will be determined by the ratio of the squares of these coefficients, all other factors being the same. Thus

$$\frac{\sigma(p + d \to {}^3\text{He} + \pi^0)}{\sigma(p + d \to {}^3\text{H} + \pi^+)} = \frac{|(\frac{1}{2}\ \ 1\ \ \frac{1}{2}\ \ 0|\frac{1}{2}\ \ \frac{1}{2})|^2}{|(\frac{1}{2}\ \ 1\ \ -\frac{1}{2}\ \ 1|\frac{1}{2}\ \ \frac{1}{2})|^2} = 2.$$

Harting et al. [30] measured this ratio at 591 MeV and found it to be 2.13 ± 0.06. The difference between theory and experiment can be accounted for if one allows for the differences in the wave functions of ^{3}H and ^{3}He due to Coulomb force, and the mass difference between the final states, which causes the phase space factor to differ.

There are nuclear reactions involving more complex nuclei which test charge symmetry or charge independence. As a simple example, consider the reaction $^{16}\mathrm{O} + d \rightarrow \alpha + {}^{14}\mathrm{N}$, leading to various excited state of ^{14}N. The initial system has $T = 0$; hence finally also we should have $T = 0$. If the α-particle remains in a $T = 0$ state (more than 20 MeV is required to excite it to a $T = 1$ state), then only the $T = 0$ states of ^{14}N can be excited. The low-lying excited state of ^{14}N at 2.3 MeV which has $T = 1$ should not, therefore, be populated. Experiments by Cerny et al. [31] show this to be true; for incident deuterons of 24 MeV the yield of this state is only $0.7 \pm 0.6\%$ of the ground-state yield.

Actually, the above observation follows also from the less general postulate of charge symmetry and hence the experiment is not a real test of charge independence. To clarify this, we introduce a charge-parity operator P_{ch}, which, operating on an i-spin wave function ϕ of Z protons and N neutrons, transforms it to ϕ' with Z neutrons and N protons, that is,

$$\phi' = P_{\mathrm{ch}}\phi. \tag{2-67}$$

Obviously, $P_{\mathrm{ch}}^2 = 1$. Formally, since T_3 is being changed to $-T_3$ by this operator, it amounts to a rotation of the axes by π about the T_2-axis,

$$P_{\mathrm{ch}} = \exp(i\pi T_2). \tag{2-68}$$

For a self-conjugate nucleus ($Z = N$), ϕ' must be the same state as ϕ; therefore

$$\phi' = P_{\mathrm{ch}}\phi = p\phi, \quad \text{where} \quad p = \pm 1. \tag{2-69}$$

In the reaction $^{16}\mathrm{O} + d \rightarrow \alpha + {}^{14}\mathrm{N}$, the ground states of ^{16}O, d, and α all have $T = 0$, so that necessarily $p = 1$ for each of these. Parity being a multiplicative quantum number, it follows that only those states of ^{14}N that have $p = 1$ can be excited. Therefore the result that the 2.3-MeV state of ^{14}N is not populated can be explained by assigning to it a negative "charge parity." Conservation of charge parity only implies charge symmetry here and does not reflect on charge independence. Other tests of charge symmetry may be found in β-decay schemes, but we shall not discuss them here.

Conservation of i-spin plays a dominant role in determining the forces between strongly interacting particles. For example, the force between two nucleons can be generated by exchanging various kinds of mesons, and Fig. 2–13a shows two nucleons exchanging a pion (which is the lightest meson) to generate the longest-range interaction, called the one-pion-exchange potential (OPEP). This will be discussed at length in Chapter 5 on the two-nucleon force. The point to note here is that a single pion exchange between two nucleons is allowed by i-spin conservation, since the process $N \rightarrow N + \pi$ can go through the channel $T = \frac{1}{2}$. The Λ particle, however, being an i-spin singlet, has to change to a $T = 1$ particle on emitting a pion: $\Lambda \rightarrow \Sigma + \pi$, where Σ has $T = 1$, and the pion has also i-spin 1, so that the two can combine to give an initial i-spin of zero. Thus the longest-range force between a Λ and N is of two-pion character. This simple process is shown in Fig. 2–13b.

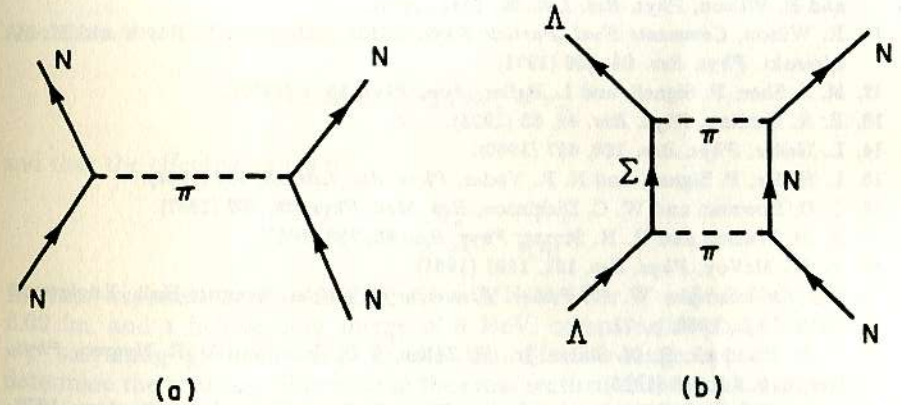

Fig. 2-13 In (a), N-N scattering is taking place via the exchange of a single pion. In (b), Λ-N scattering is displayed where two pions are exchanged. Note that the i-spin is conserved at each "vertex."

A detailed analysis of charge independence and charge symmetry in nuclear forces is available in the review article by Henley [21]. The best evidence of charge independence and charge symmetry in nuclear forces still comes from the scattering-length parameters of the p-p, n-p, and n-n forces in the $^1S_0$-state. As mentioned before, the data indicate that the n-p force is about 2% stronger than the p-p or n-n force, while the latter two are identical to within 1%, when electromagnetic corrections are made.

REFERENCES

1. D. M. Brink, *Nuclear Forces*, Pergamon Press, New York, 1965.
2. R. P. Feynman and M. Gellman, *Phys. Rev.* **109**, 193 (1958); F. C. Michel, *Phys. Rev.* **133**, B329 (1964). For a review of the subject, see the articles by B. H. McKellar, "*P*- and *T*-Violations in Nuclear Physics," and D. Hamilton, "Experimental Investigations of *P*- and *T*-Violations," in *High-Energy Physics and Nuclear Structure*, edited by S. Devons, Plenum Press, New York-London, 1970.
3. D. P. Boyd, P. F. Donovan, B. Marsh, D. E. Alburger, D. H. Wilkinson, P. Assimakopoulous, and E. Beardsworth, *Bull. Am. Phys. Soc.* **13**, 1424 (1968).
4. K. S. Krane, C. E. Olsen, J. R. Sites, and W. A. Steyert, *Phys. Rev. Lett.* **26**, 1579 (1971).
5. J. H. Bartlett, Jr., *Phys. Rev.* **49**, 102 (1936).
6. E. Majorana, *Z. Phys.* **82**, 137 (1933).
7. W. Heisenberg, *Z. Phys.* **77**, 1 (1932).
8. E. P. Wigner, *Phys. Rev.* **43**, 252; *Z. Phys.* **83**, 253 (1933).
9. T. L. Houk and R. Wilson, *Rev. Mod. Phys.* **39**, 546 (1967); Erratum, *Rev. Mod. Phys.* **40**, 672 (1968).
10. L. Koester, *Z. Phys.* **198**, 187 (1967); **203**, 515(E) (1967); T. L. Houk, D. Shambroom, and R. Wilson, *Phys. Rev. Lett.* **26**, 1581 (1971).
11. R. Wilson, *Comments Nucl. Particle Phys.* **2**, 142 (1968); H. P. Noyes and H. M. Lipinski, *Phys. Rev.* **C4**, 995 (1971).
12. M. S. Sher, P. Signell, and L. Heller, *Ann. Phys.* **58**, 1 (1970).
13. E. A. Uehling, *Phys. Rev.* **48**, 55 (1935).
14. L. Heller, *Phys. Rev.* **120**, 627 (1960).
15. L. Heller, P. Signell, and N. R. Yoder, *Phys. Rev. Lett.* **13**, 577 (1964).
16. C. D. Bowman and W. C. Dickinson, *Rev. Mod. Phys.* **39**, 592 (1967).
17. K. M. Watson and R. N. Stuart, *Phys. Rev.* **82**, 738 (1951).
18. K. W. McVoy, *Phys. Rev.* **121**, 1401 (1961).
19. See, for example, W. R. Fraser, *Elementary Particles*, Prentice-Hall, Englewood Cliffs, N.J., 1966, p. 71.
20. R. P. Haddock, R. M. Slater, Jr., M. Zeller, J. B. Czirr, and D. R. Nygren, *Phys. Rev. Lett.* **14**, 318 (1965).
21. E. M. Henley, in *Isospin in Nuclear Physics*, North-Holland, Amsterdam, 1970.
22. M. Bander, *Phys. Rev.* **134**, B1052 (1964).
23. D. R. Nygren, unpublished thesis, University of Washington, 1968.
24. E. E. Gross, E. V. Hungerford, and J. J. Manify, *Phys. Rev.* **C1**, 1365 (1970).
25. M. J. Moravcsik, *Phys. Rev.* **136**, B624 (1964).
26. H. Goldstein, *Classical Mechanics*, Addison-Wesley, Reading, Mass., 1950.
27. J. S. Leung and Y. Nogami, *Nucl. Phys.* **B7**, 527 (1968).
28. R. G. Thomas, *Phys. Rev.* **80**, 136 (1950).
29. J. B. Ehrman, *Phys. Rev.* **81**, 412 (1951).
30. D. Harting, J. C. Kluyver, A. Kusunegi, R. Rigopoulos, A. M. Sachs, G. Tibell, G. Vanderhaeger, and G. Weber, *Phys. Rev.* **119**, 1716 (1960).
31. J. Cerny, R. H. Pehl, E. Rivet, and B. G. Harvey, *Phys. Lett.* **7**, 67 (1963).
32. J. M. Blair, G. Freier, E. E. Lampi, W. Sleator, and J. H. Williams, *Phys. Rev.* **74**, 553 (1948).
33. E. Verondini, *Riv. Nuovo Cimento* **1**, 33 (1971).

PROBLEMS

2–1. Calculate v/c and λ for neutrons of the following energies: thermal, 500 keV, 5 MeV, 20 MeV, 100 MeV, 400 MeV. Comment on the significance of these values for (a) nucleon-nucleon scattering, (b) study of stable nuclei, and (c) neutron-nucleus reactions.

2–2. Suppose that n-p scattering is studied by scattering neutrons from a nylon target. Explain how you would correct for the presence of carbon and oxygen.

2–3. Consider a square well of radius r_n and depth of potential V. Show that, if two types of particles of equal mass M interact by means of this potential, and if particles of one type are initially at rest and are bombarded by a beam of particles of the other type, with energy $2E$, the scattering phase shift δ for the S-wave is given by

$$k \cot \delta = \frac{\sqrt{k^2 + K^2} + k \tan kr_n \tan \sqrt{k^2 + K^2}\, r_n}{\tan \sqrt{k^2 + K^2}\, r_n - \sqrt{1 + (K^2/k^2)} \tan kr_n}. \tag{1}$$

Also show that the scattering length is

$$a = -\frac{1}{K} \tan Kr_n + r_n,$$

and that the effective range is

$$r_0 = r_n - \frac{1}{3}\frac{r_n^3}{a^2} - \frac{1}{K^2 a}.$$

In these expressions, $k^2 = ME/\hbar^2$, $K^2 = MV/\hbar^2$. For $V = 36.2$ MeV, $r_n = 2.02$ fm, and a bombarding energy of 6 MeV, compare the phase shift for n-p scattering given by Eq. 1 with the effective-range expression and determine the resulting difference in the cross section. How would you know experimentally whether waves of angular momentum > 0 were important?

2–4. In Problem 2–3, it is shown for a square-well potential that the scattering length is

$$a = -\frac{1}{K} \tan Kr_n + r_n.$$

For a potential in the $^1S_0$-state, the quantity Kr_n is only very slightly less than $\pi/2$. Using this fact, show that, if the scattering length a changes by Δa because of a change in the depth of the potential by ΔV, then

$$\frac{\Delta a}{a} \approx -\frac{\pi^2}{8}\left(\frac{a}{r_n}\right)\frac{\Delta V}{V},$$

which is essentially Eq. 2–63 of the text.

2–5. Suppose that the central potential between nucleons in the singlet S-state is known. Denote it by ${}^1V^s(r)$. Assume similarly that the following potentials are known: ${}^1V^p$, ${}^3V^s$, ${}^3V^p$. Find expressions for the Wigner, Bartlett, Majorana, and Heisenberg potentials in terms of the four V's listed above.

2–6. Imagine two nucleons interacting only in the S-state by a hard-core potential of radius r_c:

$$V(r) = \infty \quad \text{for} \quad r \leqslant r_c,$$
$$= 0 \quad \text{for} \quad r > r_c.$$

Show that the s-wave phase shift is given by $\delta(k) = -kr_c$. Hence show that the scattering length a and the effective range r_0 are given by

$$a = r_c, \qquad r_0 = \tfrac{2}{3}r_c.$$

Verify the answer for r_0 by using Eq. 2–43 of the text.

2–7. As is stated in the text, in elastic scattering the outgoing flux of particles must equal the incoming flux, with the result that the phase shift $\delta(k)$ is real. This implies that the scattering "matrix" $S(k) = \exp[2i\,\delta(k)]$ is unitary, that is,

$$S^*(k) = \frac{1}{S(k)} \quad \text{for real } k.$$

One of the simplest forms of the S-matrix obeying unitarity is a rational function of k,

$$S(k) = \left(\frac{k + i\beta}{k - i\beta}\right)\cdot\left(\frac{k - i\alpha}{k + i\alpha}\right),$$

where we assume α and β to be real and positive. Show that for such a case the effective-range expression (Eq. 2–41) is exactly satisfied for all values of k, with

$$a = -\frac{\beta - \alpha}{\alpha\beta}, \qquad r_0 = \frac{2}{\beta - \alpha}.$$

Assuming that $a = -23.7$ fm and $r_0 = 2.7$ fm, find α and β. A potential that exactly reproduces this scattering matrix for all real k is the Bargmann potential [V. Bargmann, *Rev. Mod. Phys.* **21**, 488 (1949)], given by

$$V(r) = 2\beta^2(\alpha^2 - \beta^2)(\beta \cosh \beta r + \alpha \sinh \beta r)^{-2},$$

which asymptotically behaves as $\exp(-2\beta r)$.

2–8. (a) In the reaction

$$\pi^- + d \to n + n + \gamma,$$

show that the available energy for the reaction is 136.07 MeV.

(b) Consider the reaction

$$\pi^- + d \to n + n.$$

Assume that the capture of the pion taken place from the s-orbit of the π-mesic atom, and that the spin parity associated with the deuteron is 1^+. Noting that the spin of the pion is zero, prove that the parity associated with it is negative.

2–9. (a) The Λ particle has spin $\frac{1}{2}$, i-spin 0, and charge 0. It decays by weak interactions

$$\text{(A)} \quad \Lambda \to p + \pi^-, \qquad \text{(B)} \quad \Lambda \to n + \pi^0.$$

Charge and angular momentum are conserved in the decay, but the total i-spin T changes by $\frac{1}{2}$. Using the i-spin formalism, find the ratio of protons to neutrons observed in the decay.

(b) Consider the following strong interactions:

$$\text{(C)} \quad \pi^- + p \to K^0 + \Lambda, \qquad \text{(D)} \quad \pi^0 + n \to K^0 + \Lambda.$$

In these reactions, i-spin T and its third component T_3 are conserved. What are the possible values for the i-spin of K^0 for reactions C and D to go? Calculate $\sigma(\pi^- + p \to K^0 + \Lambda)/\sigma(\pi^0 + n \to K^0 + \Lambda)$ for each of these possible values. Knowing the ratio experimentally to be 2, can you predict the i-spin of K^0?

Hint: The i-spin wave functions needed are the following:

$$|\pi^- p\rangle = \sqrt{\tfrac{1}{3}}\,|\tfrac{3}{2}, -\tfrac{1}{2}\rangle - \sqrt{\tfrac{2}{3}}\,|\tfrac{1}{2}, -\tfrac{1}{2}\rangle,$$
$$|\pi^0 n\rangle = \sqrt{\tfrac{2}{3}}\,|\tfrac{3}{2}, -\tfrac{1}{2}\rangle + \sqrt{\tfrac{1}{3}}\,|\tfrac{1}{2}, -\tfrac{1}{2}\rangle.$$

Chapter 3

Nuclear Moments and Nuclear Shapes

3-1 ELECTROMAGNETIC MULTIPOLES

We now examine electromagnetic effects in which the nucleus interacts with electromagnetic systems separated from it by distances that are large on the nuclear scale. In such cases, it is desirable to think of the interaction of fields rather than particles. It is shown in works on electromagnetism that the external effects of any distribution of charges and currents (e.g., a nucleus) can be expressed in terms of a series of "multipole moments." In many instances only a few multipoles of the lower orders need be considered, and it is this feature that makes the use of the series convenient. The simplification depends on two conditions: (1) the velocity of the nuclear particles must be small compared with the speed of light, and (2) the fractional change of the applied field across the nucleus must be small. Clearly, to obtain information about the undisturbed nucleus, a third condition is necessary, namely, the applied field must not be so strong as to change appreciably the arrangement of charges and currents in the nucleus. For example, we must watch for possible polarization of nuclear charges in strong electric fields.

The energy of interaction between an applied electromagnetic field and a charge-current system can be written as

$$H_{\text{el}} = q\phi_0 - \mathbf{P}\cdot\mathbf{E}_0 - \mathbf{M}\cdot\mathbf{H}_0 - \frac{1}{6}\sum_{ij} Q_{ij}\left(\frac{\partial E_j}{\partial x_i}\right)_0 - \cdots, \tag{3-1}$$

where $\mathbf{E}$ and $\mathbf{H}$ are the applied electric and magnetic fields, and ϕ is the electrostatic potential of the applied field. The subscript 0 indicates that the

quantity in question is to be evaluated at the origin of coordinates, which is taken at some convenient point in the charge-current system (say the center of the nucleus in our case). The symbol q denotes the total charge of the system, $\mathbf{P}$ is the electric dipole vector, $\mathbf{M}$ is the magnetic dipole vector, and Q_{ik} is the electric quadrupole tensor. For a charge density ρ and current density $\mathbf{J}$, the explicit expressions are:

$$q = \int \rho\, dV, \tag{3-2a}$$

$$\mathbf{P} = \int \rho\mathbf{r}\, dV, \tag{3-2b}$$

$$\mathbf{M} = \tfrac{1}{2}\int \mathbf{r}\times\mathbf{J}\, dV, \tag{3-2c}$$

$$Q_{ik} = \int \rho(3x_i x_k - \delta_{ik} r^2)\, dV. \tag{3-2d}$$

In quantum mechanics the energy H_{el} becomes an operator, as do the various multipole moments. Expression 3-1 is actually an infinite series of terms of increasing multipole order. It will be observed that the values of the quantities defined in Eqs. 3-2 depend only on the radial and angular distributions of charge and current in the nucleus. Conversely, a knowledge of these multipoles gives information about the size, shape, density, and motion of the matter in nuclei.

Equation 3-1 shows that we may learn experimentally the values of the multipoles either by observing energy shifts due to the interaction of the nucleus with atomic or molecular fields, or by applying an external field of a chosen type. The latter methods are, in general, more accurate since the fields are better known. It is particularly difficult to obtain accurate values of the electric quadrupole from the energies of lines in atomic and molecular spectra, since one is required to know the value, at the nucleus, of the gradient of the electric field of the atomic or molecular electrons, a quantity which is difficult to calculate and is very sensitive to details of the electronic configuration. Experimental methods of measuring nuclear moments are described in a number of books, for example, Ramsey's *Nuclear Moments* [1].

Although the fundamental definition of $\mathbf{M}$ expresses the magnetic dipole vector in terms of the current density $\mathbf{J}$, an alternative form is very important. If $\mathbf{J}$ is produced by an electric charge of density ρ moving with

velocity $\mathbf{v}$, then $\mathbf{J} = \rho\mathbf{v}/c$.† If the charge density is actually composed of particles of charge e and mass M, the angular-momentum density is $\mathbf{L} = (M\rho/e)(\mathbf{r} \times \mathbf{v})$, and we can write

$$\mathbf{M} = \frac{1}{2}\frac{e}{Mc}\int \mathbf{L}\, dV. \tag{3-3a}$$

For Z protons moving in a nucleus, the quantal analog is

$$\mathbf{M}_{\text{orb}} = \frac{1}{2}\frac{e\hbar}{Mc}\int \psi^* \sum_1^Z \mathbf{l}_k \psi\, dV, \tag{3-3b}$$

where $\mathbf{l}_k$ is the angular-momentum operator (divided by $\hbar$) of the kth proton, ψ is the nuclear wave function, and the subscript "orb" is used with $\mathbf{M}$ to stress the fact that this magnetic moment is due to the orbital angular momentum. It will be seen from Eq. 3–3 that, when all particles have the same ratio of charge to mass, the magnetic dipole is parallel to the total angular momentum with which it is associated. The orbital magnetic dipole operator is

$$\mathbf{M}_{\text{orb}} = \mu_0 \sum_{\text{protons}} \mathbf{l}_k, \tag{3-4a}$$

where μ_0 is the nuclear magneton $e\hbar/2m_pc$. In addition to the orbital magnetic moment of the protons, there is the spin magnetic moment of each nucleon,

$$\mathbf{M}_{\text{spin}} = \mu_0 \sum g_k \mathbf{s}_k, \tag{3-4b}$$

where $g = 5.5856$ for protons and -3.8263 for neutrons (see Chapter 1). The close connection of magnetic moment and angular momentum requires that we now survey the angular momenta of nuclei.

3-2 ANGULAR MOMENTUM

The total angular momentum of a nucleus is the vector sum of the angular momenta of the constituent nucleons, which in turn consist of both orbital angular momenta due to the motion about the center of the nucleus and of the intrinsic spin angular momentum of $\frac{1}{2}\hbar$ per nucleon. We shall use capital letters to refer to angular momenta associated with the whole nucleus and lower-case letters to denote those of individual nucleons. We measure all angular momenta in units of $\hbar$. If $\mathbf{l}_k$ is the orbital angular momentum of nucleon k and $\mathbf{s}_k$ is its spin vector, we define

† The factor c is due to the use of Gaussian units.

$$\mathbf{j}_k = \mathbf{l}_k + \mathbf{s}_k = \mathbf{l}_k + \tfrac{1}{2}\boldsymbol{\sigma}_k,$$

$$\mathbf{L} = \sum_k \mathbf{l}_k, \quad \mathbf{S} = \sum_k \mathbf{s}_k,$$

$$\mathbf{J} = \sum \mathbf{j}_k = \mathbf{L} + \mathbf{S}. \tag{3-5}$$

It should be realized that the only vector mentioned which is necessarily a constant of motion is $\mathbf{J}$, the total angular momentum of the whole nucleus; the eigenvalue of J^2 is $J(J+1)$, with similar notation for the other vectors when applicable. Also, the eigenvalue of J_z is written as M, and corresponding quantities (when they exist) are m_k, m_{l_k}, m_{s_k} $(= \pm\frac{1}{2})$, m_{σ_k} $(= \pm 1)$, m_L, m_S. The quantum number J is often referred to rather loosely as the "spin" of the nucleus.

Experimentally, it is found that all nuclei have relatively low spins in their ground states. Although all constituent nucleons have angular momenta of at least $\frac{1}{2}\hbar$, the highest confirmed value of J is 6, which occurs in the ground state of ^{50}V. This indicates that the motion of the nucleons and the orientation of their spins are such that most of the angular-momentum vectors cancel each other. Indeed, with no known exception the ground states of nuclides with even Z and even N have zero spin, a fact which suggests the even stronger rule that the nucleon angular momenta cancel in pairs for each type of nucleon. In this case, we might expect that the total angular momentum of an odd-A nuclide would be just that of the last unpaired particle, and that in an odd-odd nuclide only the last proton and last neutron would contribute to $\mathbf{J}$. This provides a very natural explanation of the low values of $\mathbf{J}$ which exist.

Although the facts do not require us to adopt such an extreme degree of pairing of nucleons in order to obtain cancellation of their $\mathbf{j}$-vectors, it is clear that in any reasonable model of nuclear forces cancellation will occur, since any marked difference is unlikely between the energies of nucleons with different orientations of $\mathbf{j}$, that is, different m, but with all other quantum numbers the same. Hence for each set of quantum numbers (including a specific j), we expect to find in the ground state of lowest energy one nucleon with each of the $(2j+1)$-values of m. Of course, only one proton and one neutron can have the same m-value because of the exclusion principle. Now $2j+1$ particles of the same j have a resultant angular momentum of zero. Contributions to $\mathbf{J}$ would come only from the last few particles, which are insufficient in number $(< 2j+1)$ to provide complete cancellation for the value of j to which they belong. This picture does not necessarily imply that all even-even nuclides have spin zero, since if there are, for

example, two protons with the same j, they need not have opposite values of m in order to minimize the energy. Consequently the low actual values of J do suggest more than the minimum amount of angular-momentum cancellation. They also suggest that the j-values of individual nucleons may be constants of motions, an assumption which is implicit in the above argument.

The idea that individual nucleons have a constant angular momentum implies that each nucleon essentially follows a prescribed orbit and does not exchange angular momentum in encounters with other nucleons. In fact, this assumption appears to ignore the nucleon's interaction with other nucleons. The strength and range of the nucleon-nucleon forces might lead one to expect that this is a poor approximation, since collisions should be frequent and a constant value of j most improbable. Nevertheless, it is possible to understand a number of fundamental nuclear properties in terms of a very simple model in which the effects of the nuclear forces are represented only by confining the nucleons in a volume of nuclear dimensions, and all direct nucleon-nucleon interaction is ignored. The reconciliation of this model with the strong nuclear force will be considered in Part II; for the present we shall merely employ the model on a heuristic basis.

3-3 ELECTRIC MOMENTS

The term in the expansion 3–1 of H_{el} which involves the electric multipole of order λ can be expressed in terms of the so-called *electric 2^λ-pole moment operator*, defined by

$$Q_\lambda = e\sum_{k=1}^{Z} r_k{}^\lambda Y_\lambda{}^0(\theta_k), \tag{3–6}$$

where (r_k, θ_k, ϕ_k) are the coordinates of the kth proton, and $Y_\lambda{}^0$ is a spherical harmonic of order λ. For $\lambda = 2$ it can be shown [1] that the quantal operator for the electric quadrupole tensor is

$$Q_{ij} = \frac{Q}{J(2J-1)}[\tfrac{3}{2}(J_iJ_j + J_jJ_i) - \delta_{ij}\mathbf{J}^2], \tag{3–7a}$$

where J_i $(i = 1, 2, 3)$ are the components of $\mathbf{J}$, and

$$Q = \left(\frac{16\pi}{5}\right)^{1/2}\langle Q_2\rangle_{M=J} = \left(\frac{16\pi}{5}\right)^{1/2}\int \Psi^*_{J,J}Q_2\Psi_{J,J}\,dV. \tag{3–7b}$$

Thus the interaction energy H_{el} can be written in terms of Q; similar results hold for higher multipoles.

It will be observed that

$$\begin{aligned} Q_2 &= e\sqrt{\frac{5}{4\pi}}\sum r_k{}^2P_2(\theta_k) \\ &= e\sqrt{\frac{5}{16\pi}}\sum(3z_k{}^2 - r_k{}^2) = \sqrt{\frac{5}{16\pi}}\,Q_{33}, \end{aligned} \tag{3–8}$$

and that Q is the expectation value of Q_{33} in the state in which the z-component of $\mathbf{J}$ has its maximum value J. The quantity Q is also called the *electric quadrupole moment*, although it differs from $\langle Q_2\rangle$ by a numerical factor. There is no logical need to introduce Q instead of $\langle Q_2\rangle$, but this is done since it is the quantity Q which is conventionally quoted in experimental results.† Its units are charge times area and are usually written e cm^2 or e b.

We may note that any system with a definite parity cannot have static electric poles of odd order, since the Legendre polynomials of odd order are odd functions of z, whereas $|\psi|^2$ is an even function of (x, y, z) if ψ has definite parity. Hence the integral for the multipole moment $\int|\psi|^2Q_\lambda\,dV$ has an odd integrand and is zero. In particular, nuclei cannot have electric dipole moments, and, apart from the term $q\phi_0$, the quadrupole is the lowest order of interaction with an external electric field.‡ There are also restrictions on the angular momentum of a nucleus if it is to have a multipole of given order. Since $P_\lambda(\theta_k)$ is the mathematical form of a wave function of angular momentum λ, and since wave functions of different angular momenta are orthogonal, the factor $\psi^*\psi$ in the integral $\int\psi^*_{J,J}\psi_{J,J}Q_\lambda\,dV$ must have a term corresponding to an angular momentum λ. Also, $\psi_{J,J}$ describes a state of angular momentum J, and the product $\psi^*\psi$ therefore describes states in which two angular-momentum vectors of the same J are added. The possible resultants are all angular momenta $\leqslant 2J$. Consequently, for an electric 2^λ-pole moment to exist, J must be at least $\frac{1}{2}\lambda$. In particular, nuclides of spin 0 or $\frac{1}{2}$ cannot possess static electric quadrupole moments. (The adjective *static* has been introduced to emphasize that we are not discussing the multipole orders which can play a role in γ-radiation from nuclei. These are not so restricted.)

† The reader should be warned that even this usage is not without exceptions in the literature.

‡ It is sometimes argued that the experimental absence of electric dipole moments of nuclei and also of nucleons shows that the states are of definite parity to a very good approximation. However, it can be demonstrated that odd electric moments must vanish if our theories are invariant under time reversal only, without any assumption about parity.

The existence of a quadrupole moment means that the charge distribution is not spherically symmetric. This can be seen from Eq. 3–7b, which is zero unless the density $\psi^*\psi$ has an angular dependent term proportional to $P_2(\theta)$. Less formally, the situation may be illustrated by considering a charge uniformly distributed throughout an ellipsoid while ignoring the fact that charge is actually on the individual protons. Let us call the axis of the ellipsoid the z'-axis, let this axis have length $2a$, and let b be the other semiaxis. Then the charge density is

$$e\rho = \frac{Ze}{V} = \frac{3Ze}{4\pi ab^2}.$$

In analogy with Eqs. 3–8 and 3–2d, we define quadrupole moments with respect to the z'-axis by

$$\langle Q_2' \rangle = \sqrt{\frac{5}{16\pi}}\langle Q_{33}' \rangle = \sqrt{\frac{5}{16\pi}}\int e\rho(3z'^2 - r^2)\,dV$$

$$= \frac{Ze}{\sqrt{20\pi}}(a^2 - b^2) = \frac{3Ze}{4\pi}\sigma a^2, \tag{3–9}$$

where we have introduced as a measure of ellipticity the parameter

$$\sigma = \frac{1}{3}\sqrt{\frac{4\pi}{5}}\frac{a^2 - b^2}{a^2}. \tag{3–10}$$

(The numerical factors will be seen to be convenient later.) If σ is small so that a and b are not very different, it is convenient to define a mean radius by

$$R_0^3 = ab^2, \tag{3–11}$$

so that a sphere of radius R_0 has the same volume as the ellipsoid. Then

$$Q' = \sqrt{\frac{16\pi}{5}}\int \langle Q_2' \rangle = \frac{3Ze}{\sqrt{5\pi}}R_0^2\sigma\left(1 - 3\sqrt{\frac{5}{4\pi}}\sigma\right)^{-2/3}. \tag{3–12}$$

If we take a z-axis making an angle Θ with a z'-axis (not necessarily a symmetry axis) as in Fig. 3–1, it is not difficult to see that the quadrupole moment with respect to this axis is

$$\langle Q_2 \rangle_\Theta = \sqrt{\frac{5}{16\pi}}\int e\rho(3z^2 - r^2)\,dV = \tfrac{1}{2}(3\cos^2\Theta - 1)\langle Q_2' \rangle. \tag{3–13}$$

Equation 3–13 shows that the largest value of $\langle Q_2 \rangle_\Theta$ occurs when Θ is as

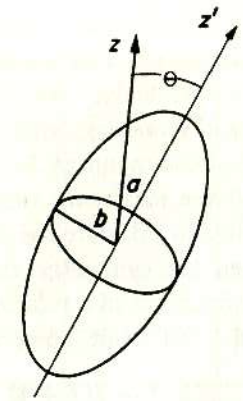

Fig. 3-1 The quadrupole moment of a spheroid.

small as possible. Classically of course it can be zero, but quantally the maximum value of $\cos\Theta$ is determined by the angular-momentum properties.

If Q' is the intrinsic moment *with respect to the spin direction*, the z'-axis is in the direction of **J**, and this maximum, which occurs when $M = J$, is

$$\cos\Theta = \frac{J}{\sqrt{J(J+1)}}.$$

It follows from Eq. 3–13 that

$$Q = \sqrt{\frac{16\pi}{5}}\langle Q_2 \rangle_{M=J} = \frac{2J-1}{2(J+1)}Q'. \tag{3–14}$$

It is now clear why the quantity Q is defined as the moment in the state $M = J$; it is the maximum observable quadrupole moment. We can think of Q' as the intrinsic quadrupole moment of the system with respect to its spin axis, but since the uncertainty principle prevents the exact location of the angular-momentum vector, only a fraction of Q' is effectively in interaction with an applied field. Indeed we see that, for $J = \frac{1}{2}$, the extent to which the vector **J** can be aligned with the z-axis is so slight that $Q = 0$. This is the "physical" reason behind the general theorem that $Q = 0$ unless $J \geqslant 1$. We note that this implies, not that nuclei with spins 0 and $\frac{1}{2}$ are spherical, but simply that their asymmetry does not show up in static electric quadrupole interactions.

If we think of the nucleus as an ellipsoid of fixed shape, rotating in space, the angular momentum **J** will have a fixed value, called K, for its component along the axis of symmetry. This is a general result in the classical mechanics of the motion of a rigid body. We can connect the quadrupole moment Q', *referred to the axis of symmetry*, with Q, referred to an axis fixed in space, along which **J** has the component $M = J$. In this case, **J** can coincide with neither axis, and the maximum value of K is J. In order to use Eq. 3–13, it must be possible to calculate the expectation value of $\cos^2\Theta$, where Θ is the angle between the symmetry axis and the axis in space. To do this, we need the wave functions of a rotating ellipsoid, which we shall not encounter until Chapter 8. The result, however, is

$$Q = Q'\frac{3K^2 - J(J+1)}{(J+1)(2J+3)}, \tag{3–15}$$

or, for $K = J$,

$$Q = Q'\frac{J(2J-1)}{(J+1)(2J+3)}. \tag{3–16}$$

Figure 3–2 shows experimental values of quadrupole moments, plotted as

$$\frac{\sqrt{5\pi}}{3}\frac{Q}{ZeR_0^2}\frac{(J+1)(2J+3)}{J(2J-1)}.$$

This ordinate provides a measure of the asymmetry parameter σ, according to Eq. 3–12, in cases where it is reasonable to think of the nucleus as an ellipsoid. For odd proton nuclides the abscissa is Z, for odd neutron nuclides it is N, and for even-even nuclides it is Z. For even-even nuclides and some others, Q' is obtained from Coulomb-excitation cross sections. The curve is drawn in Fig. 3–2 merely to show the trend of the data. Numbers for which nuclei are spherical are listed.

The assumption of an ellipsoidal charge distribution should be contrasted with the simpler picture already suggested in connection with nuclear spins in which particles in the nucleus are paired so that all the particles of a given j constitute a spherically symmetric distribution and the nuclear spin is the angular momentum of the last particle. It can be seen (Problem 3–2) that the quadrupole moment due to a single proton is

$$Q_{sp} = -e\frac{2J-1}{2(J+1)}\langle r^2\rangle, \tag{3–17a}$$

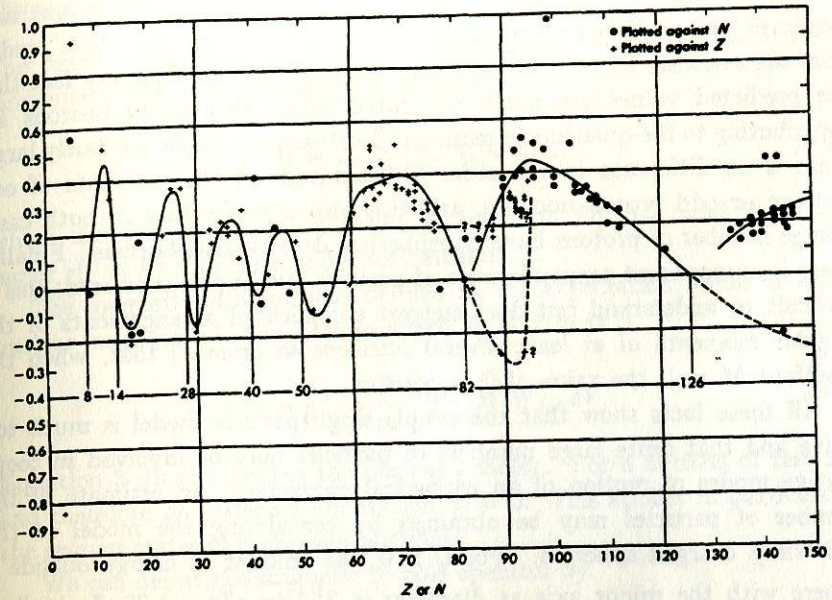

Fig. 3-2 Experimental values of electric quadrupole moments plotted to show the nuclear asymmetry.

where $\langle r^2\rangle$ is the mean-square distance of the proton from the center of the nucleus. For an odd neutron nucleus, there is a quadrupole moment due to the recoil motion of the rest of the nucleus, which is a charge Z at a distance r_n/A from the center of mass. Hence

$$Q_{sn} = \frac{Z}{A^2}Q_{sp}. \tag{3–17b}$$

In these formulas the value $\langle r^2\rangle$ will be somewhat less than the square of the nuclear radius. Consequently, if this model were valid, values of Q for odd proton nuclides would increase like $A^{2/3}$ and would range from $\sim 10^{-26}$ to $\sim 5 \times 10^{-25}\ e\ \text{cm}^2$; for single-neutron nuclei, the values would behave roughly like $A^{-1/3}$ and would lie between 10^{-28} and $10^{-26}\ e\ \text{cm}^2$. These results would imply that the ordinate in Fig. 3–2 would have the value

$$\left(\frac{2J-3}{2J}\right)\left(\frac{\langle r^2\rangle}{R_0^2}\right)\left(\frac{\sqrt{5\pi}}{3}\right)\left(\frac{1}{Z}\right) \sim \frac{1}{Z}$$

for odd proton nuclides and a value $\sim 1/A^2$ for odd neutron nuclides. Moreover, the predicted signs are all negative. It is clear that these predictions are seriously at variance with the observed values. The very fact that the predicted values are much too small shows that many protons are contributing to the quadrupole moment. Furthermore, when Q is fairly large, there is no difference in the order of magnitude of the moments of odd neutron or odd proton nuclides, and this also suggests that in both cases a large number of protons have nonspherical density distributions. Finally, there is an apparent preponderance of positive quadrupole moments; this is difficult to understand but does suggest complicated arrangements of the angular momenta of at least several nucleons so oriented that, when the resultant $M = J$, the value of Q is positive.

All these facts show that the simple single-particle model is much too naive and that quite large numbers of particles may be involved in cooperative modes of motion of an aspherical character. An estimate of the number of particles may be obtained by considering the model of the uniformly charged spheroid. For $Q > 0$, the amount of charge outside a sphere with the minor axis as diameter is $3\sqrt{5/4\pi}\,\sigma Ze = 1.89\sigma Ze$ to first order in σ. In agreement with the results for spherical nuclei, there will be some reduction of density near the edges of the nucleus, and this means that the actual value of distortion is somewhat greater than the value of σ indicated in Fig. 3–2. These values of σ are already appreciable, and it therefore appears that in many nuclei a large number of nucleons cooperate to produce a spheroidal density distribution.

Another striking feature of the graph of Q is the occurrence of zeros for certain nucleon numbers. From high positive values, Q falls through zero to small negative values not inconsistent with the single-particle value and then rises again rather abruptly to positive values. The zeros on the falling branches of the graph of Q occur for nuclides with values of Z or $N = 8, 16, 20, 28, 38, 50, 82, 126$. Nuclei with these values of Z or N are spherical, and if one or two nucleons are added, the spherical core is apparently not greatly distorted; but as the number of extra nucleons is increased, it seems that the nucleus takes on a spheroidal shape. We shall see that certain other nuclear properties have discontinuities at some of the same nucleon numbers; a fuller discussion and understanding of the behavior of Q will be possible after we have explained some less naive nuclear models. In the meantime let us note that a satisfactory model must include both the apparent single-particle behavior evident in the values of angular momentum and the collective motion implied by the large distortions of nuclei.

3-4 MAGNETIC MOMENTS

The magnetic-moment operator of a nucleus due to the orbital and spin moments of the nucleons can be written as

$$\mathbf{M} = \mu_0 \sum_{k=1}^{A} (g_k^{(l)} \mathbf{l}_k + g_k \mathbf{s}_k), \tag{3–18}$$

where the spin gyromagnetic ratios g_k are as in Eq. 3–4, and the orbital factor $g^{(l)}$ is 1 for protons and 0 for neutrons.

The magnetic moment μ is defined as the expectation value of M_Z in nuclear magnetons in the state in which $J_Z = J$, that is,

$$\mu = gJ = \frac{1}{\mu_0} \int \Psi_{J,J}^* M_Z \Psi_{J,J}\, dV. \tag{3–19}$$

Equation 3–19 also defines the nuclear g-factor. For a nucleus of zero spin and therefore no preferred orientation, $\mu = 0$. This applies in particular to the ground states of even-even nuclides.

We can define the magnetic 2^λ-pole operator by

$$M_\lambda = \mu_0 \sum_{k=1}^{A} [\nabla r_k^\lambda P_\lambda(\theta_k)] \cdot \left[g_k^{(l)} \frac{2}{\lambda+1} \mathbf{l}_k + g_k \mathbf{s}_k \right]. \tag{3–20}$$

The magnetic moment is the special case $\lambda = 1$, namely, $\mu = (1/\mu_0)\langle M_1 \rangle_{M=J}$. The magnetic octupole moment $\langle M_3 \rangle_{M=J}$ has been measured in a few instances [2], but experimental accuracy has not yet proved sufficient to detect any higher magnetic multipoles.

In the extreme single-particle model, the angular momenta and hence the magnetic moments of nucleons cancel in pairs, and the magnetic moment of the nucleus is then simply that of the last odd nucleon. The value depends on whether $J = j = l + \frac{1}{2}$ or $l - \frac{1}{2}$, and it is not difficult (Problem 3–3) to see that the results are

$$j = l + \tfrac{1}{2}: \quad \mu = (j - \tfrac{1}{2}) g^{(l)} + \mu_{n,p}, \tag{3–21a}$$

$$j = l - \tfrac{1}{2}: \quad \mu = \frac{j}{j+1} \left[\left(j + \frac{3}{2} \right) g^{(l)} - \mu_{n,p} \right], \tag{3–21b}$$

where $\mu_{n,p}$ is the free magnetic moment of the odd nucleon ($\mu_{n,p} = \frac{1}{2} g_{n,p}$). These values of the magnetic moment for a given j are referred to as the Schmidt limits [3].

Figures 3–3 and 3–4 show the measured values of the magnetic moment as a function of J for odd-A nuclei. The solid lines on the diagrams are

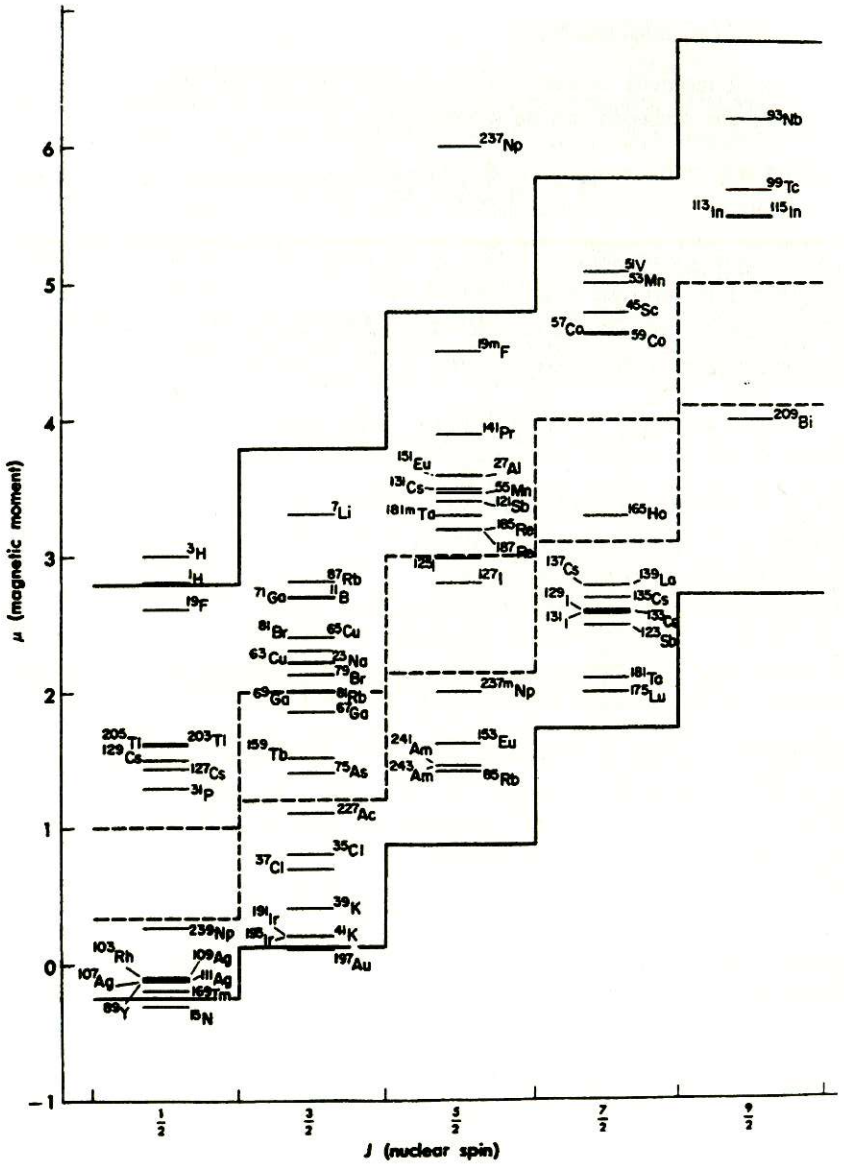

Fig. 3-3 Magnetic moments of odd proton nuclides. The solid lines are Schmidt limits; the dashed lines are single-particle moments for a fully quenched intrinsic magnetic moment.

the Schmidt limits given by Eq. 3–21. Examination of these figures shows certain general features. The moments of most nuclei are not on the Schmidt lines. However, the nuclides in each diagram fall into two rough groups, one near each of the Schmidt lines and about one nuclear magneton away.

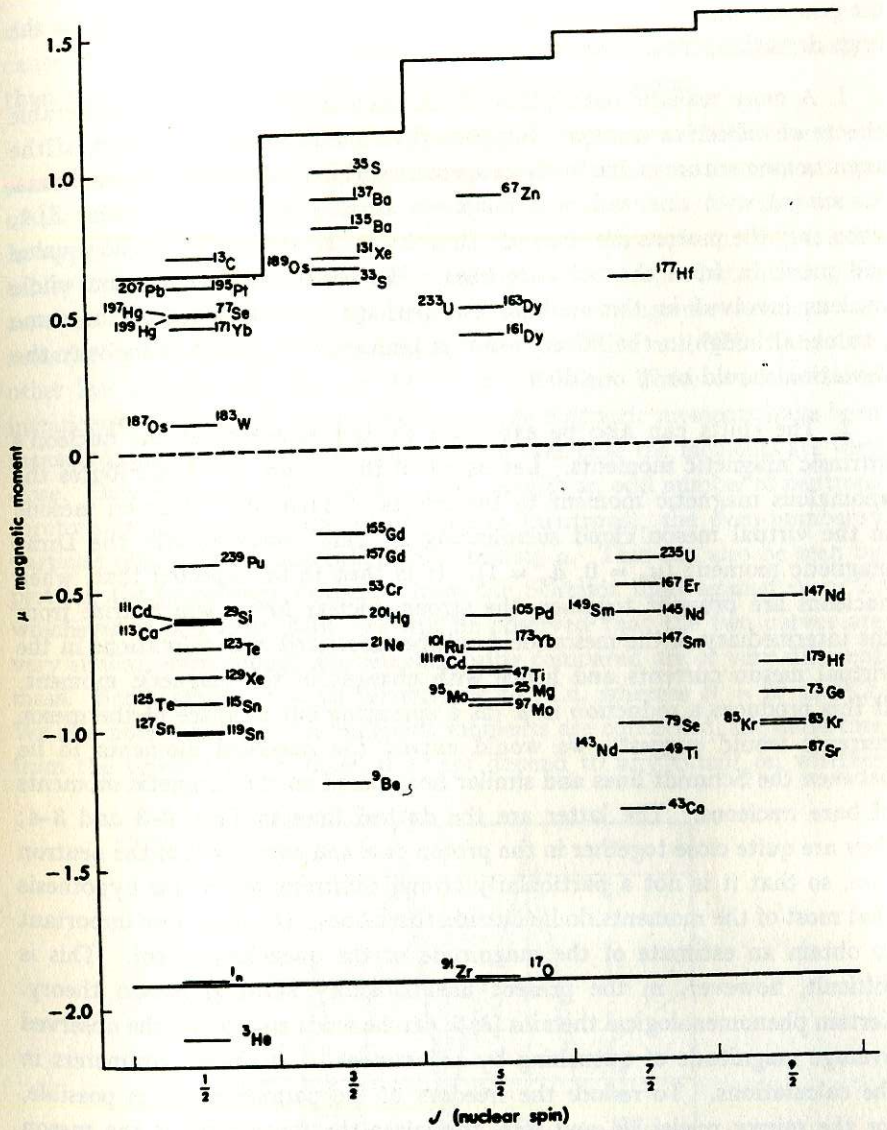

Fig. 3-4 Magnetic moments of odd neutron nuclides. The lines have the same significance as in Fig. 3–3.

It is also remarkable that, except for a few light nuclei and ^{237}Np, all deviations are inward from the Schmidt lines.

These facts stress again that the extreme single-particle model is not in accord with the details of nuclear structure, but that it does seem to explain

the general trend of some phenomena. There are two possible causes for the large deviations from the single-particle values:

1. A more realistic description of the nucleus includes very considerable effects of collective motion. Suppose that a reasonably large part of the angular momentum is due to the cooperative orbital motion of other nucleons. Associated with this will be a relatively small g-factor of the order Z/A, since only the protons are charged. It is then to be expected that the μ-value will move in from the Schmidt lines. We need consider, not the whole nucleus involved in this motion, but perhaps only nucleons of the same j-value, although in the latter case it is perhaps not so easy to see why the deviation should be in one direction.

2. The shifts can also be explained by the *quenching* of the nucleon's intrinsic magnetic moments. Let us recall the picture which attributes the anomalous magnetic moment to the effects of currents of charged mesons in the virtual meson cloud surrounding a "bare" nucleon with the Dirac magnetic moment ($\mu_n = 0$, $\mu_p = 1$). It is then to be expected that, when nucleons are brought together, the strong nuclear forces which arise from the intermediary of the meson field will be associated with alterations in the virtual meson currents and hence with changes in the magnetic moment. If this produces a reduction in μ (as a spreading out in space of the meson currents would suggest), we would expect the observed moments to lie between the Schmidt lines and similar lines based on the magnetic moments of bare nucleons. The latter are the dashed lines in Figs. 3–3 and 3–4; they are quite close together in the proton case and coincident in the neutron case, so that it is not a particularly strong confirmation of this hypothesis that most of the moments do lie outside these lines. It is therefore important to obtain an estimate of the magnitude of the quenching effect. This is difficult, however, in the present unsatisfactory state of meson theory. Certain phenomenological theories [4, 5] can be made to produce the observed average magnitude of quenching by adjustment of available parameters in the calculations. To reduce the freedom of the parameters, it is possible, for the mirror nuclei ^{3}H and ^{3}He, to isolate the magnitude of the meson exchange-current contribution with acceptable certainty, since in these simple nuclei the wave functions are reasonably well known [6]. In each case the effect on μ is 0.27 nuclear magneton to the *outside* of the Schmidt limits. With the restriction that the theory used for other nuclei must fit ^{3}He and ^{3}H, it would seem that the quenching effect will not exceed about 0.25 nuclear magneton [7, 8] and may be in the wrong direction. Although

the situation is not clear, it is reasonable to suppose that one important cause of the deviations is the inadequacy of the single-particle model, rather than to attribute them wholly to a quenching phenomenon.

Despite this evidence of the importance of cooperative effects, there are some aspects of the data on magnetic moments that stress the importance of the number of odd particles in the determination of nuclear properties. In approximately twelve odd-Z elements scattered throughout the periodic table, there are two or more isotopes having the same spin but differing by an even number of neutrons. In such cases the magnetic moments are remarkably close; one outstanding exception is ^{151}Eu and ^{153}Eu, and two other less pronounced ones are ^{81,87}Rb and ^{69,71}Ga. There are also three instances of two odd-N isotones for which the magnetic moments have been measured, namely, $N = 65$, 85, and 117; in each case the moments are very close. These facts indicate that, in a nucleus with an odd number of neutrons (protons) and an even number of protons (neutrons), the even-numbered particles play only a small role in determining μ. This can also be seen by plotting the percentage deviation from the Schmidt limit against N or Z, whichever is odd (Fig. 3–5). It will be observed that the two curves are very similar, even though the nuclides being compared are of very different mass. For example, $Z = 29$ corresponds to ^{63}Cu, whereas $N = 29$ is ^{53}Cr. We also note that, as far as magnetic moments are concerned, the departure from the single-particle model does not depend to any extent on whether

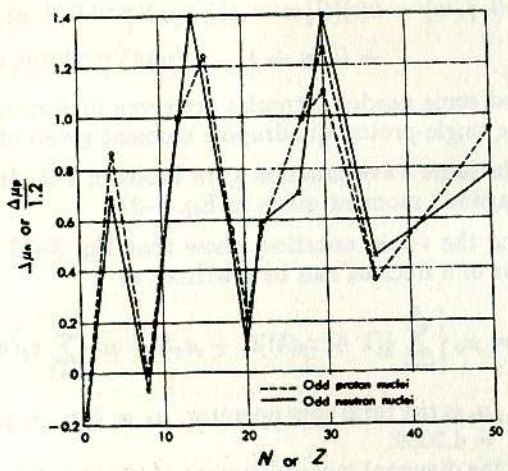

Fig. 3-5 Magnetic-moment deviation from the Schmidt limit as a function of the odd nucleon number. (After Blin-Stoyle [9]).

the odd-numbered nucleons present are neutrons or protons, but does depend rather sensitively on the value of the odd number.

REFERENCES

1. N. F. Ramsey, *Nuclear Moments*, John Wiley, New York, 1953.
2. C. Schwartz, *Phys. Rev.* **97**, 380 (1955).
3. T. Schmidt, *Z. Phys.* **106**, 358 (1937).
4. A. Miyozawa, *Progr. Theor. Phys.* **6**, 801 (1951).
5. A. Russek and L. Spruch, *Phys. Rev.* **87**, 1111 (1952).
6. R. G. Sachs, *Nuclear Theory*, Addison-Wesley, Reading, Mass., 1953.
7. M. Ross, *Phys. Rev.* **88**, 935 (1952).
8. S. D. Drell and J. D. Walecka, *Phys. Rev.* **120**, 1069 (1960).
9. R. J. Blin-Stoyle, *Theories of Nuclear Moments*, Oxford University Press, Oxford, 1957.

PROBLEMS

3–1. (a) Show that the quadrupole moment Q' of a uniformly charged spheroid about the axis of symmetry is $\frac{2}{5}Ze(b^2 - a^2)$, where a, b are the semi-axes, b being along the axis of symmetry.

(b) Show that the quadrupole moment about an axis making an angle β with the axis of symmetry is $(\frac{3}{2}\cos^2\beta - \frac{1}{2})Q'$.

(c) From the values of σ in Fig. 3–2, calculate the percentage difference between the major and minor axes of several typical distorted nuclei.

3–2. Note that in the simple model used in this chapter a nucleon has constant values of l, j, and m. Hence its wave function is

$$\psi(l, j, m) = u(r)[(l\tfrac{1}{2}m - \tfrac{1}{2}\tfrac{1}{2}|jm)\alpha Y_l^{m-(1/2)}(\theta, \phi) + (l\tfrac{1}{2}m + \tfrac{1}{2} - \tfrac{1}{2}|jm)\beta Y_l^{m+(1/2)}(\theta, \phi)].$$

The notation and some needed formulas are given in Appendix A.

Calculate the single-proton quadrupole moment given in Eq. 3–17a.

3–3. Using the same wave function as in Problem 3–2, derive the Schmidt values of the magnetic moment given in Eq. 3–21.

3–4. (a) Using the i-spin notation, show that Eq. 3–18 for the magnetic moment operator of a nucleus can be rewritten as

$$\mathbf{M} = \mu_0\left\{\sum_{k=1}^{A} \tfrac{1}{2}[1 + \tau_3(k)]\mathbf{l}_k + \mu_S\mathbf{S} + \mu_V\sum_{k=1}\tau_3(k)\mathbf{s}_k\right\}$$

where $\mathbf{S} = \sum_{k=1}^{A}\mathbf{s}_k$ is the total spin operator, $\mu_S = \frac{1}{2}(g_p + g_n) = 0.8797$, and $\mu_V = \frac{1}{2}(g_p - g_n) = 4.7059$.

(b) Denoting the diagonal matrix element of the operator M_z with respect to the nuclear state $|J, M = J; T, T_3\rangle$ as $\langle M_z\rangle_{T_3}$, show that the sum of the magnetic moments of mirror nuclei is given (in units of μ_0) by

$$\langle M_z\rangle_{T_3} + \langle M_z\rangle_{-T_3} = (\tfrac{1}{2} + \mu_S)J + \frac{1}{J+1}(\tfrac{1}{2} - \mu_S)\langle \mathbf{L}^2 - \mathbf{S}^2\rangle.$$

You will need formula A–75a of the appendix. This is known as the mirror theorem of Sachs [R. G. Sachs, *Phys. Rev.* **69**, 611 (1946)].

Chapter 4

Sizes of Nuclei

4-1 INTRODUCTION

We would like to ask these important questions: What are the shapes and sizes of nuclei, and how are the nucleons distributed throughout the nuclear volume?

In Chapter 1 we have already remarked that Rutherford showed in 1911 that nuclei have a radial extent of less than 10^{-12} cm [1]. Rutherford's calculations were based on experiments by Geiger and Marsden [2, 3, 4], in which a beam of α-particles was made to fall on gold atoms in a thin foil. A scintillation detector was used to determine how many α-particles were scattered at each of several angles. If the final direction of motion of a scattered particle is specified by polar angles (θ, ϕ), and if $d\Omega$ is an infinitesimal solid angle located around the ray (θ, ϕ), then the number of particles scattered per second into $d\Omega$ divided by the incident flux is defined as the *differential scattering cross section* and is written as $\sigma(\theta, \phi)\, d\Omega$ (Fig. 4–1). For charged particles scattered by a point charge with potential Z_2e/r, this cross section can be easily calculated classically. Here we have one formula of classical mechanics that carries over unchanged into nonrelativistic quantum theory.† The result, which does not depend on ϕ, is

$$\sigma(\theta) = \left(\frac{Z_1Z_2e^2}{2\mu v^2}\right)^2 \operatorname{cosec}^4 \tfrac{1}{2}\theta. \tag{4–1}$$

† See, for example, K. R. Symon, *Mechanics*, Addison-Wesley, Reading, Mass., p. 120; and L. I. Schiff, *Quantum Mechanics*, McGraw-Hill, New York, p. 114.

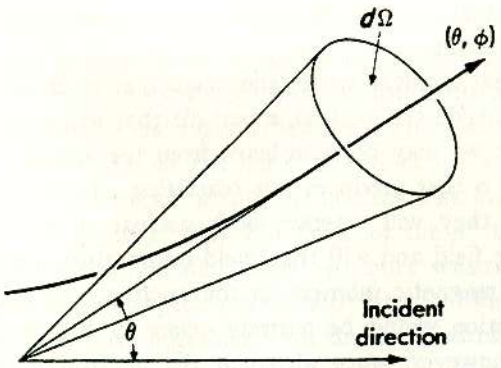

Fig. 4-1 Scattering angles and solid angle.

In this formula, θ is the scattering angle in the center-of-mass system, μ is the reduced mass, v is the initial relative velocity, and Z_1e, Z_2e are the charges of the two particles. The scattering described by Eq. 4–1 is referred to sometimes as "Coulomb scattering" and sometimes as "Rutherford scattering."

Classically, the distance of closest approach for a given energy is $(2Z_1Z_2e^2/\mu v^2) = r_C$, say. In Geiger's experiments, if r_C were less than the radius of the gold nucleus, the α-particles would be able to penetrate into the nucleus. In this region the potential would no longer be that of an isolated charge. If, for example, the electric charge Z_2e were uniformly distributed throughout a sphere of radius R, the potential inside the sphere would be (see Problem 4–11)

$$\frac{Z_2e}{R}\left[\frac{3}{2} - \frac{1}{2}\left(\frac{r}{R}\right)^2\right] \quad \text{for} \quad r < R. \tag{4–2}$$

Thus, if the α-particles entered the region of positive charge, the angular dependence of their scattering would be quite different from that given by Eq. 4–1. In the experiments that Rutherford analyzed, r_C was as small as 10^{-12} cm, and yet there was no departure from Coulomb scattering. Consequently it was deduced that nuclei have radii of less than 10^{-12} cm.

Since the scattering in question is due to electric forces, one might be tempted to say that all that had been demonstrated was that the protons are inside r_C and that nothing was learned about the location of neutrons.

However, the α-particle would have "felt" nuclear forces if any nuclear matter were outside r_C, and, of course, these forces would also have caused anomalous scattering.

It is clear that, if a scattering experiment is to teach us about the distribution of matter inside the nucleus, a particle that will enter the nucleus must be used. Then we may hope to learn from the angular scattering pattern what the force is that produces this scattering. If for a probe we use very fast electrons, they will interact with nuclear matter only through the electromagnetic field and will thus yield information about the distribution of charge and magnetic moment in the nucleus. It would seem that the charge distribution would be entirely given by the protons. This is not strictly true, however, since although the neutron is a neutral particle, experiments indicate (see Section 4–3) that it has a charge structure, with positive charge mainly in the core and negative charge distributed to a greater degree in the tail. This implies that an incoming high-energy electron may be scattered by the charge distribution of a neutron; consequently, the charge distribution in a nucleus, although governed mainly by the proton distribution, is also influenced by the neutrons. It is reasonable to state that the charge density in a nucleus is generated from the single-particle wave functions of the nucleons, convoluted with the intrinsic charge structure of the nucleons obtained experimentally, with small and spatially smooth corrections for many-body correlations and meson-exchange currents. In the magnetic-moment distribution, of course, both protons and neutrons contribute importantly.

Since the only force of any importance between the electrons and the nucleons is electromagnetic, the electron is an ideal probe particle. Electron beams can be scattered from nuclei, just as α-particles were, and if the electrons are sufficiently energetic, they are not affected by the electrons in the target, but enter the nucleus and provide very good indications of their charge distributions. It will be realized also that any electron which penetrates the nucleus, such as an s-electron in an atom, will have its motion influenced by the nuclear-charge distribution. This will affect the electron's energy, and consequently there is some hope of learning about the nuclear structure from a study of fine structure in X-ray spectra. The difficulty lies in the smallness of these effects, which is due to the fact that only a very small fraction of the motion of a bound electron lies within the nucleus. However, there is another particle which also interacts with nucleons essentially only through electromagnetic forces. This is the muon (μ). Indeed, from the present point of view, it differs importantly from the electron only by its

mass, which is $207m_e$, and its instability. It has a half-life at rest of 2.2×10^{-6} sec. However, this is ample time for negative muons (produced, say, in an accelerator) to slow down in matter and to be captured into an orbit about a nucleus. This orbit will have the same properties as an electronic orbit in an atom, except for the mass difference. The radius of the Bohr orbit is inversely proportional to the mass, and thus the μ^- has a much larger fraction of its wave function within the nucleus than has the electron. In heavy elements, the radius of the Bohr orbit for the μ^- is $\sim 10^{-12}$ cm. Consequently the spectra of muonic atoms are more sensitive to nuclear size and structure than are the spectra of ordinary atoms. We shall consider each of these methods in turn, beginning with the most instructive, namely, electron scattering [5, 55].

4-2 ELECTRON SCATTERING

The amount of detail of nuclear structure discovered in an electron-scattering experiment is, of course, governed by the de Broglie wavelength of the electron. Thus, to delineate features having dimensions of the order of 1 fm, it is necessary to use electrons of over 100 MeV. It is essential to employ relativistic wave mechanics to describe such electrons. Also, in the scattering process, electrons of quite high angular momenta are involved, and in calculations for 180 MeV on heavy nuclei as many as ten phase shifts are required to describe the scattering process. In these circumstances, it is not possible to give a closed expression for even point-charge scattering. Analytic forms of $\sigma(\theta)$ have been given for high-energy electrons scattered from a point charge Ze, where $Ze^2/\hbar c = Z/137 \ll 1$ [6, 7, 8]. The first terms of a series in $Z/137$ are

$$\sigma(\theta) = \left(\frac{Ze^2}{2E}\right)^2 \frac{\cos^2 \frac{1}{2}\theta}{\sin^4 \frac{1}{2}\theta} \left[1 + \frac{\pi Z}{137} \frac{(\sin \frac{1}{2}\theta)(1 - \sin \frac{1}{2}\theta)}{\cos^2 \frac{1}{2}\theta}\right]. \tag{4–3}$$

The factors outside the brackets are referred to as Mott scattering and may be written σ_{Mott}. The quantity E is the center-of-mass energy. For high Z this formula cannot be used, but numerical evaluations are available [9]. It holds, of course, for the center-of-mass system; hence in the laboratory system the apparently energy-independent angular distribution is modified, and the energy of the scattered electrons is a function of the scattering angle.

Departures from the cross section for a point charge reveal features of the nuclear structure. For heavy nuclei, the effects of this structure also

must be handled by numerical computation. However, for light elements with $Z \lesssim 10$, where the second term in the brackets of Eq. 4–2 can be ignored, a valid closed formula can be obtained. The cross section is expressed as the Mott cross section multiplied by a *form factor*:

$$\sigma(\theta) = \sigma_{\text{Mott}}(\theta)[F(q)]^2, \tag{4–4}$$

$$F(q) = \frac{4\pi}{q}\int_0^\infty \rho(r)\sin(qr)r\,dr. \tag{4–5}$$

In this expression, $\mathbf{q}$ is the vector representing the momentum transfer in the collision, and its magnitude q is given by

$$q = \frac{2E}{\hbar c}\sin\tfrac{1}{2}\theta = \frac{2}{\lambda\!\!\!^{-}}\sin\tfrac{1}{2}\theta, \tag{4–6}$$

where $\lambda\!\!\!^{-}$ is the reduced de Broglie wavelength of the electron (see Problem 4–1). The derivation of these formulas is valid only for spherically symmetric charge distributions; $\rho(r)$ represents the charge density, but it is normalized to unity, that is, $\int \rho(r)4\pi r^2\,dr = 1$, and the charge in the spherical shell of radius r and thickness dr is $Ze\rho(r)4\pi r^2\,dr$. Experimentally, the form factor is obtained directly for some range of q, determined by the energy and the angular range for which observations are made. It is then desirable to correlate the density $\rho(r)$ with the function F. Let us suppose that the wavelength $\lambda\!\!\!^{-}$ is large compared with nuclear dimensions. Then in Eq. 4–4, since $\rho(r)$ is zero outside the nucleus, we have $qr \ll 1$ and can write

$$\begin{aligned} F(q) &= \frac{4\pi}{q}\int \rho(r)(qr - \tfrac{1}{6}q^3r^3 + \cdots)r\,dr \\ &= \int \rho(r)4\pi r^2\,dr - \tfrac{1}{6}q^2\int r^2\rho(r)4\pi r^2\,dr + \cdots \\ &= 1 - \tfrac{1}{6}(qa)^2 + \cdots. \end{aligned} \tag{4–7}$$

We have put $a^2 = \int r^2\rho(r)4\pi r^2\,dr$, and it is seen that a^2 is the mean-square radius of the charge distribution. It is clear that, until $\lambda\!\!\!^{-}$ is decreased to at least nuclear dimensions, it will not be possible to learn anything more than the value of a^2. This is a reflection of the general remark that we must use high energies to learn the finer details of nuclear structure.

It is possible to give an expression for $\rho(r)$, for the Fourier transform of Eq. 4–5 yields

$$\rho(r) = \frac{1}{2\pi^2 r}\int_0^\infty F(q)\sin(qr)q\,dq. \tag{4–8}$$

This formula is of limited usefulness until experiments are carried out that give the form factor with considerable accuracy and over a sufficient range of q. The alternative procedure, which is the only one available whenever formula 4–3 does not apply, is to assume many possible forms of the function $\rho(r)$ and, by substitution in Eq. 4–4, discover which are consistent with experiment.

One of the principal results of the electron-scattering experiments is the conclusion that nuclei do not have sharp edges, but rather that there is an appreciable region over which the nucleon density falls away. One form of density dependence that has been studied extensively is

$$\rho_F(r) = \frac{\rho_0}{1 + \exp[(r - c)/a_0]}. \tag{4–9}$$

This distribution has been referred to in the literature as a Fermi density function. It has the property that, for $c \gg a_0$, ρ is essentially ρ_0 until $c - r$ is a few times a_0, and then it falls to negligible values in a distance determined by a_0 and independent of c.

Hence for the same a_0 we obtain density distributions of the type shown in Fig. 4–2, with uniform density in central cores of varying radii, but with the same thickness of boundary layer. For any density distribution with a symmetrical skin, we shall define c as the radius at which the density has fallen to half its maximum value, and shall use the letter t to denote the

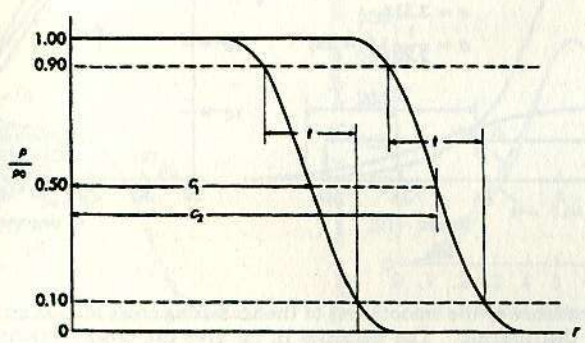

Fig. 4-2 The Fermi-density distributions for two nuclei of different radii.

distance in the surface layer over which the density decreases from 90% to 10% of its maximum.† For the Fermi distribution, $t = 4.40a_0$. It will be realized that, as a_0 approaches zero, the distribution approaches that of a uniform sphere of radius c.

The form factors for many shapes of $\rho(r)$ have been calculated. A general result is that the sharper the cutoff of the density, the more pronounced are the oscillations in the cross section, as would be expected, since the cross section is essentially a diffraction pattern for the electron wave. This behavior is also confirmed, by numerical calculation, in the range for which the form-factor approximation is not valid. An example is illustrated in Fig. 4–3, based on calculations carried out by Yennie, Ravenhall, and Wilson [10]. The scattering cross section is shown for 125-MeV electrons incident on gold for three different shapes of charge density. It is seen that the smoothest curve arises from the smoothest (i.e., the exponential) distribution, and the most oscillatory curve is associated with the sharp cutoff of a

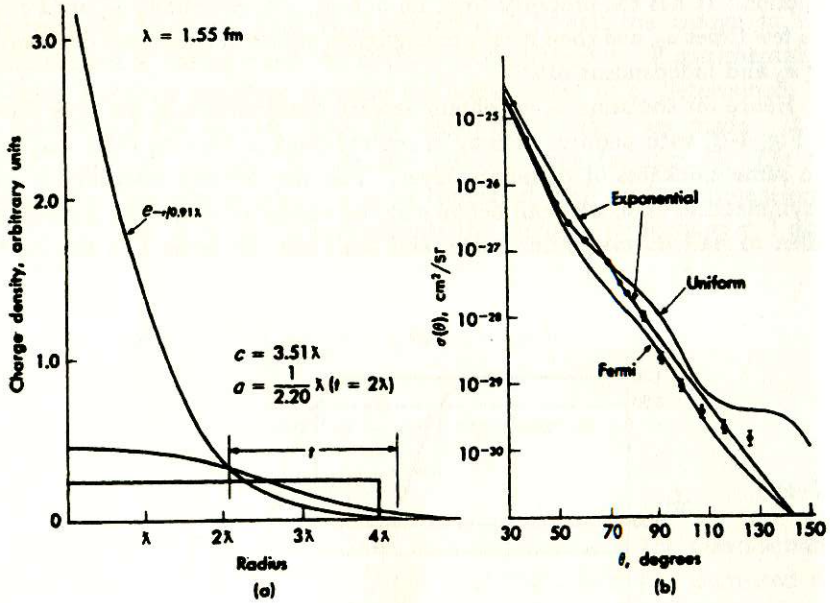

Fig. 4-3 Dependence of the smoothness of the scattering cross section on the smoothness of the density distribution. The densities in (a) give the cross sections in (b). (After Yennie et al. [10].)

† Strictly speaking, the definition of c used in the literature is $c\rho(0) = \int_0^\infty \rho(r)\,dr$.

uniform sphere. The intermediate Fermi distribution is nearer to the experimental points than either of these extremes.

The calculations require first evaluating the potential energy inside the nucleus due to the assumed spherically symmetric charge distribution, given by

$$(4\pi)^{-1}V(r) = \left[\frac{1}{r}\int_0^r \rho(r')r'^2\,dr' + \int_r^\infty \rho(r')r'\,dr'\right](-Ze^2). \qquad (4\text{–}10)$$

The wave function describing the electron scattering is determined by solving Dirac equations for all necessary angular momenta, using Eq. 4–10 for the potential function. This is done numerically, and phase shifts are found. The cross section, which is a known function of the phase shifts, is then calculated. This procedure resembles the methods discussed in Chapter 2 for neutron-proton scattering, but is complicated by the fact that the electrostatic forces are not of short range. We shall not discuss the details here; they are given in the original paper [10].

We first discuss an early experimental study on gold made by Hahn, Ravenhall, and Hofstadter [11], using 153- and 183-MeV electrons. This will illustrate the fact that, with electrons in this energy range, it is not possible to determine the details of $\rho(r)$ for $r < 4$ fm. Previous results, such as those at 125 MeV described above, had made it clear that the density should have a "tail" rather like the Fermi shape and be fairly flat inside. Actually the density at small r is very hard to determine, since there is not much charge in a sphere of small radius, say 3 fm. [This geometrical factor is

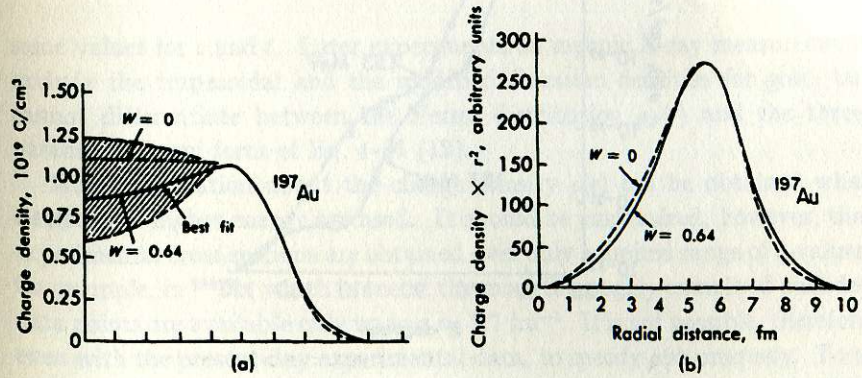

Fig. 4-4 Possible charge densities for gold. (After Hofstadter [5].)

easily taken into account by plotting $4\pi r^2\rho(r)$, a quantity that is associated with the charge in a spherical shell and that portrays more graphically than $\rho(r)$ itself the distances most important for scattering.] Consequently, in addition to using the Fermi distribution F, Hahn et al. studied shapes with central depressions or elevations, given by

$$\rho(r) = \left(1 + \frac{wr^2}{c^2}\right)\rho_F(r), \tag{4-11}$$

which is also called the three-parameter Fermi distribution. The best fit to experiment was obtained with a slight reduction in central density corresponding to $w = 0.64$. However, any curve passing through the shaded area of Fig. 4-4a gives a cross-section curve within experimental error. Figure 4-4b shows clearly the effect of the spherical geometry in reducing the contribution from near the center. On the other hand, the density from about 5 fm out, that is, in the nuclear skin, is quite closely determined. The quality of the agreement with experiment is illustrated in Fig. 4-5.

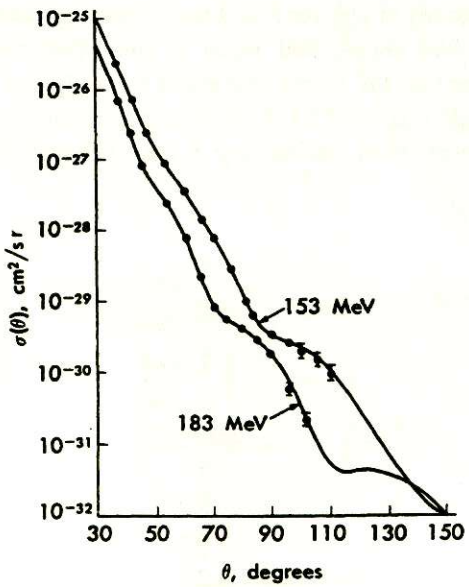

Fig. 4-5 The best-fitting Fermi density for gold gives this excellent agreement with experiment. (After Hofstadter [5].)

Hahn et al. also evaluated the scattering for a trapezoidal density and for the density

$$\rho(r) = \rho_0\left[1 + \exp\left(\frac{r^2 - c^2}{a^2}\right)\right]^{-1}. \tag{4-12}$$

It was found possible to fit the data equally well with these shapes, but, as a glance at Fig. 4-6 shows, the actual densities are very similar, particularly in the skin. In fact, all shapes that agree with experiment have the

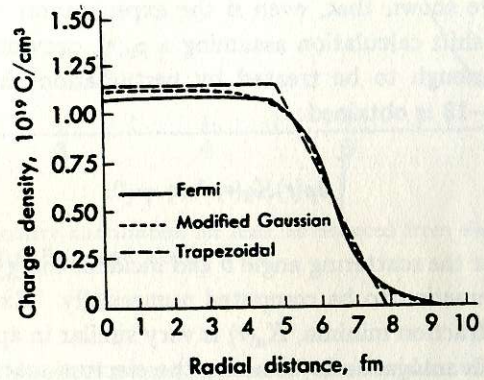

Fig. 4-6 Densities for gold, all of which fit the electron-scattering data. (After Hofstadter [5].)

same values for c and t. Later experiments on muonic X-ray measurements exclude the trapezoidal and the modified Gaussian densities for gold, but cannot differentiate between the Fermi distribution $\rho_F(r)$ and the three-parameter Fermi form of Eq. 4-11 [12].

More information about the charge density $\rho(r)$ can be obtained when electrons of higher energy are used. It should be emphasized, however, that experimental cross sections are obtained over only a limited range of q-values; for example, in ^{208}Pb, which is one of the most thoroughly examined nuclides, data points are available only up to $q \approx 2.7$ fm^{-1}. It is not possible, therefore, even with the present-day experimental data, to specify $\rho(r)$ uniquely. To be more explicit, we assume that there are N data points, $q_1 \cdots q_N$, at which $F(q)$ has been determined experimentally. Let $\rho_0(r)$ be a density distribution

that can fit these experimental data within errors. For simplicity, we assume that the Born formula Eq. 4–5 may be used for $F(q)$, although essentially the same conclusions are reached by more rigorous arguments [13]. If we now change $\rho_0(r)$ to $\rho_0(r) + \delta\rho(r)$, with the constraints

$$\int \delta\rho(r) r^2\, dr = 0,$$

$$\int \delta\rho(r) j_0(q_i r) r^2\, dr = 0, \quad i = 1 \text{ to } N, \tag{4–13}$$

it follows that the same experimental $F(q)$'s will be reproduced. Friar and Negele [13] have shown that, even if the experimental $\sigma(\theta)$'s are fitted by an exact phase-shift calculation assuming a $\rho_0(r)$, provided that the change $\delta\rho(r)$ is small enough to be treated by perturbation theory, a constraint similar to Eq. 4–13 is obtained:

$$\int \delta\rho(r) K_\alpha(r) r^2\, dr = 0. \tag{4–14}$$

Here α stands for the scattering angle θ and incident energy E of the electron, and $K_\alpha(r)$ is a function to be computed numerically. Except at the values of q near the diffraction minima, $K_\alpha(r)$ is very similar in appearance to $j_0(qr)$.

It is most advantageous to combine the electron-scattering data at low and high energies with muonic X-ray data to determine the characteristics of the nuclear-charge distribution. As we saw from Eq. 4–7, at low energies only the rms radius a is obtained from elastic electron-scattering measurements. We shall see in Section 4–4 that the muonic data also determine a accurately. The high-energy measurements, however, scan the regions of the density that have the steepest slope [14, 15]. A careful analysis of ^{208}Pb data on electron scattering and muon X-rays shows [13] that, although the charge distribution $\rho(r)$ can be obtained unambiguously beyond $r > 5$ fm, ambiguities in $\rho(r)$ for the interior region remain, the uncertainty in the central region being the largest, of the order of 4–5%. The charge distribution of ^{208}Pb that yields the best fit to the latest Stanford data on electron scattering and the muonic X-ray data is shown in Fig. 4–7, the ambiguity in $\rho(r)$ being indicated by the shaded envelope [13]. The rms radius a of this distribution is 5.502 ± 0.006 fm. An earlier analysis by Bethe and Elton [15] indicated that there is a 7–10% depression in the central density of ^{208}Pb; the more careful analysis of Friar and Negele [13], on the other hand, shows only a slight depression at $r \approx 1.5$ fm (see Fig. 4–7). The central depression is very

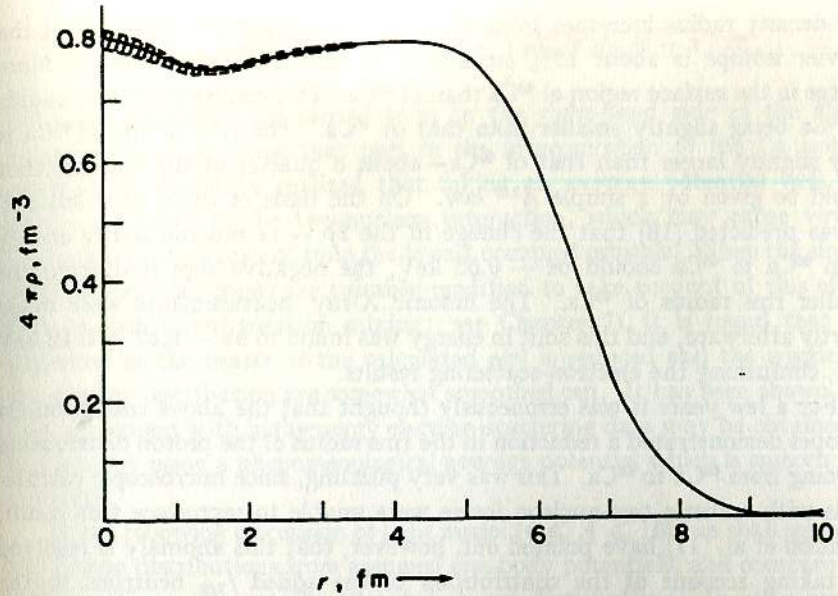

Fig. 4-7 Charge-density distribution for lead, as deduced from electron scattering and muonic X-ray. (After Friar and Negele [13].)

sensitive to the absolute normalization of the incident electron beam, and a 4% change in the normalization can eliminate the depression shown in Fig. 4–7. Furthermore, earlier analysis of high-energy electron-scattering data [16] indicated that minute oscillations in $\rho(r)$ superimposed on a smooth density improve the fit; the analysis of Friar and Negele [13] shows that there is nothing unique about these wiggles and that the data may be fitted with or without them, so long as the constraints of Eq. 4–14 are obeyed. We can state, therefore, that there is no positive evidence for the wiggles in $\rho(r)$ found earlier, but the data do not exclude them either.

Interesting work by electron scattering has also been done on calcium isotopes [18, 19, 20]. It was found that the electron-scattering data at 250 MeV on ^{40}Ca, ^{44}Ca, and ^{48}Ca could be well fitted by the three-parameter Fermi distribution given by Eq. 4–11. The best fit to ^{40}Ca yielded the parameters $c = 3.6685$ fm, $a_0 = 0.5839$ fm, and $w = -0.1017$, indicating a slight elevation at the center. The corresponding values for ^{48}Ca were found to be $c = 3.7369$ fm, $a_0 = 0.5245$ fm, and $w = -0.0300$. Since w is so small, we may still consider c to be the half-density radius, and the surface thickness $t \approx 4.4a_0$. The above parameters then reveal that, although the

half-density radius increases from ^{40}Ca to ^{48}Ca, the surface thickness of the heavier isotope is about 10% smaller, with the result that there is more charge in the surface region of ^{40}Ca than of ^{48}Ca. This results in the rms radius of ^{48}Ca being slightly smaller than that of ^{40}Ca. The rms radius of ^{44}Ca is only slightly larger than that of ^{40}Ca—about a quarter of the increase that would be given by a simple $A^{1/3}$ law. On the basis of these distributions, it was predicted [18] that the change in the $2p \to 1s$ muonic X-ray energy from ^{40}Ca to ^{48}Ca should be -0.52 keV, the negative sign indicating the smaller rms radius of ^{48}Ca. The muonic X-ray measurements were made shortly afterward, and this shift in energy was found to be -0.47 ± 0.12 keV [21], confirming the electron-scattering results.

For a few years it was erroneously thought that the above results on Ca isotopes demonstrated a reduction in the rms radius of the proton distribution in going from ^{40}Ca to ^{48}Ca. This was very puzzling, since microscopic calculations with realistic two-nucleon forces were unable to reproduce this result. Bertozzi et al. [17] have pointed out, however, that this anomaly is resolved by taking account of the contribution of the added $f_{7/2}$ neutrons to the charge distribution. These neutrons contribute negatively to the charge distribution in the surface, and more than compensate for the increase in the rms radius of the proton distribution. The result is a net decrease in the charge rms radius in going from ^{40}Ca to ^{48}Ca.

In the independent-particle model of the nucleus, each nucleon moves in an average one-body potential well, the latter in general being different for protons and neutrons. The energy levels of the potential well are occupied in accordance with the Pauli exclusion principle. For example, in the lowest s-state, there can be only two protons and two neutrons, since the z-component of the spin of each particle can be up or down. By filling up the orbitals in this manner, one can calculate the resulting density distribution of point nucleons from a knowledge of the single-particle wave functions (see Problem 4–10). Such a "shell-model" calculation of the density distribution shows some wiggles due to shell structure and a somewhat pronounced peaking at the center caused by the filling of s-wave orbitals. In order to obtain the charge distribution, it is necessary to convolute the intrinsic charge structure of the nucleons (Section 4–3) with the appropriate densities. Let $\rho_{SM}^{(p)}(\mathbf{r})$ and $\rho_{SM}^{(n)}(\mathbf{r})$ denote the point distributions of the protons and the neutrons, respectively, as obtained from the single-particle wave functions; and $f_{Ep}(\mathbf{r})$ and $f_{En}(\mathbf{r})$ the spatial charge distributions of the proton and the neutron in the nonrelativistic limit (see Eq. 4–31). Then the charge distribution of the nucleus in this model is

$$\rho(\mathbf{r}) = \int \rho_{SM}^{(p)}(\mathbf{r}')f_{Ep}(\mathbf{r}-\mathbf{r}')\,d\mathbf{r}' + \int \rho_{SM}^{(n)}(\mathbf{r}')f_{En}(\mathbf{r}-\mathbf{r}')\,d\mathbf{r}'.$$

We have seen that the second term in the right-hand side of the above equation plays an important part in the interpretation of the Ca isotope results. It should be realized that taking an average potential well still leaves out parts of the two-nucleon interaction, which may cause virtual excitation of the nucleons from the lowest occupied orbitals. When the single-particle wave functions are suitably modified to take account of this effect (this is called configuration mixing; see Chapter 7), it is found that the elevation at the center of the calculated $\rho(r)$ is reduced and the wiggles in the density distribution are somewhat smoothed out. It has been shown [22] that agreement with high-energy electron-scattering data may be obtained in this way by using a phenomenological average potential which is smooth and nonlocal.

In the following discussion of light nuclei ($4 \leqslant A \leqslant 16$), we shall generate the proton distributions from assumed one-body potentials, and compare the results with experimentally extracted charge distributions. In other words, we are going to neglect the contribution of the neutrons to the charge distribution by assuming that $f_{En}(r) = 0$, which, as we have pointed out, is not quite right. Detailed elastic scattering data are available for many nuclei, including ^{16}O, ^{12}C, ^{6}Li, and ^{4}He [23]. In the earlier analyses of these results, good agreement was generally obtained by assuming that each proton moves in a harmonic-oscillator shell-model potential, given by

$$V = -V_0 + \tfrac{1}{2}M\omega^2 r^2,$$

where V_0 is a constant, M is the proton mass, ω is a parameter determining the spread of the wave function, and r is the proton coordinate with respect to the center of the well. By putting two protons in the s-shell and $Z-2$ protons in the p-shell of such a well, the density distribution is given by (see Problem 4–10)

$$\rho_{SM}(r) = \rho_0\left[1 + \frac{Z-2}{3}\left(\frac{r}{b}\right)^2\right]\exp\left(-\frac{r^2}{b^2}\right), \tag{4–15}$$

where by ρ_{SM} we denote the "shell-model" density, ρ_0 is the normalization constant, and $b = \sqrt{\hbar/m\omega}$ is called the oscillator parameter. In order to obtain the charge density $\rho(r)$ from this, it is necessary to take account of the finite size of the protons and to correct for the center-of-mass motion. For these details, the reader is referred to Elton's book [23]. When these

corrections are made, it is found that good fits to the ^{12}C and ^{16}O data can be obtained for $q \leqslant 400$ MeV/c, with $b = 1.64$ fm for ^{12}C and $b = 1.76$ fm for ^{16}O. However, the experimental form factor of ^{16}O, shown in Fig. 4–8, has two diffraction minima, the first at $q \approx 300$ MeV/c and the second at $q \approx 600$ MeV/c [24]. The form factor generated by a harmonic-oscillator

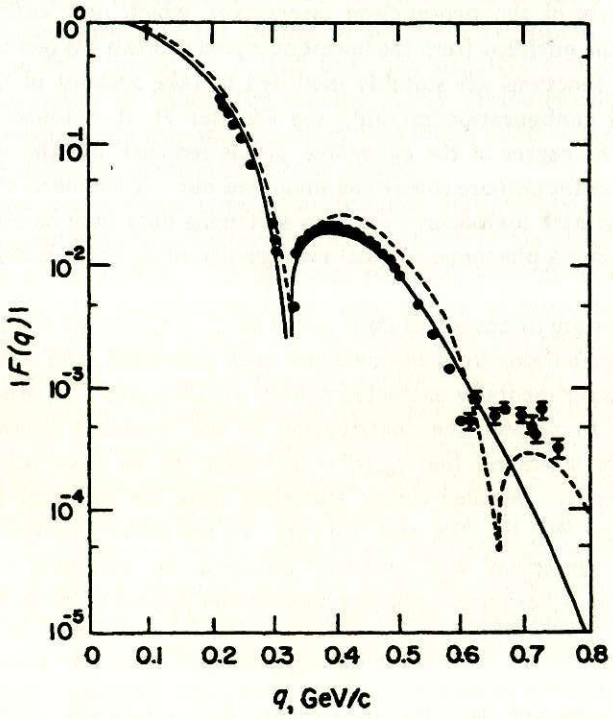

Fig. 4-8 Electron elastic-scattering form factor for ^{16}O. The experimental data of McCarthy and Sick [24] are shown by dots. The full line is the theoretical fit obtained by assuming a closed-shell configuration and using harmonic-oscillator wave functions; the dashed curve is obtained from Woods-Saxon wave functions. (After Donnelly and Walker [25].)

potential yields only one diffraction minimum and therefore cannot fit the high-energy data. A harmonic potential is rather unrealistic in the sense that it keeps increasing with increasing distance, rather than falling off to zero. Any potential with a finite range, on the other hand, gives rise to a form factor that continues to undulate with increasing momentum transfer, giving a series of diffraction minima. Donnelly and Walker [25] have shown that a reasonable fit to the ^{16}O data, including the second diffraction minimum, can be obtained by a suitably chosen potential well of the form

$$V(r) = \frac{V_0}{1 + \exp[(r - c)/a_0]}. \tag{4–16}$$

This is known as the Woods-Saxon potential; it falls to half its central value at $r = c$. The form factor of ^{16}O generated by such a well is also shown in Fig. 4–8.

The situation for ^{12}C is shown in Fig. 4–9. The Woods-Saxon potential well predicts a second minimum in the form factor at $q \sim 700$ MeV/c, which is the upper limit of the existing data.

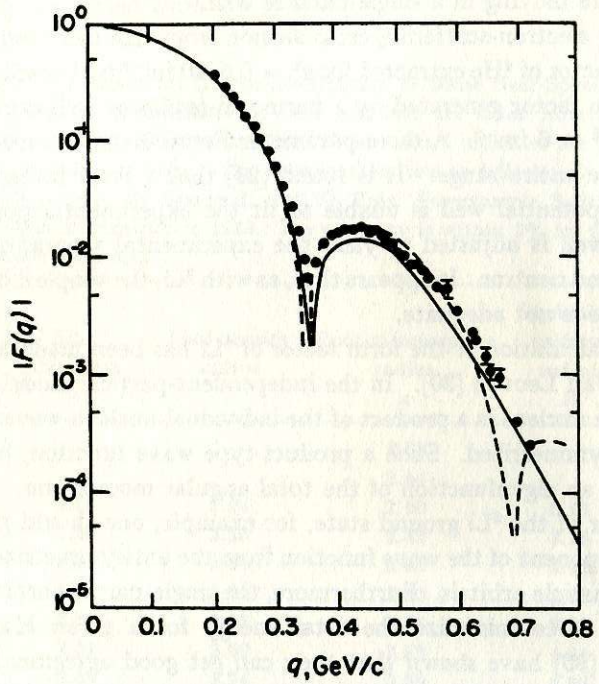

Fig. 4-9 Same as in Fig. 4–8, but for ^{12}C. (After Donnelly and Walker [25].)

The nucleus ^6Li is the lightest stable nucleus with two p-shell nucleons. Its ground-state spin J is 1; consequently it has magnetic dipole and electric quadrupole moments. The simple formula 4–4 should be modified to take account of the fact that these also can contribute to the form factor [26]. The quadrupole moment of ^6Li being very small, $Q = (-8.0 \pm 0.8) \times 10^{-2}$ fm^2, the charge part of the form factor may still be assumed to be spherically

symmetric, as in Eq. 4–5. There is an additional term in the form factor due to the magnetic interaction, which becomes more important for backward scattering. The charge form factor of ^{6}Li has been extracted experimentally [27] in the range $0.7 < q < 2.62$ fm^{-1}. An excellent fit to the data can be made with

$$|F(q)|^2 = \exp(-a^2q^2) - c^2 \exp(-b^2q^2),$$

where $a^2 = 0.87$ fm^2, $b^2 = 1.70$ fm^2, and $c^2 = 0.205$, yielding an rms radius of 2.54 fm. However, the data cannot be fitted by taking a model in which the nucleons are moving in a single-particle well.

The elastic electron-scattering cross section from ^{4}He has been measured and the form factor of ^{4}He extracted for $q^2 = 0.5$–20 fm^{-2} by Frosch et al. [28]. Again the form factor generated by a harmonic-oscillator well cannot fit the data beyond $q^2 = 6$ fm^{-2}. A three-parameter Fermi distribution for $\rho(r)$ fits the data in the entire range. It is found [29] that a form factor produced from a finite potential well is unable to fit the experimental points if the depth of the well is adjusted to yield the experimental separation energies of the proton and neutron. It appears that, as with ^{6}Li, the simple independent-particle picture is not adequate.

A careful calculation of the form factor of ^{6}Li has been made by Bouten, Bouten, and Van Leuven [30]. In the independent-particle model, the wave function of the nucleus is a product of the individual nucleon wave functions, properly antisymmetrized. Such a product-type wave function, however, is not in general an eigenfunction of the total angular momentum. To obtain the form factor of the ^{6}Li ground state, for example, one should project out the $J = 1$ component of the wave function from the antisymmetrized product of the single-particle orbitals. Furthermore, the single-particle orbitals should be chosen so as to minimize the total energy for a given Hamiltonian. Bouten et al. [30] have shown that they can get good agreement with the experimental results of ^{6}Li, starting with reasonable forms of the nuclear Hamiltonian. Such a generalized shell model, therefore, seems to be adequate for light nuclei.

Finally, we mention that the electromagnetic form factors for ^{3}He [31] and the deuteron [32] have been extracted from the elastic scattering data over a wide range of q. For ^{3}He, the charge form factor is known up to $q^2 = 20$ fm^{-2}, while the magnetic form factor is determined up to $q^2 = 12.5$ fm^{-2}. The neutron-proton interaction in the deuteron would be uniquely determined if the deuteron wave function were known for all values of r. The form factor is the most directly related quantity to the wave function

that can be determined experimentally, and it is clear that the deuteron form factor can provide some insight into the details of the n-p interaction. To perform the analysis, it is necessary to know the form factors of neutron and proton, which we discuss in the next section. It turns out that most n-p potentials with short-range repulsion which fit the scattering data also fit the deuteron electric form factor reasonably well [32] (see Section 5–2, where we discuss this topic in detail).

For all but these very light nuclei, certain regularities in the behavior of the charge density are important. For each nucleus studied, a rms charge radius a is calculated from

TABLE 4-1 Parameters of Charge Distribution of Some Near-Spherical Nuclei. The distances are given in femtometers. The numbers are taken from a compilation by Überall [55, p. 210]. The last column, "Comments," indicates the place and year in which the analysis was done. The abbreviations are as follows: D: Darmstadt; K: Khartov; O: Orsay; S: Stanford; and Y: Yale. For example, S 59 indicates that the work was done at Stanford in 1959. The accuracy is within 2% for the radii and 10% for the surface thickness.

Nuclide	Skin thickness t	Half-density radius c	Root-mean-square radius a	Equivalent uniform radius R	Comments
^{4}He			1.63		[34]
^{6}Li			2.54		[27]
^{12}C	2.20	2.24	2.50	3.23	S 59
^{14}N	2.20	2.30	2.45	3.16	S 59
^{16}O	1.8	2.60	2.65	3.42	
^{24}Mg	2.6	2.85	2.98	3.85	S 56
^{28}Si	2.8	2.95	3.04	3.93	S 56
^{40}Ca	2.51	3.60	3.52	4.54	S 65
^{48}Ti	2.49	3.74	3.59	4.63	D 66
^{52}Cr	2.33	3.97	3.58	4.62	O 64
^{56}Fe	2.5	4.16	3.76	4.85	O 62
^{58}Ni	2.46	4.14	3.83	4.94	K 68
^{89}Y	2.51	4.76	4.24	5.47	K 67
^{93}Nb	2.52	4.87	4.33	5.59	K 67
^{116}Sn	2.37	5.27	4.55	5.87	O 67
^{120}Sn	2.53	5.31	4.64	5.99	O 67
^{139}La	2.35	5.71	4.85	6.26	K 67
^{142}Nd	1.79	5.83	4.76	6.15	Y 69
^{197}Au	2.32	6.38	5.33	6.88	S 56
^{208}Pb	2.33	6.54	5.50	7.10	[13]

$$a^2 = \int r^2 \rho(r) 4\pi r^2 \, dr. \tag{4–17}$$

The equivalent uniform distribution is defined as the uniform distribution with the same value of a. Its radius R is given by $R = (5/3)^{1/2}a$. Both these quantities are tabulated in Table 4–1, which lists also the values of the skin thickness t and the half fall-off radius c.

The size and density of a nucleus are determined mainly by the nuclear forces, to which the electrostatic forces are a relatively small correction. If the numbers of neutrons and protons in the nucleus are the same, the nuclear forces being charge independent, we would expect the neutrons and protons to have nearly the same spatial distribution. In heavier nuclei, the neutron number being large, the protons should move in a deeper potential well. However, this will be somewhat offset by the average repulsive Coulomb potential that the proton experiences. There is the additional fact that the single-particle wave function of the proton should decay more rapidly in the asymptotic region than that of the neutron because of the Coulomb barrier. We may expect, therefore, that in the outer edge of the surface there are more neutrons than protons. The densities for protons and neutrons should otherwise be very similar (except for the normalization factor). Experimentally, the absorption of K^--mesons in the nuclear periphery [33] seems to support the view that the distant surface [$r > (c + 1)$ fm] of a heavy nucleus contains more neutrons than protons.

In summary, elastic electron scattering has provided the following information about the spatial distribution of charge in nuclei:

1. For nuclei with $A > 30$, the main features of the charge density may be represented by two- or three-parameter Fermi distributions which have almost uniform central cores.

2. For nuclei with $A \gtrsim 20$, the half-density radius c and the rms radius a are both roughly proportional to $A^{1/3}$. As illustrated in Figs. 4–10 and 4–11, good fits are found to be as follows [34]:

$$c = 1.18A^{1/3} - 0.48 \text{ fm}, \qquad a = 0.82A^{1/3} + 0.58 \text{ fm}. \tag{4–18}$$

3. For lighter nuclei ($4 \leqslant A \leqslant 20$), the central core is not well developed and the density falls steadily with r. The low-q data may be fitted by form factors generated in harmonic-oscillator wells, but refinements are necessary to obtain agreement at higher momentum transfers. The rms radii for these nuclei do not obey Eq. 4–18; they fluctuate a great deal for $A < 6$ and are almost constant for $6 < A < 16$. This is shown in Fig. 4–12.

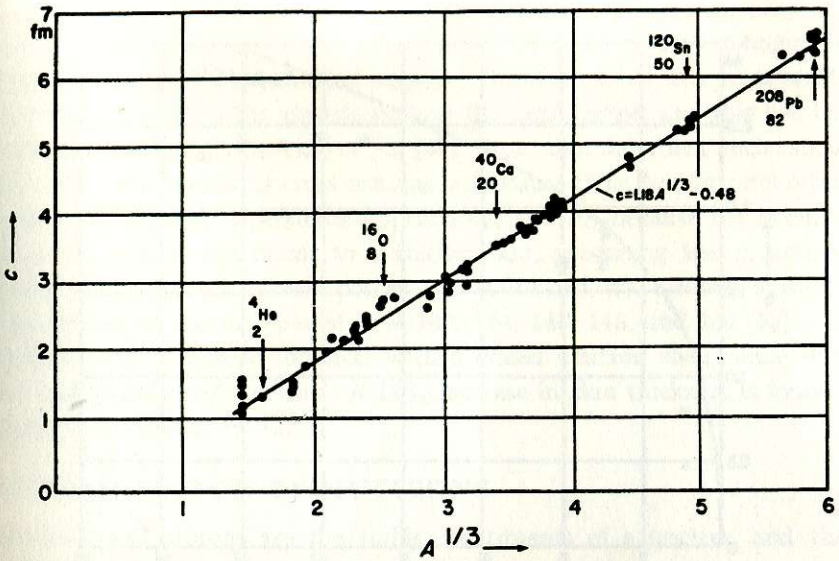

Fig. 4-10 Half-density radius c of the nuclear charge density, plotted as a function of $A^{1/3}$. For many nuclei, more than one experimental point is shown, corresponding to different assumed forms of the distribution. (After Hofstadter [34].)

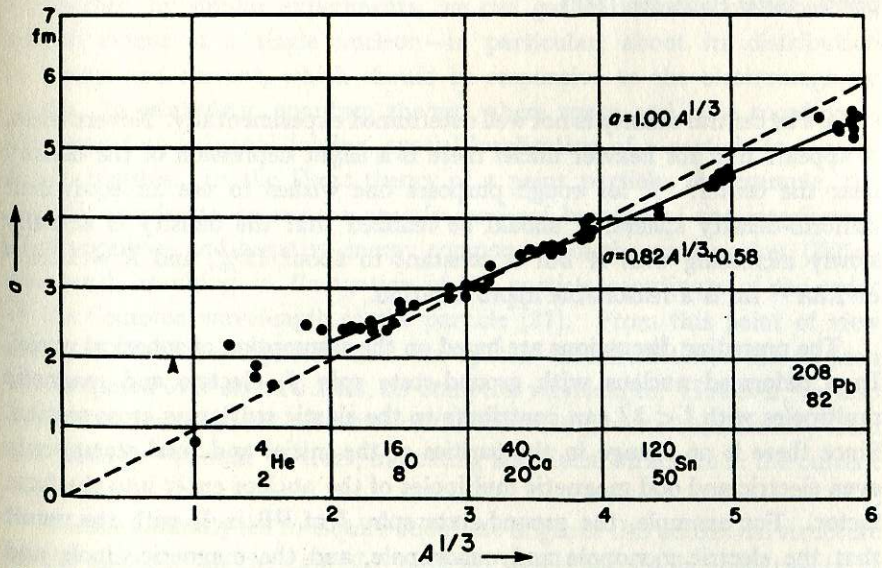

Fig. 4-11 The rms radius, a, of the nuclear charge density, plotted as a function of $A^{1/3}$. Multiplicity of experimental points, for the same value of $A^{1/3}$, corresponds to different assumed charge distributions. (After Hofstadter [34].)

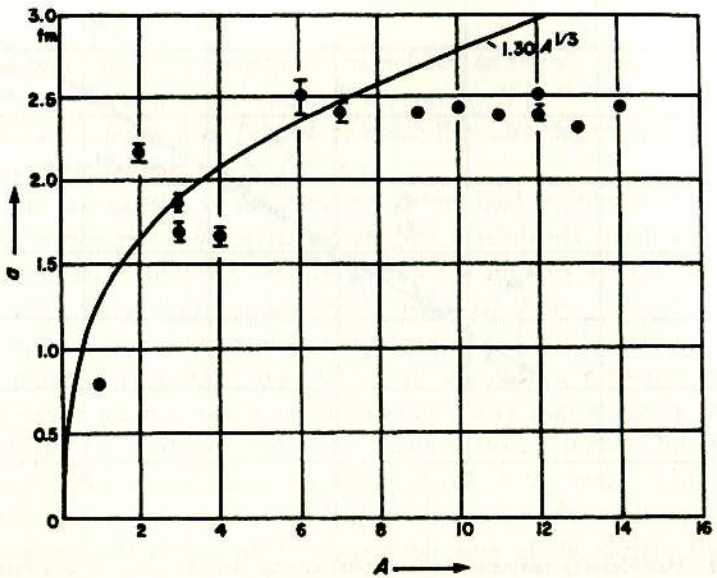

Fig. 4-12 The rms radius, a, of the nuclear charge density for light nuclei ($A \leqslant 14$) as a function of A. The full line is the curve $1.30A^{1/3}$, which fails to fit the experimental points. (After Hofstadter [34].)

4. The central density is not well determined experimentally. Nevertheless, it appears that for heavier nuclei there is a slight depression of the density near the center. If for rough purposes one wishes to use an equivalent uniform-density sphere, it should be realized that the density is actually slowly increasing with A but is constant to about 12%, and $R = 1.2A^{1/3}$ or $1.3A^{1/3}$ fm is a reasonable approximation.

The preceding discussions are based on the assumption of spherical nuclei. In a deformed nucleus with ground-state spin J, electric and magnetic multipoles with $l < 2J$ can contribute to the elastic scattering cross section. Since there is no change in the parities of the initial and final states, only even electric and odd magnetic multipoles of the nucleus enter into the form factor. For example, the ground-state spin J of ^{11}B is $\frac{3}{2}$, with the result that the electric monopole and quadrupole, and the magnetic dipole and octupole, moments of the nucleus contribute to elastic scattering. In the Born approximation (which is reasonable for light nuclei), the charge and

magnetic parts of the form factor can again be expressed neatly [35]. The magnetic form factors contribute negligibly for small scattering angles but become important at backward angles. Therefore these can be separated experimentally from the electric part of the form factor, and this has been done, for example, in the case of ^{11}B [36]. Note that deformed nuclei should have smoother scattering cross sections (a) because their random orientations reduce the angular dependence appreciably, and (b) because the extension along the axis is equivalent to a thicker skin, producing less pronounced diffraction minima. These points are confirmed by electron-scattering experiments on Nd isotopes of $A = 142$, 144, 146, 148, and 150 [53]. The nuclide ^{142}Nd is nearly spherical with a closed neutron shell, while ^{150}Nd is a highly deformed nucleus. A 13% increase in skin thickness is found in going from ^{142}Nd to ^{150}Nd.

4-3 FORM FACTOR OF NUCLEONS

Neutrons and protons are the stable constituents of a nucleus, and their distribution in a localized volume, resulting from the attractive nature of the nucleonic forces, gives rise to the finite size of the nucleus. In Sections 4–1 and 4–2 we inquired in particular about the distribution of the electric charge in various nuclides by electron-scattering experiments. A logical question is whether, by similar experiments, we can gather information about the spatial extent of a single nucleon—in particular, about its distribution of charge and current, which should be responsive to the electromagnetic probe. In relativistic quantum theory, where space and time coordinates are treated on an equal footing, spatial localization of a particle to a point is not possible. In the Dirac theory of a point particle, for example, the particle coordinate cannot be exactly *localized* because of the interference of the positive- and negative-energy components of the wave packet (*Zitterbewegung*), resulting in fluctuation of the particle coordinate of the order of the Compton wavelength of the particle [37]. From this point of view alone, it would be expected that the spatial distribution for the nucleon would spread over about 0.2 fm, its Compton wavelength. However, we also know that the magnetic moments of the nucleons deviate considerably from the Dirac (or "normal") values, indicating additional structure in the current distributions.

We are naturally led to inquire about the origin of this additional structure in the nucleon. In the case of a nucleus, which has stable constituents, it arises from the distribution in space of the constituents themselves. One point of view, to answer the question, would be to assume that a nucleon itself

is made up of stable, subnucleonic particles. Indeed, a large body of experimental data for a host of strongly interacting elementary particles can be analyzed by postulating three such basic constituents, called "quarks" [38]. Experimentally, however, these have not been detected as separate entities to date. From a more conventional point of view, the origin of the nucleonic structure can be traced to the Yukawa theory of nuclear force. We noted in Chapter 2 that the force between two nucleons may be considered as due to the exchange of virtual mesons. By the uncertainty principle, it is admissible for a nucleon to create one or more mesons, violating energy conservation by an amount ΔE if these mesons are reabsorbed, either by the nucleon itself or by another nucleon, within a time period $\Delta\tau \sim \hbar/\Delta E$. When the meson is absorbed by a neighboring nucleon, it is the source of the nuclear force; if, on the other hand, the absorption occurs by the same nucleon that emitted the meson, this can be the source of additional structure. The mesons are virtual in the sense that their existence is transitory; a nucleon is continually emitting and absorbing them to form a cloud around it. The electromagnetic composition of a meson-clothed nucleon should therefore reflect the charge and current distributions of this composite system [39]. An electron, since it does not interact strongly, has no meson cloud around it. Nonetheless, it has the same charge as a proton because, in all these virtual processes of emission and absorption of mesons reflecting strong interaction, the charge is conserved.

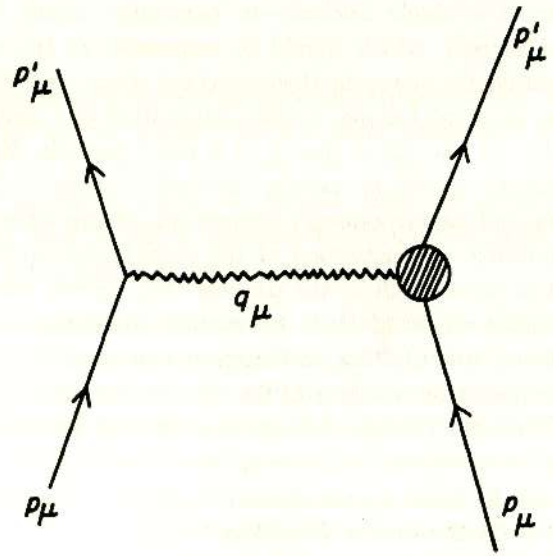

Fig. 4-13 Electron-nucleon scattering by the exchange of a virtual photon of four-momentum q_μ. The structure of the nucleon is schematically shown by the shaded blob.

To probe the structure of a nucleon by elastic electron scattering, very high-energy electrons, whose momenta are of the order of a few GeV/c, are used. It is necessary, therefore, to use a fully relativistic formalism to define the form factors. Furthermore, the recoil of the nucleon cannot be ignored, so that even for elastic scattering the initial and final electron energies are not the same. Figure 4–13 is a schematic diagram of an electron scattering off a nucleon by the exchange of a single photon. In the notation of Sections A–3 and A–4, the initial four-momentum of the electron is denoted by $p_\mu(\mathbf{p}, iE_e)$ and its final four-momentum by $p_\mu'(\mathbf{p}', iE_e')$, and likewise for the nucleon. The shaded blob at the nucleon vertex indicates the composite structure of the proton. The four-momentum transferred by the photon is expressed as $q_\mu = p_\mu - p_\mu'$. With the metric defined in Section A–3, it follows ($c = \hbar = 1$) that

$$p_\mu^2 = p_\mu'^2 = -m^2,$$

$$P_\mu^2 = P_\mu'^2 = -M^2,$$

$$q_\mu^2 = (\mathbf{p} - \mathbf{p}')^2 - (E_e - E_e')^2 \geqslant 0. \tag{4–19}$$

The last equation shows that the exchanged photon is virtual, since for a real photon the mass is zero; hence $q_\mu^2 = 0$. In a relativistic theory, the three components of the electric current and the charge form a four-vector j_μ. This current for the Dirac electron is given by (see Section A–4)

$$j_{e\mu}(x) = ie\bar{\psi}_{p'}(x)\gamma_\mu\psi_p(x), \tag{4–20}$$

where $\psi_p(x)$ is the free four-component Dirac spinor,

$$\psi_p(x) \equiv \psi_p(\mathbf{x}, t) = \psi(\mathbf{p}) \exp[i(\mathbf{p}\cdot\mathbf{x} - Et)]. \tag{A–90}$$

It is straightforward to prove that

$$j_{e\mu}(x) = j_{e\mu}^{(1)}(x) + j_{e\mu}^{(2)}(x),$$

with

$$j_{e\mu}^{(1)}(x) = \frac{ie}{2m}\left[-\bar{\psi}_{p'}(x)\frac{\partial\psi_p(x)}{\partial x_\mu} + \frac{\partial\bar{\psi}_{p'}(x)}{\partial x_\mu}\psi_p(x)\right], \tag{4–21}$$

$$j_{e\mu}^{(2)}(x) = \frac{e}{2m}\frac{\partial}{\partial x_\nu}[\bar{\psi}_{p'}(x)\sigma_{\mu\nu}\psi_p(x)], \tag{4–22}$$

where $\sigma_{\mu\nu}$ is defined by Eq. A–134. The quantity $j_\mu^{(1)}$ is analogous to the nonrelativistic quantum-mechanical current of a particle without spin, while $j_\mu^{(2)}$ is the current from a magnetic dipole of "normal" moment $e/2m$. When

the electron interacts with an electromagnetic field $A_\mu(\mathbf{A}, i\phi)$, the interaction Hamiltonian is given by

$$H^e_{\text{int}} = -\int j_\mu{}^e(\mathbf{x}) A_\mu(\mathbf{x})\, d^3x. \tag{4–23}$$

In the static limit, this gives rise to the usual electrostatic term $e\phi$ and the normal magnetic term $-(e/2m)\,\mathbf{B}\cdot\boldsymbol{\sigma}$.

For the case of a nucleon, we know that the nucleon four-current $j_{N\mu}$ is modified because of the meson clothing around it. Even in the static limit, the magnetic interaction is changed to $-(e/2M)(1+\kappa)\mathbf{B}\cdot\boldsymbol{\sigma}$, where κ is the anomalous contribution. Furthermore, the structure of the meson cloud must be taken into account. The phenomenological form of the current is now considered to consist of a normal term of the form of Eq. 4–20, and an additional magnetic term of the form of Eq. 4–22:

$$j_{N\mu} = \left[F_1(q_\mu{}^2) ie\bar{\psi}_p \cdot \gamma_\mu \psi_p + F_2(q_\mu{}^2) i \frac{\kappa e}{2M} q_\nu \bar{\psi}_p \cdot \sigma_{\mu\nu} \psi_p\right]. \tag{4–24}$$

The functions F_1 and F_2 describe the finite electromagnetic structure of the nucleon; for a point particle these should be independent of $q_\mu{}^2$. The normalizations of F_1 and F_2 are so chosen that they yield the correct static values for the charge and magnetic moment, that is,

$$F_1(0) = F_2(0) = 1 \qquad \text{for the proton,}$$

$$F_1(0) = 0, \qquad F_2(0) = 1 \qquad \text{for the neutron.} \tag{4–25}$$

In order to obtain the correct static magnetic moments, $\kappa = 1.79$ for the proton and -1.91 for the neutron in nuclear magnetons.

The functions $F_1(q_\mu{}^2)$ and $F_2(q_\mu{}^2)$ are called the Dirac and Pauli form factors, respectively. These are still not related directly to the charge and magnetic-moment distributions in the nucleon, since, although the static charge is $eF_1(0)$, the static magnetic moment, in nuclear magnetons, is $F_1(0) + \kappa F_2(0)$. It is customary, therefore, to define the electric and magnetic form factors $G_E(q_\mu{}^2)$ and $G_M(q_\mu{}^2)$:

$$G_E = F_1 - \left(\frac{q_\mu{}^2 \kappa}{4M^2}\right) F_2, \qquad G_M = F_1 + \kappa F_2, \tag{4–26}$$

which yield the charge and magnetic moment of the physical nucleon in the static limit and also give a simpler form for the cross section.

Experimentally, for protons, G_E and G_M are determined as functions of $q_\mu{}^2$ from a measurement of the electron-proton scattering cross section.

For a point charge with no spin, the differential scattering cross section is given, up to the order $\alpha^2 = 1/137$, by the first term in Eq. 4–3, which is the Mott scattering cross section $\sigma_{\text{Mott}}(\theta)$. For a proton with form factors G_E and G_M, this expression is modified by Rosenbluth [40] to

$$\sigma(\theta) = \sigma_{\text{Mott}}(\theta)\left[\frac{G_E{}^2 + (q_\mu{}^2/4M^2)G_M{}^2}{1 + (q_\mu{}^2/4M^2)} + \frac{q_\mu{}^2}{2M^2} G_M{}^2 \tan^2\frac{\theta}{2}\right]. \tag{4–27}$$

Thus a plot of the ratio of the observed cross section to that of $\sigma_{\text{Mott}}(\theta)$, against $\tan^2\theta/2$ for fixed $q_\mu{}^2$, should give a straight line, from which values

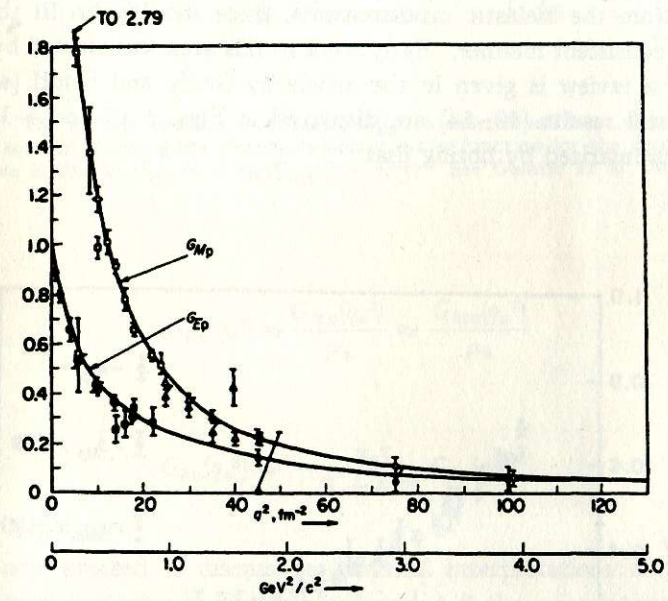

Fig. 4-14 Experimental values of the proton electromagnetic form factors, as determined by elastic electron-proton scattering. The compilation of experimental points is taken from Griffy and Schiff [48]. ΔG_{Mp}, $\blacktriangle G_{Ep}$, Berkelman et al. [41]; $\square G_{Mp}$, $\blacksquare G_{Ep}$, Bumiller et al. [42]; $\otimes G_{Ep}$, Dunning et al. [43]; $\diamond G_{Mp}$, Janssens et al. [44]; $\blacktriangledown G_{Ep}$, Lehmann et al. [45]; $\circ G_{Mp}$, $\bullet G_{Ep}$, Chen et al. [46].

of $G_E{}^2(q_\mu{}^2)$ and $G_M{}^2(q_\mu{}^2)$ can be readily deduced. In Fig. 4–14, we show the experimentally determined form factors of G_{Ep} and G_{Mp} of the proton as functions of the four-momenta squared, the signs having been fixed from the known static values.

Before discussing the physical implication of these results, we present briefly the experimental results for the neutron form factors. Since it is not possible to obtain free neutron targets, the chief source of information is electron-deuteron scattering, where the neutron is loosely bound to the proton. There appear to be some obvious difficulties in the analysis of the experimental data to extract the neutron form factors from this approach. Even if, for simplicity, the deuteron is treated nonrelativistically, the results depend on the form of the deuteron wave function and the meson-exchange currents in the deuteron itself. Both elastic *e-d* scattering and inelastic scattering leading to deuteron disintegration have been performed. If, assuming some form of deuteron wave function, the neutron form factors are deduced from the inelastic measurements, these should also fit the elastic data in a consistent manner. Early work in this area was started by Jankus [47], and a review is given in the article by Griffy and Schiff [48]. The experimental results [49, 54] are displayed in Figs. 4–15 and 4–16, which may be summarized by noting that

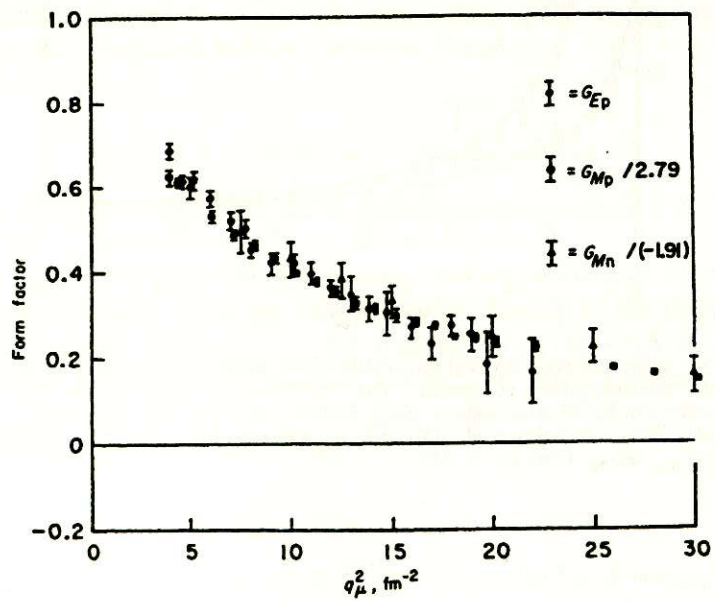

Fig. 4-15 The magnetic form factors of the neutron, as determined from deuteron electrodisintegration (after Hughes et al. [49]). For comparison, the proton form factors G_{Ep} and G_{Mp}/μ_p are also plotted.

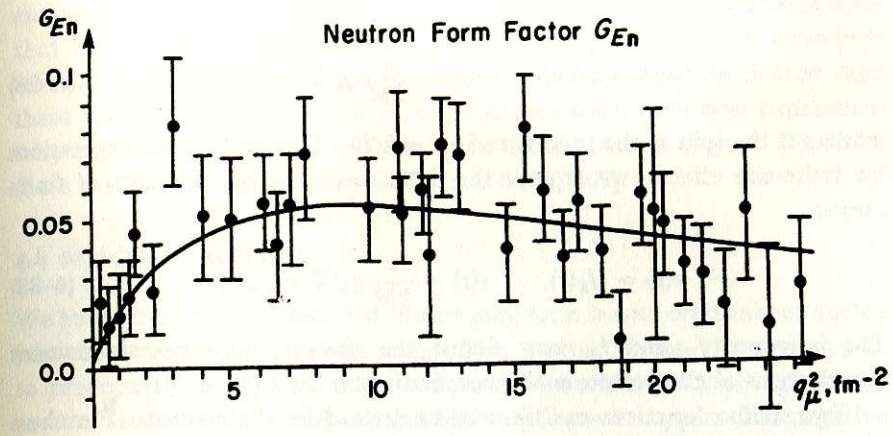

Fig. 4-16 The electric neutron form factor G_{En}, as determined from elastic electron-deuteron scattering, using the Feshbach-Lomon wave function for the deuteron. The solid curve is the fit $G_{En} = -\mu_N \tau G_{Ep}/(1 + 5.6\tau)$. See Galater et al. [54] for more details.

$$G_{Ep}(q_\mu^2) \approx \frac{G_{Mp}(q_\mu^2)}{\mu_p} \approx \frac{G_{Mn}(q_\mu^2)}{\mu_n} \tag{4–28a}$$

and

$$G_{En}(q_\mu^2) \approx -\frac{\mu_n \tau}{1 + 5.6\tau} G_{Ep}(q_\mu^2), \tag{4–28b}$$

where $\tau = q_\mu^2/4M^2$.

We now proceed to discuss the physical interpretations of these relativistic form factors. In Sections 4–1 and 4–2 the nonrelativistic charge form factor was simply the Fourier transform of the spatial charge distribution. Can we make similar interpretations in the relativistic case? To answer this question, we note that, from Eq. 4–19, the form factors are defined only for space-like $q_\mu^2 \geqslant 0$. It is possible, therefore, to go to a special Lorentz frame in which q_μ has no time-like component, and to define the spatial distributions of charge and magnetic moment as the inverse Fourier transforms of $G_E(\mathbf{q}^2)$ and $G_M(\mathbf{q}^2)$. These spatial distributions, however, are not Lorentz invariant, and, therefore, relativistically it is not possible to define spatial distributions uniquely. The other alternative is to go to the nonrelativistic limit. In this limit, the charge and the current-density operators

for a *point* proton fixed at the origin are

$$\rho(\mathbf{r}) = e\,\delta(\mathbf{r}), \qquad j(\mathbf{r}) = \frac{e}{2M} g_p[\nabla \times \mathbf{s}\,\delta(\mathbf{r})], \tag{4-29}$$

where s is the spin of the proton and $g_p = 2.79$. To modify these expressions for finite-size effects, we replace the delta functions by functions of finite range:

$$\rho(\mathbf{r}) = e f_E(r), \qquad j(\mathbf{r}) = \frac{e}{2M} g_p[\nabla \times \mathbf{s} f_M(r)]. \tag{4-30}$$

The functions f_E and f_M now define the charge and magnetic-moment distributions of the proton in the nonrelativistic limit ($\hbar q \ll Mc$).

Two similar functions can likewise be defined for the neutron. For these small values of q, we may write

$$G_E(\mathbf{q}^2) = \int f_E(r) \exp(i\mathbf{q}\cdot\mathbf{r})\, d^3r,$$

$$G_M(\mathbf{q}^2) = \mu \int f_M(r) \exp(i\mathbf{q}\cdot\mathbf{r})\, d^3r. \tag{4-31}$$

Here μ is the static magnetic moment of the nucleon. Small values of $\mathbf{q}$ give information for large $\mathbf{r}$, and we can make the following interpretations from the experimental data:

1. For the proton, $f_{Ep}(r)$ and $f_{Mp}(r)$ are very similar in shape for large r, being roughly exponential in character with a rms radius of about 0.8 fm.

2. For the neutron, the magnetic-moment distribution is very similar to that of a proton. The data for the electric part G_{En} are less certain, although the rms radius of the charge distribution of the neutron is precisely known to be 0.36 fm.† Recent data [54] indicate that in the nonrelativistic limit the charge distribution of the neutron, $f_{En}(r)$, may be taken to be a superposition of a short-range exponential distribution of positive charge $+e$ and a longer-range exponential of negative charge $-e$ [17].

Finally, we should remark that on the theoretical side substantial progress has been made in understanding the nucleon structure from the meson cloud point of view. The simplest virtual process in which a charged meson is created and annihilated, with virtual photon coupling to the meson, is not

† Note that by means of slow neutron scattering from atomic electrons it is known precisely that $(\partial/\partial q^2)G_{En}|_{q^2=0} = 0.021 \pm 0.001$ fm², yielding the neutron rms radius for the electric part to be 0.36 fm [52].

enough to explain the data. In fact, it was this kind of theoretical analysis that first suggested the necessity to include strong two-pion and three-pion correlated states in the meson cloud that can couple to the photon, and these multipion resonances (the ρ-, ω-, and ϕ-mesons) were later experimentally observed (see Section 5–10 for more details on this topic). Details of these calculations are given by Griffy and Schiff [48].

4-4 MUONIC ATOMS

We have already mentioned that muons may form bound orbits about nuclei, just as electrons do. In order to produce muonic atoms, the first step is to produce negative pions in the collisions between a beam of high-energy protons (400–900 MeV) and a target like beryllium or copper. The negative muons are produced in the decay of these pions in flight. The muons thus produced have energies of a few hundred MeV with considerable spread.

TABLE 4-2 Comparison of Characteristics of Muonic and Electronic Atoms. The expressions are for a point-nucleus, Coulomb-field case.

Quantity	Expression	Ratio between muonic and electronic atoms	Typical values for muonic atoms
Orbit radius	$\frac{n^2\hbar^2}{Ze^2}\cdot\frac{1}{m}$	$\frac{m_e}{m_\mu} \approx \frac{1}{207}$	5 fm ($Z \approx 50$)
Energy levels E_n	$-\frac{(Z\alpha)^2c^2}{2n^2}m$	$\frac{m_\mu}{m_e} \approx 207$	-6 MeV ($Z \approx 50$) ($n = 1$)
Fine structure $\left\langle\frac{(\mathbf{l}\cdot\boldsymbol{\sigma})Z}{m^2r^3}\right\rangle$	$\alpha Z^4 m$	$\frac{m_\mu}{m_e} \approx 207$	550–200 keV in heavy elements
Hyperfine electric quadrupole $\left\langle\frac{e^2Q_N}{r^3}\right\rangle$	$\sim Q_N Z^3 m^3$	$\frac{m_\mu^3}{m_e^3} \sim 10^7$	50–500 keV in highly deformed heavy nuclei
Hyperfine magnetic dipole $\left\langle\frac{\mu_N\mu_{\text{lepton}}}{r^3}\right\rangle$	$\sim \mu_N Z^3 m^2$	$\frac{m_\mu^2}{m_e^2} \sim 4 \times 10^4$	$\sim$ A few keV in heavy nuclei

These muons have to be slowed down to thermal energies by passage through the target material before being captured in atomic orbits. The density of states of high-angular-momentum orbits being large, a muon first enters a bound state in one of these orbits and then cascades down to the ground state.

The muonic atom has characteristics considerably different from those of the electronic one since the muon mass is about 207 times heavier than the electron mass and also because there is no shielding of the nuclear charge in the lower orbits of the muonic atoms. The characteristics of the two types are compared in Table 4–2, following Wu and Wilets [50]. It will be noticed that a muonic orbit with principal quantum number n around 14 has the same radius as the lowest electronic orbit. Therefore, while a muon is in its higher orbits, it interacts strongly with the electrons, and emission of electrons predominates over radiation as a de-excitation mechanism. By the time the principal quantum number n of the muonic orbit reaches a value of 6 or less, its interaction with the electron structure is very small, and one is dealing essentially with a bare, hydrogen-like muonic atom. Transitions involving these low quantum numbers result in the emission of photons, which may have energies up to several MeV. These are still called muonic X-rays, because of the similarity of the processes in which they arise. On reaching the lowest 1s-level, the muon either decays with a half-life of 2.2×10^{-6} s or is captured by a proton in the nucleus in a comparable time, with emission of a neutron and neutrons. It is therefore only possible to study one-muon atoms.

The radius of the lowest muonic orbit in a heavy or medium-heavy nucleus is comparable to the half-density radius of the nucleus. For example, in lead, the orbit with $n = 1$ (the 1s-state) has a radius of 3.1 fm, and the $n = 2$ state radius is about 12 fm. The half-density radius of lead is 6.5 fm, and therefore the muon spends a substantial fraction of its time inside the nucleus, especially in the 1s-orbit. Since it will experience an electrostatic potential of non-Coulomb shape inside the nucleus, its energy levels will be appreciably different from those given by the simple theory for a hydrogen-like atom. This finite-size effect reduces the binding of the 1s-level drastically in a heavy nucleus. For example, the binding of the 1s-level in lead should be about 21 MeV for a point nucleus according to the Dirac theory, whereas the experimental value is approximately 10.6 MeV.

It will also be seen from Table 4–2 that the hyperfine electric quadrupole interaction in a heavy deformed element can be as large as the fine-structure splittings, and these are of the same order as the spacings of the low-lying

collective states of a nucleus. With the development of lithium-drifted germanium and silicon detectors, having resolutions of a few keV even for a γ-ray of energy 5 MeV, it has become possible to measure these splittings in heavy nuclei.

As we have seen, measurement of the energies of the X-rays of a muonic atom should provide information about the charge distribution in a nucleus. The first quantitative studies of the X-ray energies, made by Fitch and Rainwater [51], resulted in the determination of the $2p \rightarrow 1s$ transition energy of nine elements with Z ranging from 13 to 83. It is clear that measurement of one energy will provide only one parameter of the nuclear-charge distribution and therefore will not by itself give information about the shape of the radial dependence. Rather, some gross feature of the charge distribution (like the rms radius or some moment of the radius) may be fixed by this form of data.

We have noted that, for a heavy element like lead, the shift in the 1s-level due to the finite-size effect is very large. For light nuclides, however, the muonic X-ray energies are a rather insensitive measure of nuclear size, since the radii of the Bohr orbits are inversely proportional to Z (see Table 4–2), while the nuclear dimensions are proportional to $A^{1/3}$. Consequently, only a small fraction of the muonic orbit is inside the nucleus. Thus the shift in the 1s-level for ^{40}Ca is only about 0.07 MeV. For even lighter nuclei, only the s-state energies are much affected, and an estimate of this effect can be made by first-order perturbation calculation. Because of the finite size of the nucleus, the muon experiences a potential $V(r)$, given by Eq. 4–10, instead of the point Coulomb field Ze^2/r, so that the first-order energy shift is

$$\Delta E = \langle \psi_0 | V - \left(-\frac{Ze^2}{r} \right) | \psi_0 \rangle, \tag{4–32}$$

where ψ_0 is the muonic wave function for a point nucleus, obtained by solving the Dirac equation in a Coulomb field. This wave function has a singularity at the origin that goes like $r^{\sigma-1}$, where $\sigma = (1 - \alpha^2 Z^2)^{1/2}$, α being the fine-structure constant $e^2/\hbar c$. The actual wave function for a finite nucleus does not have this singularity, but remains finite. The singularity of ψ_0 at the origin presents no difficulty in the integration indicated in Eq. 4–32, but it is true that ψ_0 is not realistic for very small values of r. This is not significant in lighter nuclei, but we cannot expect Eq. 4–32 to be valid for heavy nuclei. When Eq. 4–32 is simplified, it is found that

$$\Delta E = \frac{2^{2\sigma-1}}{\pi(2\sigma+1)!} (\alpha Z)^{2\sigma+2} \langle r^{2\sigma} \rangle \left(\frac{\hbar}{\mu c} \right)^{-2\sigma} \mu c^2, \tag{4–33}$$

where

$$\langle r^{2\sigma} \rangle = 4\pi \int \rho(r)^{2\sigma+2}\, dr.$$

For lighter nuclei, σ is nearly unity, and we see that the energy shift measures essentially the mean-square radius. We further note that $\Delta E \propto Z^4$, a result that turns out to be approximately true throughout the periodic table. Thus the experiments of Fitch and Rainwater may be regarded as determining the value of the mean-square radius.

Since these early measurements, great progress has been made in precise measurements of the muonic X-rays, and many transitions can now be accurately determined. In the medium- and heavy-Z regions several energy differences have been measured, but all that is effectively obtained is the shifts in the energy levels of the $1s_{1/2}$-, $2p_{1/2}$-, and $2p_{3/2}$-levels, because the shift in the $3d$-level is not sensitive to charge distribution. For most nuclides, the $3d$-level shift is considerably smaller than the experimental accuracy, and even for $Z \sim 80$ this shift is only about 4 keV, while the accuracy of measurements is of the order of 1 keV. In principle, to analyze the experiments, a nuclear charge distribution $\rho(r; a, b, c, \ldots)$ with appropriate parameters may be assumed and the resulting potential $V(r)$ calculated from Eq. 4–10. The Dirac equations are then solved with this potential inserted, and the energy levels determined. The parameters a, b, c, etc., of the density distribution are adjusted to give agreement between the experimental and theoretically determined energy levels.

At best, the number of nuclear parameters deduced in this way can be only as large as the independent number of levels measured. Actually, when one considers the diminishing sensitivity of the higher energy levels to the nuclear parameters and the limited experimental accuracy, the significant number of parameters deduced is much less. For example, although for most medium and heavy nuclei the $1s_{1/2}$-, $2p_{3/2}$-, and $2p_{1/2}$-levels are accurately determined, information about the $n = 2$ levels becomes sensitive to charge distributions only for $Z \gtrsim 50$. The sensitivity of the fine-structure components $2p_{3/2}$ and $2p_{1/2}$ to the charge distribution is not sufficiently different to yield significant information. For light nuclei, then, only one parameter of the charge distribution (like $\langle r^2 \rangle$) is obtained, whereas for heavier nuclei some additional constraint on $\rho(r)$ can also be found. Typically, a two-parameter Fermi distribution for $\rho(r)$ is assumed. Measurement of the $1s_{1/2}$-level then provides a single relation between the half-density radius c and the surface thickness t, which can be plotted as an isoenergetic contour, as

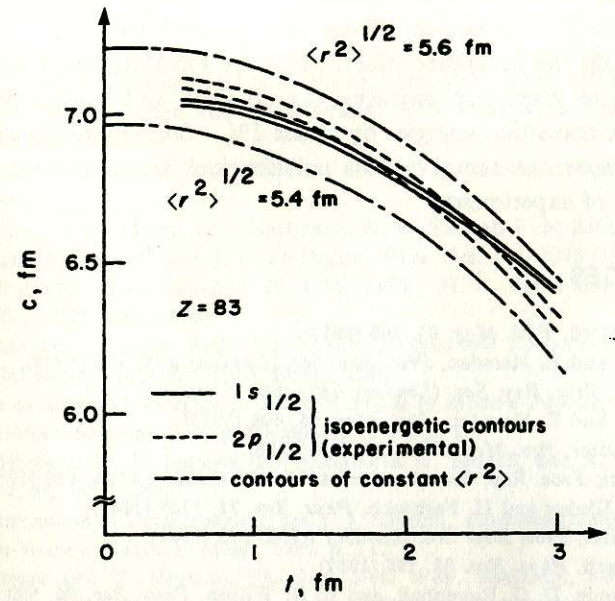

Fig. 4-17 Dependence of the isoenergetic contours of the muonic states on the parameters c and t of the Fermi distribution for the nuclear charge of ^{209}Bi. The contours are for the energies $E(1s_{1/2}) = 5225.5 \pm 3.9$ keV and $E(2p_{1/2}) = 1812.7 \pm 2.7$ keV. The curves for constant $\langle r^2 \rangle^{1/2}$ show that it is determined more accurately than either c or t. [From S. Devons and I. Duerdoth, *Advan. Nucl. Phys.* **2**, 295 (1969).]

shown in Fig. 4–17 for $Z = 83$. Measurement of the $2p$-level gives a different relation between c and t, which is plotted as another contour in the same figure. Intersection of these contours should determine c and t. In practice, however, because of experimental inaccuracies, c and t are determined only within certain limits, with a rather wide variation of t-values possible. In contrast, as is shown in the figure, the value of $\langle r^2 \rangle$ is quite well determined, independently of the $c - t$ combinations permissible by the above procedure. Typically, for the assumed Fermi distribution, c is determined to about $\pm 1\%$ and t to about $\pm 10\%$ for heavy nuclei ($Z \sim 80$). The uncertainties in c and t are strongly correlated, so that a single parameter like $\langle r^2 \rangle^{1/2}$ is found to within about 0.02 fm. In this sense, the accuracy is better than that obtained in the electron-scattering experiments. The results for c and t obtained for heavy nuclei from muonic data are consistent with the electron-scattering results. As already noted, it is often fruitful to analyze the com-

bined muonic X-ray and electron-scattering data to deduce information about the charge distribution, as was done for lead and gold.

Apart from the finite-size effect, which we have discussed, several other effects (such as vacuum polarization, Lamb shift, and nuclear polarization) can alter the transition energies by about 1%. Corrections for these effects (the most important being vacuum polarization) are taken into account in the analyses of experiments.

REFERENCES

1. E. Rutherford, *Phil. Mag.* **21**, 669 (1911).
2. H. Geiger and E. Marsden, *Proc. Roy. Soc.* (*London*) **A82**, 495 (1909).
3. H. Geiger, *Proc. Roy. Soc.* (*London*) **A83**, 482 (1910).
4. H. Geiger and E. Marsden, *Phil. Mag.* **25**, 604 (1913).
5. R. Hofstadter, *Rev. Mod. Phys.* **28**, 214 (1956).
6. N. F. Mott, *Proc. Roy. Soc.* (*London*) **A135**, 429 (1932); **A124**, 426 (1929).
7. W. A. McKinley and H. Feshbach, *Phys. Rev.* **74**, 1759 (1948).
8. R. H. Dalitz, *Proc. Roy. Soc.* (*London*) **A206**, 509 (1951).
9. H. Feshbach, *Phys. Rev.* **88**, 295 (1952).
10. D. R. Yennie, D. G. Ravenhall, and R. N. Wilson, *Phys. Rev.* **95**, 500 (1954).
11. B. Hahn, D. G. Ravenhall, and R. Hofstadter, *Phys. Rev.* **101**, 1131 (1956).
12. D. G. Ravenhall, in *Proceedings of the Williamsburg Conference on Intermediate Energy Physics, 1966.* Quoted in "Muonic Atoms," by S. Devons and I. Duerdoth, *Adv. Nucl. Phys.* **2**, 363 (1969).
13. J. L. Friar and J. W. Negele, *Nucl. Phys.* **A212**, 93 (1973).
14. Y. C. Lin, private communication, as reported by H. A. Bethe, *Phys. Rev.* **167**, 879 (1968).
15. H. A. Bethe and L. R. B. Elton, *Phys. Rev. Lett.* **20**, 745 (1968).
16. J. Heisenberg, R. Hofstadter, J. S. McCarthy, I. Sick, B. C. Clark, R. Herman, and D. G. Ravenhall, *Phys. Rev. Lett.* **23**, 1402 (1969).
17. W. Bertozzi, F. Friar, J. Heisenberg, and J. W. Negele, *Phys. Lett.* **41B**, 408 (1972).
18. K. J. van Oostrum, R. Hofstadter, G. K. Nöldeke, M. R. Yearian, B. C. Clark, R. Herman, and D. G. Ravenhall, *Phys. Rev. Lett.* **16**, 528 (1966).
19. J. B. Bellicard, P. Bounin, R. F. Frosch, R. Hofstadter, J. S. McCarthy, F. J. Uhrhane, M. R. Yearian, B. C. Clark, R. Herman, and D. G. Ravenhall, *Phys. Rev. Lett.* **19**, 527 (1967).
20. R. F. Frosch, R. Hofstadter, J. S. McCarthy, G. K. Nöldeke, K. J. van Oostrum, M. R. Yearian, B. C. Clark, R. Herman, and D. G. Ravenhall, *Phys. Rev.* **174**, 1380 (1968).
21. R. D. Ehrlich, D. Fryberger, D. A. Jensen, C. Nissim-Sabat, R. J. Powers, V. L. Telegdi, and C. K. Hargrove, *Phys. Rev. Lett.* **18**, 959 (1967); **19**, 334(E) (1967).
22. L. R. B. Elton and S. J. Webb, *Phys. Rev. Lett.* **24**, 145 (1970).
23. L. R. B. Elton, *Nuclear Sizes*, Oxford University Press, Oxford, 1961.
24. J. S. McCarthy and I. Sick: their data are displayed in ref. 25.
25. T. W. Donnelly and G. E. Walker, *Phys. Rev. Lett.* **22**, 1121 (1969).

26. R. H. Pratt, J. D. Walecka, and T. A. Griffy, *Nucl. Phys.* **64**, 677 (1965).
27. L. R. Suelzle, M. R. Yearian, and H. Crannel, *Phys. Rev.* **162**, 992 (1967).
28. R. F. Frosch, J. S. McCarthy, R. E. Rand, and M. R. Yearian, *Phys. Rev.* **160**, 874 (1967).
29. B. F. Gibson, A. Goldberg, and M. S. Weiss, *Nucl. Phys.* **A111**, 321 (1968).
30. M. Bouten, M. C. Bouten, and P. van Leuven, *Nucl. Phys.* **A100**, 105 (1967); *Phys. Lett.* **26B**, 191 (1968).
31. J. S. McCarthy, I. Sick, R. R. Whitney, and M. R. Yearian, *Phys. Rev. Lett.* **25**, 884 (1970).
32. J. E. Elias, J. I. Friedman, G. C. Hartmann, H. W. Kendall, P. N. Kirk, M. R. Sogard, L. P. van Speybroeck, and J. K. de Pagter, *Phys. Rev.* **177**, 2075 (1969).
33. C. E. Wiegand, *Phys. Rev. Lett.* **22**, 1235 (1969); H. A. Bethe and P. J. Siemens, *Nucl. Phys.* **B21**, 589 (1970).
34. R. Hofstadter, "Nuclear Radii," in *Nuclear Physics and Technology*, Vol. 2, edited by H. Schopper, Springer-Verlag, Berlin, 1967.
35. See, for example, H. Überall, in *Springer Tracts in Modern Physics*, Vol. 39, edited by G. Höhler, Springer-Verlag, Heidelberg, 1969, p. 18.
36. J. Goldemberg, D. B. Isabelle, D. Vinciguerra, T. Stovall, and A. Bottino, *Phys. Rev. Lett.* **16**, 141 (1965).
37. For a discussion of *Zitterbewegung*, see J. J. Sakurai, *Advanced Quantum Mechanics*, Addison-Wesley, Reading, Mass., 1967, p. 117.
38. M. Gellman and Y. Neeman, *The Eight-Fold Way*, Benjamin, New York, 1964.
39. S. D. Drell and F. Zachariasen, *Electromagnetic Structure of Nucleons*, Oxford University Press, Oxford, 1961, Chap. 1.
40. M. N. Rosenbluth, *Phys. Rev.* **79**, 615 (1960).
41. K. Berkelman, M. Feldman, R. M. Littauer, G. Rouse, and R. R. Wilson, *Phys. Rev.* **130**, 2061 (1963).
42. F. Bumiller, M. Croissiaux, E. Dally, and R. Hofstadter, *Phys. Rev.* **124**, 1623 (1961).
43. J. R. Dunning, K. W. Chen, N. F. Ramsay, J. R. Rees, W. Shlaer, J. K. Walker, and R. Wilson, *Phys. Rev. Lett.* **10**, 500 (1963).
44. T. Janssens, R. Hofstadter, E. Hughes, and M. Yearian, *Phys. Rev.* **142**, 922 (1966).
45. P. Lehmann, R. Taylor, and R. Wilson, *Phys. Rev.* **126**, 1183 (1962).
46. K. W. Chen, A. A. Cone, J. R. Dunning, S. G. T. Frank, N. F. Ramsay, J. K. Walker, and R. Wilson, *Phys. Rev. Lett.* **11**, 561 (1963).
47. V. Z. Jankus, *Phys. Rev.* **102**, 1586 (1956).
48. T. A. Griffy and L. I. Schiff: see the article "Electromagnetic Form Factors," in *High Energy Physics*, Vol. I, edited by E. H. Burhop, Academic Press, New York, 1967.
49. E. B. Hughes, T. A. Griffy, R. Hofstadter, and M. R. Yearian, *Phys. Rev.* **139B**, 458 (1965).
50. C. S. Wu and L. Wilets, *Ann. Rev. Nucl. Sci.* **19**, 527 (1969).
51. V. L. Fitch and J. Rainwater, *Phys. Rev.* **92**, 789 (1953).
52. L. L. Foldy, *Rev. Mod. Phys.* **30**, 471 (1958).
53. J. H. Heisenberg, J. S. McCarthy, I. Sick, and M. R. Yearian, *Nucl. Phys.* **A164**, 340 (1971).
54. S. Galster, H. Klein, J. Mortiz, K. H. Schmidt, D. Wegener, and J. Bleckwenn, *Nucl. Phys.* **B32**, 221 (1971).
55. H. Überall, *Electron Scattering from Complex Nuclei*, Vols. A and B, Academic Press, New York, 1971.

PROBLEMS

4–1. Calculate the magnitude of q (Eq. 4–6) for 60-, 183-, and 550-MeV electrons. For what range of θ would expression 4–7 give cross sections reliable to 10% for 60-MeV electrons on ^{14}N?

4–2. For the density $\rho(r) = \rho_0 \exp(-r/\alpha)$, show that the rms radius $a = \alpha\sqrt{12}$ and that the form factor is $(1 + \alpha^2 q^2)^{-2}$. Find also a and F for a uniform distribution of radius R. For 183-MeV electrons on ^{14}N, compare the cross sections predicted by the two distributions, using the same a for both.

4–3. (a) Show that, if E ($\gg mc^2$) is the laboratory energy of electrons incident on a nucleus of mass M, the nucleus will acquire kinetic energy

$$E_n = \frac{E^2}{Mc^2}\frac{1-\cos\theta}{1+(E/Mc^2)(1-\cos\theta)}.$$

Evaluate this result for ^{40}Ca and 550-MeV electrons.

(b) Describe some processes other than elastic scattering which electrons of high energy would initiate. Draw a schematic curve representing the number of electrons counted versus energy for a fixed angle of scattering for (i) 180 MeV and (ii) 550 MeV.

4–4. The "elastic peak" in electron scattering is broadened and its intensity is reduced by emission of radiation (both real and virtual) by the scattered electrons. The correction for bremsstrahlung is given by

$$I_1 = I\exp(\delta_B),$$

with

$$\delta_B = \frac{t}{\ln 2}\ln\left(\frac{E}{\Delta E}\right),$$

where I_1 is the corrected intensity at energy E, I is the observed intensity, ΔE is the full width of the peak at half-maximum, and t is the target thickness through which the electrons scattered at the specified angle pass. There is also the correction for radiation processes of energy less than $\Delta' E$, where $\Delta' E$ is the smallest energy resolvable from the main peak. This is given by

$$I_0 = I_1\exp(\delta_r),$$

where I_0 is the intensity to be compared with a theory of elastic scattering and

$$\delta_r = \frac{4\alpha}{\pi}\left\{K\left[\ln\left(\frac{2E}{mc^2}\sin\tfrac{1}{2}\theta\right) - \frac{1}{2}\right] + \frac{17}{12}\right\},$$

$$K = \ln\frac{E}{\Delta' E} - \frac{13}{12}, \qquad \alpha = \frac{e^2}{\hbar c}.$$

These formulas are discussed by H. A. Bethe and J. Ashkin, *Experimental Nuclear Physics*, edited by E. Segré (John Wiley, New York, 1953), and by J. Schwinger, *Phys. Rev.* **75**, 898 (1949).

Consider 550-MeV electrons; assume that $\Delta' E = \Delta E = 5$ MeV and calculate δ_r at 30°. Demonstrate that the effect of δ_r on the differential cross section is very slight for angles from $\theta = 30$–$150°$.

4–5. By assuming a trapezoidal density function

$$\rho(r) = \begin{cases} \rho_0, & r < c - \tfrac{1}{2}t, \\ \rho_0\left(\dfrac{1}{2} - \dfrac{r-c}{t}\right), & c - \tfrac{1}{2}t < r < c + \tfrac{1}{2}t, \\ 0, & r > c + \tfrac{1}{2}t, \end{cases}$$

show that $c \sim A^{1/3}$ implies that the density is independent of A to a good approximation inside the core, that is, for $r < c - \frac{1}{2}t$, but that $c - \frac{1}{2}t \sim A^{1/3}$ would not have this implication.

4–6. It might be possible to discover by electron-electron scattering whether the apparent structure of the proton is in part a reflection of the breakdown of the Coulomb law. What velocity would be necessary in the center-of-mass system? What energy would be required in the laboratory system?

4–7. Deduce Eq. 4–33, recalling that

$$\int |\psi_0|^2\, d\Omega\, r^2\, dr = \left(\frac{2\alpha Z\mu c}{\hbar}\right)^{2\sigma+1}[(2\sigma)!]^{-1}\int_0^\infty r^{2\sigma-2}\exp\left(\frac{-2\alpha Z r\mu c}{\hbar}\right) r^2\, dr,$$

$$\nabla^2 r^\lambda = \lambda(\lambda+1)r^{\lambda-2},$$

and $\int (U\nabla^2 V - V\nabla^2 U)\, dr = 0$ if V vanishes sufficiently quickly at large r.

The experimental values of the $2p \to 1s\mu^-$ X-rays in titanium and copper are 0.995 and 1.548 MeV, respectively [51]. Show that the values for point nuclei are 1.045 and 1.826 MeV and use the above equation to deduce the value of R, the radius of the equivalent uniform well, in each case.

4–8. Consider a charge density defined by

$$\rho(r) = \rho_0 f(x) = \frac{1}{1-\frac{1}{2}e^{-n}}\begin{cases} 1 - \frac{1}{2}e^{-n}e^{x}, & x \leqslant n, \\ \frac{1}{2}e^{n}e^{-x}, & x \geqslant n; \end{cases}$$

$$x = \frac{nr}{c}.$$

Show that, as n varies from 0 to ∞, this shape varies from exponential through Gaussian and Fermi shapes to a uniform density. Show also that $n = 2\ln 5(c/t)$, where c is the half-density radius and t is the thickness parameter.

This is family II of a set of functions ρ considered by D. L. Hill and K. W. Ford, *Phys. Rev.* **94**, 1617 and 1630 (1954). Use Eq. 34 of their second

paper and the integrals given for family II(a) in their appendices to show that, for $A \gtrsim 12$, it is a good approximation to write

$$\frac{Ec}{(Ze)^2} = \frac{3}{5}\frac{1}{c}(1+6n^{-2})^{-1}\left[1 - \frac{n^{-2}}{1+6n^{-2}}\left(1 - \frac{75}{8n} + \frac{15}{n^2} - \frac{315}{16}\frac{1}{n^3}\right)\right].$$

4–9. (a) Consider electron-proton scattering at an incident electron energy E_e so high that we can write $E_e = p$ (we use units $c = \hbar = 1$ here), where p is the magnitude of its three-momentum. Then show that the quantity q_μ^2, defined in Eq. 4–19, is given by

$$q_\mu^2 = 4E_eE_e' \sin^2\frac{\theta}{2},$$

where E_e' is the energy of the electron scattered at an angle θ.

(b) Using the result of Problem 4–3a, show that

$$q_\mu^2 = \frac{4E_e^2 \sin^2\theta/2}{1 + (2E_e/M)\sin^2\theta/2}.$$

Note that $q_\mu^2 \geqslant 0$.

4–10. In a very simple model of the nucleus, assume that each nucleon is moving in the field of a common central one-body potential. Then the spatial wave function of a nucleon may be written as

$$\phi_{nlm}(\mathbf{r}) = R_{nl}(r)Y_l^m(\hat{r}), \tag{1}$$

where n, l, and m are the principal, orbital, and azimuthal quantum numbers, respectively, of a nucleon; and $R_{nl}(r)$ is the radial and Y_l^m the angular wave function (defined in Eq. A–13a). If, in a given shell (defined by n, l), all the azimuthal states are occupied, the shell is called closed. For such a closed-shell nucleus, show that the single-particle proton density ρ is spherically symmetric:

$$\rho = 2\sum_{\substack{n,l\\ \text{occupied}}} \frac{2l+1}{4\pi}[R_{nl}(r)]^2. \tag{2}$$

If one assumes a harmonic-oscillator potential $\frac{1}{2}M\omega^2r^2$ for the one-body potential, then $[\alpha = (M\omega/\hbar)^{1/2}]$

$$R_{nl}(r) = \sqrt{\frac{2n!\alpha^3}{\Gamma(n+l+\frac{3}{2})}}(\alpha r)^l \exp(-\tfrac{1}{2}\alpha^2r^2)\, L_n^{l+1/2}(\alpha^2r^2), \tag{3}$$

where the associated Laguerre polynomial is defined by

$$L_n^\beta(x) = \sum_{m=0}^{n} \frac{(n+\beta)!}{(n-m)!(\beta+m)!}\frac{(-x)^m}{m!}, \tag{4}$$

which yields, for example,

$$L_0^{1/2} = 1, \qquad L_0^{3/2} = 1,$$
$$L_1^{1/2} = \tfrac{3}{2} - x, \quad L_1^{3/2} = \tfrac{5}{2} - x,$$
$$L_2^{1/2} = \tfrac{15}{8} - \tfrac{5}{2}x + \tfrac{1}{2}x^2, \quad \text{etc.}$$

Assuming, for ^{16}O, that there are two protons in the $1s$ ($n = 0$, $l = 0$) and six in the $1p$ ($n = 0$, $l = 1$) state, show, using Eqs. 2 and 3, that the proton density is

$$\rho(r) = \frac{2\alpha^3}{\pi\sqrt{\pi}}\exp(-\alpha^2r^2)(1 + 2\alpha^2r^2). \tag{5}$$

If the form factor $F(q)$ is defined by

$$F(q) = 4\pi\int_0^\infty \rho(r)j_0(qr)r^2\,dr,$$

show that the form factor $F(q)$ for the ^{16}O-distribution (Eq. 5) is

$$F(q) = \exp\left(-\frac{q^2}{4\alpha^2}\right)\left(8 - \frac{q^2}{\alpha^2}\right), \tag{6}$$

which shows that $F^2(q)$ has only one minimum. Note that this is not true if the nucleons are assumed to move in a finite potential, in which case the tail of the density distribution decays exponentially.

4–11. Isotope shift in atomic X-rays.

From the expression for the orbital radius of an electron given in Table 4–2, show that the lowest electron orbital radius in a heavy atom is about 100 times larger than the nuclear radius R. Even then, the electronic binding energy would undergo a small shift because of the finite size of the nucleus, and the shifts for two different isotopes would not be the same. This is called the isotope shift in X-rays.

A rough estimate of this effect may be made by making the following simplifying assumptions:

1. Screening effects are identical for the two isotopes and cancel out in the isotope shift.

2. The nuclear charge distribution is uniform over a radius R with sharp cutoff, and $R = 1.2A^{1/3}$ fm.

3. The nonrelativistic electronic wave function for a point nucleus is used for a first-order perturbation calculation of the effect. For the lowest electronic state, this wave function is

$$u_0 = \frac{\gamma^{3/2}}{\sqrt{\pi}}\exp(-\gamma r), \qquad \gamma = Z\frac{me^2}{\hbar^2},$$

and the unperturbed energy is

$$E_0 = -\tfrac{1}{2}Z^2\frac{me^4}{\hbar^2}.$$

(a) Using Eq. 4–10, show that the potential energy of an electron in the field of the nucleus is

$$V(r) = -\frac{Ze^2}{r} \qquad \text{for} \quad r > R$$

$$= \frac{Ze^2}{R}\left(\frac{r^2}{2R^2} - \frac{3}{2}\right) \qquad \text{for} \quad r < R.$$

(b) Using perturbation theory, show that the energy shift in the lowest state due to the finite nuclear size is

$$\Delta E = \frac{4Ze^2}{R}\gamma^3 \int_0^R \left(\frac{r^2}{2R^2} - \frac{3}{2} + \frac{R}{r}\right)\exp(-2\gamma r)\, r^2\, dr.$$

(c) Even for heavy atoms $\gamma R \ll 1$, and we may replace the exponential $\exp(-2\gamma r)$ by unity in the above integrand. Show that

$$\Delta E \approx \frac{4}{5} Z^2 |E_0| \left(\frac{R}{a_0}\right)^2,$$

where $a_0 = \hbar^2/me^2$. This shows that $\Delta E \propto Z^4$. For Tl ($Z = 81$), check that this expression yields $\Delta E = 8.25$ eV.

(d) The isotope shift S in K X-ray between ${}^{203}_{81}$Tl and ${}^{205}_{81}$Tl may be found from

$$S = \frac{d}{dR}\Delta E \cdot \frac{dR}{dA} \cdot \Delta A.$$

Show that

$$S = \frac{2}{3}\frac{\Delta A}{A} \cdot \Delta E.$$

The isotope shift S between ${}^{203}_{81}$Tl and ${}^{205}_{81}$Tl is thus only of the order of 0.05 eV.

Chapter 5

Internucleon Forces: II

5-1 ELECTROMAGNETIC MOMENTS OF THE DEUTERON AND TENSOR FORCES

The deuteron has been observed to have an electric quadrupole moment $Q = 0.2860 \pm 0.0015$ fm^2 [1, 2] and a magnetic moment $\mu_d = 0.857406 \pm 0.000001$ [3]. Its total angular momentum $J = 1$. We saw in Chapter 2 that the binding energy and angular momentum are consistent with the assumption that the deuteron is in a ${}^3S_1$-state. However, a system in an S-state can have no quadrupole moment, since its wave function has no angular dependence and the density distribution is therefore isotropic. For two spin-$\frac{1}{2}$ particles whose total angular momentum is 1, the only possible angular-momentum states are ${}^1P_1$, ${}^3S_1$, ${}^3P_1$, ${}^3D_1$. For central forces, the magnitude of the orbital angular momentum is a constant of motion, but if we consider noncentral forces it is possible to have a combination of states with different values of L but the same J. If parity is to be a good quantum number, we may combine only states of the same parity. Therefore, in addition to the states of definite $\mathbf{L}^2$, we should consider the possible deuteron wave functions,

$$\psi(SD) = \cos\omega\psi({}^3S)^1(\tau)_0 + \sin\omega\psi({}^3D)^1(\tau)_0, \tag{5–1a}$$

$$\psi(PP) = \cos\omega\psi({}^1P)^1(\tau)_0 + \sin\omega\psi({}^3P)^3(\tau)_0. \tag{5–1b}$$

The amount of mixing of the individual states is described by the parameter ω, which is introduced in the form of trigonometric functions, so that $\psi(SD)$ and $\psi(PP)$ are automatically normalized to unity. Both wave functions

describe states in which a measurement of J will yield the value 1, but in the state described by Eq. 5–1a a measurement of L will sometimes yield 0 and sometimes 2, the respective probabilities being $\cos^2\omega$ and $\sin^2\omega$. Similarly, in the state of Eq. 5–1b, a measurement of S yields 0 or 1 with respective probabilities $\cos^2\omega$ and $\sin^2\omega$. The choice among the five possible alternatives for a pure ^3S-state is determined by the value of the magnetic moment.

To calculate the magnetic moment of the deuteron, we make use of the Sachs formula, given in Problem 3–4:

$$[\langle M_z\rangle_{T_3} + \langle M_z\rangle_{-T_3}] = (\tfrac{1}{2} + \mu_s)J + \frac{1}{J+1}(\mu_s - \tfrac{1}{2})\langle \mathbf{S}^2 - \mathbf{L}^2\rangle, \quad (5\text{–}2)$$

where $\mu_s = (\mu_p + \mu_n)$ is the isoscalar part of the nucleon magnetic moment. Noting that for the deuteron $T_3 = 0$, $J = 1$, we immediately get its magnetic moment operator in nuclear magnetons as

$$\mu_d = \tfrac{1}{2}[(\tfrac{1}{2} + \mu_s) + \tfrac{1}{2}(\mu_s - \tfrac{1}{2})(\mathbf{S}^2 - \mathbf{L}^2)]. \quad (5\text{–}3)$$

When μ_d acts on a state of fixed S and L, the operators $\mathbf{S}^2$ and $\mathbf{L}^2$ are to be replaced by the values $S(S+1)$ and $L(L+1)$.

For various possible states the results are as follows:

$$\begin{aligned}
&^1P_1: && \mu_d = \tfrac{1}{2},\\
&^3S_1: && \mu_d = \mu_s = 0.879,\\
&^3P_1: && \mu_d = \tfrac{1}{2}(\mu_s + \tfrac{1}{2}) = 0.689,\\
&^3D_1: && \mu_d = \tfrac{1}{2}(-\mu_s + \tfrac{3}{2}) = 0.310,\\
&^3S + {}^3D: && \mu_d = 0.879 - 0.569\sin^2\omega,\\
&^1P + {}^3P: && \mu_d = 0.500 + 0.189\sin^2\omega + 3.327\sin 2\omega \int {}^1f\,{}^3f\,dr. \quad (5\text{–}4)
\end{aligned}$$

In the last of these equations ${}^1f(r)/r$ and ${}^3f(r)/r$ are the radial wave functions in the $^1P_1$- and $^3P_1$-states, respectively.

Only the last two states are capable of yielding the experimental value of 0.857, and the P-state is ruled out by later considerations. At least, this is true if we ignore the possibility of very strong velocity-dependent forces or very considerable meson-exchange magnetic moments. As indicated in Chapter 3, these are not thought to be very large. If all such corrections are ignored, we see from Eq. 5–4 that the deuteron magnetic moment is

$$\mu_d = 0.879 - 0.569\sin^2\omega, \quad (5\text{–}5)$$

and a value of $\sin^2\omega = 0.04$, that is, a D-state admixture of 4% is needed to give the experimental value of 0.857 nuclear magneton. Note that in Eq. 5–5 only the isoscalar part of the nucleon magnetic moment is involved, and also that an increase in the D-state probability would reduce the magnetic moment. We shall see in the next section that a variety of other experimental data, like those on nucleon-nucleon scattering and the deuteron electromagnetic form factor, as well as results on elastic π-d scattering, indicate that a D-state admixture of about 6–7% is present in the deuteron. This implies that Eq. 5–5 for μ_d must be corrected for meson-exchange currents and other relativistic effects, which must contribute positively to the deuteron magnetic moment to offset the effect of the increase in the D-state probability to more than 4%.

The calculation of the quadrupole moment of the deuteron is straightforward. The wave function (Eq. 5–1a) can be written as

$$\psi(SD) = \frac{1}{r}[\cos\omega\, f_S(r)\mathscr{Y}^1_{1,10} + \sin\omega\, f_D(r)\mathscr{Y}^1_{1,12}], \quad (5\text{–}6)$$

where $\mathscr{Y}^M_{J,SL}$ is an angular-momentum function, and $f_S(r)$ and $f_D(r)$ are the radial parts of the wave functions, normalized so that $\int_0^\infty f(r)\,dr = 1$. In these expressions, r is the neutron-proton distance, and therefore expression 3–7b yields

$$Q = \left(\frac{16\pi}{5}\right)^{1/2}\int |\psi(SD)|^2\left(\frac{r}{2}\right)^2 Y_2^0\,dV, \quad (5\text{–}7)$$

which leads to

$$Q = \tfrac{1}{10}\left[\sqrt{2}\cos\omega\sin\omega\int f_S(r)f_D(r)r^2\,dr - \tfrac{1}{2}\sin^2\omega\int f_D^2(r)r^2\,dr\right]. \quad (5\text{–}8)$$

We note that a pure D-state would have a negative Q, but if the relative phase of the S- and D-wave functions is positive, a positive Q can be obtained. Indeed, for $\sin^2\omega \sim 0.04$, the leading term of Eq. 5–8 is the more important one, and the observed value of Q requires that $\int f_S f_D r^2\,dr \sim 10 \times 10^{-26}\ \text{cm}^2$. Since low values of r will contribute little to this integral, the wave function should have a range of 4 or 5 fm. This is quite consistent with the size of the deuteron suggested in Chapter 2, where we saw that outside an effective range of about 1.7 fm the deuteron wave function decays like $e^{-\gamma r}$, with $1/\gamma = 4.31$ fm, the latter value often being loosely referred to as the "radius

of the deuteron." It will be realized that the deuteron is a quite loosely bound nucleus with a large radius comparable to that of a nucleus with as many as 20 nucleons.

Since Q is not subject to uncertain small corrections, as is the magnetic moment, it might be thought that the values of Q would allow a more precise estimate of the percentage of D-state in the wave function. However Eq. 3–29 shows that such a calculation requires knowledge of the radial wave functions, which in turn can be determined only if the nucleon forces are known in some detail. If a specific nucleon force is proposed, both Q and ω can be calculated; the experimental value of the former provides a fairly precise datum which the suggested interaction must fit, but the latter is only roughly fixed by the magnetic moment.

The type of nucleon forces that we have so far considered are essentially central and cannot mix orbital angular momenta. We can generalize the forces by considering velocity-dependent forces or, as we remarked in Section 2–2, by taking a force dependent on the angles between the spin vectors and the join of the two nucleons. A possible noncentral potential which can be formed from the three vectors $\boldsymbol{\sigma}_1$, $\boldsymbol{\sigma}_2$, and $\mathbf{r} = r\hat{\mathbf{r}}$ is

$$V_T = V_T(r)(3\boldsymbol{\sigma}_1 \cdot \hat{\mathbf{r}}\, \boldsymbol{\sigma}_2 \cdot \hat{\mathbf{r}} - \boldsymbol{\sigma}_1 \cdot \boldsymbol{\sigma}_2) = V_T(r) S_{12}. \tag{5–9}$$

The subscript T is used because this potential is called the *tensor* interaction; it is actually a scalar product of two second-rank tensors. It can be demonstrated that this and the exchange potentials considered in Chapter 2 are the only velocity-independent potentials for two nucleons which conserve energy, momentum, total angular momentum, parity, and charge.† Since $\mathbf{L}^2$ does not commute with S_{12}, the addition of a potential of this form to the Hamiltonian will mean that $\mathbf{L}^2$ is not a constant of motion and that the states are mixtures of states of different L-values, for example, a mixture of S- and D-states. Consequently the tensor force is capable of explaining the deuteron quadrupole moment. On the other hand, $S^2 = (\boldsymbol{\sigma}_1 + \boldsymbol{\sigma}_2)^2$ does commute with V_T, and S_{12} applied to a singlet wave function gives zero, with the result that a tensor force couples together neither singlet and triplet states nor different singlet states. We may also note that it conserves parity and couples together only states that are both of even L or both of odd L.

The effect on the deuteron quadrupole moment can be understood in a qualitative way by treating the spins classically. In the triplet state they

† The simplest kind of velocity-dependent force, namely an $\mathbf{L} \cdot \mathbf{S}$-force, does not mix states of different L. Whether or not there are such forces in the nuclear interaction, the deuteron properties show that another type of noncentral force is also present.

are then parallel, and if each makes an angle θ with $\mathbf{r}$, we have

$$V_T = V_T(r)(3\cos^2\theta - 1). \tag{5–10}$$

The corresponding force, $-$ grad V, has a component in the direction of increasing θ equal to $(6/r)V_T(r)\cos\theta\sin\theta$. If $V_T(r)$ is negative, this force will move the vector $\mathbf{r}$ to angles near the z-axis, that is, it will tend to concentrate the motion near $\theta = 0$ and π. Hence, if the other forces by themselves were to produce an S-state, the addition of a small tensor force would modify the density, so that instead of being isotropic it would be peaked along the axis ($Q > 0$). However, if the system were in a pure D-state under central forces, the density (proportional to $\sin^4\theta$) would be greatest perpendicular to the axis ($Q < 0$). The addition of the tensor force with $V_T < 0$ would then reduce the magnitude of this negative quadrupole moment. These effects are seen to correspond to the values of Q which are predicted by Eq. 5–8 for a mixed S- and D-state, provided that $\cos\omega\sin\omega > 0$. In other words, a tensor force with $V_T < 0$ produces a state in which the wave functions of the S- and D-states are mixed with coefficients of the same sign, and it is clearly possible, by adjusting the parameters in $V_T(r)$ (of which there must be at least two), to obtain values of Q and ω consistent with experiment.

The quantitative calculation requires the solution of the wave equation:

$$-\nabla^2\psi + (V_{te}(r) + V_T(r)S_{12})\psi = -\gamma^2\psi, \tag{5–11}$$

where $(\hbar^2/M)V_{te}$ is the central potential in triplet even states, $(\hbar^2/M)V_T$ is the tensor potential, and $(\hbar^2/M)\gamma^2$ is the binding energy of the deuteron. Equation 5–11 is simplified by writing ψ in the form of Eq. 5–6, multiplying in turn on the left by $\mathscr{Y}^1_{1,10}$ and $\mathscr{Y}^1_{1,12}$, and using their orthogonality, together with the matrix elements of S_{12} found in Problem 5–2, namely,

$$(\mathscr{Y}^1_{1,10}|S_{12}|\mathscr{Y}^1_{1,10}) = 0, \qquad (\mathscr{Y}^1_{1,12}|S_{12}|\mathscr{Y}^1_{1,12}) = -2,$$
$$(\mathscr{Y}^1_{1,12}|S_{12}|\mathscr{Y}^1_{1,10}) = \sqrt{8}.$$

The results are:

$$\frac{d^2 f_S}{dr^2} - (\gamma^2 + V_{te})f_S = \sqrt{8}\, V_T \tan\omega\, f_D, \tag{5–12a}$$

$$\frac{d^2 f_D}{dr^2} - \left(\gamma^2 + V_{te} + \frac{6}{r^2} - 2V_T\right) f_D = \sqrt{8}\, V_T \cot\omega\, f_S. \tag{5–12b}$$

These radial wave equations are referred to as "coupled", they show that, if a tensor force exists, the system cannot have a fixed L-value, since

nonzero values of $\cos \omega f_S$ require nonzero values of $\sin \omega f_D$, and vice versa. At distances greater than the range of nucleon forces, the equations are uncoupled, and the wave functions for a bound state can be written explicitly as

$$f_S = N_S e^{-\gamma r}, \tag{5–13a}$$

$$f_D = N_D e^{-\gamma r}\left(1 + \frac{3}{\gamma r} + \frac{3}{\gamma^2 r^2}\right), \tag{5–13b}$$

for r such that V_T and $V_{te} \ll \gamma^2$. The quantities N_S and N_D are normalizing constants. In addition to satisfying these equations for large r, f_S and f_D must also vanish at the origin or, if one postulates an impenetrable core, at the core radius. For a given set of potentials V_{te} and V_T, these conditions constitute an eigenvalue problem for the binding energy (γ^2) and the proportion of D-state ($\sin^2 \omega$). When these values are found and f_S and f_D are known, the quadrupole moment can be calculated in accordance with Eq. 5–8. The values of γ^2 and Q, and to a lesser degree the value of $\sin^2 \omega$, provide quantities for comparison with experiment, on the basis of which the proposed potentials may be rejected or tentatively accepted. A further test is supplied by the predicted triplet scattering cross section. In a scattering experiment, the wave functions will satisfy equations like 5–12 with $-\gamma^2$ replaced by k^2 and with asymptotic forms of f_S and f_D appropriate to a scattering problem.

The eigenvalue equations 5–12 cannot be solved analytically even for simple square-well potentials. The first numerical calculations were done by Rarita and Schwinger [4], who took V_T and V_{te} to be square-well potentials of the same range but different depths. A large variety of potentials can yield the experimental binding energy, the magnetic dipole moment, and the electric quadrupole moment of the deuteron, provided that the tensor force is strong and has a range comparable to that of the central part. Although the admixture of D-state is only a few per cent, the tensor force makes a substantial contribution to the binding energy. We shall see in a later section that the long-range part of the two-nucleon force is given by the one-pion-exchange potential, which for the triplet-even state is given by

$$-V_0\left[1 + \left(1 + \frac{3}{x} + \frac{3}{x^2}\right)S_{12}\right]\frac{e^{-x}}{x},$$

with $x = r/1.41$ fm, and $V_0 = 11$ MeV. This prediction is modified for $r < 3$ fm by two-meson terms, but it is the outer region which mainly controls a low-energy system such as the deuteron. It will be observed that

for $x = 1$ the tensor force is 10 times the central, and even for $x = 3$, at which distance the nuclear force has become quite small, the tensor force is still twice the central force, allowing for the value of S_{12}. Most modern potentials contain the one-pion-exchange tail and fit the deuteron data.

TABLE 5-1 Deuteron Properties of Some Potentials

Potential	Ref.	Per cent D-state	Predicted magnetic moment in nuclear magnetons	Predicted quadrupole moment, fm²
Hamada-Johnston	36	6.96	0.840	0.281
Feshbach-Lomon	42	4.31	0.854	0.268
Reid hard-core	39	6.50	0.842	0.277
Reid soft-core	39	6.47	0.842	0.280
Ueda-Green	58	5.5	0.856	0.280
Experimental			0.857406 ± 0.000001	0.282 ± 0.002[a]

[a] This was the accepted experimental value of Q before 1972, which the potential models attempted to reproduce. The current value of Q is 0.2860 ± 0.0015 fm² [2].

In Table 5–1, the low-energy properties of some of these potentials are listed. These potentials also fit the high-energy phase-shift data and are described in some detail in Sections 5–8 and 5–12. Table 5–1 illustrates the

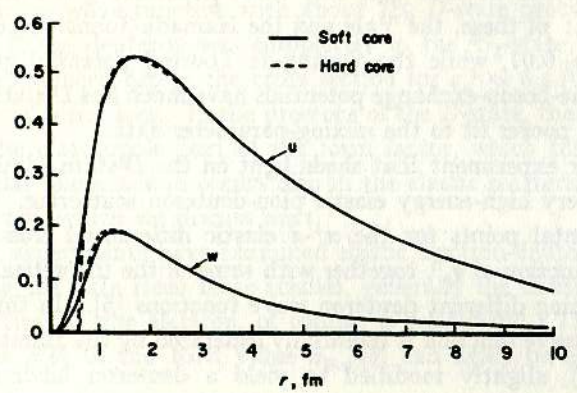

Fig. 5-1 Normalized deuteron wave functions for the Reid soft-core and hard-core potentials [39].

points that the low-energy parameters of the deuteron do not determine a unique potential and that the percentage of D-state admixture (and therefore the central-to-tensor ratio) can vary from potential to potential, even after roughly fitting the deuteron data. We discuss this question in more detail in the next section.

The normalized deuteron wave functions $\cos\omega f_S(r)$ and $\sin\omega f_D(r)$ for the Reid hard-core and soft-core potentials [39] are sketched in Fig. 5–1. Note that the S-state wave function is not negligible even at a distance of 10 fm!

5-2 THE D-STATE ADMIXTURE IN THE DEUTERON- AND MESON-EXCHANGE CURRENTS

We stated in Section 5–1 that a variety of experiments indicate that the D-state probability in the deuteron is in the range of 6–7%. We now briefly list some of these approaches.

1. The most direct method of obtaining information about the nuclear force is to perform nucleon-nucleon scattering, a subject that we shall study in detail in this chapter. The characteristics of the n-p force in the $T = 0$, $J = 1$ channel can be extracted from the scattering data by phase-shift analysis. A measure of the strength of the tensor force is the mixing parameter ε_1 (see Section 5–5), which indicates the proportion of the $^3S_1$- and the $^3D_1$-states in the triplet state. In Fig. 5–18, we show some experimentally determined values of the mixing parameter as a function of the laboratory energy, together with the values computed from various phenomenological potentials. It will be seen that only three potentials give some agreement with the data: of these, the Yale and the Hamada-Johnston potentials also yield $\sin^2\omega \approx 0.07$, while the Sprung-de Tourreil potential gives ≈ 0.05. Most of the one-boson-exchange potentials have much less D-state probability and also give poorer fit to the mixing-parameter data.

2. Another experiment that sheds light on the D-state admixture in the deuteron is very high-energy elastic pion-deuteron scattering. In Fig. 5–2, the experimental points for the π^+-d elastic differential cross section are shown as a function of q_μ^2, together with some of the theoretically predicted results, assuming different deuteron wave functions [5]. In this figure, the Humberston wave function is essentially generated by the Hamada-Johnston potential [36], slightly modified to yield a deuteron binding energy of 2.226 MeV (the H-J potential gives 2.27 MeV) and $\sin^2\omega = 0.06953$. The wave function GK8 is generated by potential 8 of Glendenning and Kramer [6]; it has a hard core of 0.5 fm and gives $\sin^2\omega = 0.05622$. Each of the

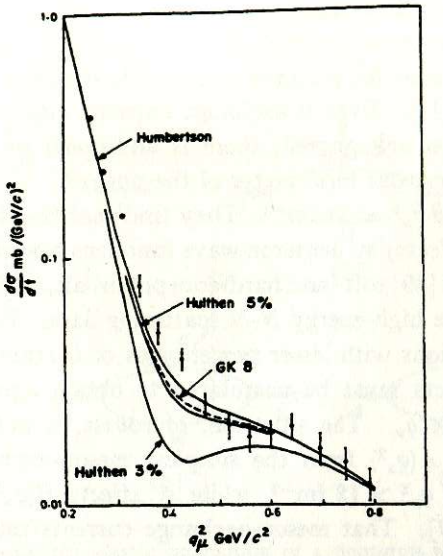

Fig. 5-2 Differential cross section for elastic π^+-d scattering for pions of momentum 3.75 GeV/c, plotted against q_μ^2. The theoretical curves are obtained using the Glauber formalism for high-energy scattering [5], employing different deuteron wave functions of varying D-state probability (see text).

two Hulthen wave functions have a hard core of 0.43 fm, with $\sin^2\omega = 0.03$ and 0.05. The radial dependence of $f(r)$ in the Hulthen wave function is simply the difference of two exponentials of differing range, with the longer one corresponding to the binding energy. It will be seen from Fig. 5–2 that the Humberston wave function with about 7% D-state probability fits the data best. If the deuteron was completely in the $^3S_1$-state, theory would predict a pronounced dip in the cross section for $q_\mu^2 \approx 0.4$ (GeV/c)^2, which is experimentally not seen. In the presence of the D-state, there is scattering also from the quadrupole part of the form factor, which fills up this dip. A very similar phenomenon occurs also in the elastic scattering of electrons from deuterons, which we discuss next.

3. Other experiments have examined elastic electron-deuteron scattering. In analyzing the data from these studies, generally the deuteron is treated nonrelativistically; the electron, of course, is relativistic. The ratio of the cross section $\sigma(\theta)$ to the Mott value $\sigma_{\text{Mott}}(\theta)$ can again be expressed as in Eq. 4–27:

$$\frac{\sigma(\theta)}{\sigma_{\text{Mott}}(\theta)} = \left[A(q_\mu^2) + B(q_\mu^2)\tan^2\frac{\theta}{2}\right],$$

where $A(q_\mu^2)$ contains dominantly the electric monopole and quadrupole form factors of the deuteron (multiplied by the isoscalar electric form factor of the nucleon to account for its finite size), while $B(q_\mu^2)$ is the contribution of the magnetic part [7]. Even if exchange currents and relativistic corrections for the deuteron are ignored, there is additional uncertainty due to the presence of the isoscalar form factor of the nucleon. Elias et al. [8] have measured $A(q_\mu^2)$ up to $q_\mu^2 = 34\ \text{fm}^{-2}$. They find that the data can be fitted (ignoring exchange effects) by deuteron wave functions generated by Hamada-Johnston [36] or Reid [39] soft- and hard-core potentials, which have $\sin^2\omega \approx 0.065$–$0.07$ and fit the high-energy N-N scattering data. For other types of deuteron wave functions with lesser percentages of D-state, relatively large meson-exchange effects must be postulated to obtain agreement with the electric data for large q_μ. The situation, of course, is not very clear cut. The contribution to $A(q_\mu^2)$ from the simplest meson-exchange currents is appreciable only for $q_\mu^2 > 12\ \text{fm}^{-2}$, while it affects $B(q_\mu^2)$ even for very small values of q_μ^2 [7]. That meson-exchange currents must be important for the magnetic part is clear even from the static magnetic moment of the deuteron: a 7% D-state yields a static magnetic moment of 0.840 nm in the absence of exchange effects, compared to the experimental value of 0.857 nm. It is found [7] that this discrepancy for $B(q_\mu^2)$ increases with higher values q_μ^2, the experimental points lying above the ones calculated using deuteron wave functions with 7% D-state and ignoring exchange currents. Summarizing the above statements, we may remark that the electric form factor of the deuteron favors a 6–7% D-state probability, that the behavior of the magnetic form factor clearly points to meson-exchange currents, and finally that the correction due to such currents should be very small for $A(q_\mu^2)$ and should be appreciable only for $B(q_\mu^2)$.

We now explain very briefly the simplest meson-exchange currents that are of importance to the deuteron. As discussed in Section 4–3, an electron can interact with a nucleon by the exchange of a virtual photon—the photon carries an electromagnetic field (or four-potential A_μ) which couples with the nucleonic current. In the deuteron, there are two nucleons, each clothed with its meson cloud. The photon can couple to either one or the other nucleon; it can also couple, as shown in Fig. 5–3a, to a charged pion which is being exchanged between the two nucleons. Since the deuteron has i-spin $T = 0$, it is not difficult to show, however, that this simplest process with the π-π-γ vertex does not contribute to the deuteron form factor. It is desirable to express the pionic exchange current in terms of nucleon variables

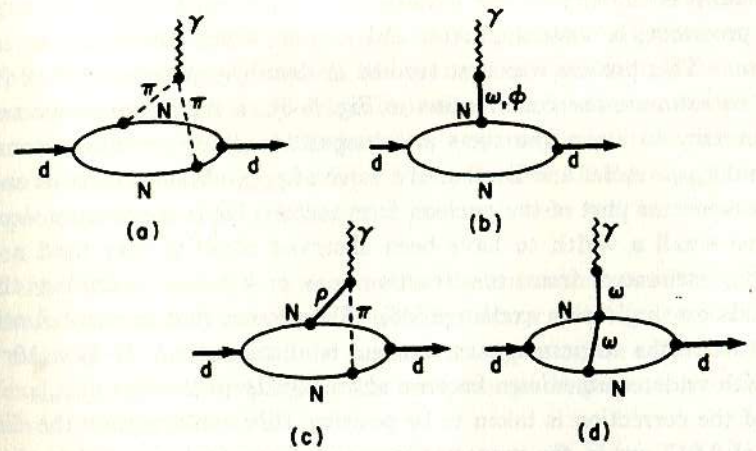

Fig. 5-3 Diagrams for the elastic interaction of a deuteron with an electromagnetic field. Note that (a) is forbidden; (b) is included in the form factor of the nucleon; (c) represents the simplest exchange-current contribution; and (d) is a double-scattering process.

by integrating over the intermediate states. Such a procedure [65] yields for the one-pion exchange current a term proportional to $(\boldsymbol{\tau}_1 \times \boldsymbol{\tau}_2)_3$. This has zero matrix elements between states of the same T. For $T = 0$ states, this is because the current is an isovector, for $T = 1$ states it follows from symmetry under exchange of particles 1 and 2. This exchange current does contribute to electromagnetic transitions between $T = 0$ and $T = 1$ states, such as the photodisintegration of the deuteron. Of course, charged pionic exchange contributes to the nuclear force in $T = 0$ as well as $T = 1$ states; indeed it gives a dependence $\boldsymbol{\tau}_1 \cdot \boldsymbol{\tau}_2$ in the nucleon variables.

The formal result that the one-pion exchange current gives no contribution to matrix elements diagonal in T may appear intuitively reasonable from the following physical picture. Consider each nucleon in a neutron-proton system as spending half its time in each charge state, with the result that positive and negative virtual pions are emitted in such a way that the net charged pionic current is zero. However, the result does, of course, involve a sum over intermediate quantum states and their relative phases are significant, and are such that a contribution arises for matrix elements between two-nucleon states that are not diagonal in T.

The simplest exchange-current contribution is shown in Fig. 5–3c, where a virtual ρ is emitted by one nucleon, it interacts with the electromagnetic field producing a virtual photon and a pion which lands on the second nucleon. This process was first studied in detail by Adler and Drell [9]. In order to estimate the contribution of Fig. 5–3c to the magnetic moment, it is necessary to know the signs and magnitudes of the coupling constants $g_{\rho\pi\gamma}$ and $g_{\rho NN}$. Adler and Drell used a value of $g_{\rho NN}$ obtained from an analysis of the isovector part of the nucleon form factor. Since the decay $\rho \to \pi + \gamma$ has too small a width to have been observed directly, they used a value for $g^2_{\rho\pi\gamma}$ estimated from the reaction $\gamma + p \to p + \rho$, assuming that it proceeds by single pion exchange [66]. They found that the contribution of Fig. 5–3c to the static magnetic moment is of the order of (1–2) $\times 10^{-2}$ nm, but with undetermined sign because of ambiguity in the sign of $g_{\rho\pi\gamma}$. If the sign of the correction is taken to be positive, this would explain the discrepancy of 0.017 nm in the magnetic moment of the deuteron that is obtained with 7% D-state.

Although this simple meson-exchange current is also able to improve the fit with $B(q_\mu^2)$, it is possible that many other more complicated processes are also important. For one thing, the simple diagram 5–3c seems to make the fit of $A(q_\mu^2)$ poorer for $q_\mu^2 > 14$ fm^{-2} [7], although its effect on the static quadrupole moment is very small. Blankenbecler and Gunion [10] have recently considered the double-scattering process of Fig. 5–3d, which is not an exchange-current effect. It seems to yield a good fit to the form-factor data of the deuteron (including the magnetic part) with 7% D-state.

Summarizing the present section, it seems reasonable to say that current experimental data favor 6–7% D-state probability in the deuteron wave function, with meson-exchange currents giving important corrections to the magnetic moment and the magnetic form factor.

5-3 THE NUCLEAR FORCE AND GENERAL FEATURES OF HIGH-ENERGY SCATTERING

The nuclear force between two nucleons may be regarded as arising from the exchanges of mesons between them. This basic idea, due to Yukawa [11], is in analogy to the electromagnetic case, where the Coulomb force is regarded as arising from a photon exchange between two charged particles. From the field-theoretical point of view, there is an interaction between the meson and nucleon fields, which gives rise to processes like $N \to N + \pi$. Since energy cannot be conserved in such a process, it is called "virtual." Since the energy conservation is being violated by $\Delta E \sim m_\pi c^2$, the pion, by the

uncertainty principle, has to be reabsorbed within a time Δt, such that $\Delta E\, \Delta t \sim \hbar$. If the virtual pion is absorbed by the same nucleon that emitted it, it contributes to the "self-energy" of the nucleon. If, however, it is absorbed by a neighboring nucleon, there is a contribution to the energy of the two nucleons, which really arises because of the interaction between the meson and nuclear fields. Alternatively, one may eliminate the meson-nucleon interaction and replace it by a N-N potential. The precise definition of a potential from the field-theoretic point of view will be discussed in Section 5–9.

If the pion is assumed to move with the maximum possible speed c, the distance traveled by it in time Δt is $c\,\Delta t = \hbar/m_\pi c = 1.4$ fm, which should be a measure of the range of the nuclear force arising as a result of one-pion exchange. The derivation of this one-pion-exchange potential (OPEP) is given in Section 5–11; it is

$$V(\text{OPEP}) = g^2 \frac{m_\pi{}^3 c^2}{12M^2} (\boldsymbol{\tau}_1 \cdot \boldsymbol{\tau}_2) \left[\boldsymbol{\sigma}_1 \cdot \boldsymbol{\sigma}_2 + S_{12} \left(1 + \frac{3}{x} + \frac{3}{x^2} \right) \frac{e^{-x}}{x} \right], \tag{5–14}$$

where $g^2 = 15$ is the pseudoscalar coupling constant, and $x = \mu r$, with $\mu = m_\pi c/\hbar$. We shall discuss later the experimental evidence for the fact that the actual nuclear interaction beyond $r > 3$ fm is dominantly V(OPEP). Multiple exchanges of pions would lead to shorter-range forces, since the range is seen to be inversely proportional to the mass of the exchanged particles. For example, the two-pion-exchange potential (TPEP) becomes increasingly dominant as we go to shorter distances, and is much stronger than V(OPEP) for $r \leqslant 1$ fm.

Consider the nucleon that is emitting the virtual pion to be at point $\mathbf{r}_1$. Since the linear momentum is conserved in a virtual process, the nucleon would recoil after emitting the pion to some point $\mathbf{r}_1'$. The second nucleon, in its turn, would also recoil from $\mathbf{r}_2$ to $\mathbf{r}_2'$ while absorbing the pion. Thus, if recoil is taken into account, the interaction potential cannot be only a function of $\mathbf{r}_1 - \mathbf{r}_2$; other relative distances are involved as well. When a potential depends only on $\mathbf{r} = \mathbf{r}_1 - \mathbf{r}_2$, it is called a "local" potential. Quantum-mechanically, the potential V is an operator which, acting on a state vector $|\psi\rangle$, yields a new state $V|\psi\rangle$. In r-space, we can write

$$\begin{aligned} \langle \mathbf{r}|V|\psi\rangle &= \int \langle \mathbf{r}|V|\mathbf{r}'\rangle\langle \mathbf{r}'|\psi\rangle\, d^3r' \\ &= \int V(\mathbf{r}, \mathbf{r}')\psi(\mathbf{r}')\, d^3r'. \end{aligned} \tag{5–15}$$

If $V(\mathbf{r}, \mathbf{r}')$ is a function only of $\mathbf{r}$, then

$$V(\mathbf{r}, \mathbf{r}') = V(\mathbf{r})\,\delta(\mathbf{r} - \mathbf{r}'); \tag{5–16}$$

hence $\langle \mathbf{r}|V|\psi\rangle = V(\mathbf{r})\psi(\mathbf{r})$ for a local potential.

From the meson-theoretical viewpoint, it is natural to assume that the actual N-N potential would be "nonlocal" in nature, obeying Eq. 5–15. The ratio of the spatial extent of the nonlocality to the range of the nuclear force goes roughly as $m_\pi/M \ll 1$. We shall return to the consideration of nonlocal potentials in a later section.

We stressed previously that, to discover the fine details of a charge distribution or of a force field, it is necessary to use probe particles with de Broglie wavelengths comparable to the dimensions of the details to be investigated. We also pointed out that the impact parameter governs the scattering of partial waves and that the higher-angular-momentum components of an incident wave are not scattered at all by the nuclear force at low energies. Both considerations indicate that it is necessary to resort to high-energy scattering to investigate details of the potential shape and to learn about the two-nucleon force in states other than the S-state.

We can make these ideas more quantitative by asking what regions in the space between two nucleons contribute to the scattering of a given angular-momentum state. The impact parameter $b_l = \sqrt{l(l+1)}\,\hbar/p$ represents classically the distance of closest approach. Actually the wave function of the lth wave is nonzero at distances smaller than b_l, so that the potential at closer approaches does affect the scattering of the relevant partial wave. By numerical calculations with simple representative potentials, Matsumoto and Watari [12] have shown that changes in the potential for distances of separation less than about $\frac{1}{2}b_l$ have essentially no effect on the lth partial wave. This means, for example, that, whereas the S-wave always senses the whole potential, the P-wave is insensitive to details of the potential for $r < 0.7$ fm, so long as the energy is below 100 MeV. Again, the shape of the potential inside $r < 2.0$ fm is first sensed by the P-wave at about 20 MeV center-of-mass energy, by the D-wave at 60 MeV, and by the F-wave at 120 MeV.

We have thus arrived at the important result that, as the energy is gradually increased, a study of the phase shifts of the higher-angular-momentum states allows us to acquire information about the nuclear potential at steadily decreasing distances of separation. Consequently, it is important to consider higher-energy experiments. There is one restriction to be mentioned; this concerns energies so high that the nucleons have speeds

comparable with the speed of light and energies sufficient to create real mesons. In such instances, it is necessary to use relativistic mechanics, in which the very idea of a static potential is an approximation, becoming increasingly poorer as the energy rises. It may be that no potential exists which will precisely fit all data up to 400 MeV, although a potential description for energies up to about 200 MeV should be possible. Indeed, it is to be expected that there is more than one such potential, since any arbitrary energy cutoff precludes a unique determination of the potential at short distances. Fortunately, for a study of atomic nuclei detailed knowledge of relativistic behavior is not necessary, since the momentum distributions of bound nucleons do not extend appreciably above momenta corresponding to about 150–200 MeV.

5-4 POLARIZATION

In addition to differential and total cross-section determinations, experiments on polarization yield important information. A beam of nucleons is polarized if the spins are not randomly distributed but have some preferred orientation. If the number of particles in the beam with spin component parallel to this preferred direction is N_+ and the number with antiparallel spin component is N_-, the polarization is defined† (for spin-$\frac{1}{2}$ particles) as

$$P = \frac{N_+ - N_-}{N_+ + N_-}. \tag{5–17}$$

A beam can be polarized if some force acts preferentially on particles with one or the other spin direction. Such a force is provided by an inhomogeneous magnetic field, which deflects in opposite directions particles of opposite magnetic-momentum orientation. This is not the most important polarizing force in nuclear physics, however. The tensor force will produce polarization, for in the two cases in which the spins of incident and target nucleons are parallel or antiparallel, the tensor force will have opposite signs and will produce entirely different angular distributions. Consequently, with a mixture of central and tensor forces acting, the beam of particles

† It will be noted that Eq. 5–17 is equivalent to $P = \langle\sigma_d\rangle$, the expectation value of the component σ_d of the spin operator $\boldsymbol{\sigma}$ along the preferred direction d. If this direction is not selected in advance, P can be defined with respect to arbitrary axes and the direction also found. We have

$$P^2 = \langle\sigma_x\rangle^2 + \langle\sigma_y\rangle^2 + \langle\sigma_z\rangle^2,$$

and the preferred direction is specified by the polarization vector

$$\bar{\boldsymbol{\sigma}} = \langle\sigma_x\rangle\mathbf{i} + \langle\sigma_y\rangle\mathbf{j} + \langle\sigma_z\rangle\mathbf{k}.$$

deflected through a given angle will be partially polarized. Other possible noncentral forces depending on the spin vectors would similarly produce differently polarized beams at different scattering angles. Even with an unpolarized beam falling on a target with random spin orientation, partially polarized beams may result, owing to interference between the wave describing particles that are scattered without change of spin direction and the wave describing spin-flipped particles. The phenomenon is an essentially quantum-mechanical effect, and semiclassical reasoning cannot lead to the correct results. Thus, in any scattering process involving a suitable force coupling spin and space coordinates, there is polarization, its sign and magnitude depending on the angle of scattering.

Conversely, one may analyze the polarization of a beam by using the fact that the differential cross section depends on the polarization if the scattering force is spin dependent. If the spins are predominantly up, say, the scattering will be mainly to one or the other side of the beam, in contrast to the scattering of an unpolarized beam, which is always symmetric about the direction of incidence.

To illustrate these points let us consider a double-scattering experiment in which first an unpolarized beam is scattered on an unpolarized target and then a part of the scattered beam undergoes a second scattering, for which the differential scattering cross section is measured (see Fig. 5–4). As a result of the first scattering, the beam incident on the second target is partially polarized, so that the measured scattering has left-right asym-

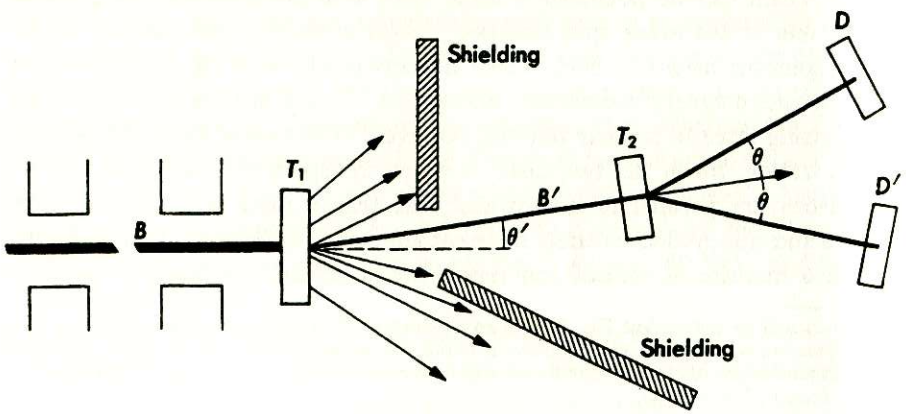

Fig. 5-4 A double-scattering experiment. An unpolarized beam B is scattered from the unpolarized target T_1. The partially polarized beam B' is scattered from a second unpolarized target T_2, and the differential scattering cross section is measured by detector D.

metry about the direction of the intermediate beam. This asymmetry is a simple function of the polarizations of the two scatterings. A number of general results concerning polarization follow from the assumptions of invariance of the forces under coordinate rotations and parity and time reversals. We shall simply state two of these results:†

1. For a given scattering angle θ, and for an initial beam with polarization $P_0\boldsymbol{\mu}$, the dependence of the differential cross section on the azimuthal angle ϕ after a single scattering with an unpolarized target is given by a proportionality factor,

$$1 + PP_0\mathbf{n}\cdot\boldsymbol{\mu} = 1 + PP_0\cos\phi, \tag{5–18}$$

where P is a number characteristic of the scattering process, and $\mathbf{n}$ is a unit vector perpendicular to the plane of scattering, with an opposite direction for left and right scattering. Precisely,

$$\mathbf{n} = \frac{\mathbf{p}_i \times \mathbf{p}_f}{|\mathbf{p}_i \times \mathbf{p}_f|}, \tag{5–19}$$

where $\mathbf{p}_i$ and $\mathbf{p}_f$ are the initial and final center-of-mass momenta. These quantities are shown in Fig. 5–5, where the initial and final center-of-mass momenta $\mathbf{p}_i$ and $\mathbf{p}_f$ define the scattering plane, $\mathbf{p}_f$ is defined as a left scattering, and $\mathbf{p}_f'$ is a right scattering in the same plane. The corresponding perpendiculars $\mathbf{n}$ and $\mathbf{n}'$ are shown. The unit vector $\boldsymbol{\mu}$ is the direction of the polarization of the incident beam, its component perpendicular to the incident direction is $\boldsymbol{\mu}_\perp$, and ϕ is the angle between $\boldsymbol{\mu}_\perp$ and $\mathbf{n}$. The corresponding angle ϕ' for

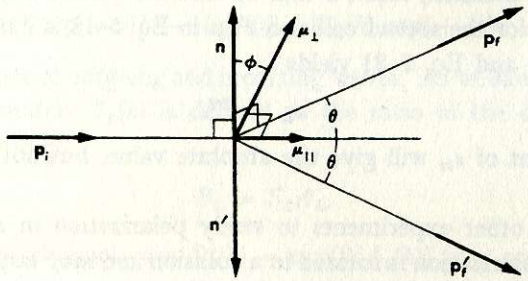

Fig. 5-5 Polarization and left-right asymmetry.

† Full details of the theory are given in an article by Wolfenstein [13].

the right scattering is seen to be $\pi - \phi$, since $\mathbf{n}' = -\mathbf{n}$. Note that any component $\boldsymbol{\mu}_{\parallel}$ is undetected in a single scattering of a polarized beam.

2. After scattering from an unpolarized traget, an initially unpolarized beam has polarization $P\mathbf{n}$, where the polarization P is the quantity that occurs in Eq. 5–18. It depends on the parameters of the specific collision in question, namely, the types of particles, the energy, and the scattering angle θ.

The first result (Eq. 5–18) gives the basic relation between polarization and differential scattering cross section or, equivalently, left-right asymmetry in a scattering plane. The relative difference between the intensities of the two beams $\mathbf{p}_f$ and $\mathbf{p}_f'$ in Fig. 5–5 is

$$e_{lr} = \frac{\sigma(\theta, \phi) - \sigma(\theta, \phi')}{\sigma(\theta, \phi) + \sigma(\theta, \phi')}, \tag{5–20}$$

which, by means of Eq. 5–18, gives

$$e_{lr} = PP_0 \cos \phi. \tag{5–21}$$

With this result we can understand the use of double scattering to determine polarization in a single scattering. Let the two scatterings be in the same plane so that $\mathbf{n}_1$ and $\mathbf{n}_2$ are either parallel or antiparallel, depending on whether the second scattering is to left or right, the first one being to the left as in Fig. 5–4. It is also arranged that the two scattering angles are identical, and the center-of-mass energies are assumed to be the same. This last requirement restricts the usefulness of the method to high energies or heavy targets and even then introduces some error. Within the stated conditions, the collisions are identical and will have the same value of P. After the first collision, result 2 tells us that the beam has polarization $P\mathbf{n}_1$, and therefore for the second collision $P_0\boldsymbol{\mu}$ in Eq. 5–18 is $P\mathbf{n}_1$. Consequently $\cos \phi$ is unity, and Eq. 5–21 yields

$$e_{lr} = P^2. \tag{5–22}$$

A measurement of e_{lr} will give the absolute value, but not the sign of the polarization.

There are other experiments to study polarization in more detail. In general, the polarization is rotated in a collision and may acquire components in the plane of scattering, both along and perpendicular to the final momentum. To study such effects, the beam must first be polarized and then scattered, and its polarization must be analyzed, that is, triple scattering is required. Analysis of polarization by scattering is valid only for the component perpendicular to the scattering plane. Consequently, various different planes must be used in the final scattering. One particular quantity determined is the depolarization D, which enters into a triple-scattering experiment in which all three planes are parallel. Such an experiment determines the polarization after the second scattering, according to Eq. 5–21. The quantity D is so defined that the polarization along $\mathbf{n}$ after the second scattering is $(P_2 + DP_1)/(1 + P_1P_2)$; it is seen that, if the first scattering completely polarized the beam ($P_1 = 1$), $D = 1$ would mean no depolarization in the second scattering. Depolarization is one of the easiest parameters to measure. Determination of three other parameters requires triple scattering in other planes, simultaneous measurement of the polarization of the scattered particle and the recoiling target, and application of magnetic fields to rotate the direction of polarization between collisions [14]. With the availability of polarized proton beams, conventional double- and triple-scattering experiments reduce to single and double scattering; while a polarized target with a polarized beam makes it possible to use single scattering throughout.

5-5 THE SCATTERING MATRIX FOR COUPLED WAVES

In any scattering experiment, the particles are detected only when they have come out of the force range of the target. All the information about the detected particle in these experiments is therefore contained in the asymptotic part of the wave function. For elastic scattering in a central force, we found in Chapter 2 that the asymptotic wave function in the S-state is characterized by phase shifts $\delta_0(k)$. Similar considerations hold also for higher partial waves. The radial wave function in the asymptotic region may be written as

$$u_L \sim A_L(k) \exp[-i(kr - L\pi/2)] - B_L(k) \exp[+i(kr - L\pi/2)],$$

which is a mixture of outgoing and incoming waves. As we saw in Section 2–3, the scattering matrix $S_L(k)$ is defined as the ratio of the outgoing to the incoming amplitude:

$$B_L = S_L A_L, \tag{5–23}$$

and for this one-channel case $S_L(k) = \exp[2i\,\delta_L(k)]$ is a complex number. Now we consider the more complicated case in which a tensor force is present. As discussed in Section 5–1, such a force mixes states of different L, and a further coupling parameter has to be introduced to describe scattering. For example, consider the triplet case with $J = 2$. With $S = 1$, we can have

$L = 1, 2$, or 3. Since the tensor force cannot mix parity, the $L = 2$ partial wave remains uncoupled, while the other two, with $L = J - 1$ and $L = J + 1$, are mixed in any state, namely,

$$\Psi_J = \frac{1}{r}[U_J(r)\mathscr{Y}^M_{J,1,J-1} + W_J(r)\mathscr{Y}^M_{J,1,J+1}]. \tag{5–24}$$

In the asymptotic force-free region, each term corresponds to a simple partial wave for $L = J - 1$ or $L = J + 1$. We can then write

$$U_J(r) \sim A_1 \exp\{-i[kr - (J-1)\pi/2]\} - B_1 \exp\{i[kr - (J-1)\pi/2]\},$$
$$W_J(r) \sim A_2 \exp\{-i[kr - (J+1)\pi/2]\} - B_2 \exp\{i[kr - (J+1)\pi/2]\}. \tag{5–25}$$

In this case also, we can define a scattering matrix by the matrix equation

$$\begin{pmatrix} B_1 \\ B_2 \end{pmatrix} = \begin{pmatrix} S_{11} & S_{12} \\ S_{21} & S_{22} \end{pmatrix} \begin{pmatrix} A_1 \\ A_2 \end{pmatrix}, \tag{5–26}$$

where S_{11}, S_{12}, etc., are complex. There are thus eight real parameters in the S-matrix. But conservation of incoming and outgoing flux requires $B^+B = A^+A$, where

$$B = \begin{pmatrix} B_1 \\ B_2 \end{pmatrix} \quad \text{and} \quad B^+ = (B_1{}^* B_2{}^*).$$

Combining this with Eq. 5–26, we obtain

$$S^+S = 1, \tag{5–27}$$

which means that S is unitary. This gives us three equations and reduces the number of parameters to five. If we now invoke time-reversal invariance, which essentially amounts to interchanging the incoming and outgoing waves and taking the complex conjugate of the amplitudes, we get

$$A^* = SB^*. \tag{5–28}$$

When this is combined with $B = SA$, we find that the S-matrix has to be symmetric, that is,

$$S_{12} = S_{21}, \tag{5–29}$$

which provides two more conditions. Thus there are only three independent real parameters in the S-matrix describing scattering in a coupled triplet

state of specified J and parity. These are taken to be the two phase shifts and a coupling parameter ε_J.

There are various ways of defining the S-matrix in terms of these parameters, but the one that is most extensively used is due to Stapp, Ypsilantis, and Metropolis [15]. In this definition,† the S-matrix for a given J and parity is

$$S_J = \begin{pmatrix} \exp(i\delta_{J\alpha}) & 0 \\ 0 & \exp(i\delta_{J\beta}) \end{pmatrix} \begin{pmatrix} \cos 2\varepsilon_J & i \sin 2\varepsilon_J \\ i \sin 2\varepsilon_J & \cos 2\varepsilon_J \end{pmatrix} \begin{pmatrix} \exp(i\delta_{J\alpha}) & 0 \\ 0 & \exp(i\delta_{J\beta}) \end{pmatrix}. \tag{5–30}$$

Phase shifts so defined are often called "bar" phases, because in early papers they were written as $\bar{\delta}$. It is incorrect to consider $\delta_{J\alpha}$ and $\delta_{J\beta}$ as the phase shifts for $L = J - 1$ and $L = J + 1$, respectively, since neither of these is an eigenstate of the Hamiltonian, and the complex of three quantities, ε_J, $\delta_{J\alpha}$, $\delta_{J\beta}$, is required to prescribe the possible scattered states. Only in the limit of $E \to 0$ does $\varepsilon_J \to 0$, and then $\delta_{J\alpha} = \delta(L = J - 1, J = J)$, $\delta_{J\beta} = \delta(L = J + 1, J = J)$. However, in the current literature, this loose description is often used. For example, $\delta_{2\alpha}$ and $\delta_{2\beta}$ are denoted by the symbols $^3P_2$ and $^3F_2$, a notation that we shall also follow. We should mention here that in the above analysis we have not considered inelastic scattering, which may occur for energies above the meson-production threshold, that is, $E_{\text{lab}} > 280$ MeV. At energies up to $E_{\text{lab}} \approx 400$ MeV, meson production is so small that the S-matrix may be approximated as unitary in the elastic channel.

At this point, we stress that the analysis of the N-N interaction is a complicated procedure that advances in several steps. The first important step is to measure the elastic-scattering data. For the range of $E_{\text{lab}} =$ 0–400 MeV, there are over 2000 items of experimental data involving p-p and n-p scattering. These are measurements of differential cross section, polarization, triple-scattering parameters, and spin-spin correlation coefficients at various energies and angles. The second step is to find a unique set of phase shifts that can reproduce the experimental data consistently. Finally, an attempt is made to construct, either theoretically or phenomenologically, models (like a N-N potential) that can yield the same phase shifts.

† A different convention sometimes used is due to J. M. Blatt and L. C. Biederharn, *Phys. Rev.* **86**, 399 (1952). Transformation formulas relating the Blatt-Biederharn phases and the "bar" phases are given by Stapp et al. [15]. Unless stated specifically to the contrary, we shall use the bar phases.

In order to appreciate the logic of these steps, it is useful to gain more understanding of the scattering matrix and its relation to experiments. Although we have seen that the S-matrix at a given energy and for specified values of J and parity is determined by three real parameters, it does not follow that only three independent experiments are needed to specify the complete S-matrix at a given energy because, for a beam of high-energy particles, many possible L- (and consequently J-) values are involved, and all these can contribute to the total S-matrix. A particularly simple situation exists for very low-energy scattering where only the $L = 0$ wave contributes and the phases are essentially determined by cross-section measurements alone. But for higher energies, it is more convenient to express the experimental results in terms of a matrix M involving the incident energy k^2 and the scattering angle θ in the CM frame.

In Section 2–3 we considered scattering with a central force in the S-state, and found that (see Eq. 2–29) the scattered wave could be written as $(e^{ikr}/r)[(1/2ik)(e^{2i\delta_0(k)} - 1)]$. In this case, we could have alternatively written

$$u_{sc} = \frac{e^{ikr}}{r} M(\mathbf{k}, \mathbf{k}'), \quad k^2 = k'^2, \tag{5–31}$$

with

$$M(\mathbf{k}, \mathbf{k}') = \frac{1}{2ik} \langle \mathbf{k} | (S - 1) | \mathbf{k}' \rangle. \tag{5–32}$$

For the S-state in particular, there was no θ-dependence in M. In the more complicated case in which the spin has to be taken into account explicitly, we can generalize this by writing the asymptotic wave function as

$$u \sim e^{ikz}\chi_s^{m_s} + \frac{e^{ikr}}{r} \sum_{m_s'} \langle \chi_s^{m_s'} | M(k^2, \theta) | \chi_s^{m_s} \rangle \chi_s^{m_s'}. \tag{5–33}$$

Here $M(k^2, \theta)$ is a matrix in the spin space, related to the total S-matrix as before, and describes the scattering through an angle θ, of an incident particle of spin (s, m_s) with momentum k along the z-axis (J is unspecified), its spin state changing from $\chi_s^{m_s}$ to $\chi_s^{m_s'}$.

The number of independent parameters in M connected with the change of spin orientations in a collision depends on the intrinsic spin of the colliding particles. For illustration, take the simple case of a nucleon scattering off a spin-zero target like ^{12}C. Then the matrix M can be expanded in the complete set of operators of the incident-particle spin space, which are just the unit matrix and $\boldsymbol{\sigma}$. Thus

$$M = B + \mathbf{C} \cdot \boldsymbol{\sigma},$$

where B and $\mathbf{C}$ are functions of (k^2, θ). Since M has to be invariant under rotation, it must be a scalar. But $\boldsymbol{\sigma}$ is a pseudoscalar; therefore so should be $\mathbf{C}$. The only pseudoscalar other than $\boldsymbol{\sigma}$ in this problem is $\mathbf{k} \times \mathbf{k}'$, where $\mathbf{k}$ and $\mathbf{k}'$ are the initial and final wave vectors in the CM frame. Hence we can finally write

$$M = B(k^2, \theta) + C(k^2, \theta)\boldsymbol{\sigma} \cdot \mathbf{n} \tag{5–34}$$

with $\mathbf{n} = (\mathbf{k} \times \mathbf{k}')/|(\mathbf{k} \times \mathbf{k}')|$ being a unit vector normal to the plane of scattering. In Eq. 5–34 there are four independent real parameters at each energy and angle, since B and C can each be complex. One of these can be regarded as an overall phase factor, leaving three real parameters to be determined by experiments.

In the more complicated case of N-N scattering, similar analysis shows that nine parameters† are required to specify M. However, the unitarity requirement on S (and therefore M) reduces the number to five. Thus, at any given energy, five independent experiments must be performed at each angle to determine the scattering matrix completely, for each i-spin state ($T = 0$ or 1).

5-6 EXPERIMENTAL RESULTS AND PRELIMINARY INTERPRETATIONS

Data on nucleon-nucleon scattering are presented in this section in graphical form, based mainly on a summary compiled by Hess [18]. Figure 5–6 shows the differential n-p cross section at various energies from 14 to 580 MeV. Experimental points are not shown, but the curves are drawn through them. Typical errors are of the order of 10%, so that fine details of the curves are not reliable; for example, curves for different energies probably do not cross each other, although there are a few instances in which they appear to do so. The threshold for π-meson production is 290 MeV. Below this energy only elastic scattering is possible, but above it the total and the elastic cross sections differ. The data on total cross section are summarized

† More precisely, invariance requirements specify nine parameters for proton-proton scattering. When the nucleons are not identical, an extra term proportional to $(\boldsymbol{\sigma}_i - \boldsymbol{\sigma}_t) \cdot \mathbf{n}$ may occur in the scattering amplitude, where $\boldsymbol{\sigma}_i$ is the spin of the incident particle and $\boldsymbol{\sigma}_t$ that of the target. This term would imply that polarized neutrons would scatter from hydrogen differently than polarized protons from target neutrons. Both experiments have been done [16, 17], and the results are similar. Also, on the basis of charge symmetry, the extra term should not be present since charge symmetry implies no change if all neutrons and protons are interchanged.

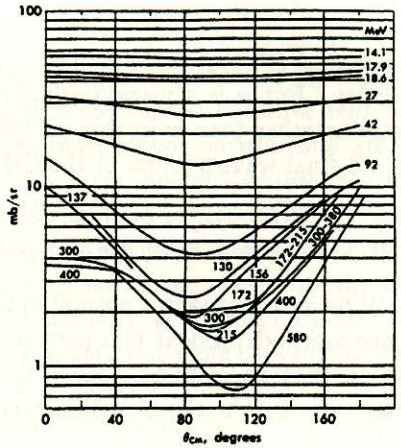

Fig. 5-6 Experimental values of the differential n-p cross section at various energies. (After Hess [18].)

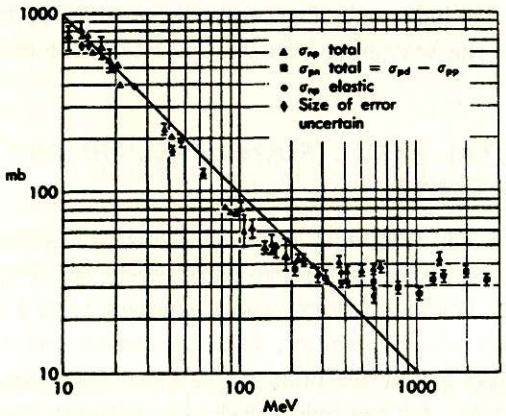

Fig. 5-7 Experimental values of total and elastic n-p scattering. (After Hess [18].)

in Fig. 5–7 [18]. The points labeled σ_{np} are from experiments in which neutrons are incident on hydrogeneous targets. Those labeled σ_{pn} are from an experiment in which protons are incident on deuterium, and the proton-proton cross section is subtracted. This is only an approximation to σ_{np} since it ignores interference terms in the deuteron scattering. The approximation improves, however, as the energy increases, and at the energies shown the correction is about 6 mb. The straight line is proportional to $1/E$.

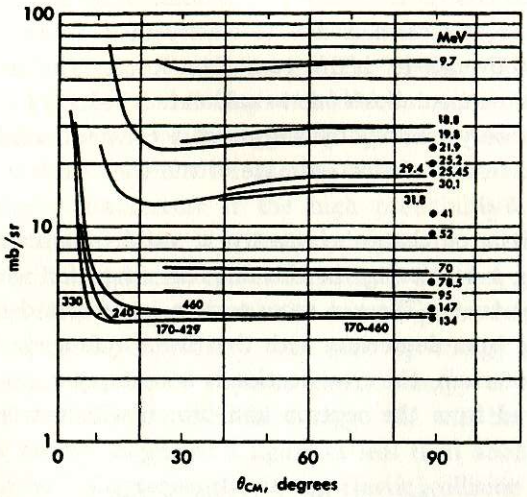

Fig. 5-8 Experimental values of the differential p-p cross section at various energies. (After Hess [18].)

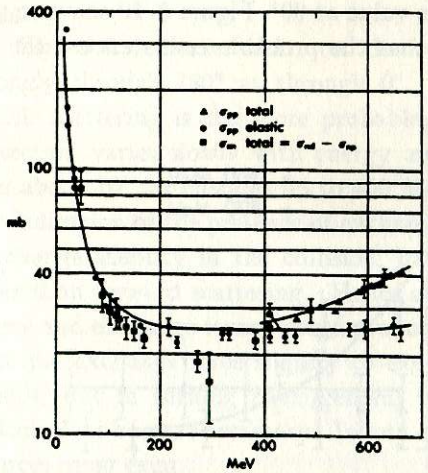

Fig. 5-9 Experimental values of the "total" and "elastic" p-p nuclear cross sections, that is, with Coulomb scattering subtracted, and of the n-n elastic cross section, as determined approximately from $\sigma_{nd} - \sigma_{np}$. (After Hess [18].)

For p-p scattering, the differential cross sections are shown in Fig. 5–8 for energies up to 500 MeV; this is as high as we need go, since we intend to restrict our attention to nuclear structure. We remarked in Chapter 2 that, as the energy increases, the effects of Coulomb scattering are confined

to smaller and smaller angles. This is clearly seen in the figure, in which the large small-angle cross section is due to electrostatic forces and the cross section at angles above 20–40° is due to nuclear forces. The marked flatness of the nuclear cross section allows one to calculate a "total" p-p cross section for nuclear forces only, simply by assuming a constant value of $\sigma(\theta)$ for each energy. The results of this estimate of the total nuclear cross section are shown in Fig. 5–9.

If the hypothesis of charge symmetry is valid, n-n scattering should be the same as p-p scattering, in the angular range for which Coulomb effects are unimportant. The n-n cross section is estimated by comparing neutron scattering from deuterium with that from hydrogen. For neutrons scattered from deuterium, the cross section is not simply $\sigma_{nn} + \sigma_{np}$, because the waves scattered from the neutron and proton will interfere coherently and, consequently,

$$\sigma_{nd}(\theta) = \sigma_{nn}(\theta) + \sigma_{np}(\theta) + I(\theta).$$

The interference term $I(\theta)$ is most important at low energies and small scattering angles. At 300 MeV, $I(\theta)$ is estimated to fall rapidly from 0.6 mb/sr at 40° to one-tenth this value at 90°. Figure 5–10 shows $\sigma_{nd} - \sigma_{np}$ for angles above 30°. It is seen that the probable errors exceed the estimated values

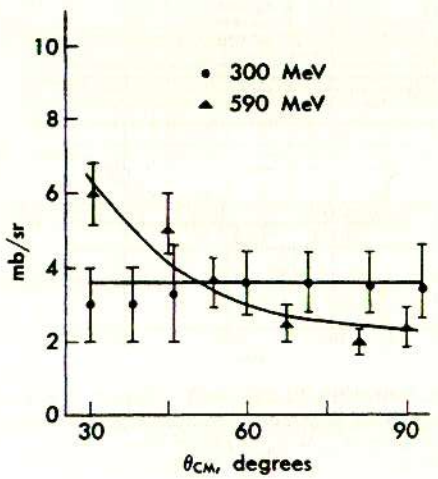

Fig. 5-10 The points show the experimental values of the differential n-n cross section at 300 and 590 MeV, estimated from $\sigma_{nd}(\theta) - \sigma_{np}(\theta)$. The curves show $\sigma_{pp}(\theta)$ at 300 MeV (from Fig. 5–8) and at 590 MeV. Points are available at 300 MeV at angles less than 30°, but these are not shown since at these angles $I(\theta)$ is important for σ_{nd} and the Coulomb scattering is important for σ_{pp}.

of $I(\theta)$. Also, one can estimate that the total cross section may have an error of 6 or 7 mb at about 300 MeV. Some points of σ_{nd} (total) $- \sigma_{np}$ (total) are shown in Fig. 5–9. Comparison of the neutron-neutron and proton-proton data in Figs. 5–9 and 5–10 gives additional support to the assumption of charge independence, already suggested by the low-energy results.

We shall now consider some of the salient features of these results. An outstanding characteristic is the high probability in neutron-proton collisions that the neutron is scattered backward in the center-of-mass system. For ordinary forces, this is impossible as soon as the bombarding energy becomes large compared with the average potential, since the proton, initially at rest in the laboratory, can pick up energy only through the internucleon force and hence acquires kinetic energy of the same order of magnitude as the nuclear potential energy. It will be recalled that the results at low energy suggested a figure of less than about 50 MeV for the average potential. Consequently, in an elastic collision at energies over 100 MeV, the scattered neutron would have more energy than the recoil proton and, by the conservation laws for a collision, would be scattered forward with a deflection less than 45° in the laboratory or 90° in center-of-mass coordinates.

Reference to Fig. 5–6 indicates that, on the contrary, neutrons are scattered as strongly through 180° as through 0°. Indeed, above about 100 MeV, the back scattering is the more probable. The position of the minimum cross section varies slowly with energy and does not shift from 90° by more than about 10° for energies up to 400 MeV.

This is a clear indication of the presence of exchange forces, for if neutron and proton interchange identity in the collision, backward scattering will be expected rather than forward scattering. Hence an approximately equal mixture of ordinary and exchange forces would produce the observed results. One might expect the exchange force slightly to exceed the ordinary force because $\sigma(\pi) > \sigma(0)$, but in turning from general features to matters of detail, precise calculations become necessary. In any event, it is evident that large exchange forces must exist.

Before the experiments above 100 MeV were done, Robert Serber proposed an equal mixture of ordinary and Majorana forces:

$$V(r)(1 + P_x). \tag{5–35}$$

Since $P_x = -1$ in states of odd parity, the Serber hypothesis implies no interaction between nucleons in states of odd L, with consequent symmetry about 90°. We shall see below that forces do act in P- and F-states, but

they are weaker than in S-, D-, and G-states. Nevertheless, because of its simplicity, the Serber force has been used in many calculations.

Total n-p and p-p cross sections are markedly different. The n-p cross section follows roughly the $1/E$ law ($\sigma \propto \lambda\!\!\!^{-2}$) up to energies at which inelastic processes are important. The small departures from $1/E$ are attributable to the variation of the phase shifts of the different angular-momentum states as these become important. On the other hand, the p-p elastic cross section is amazingly constant at about 23 mb from 150 to 600 MeV. Above this energy it decreases. Moreover, the p-p cross section has very little angular dependence at any energy except in the small-angle Coulomb scattering region.

This constant flat differential cross section is evidence that we are not dealing with an ordinary attractive force. Of course an S-wave gives an isotropic scattering, and it might be supposed that no forces are evident in the higher-angular-momentum states, even up to 400 MeV. However, this hypothesis is untenable, since the maximum total cross section for an S-wave is $2\pi\lambda\!\!\!^{-2}$ or about 11 mb, which is only half the observed value. The differential p-p scattering cross section is given in Appendix B as

$$\sigma_{pp}(\theta) = |f(\theta)|^2 + |f(\pi - \theta)|^2 - \mathrm{Re}\,[f^*(\theta)f(\pi - \theta)], \tag{5-36}$$

where

$$f(\theta) = f_C(\theta) + f_N(\theta), \tag{5-37}$$

$f_C(\theta)$ is the Coulomb scattering amplitude, and f_N contains all the effects of nuclear scattering. The formula

$$f_N(\theta) = -\frac{1}{2ik}\sum_l (2l+1)e^{2i\eta_l}(e^{2i\delta_l} - 1)P_l(\cos\theta), \tag{5-38}$$

in which η_l is a Coulomb phase shift and δ_l is a nuclear phase shift, makes clear that the nearly isotropic distribution at high energies must be due to a remarkable compensation among the coefficients of the Legendre polynomials. In the energy region where only S-, P-, and D-waves need be considered, the cross section is made up of an isotropic term proportional to $\sin^2\delta_0$ due to the ^1S-wave, a term proportional to $\sin^2\delta_2\,[P_2(\cos\theta)]^2$ due to the ^1D-wave, a term proportional to $\sin\delta_0 \sin\delta_2$ and $P_2(\cos\theta)$ due to S-D interference, and terms due to the ^3P-wave. For central forces, a P-wave gives a contribution proportional to $\cos^2\theta$, but when tensor forces act, the various substates $^3P_0$, $^3P_1$, and $^3P_2$ have different phase shifts, and a term in $|Y_1{}^1|^2$ or $\sin^2\theta$ appears. Also, the $J = 2$ state is a mixture

of $^3P_2$ and $^3F_2$, and interference terms appear in $\sigma(\theta)$ proportional to the products of first- and third-order spherical harmonics. At energies at which the F-wave separately would have negligible phase shift, the coupling due to the tensor force makes the $^3F_2$-contribution appreciable, and squares of third-order harmonics also appear.

We are now able to see how a flat cross section might arise. The major contributions to $\sigma(\theta)$ come from the ^1S- and ^1D-states, since the force in states of odd L is comparatively weak. The function $P_2(\cos\theta)$ has a zero at 55° and is negative at 90°. Hence the D-wave contributions are as shown in Fig. 5-11. To obtain $\sigma(\theta)$ we combine curves (a) and (b) with the constant S-wave contribution, in proportions determined by δ_0 and δ_2. It is evident that, if curve (a) is added in with a positive coefficient, forward scattering will predominate. However, if curve (a) is added with a negative coefficient, the scattering at 90° can be built up and a curve of the general nature of (c) or (d) can be obtained for $\sigma(\theta)$. This is still not the observed isotropic scattering, since there is a minimum around 45° due to the zero of P_2, but a tensor force acting in the P-states will fill in the minimum. A central-force P-wave merely builds up the forward scattering with a $(\cos^2\theta)$-term, but the $\sin^2\theta$ provided by the interference waves between the different P-states

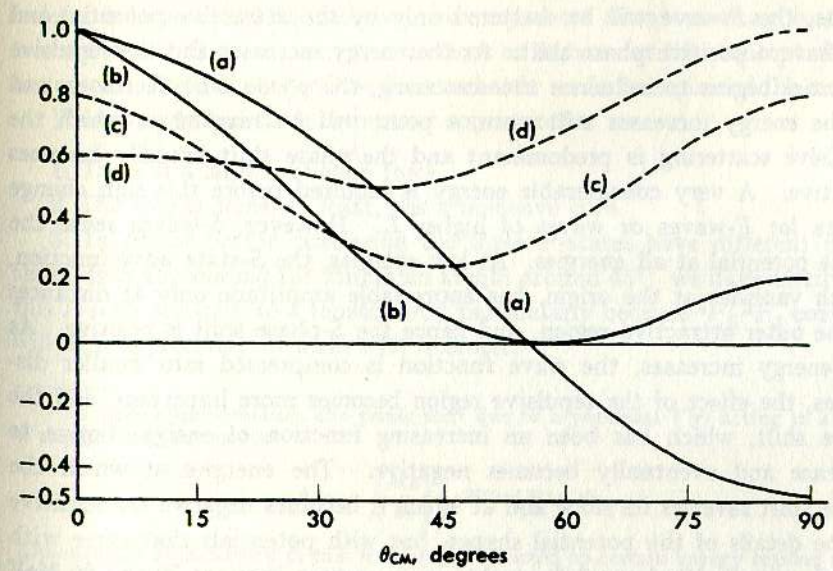

Fig. 5-11 Contributions of S- and D-waves to p-p scattering. Curve (a) is $P_2(\cos\theta)$, curve (b) is $[P_2]^2$, curves (c) and (d) are arbitrary combinations which might represent $\sigma(\theta)$. Curve (c) is $0.3 + P_2(P_2 - 0.5)$, and curve (d) is $0.6 + P_2(P_2 - 1)$.

tends to smooth out this effect, and the P-F interference terms provide angular functions, similar to $\sin^2\theta\cos^2\theta$, which maximize around 45°.

These considerations show that the isotropic proton-proton cross section can be understood on the basis of two essential hypotheses, stipulating (1) a force such that the coefficient of the S-D interference will be negative and (2) tensor forces in the triplet states to build up the central portion of the distribution. It is easy to believe that the relative strengths of the various forces involved might be such as to produce isotropy at one energy; what is not so simple is to achieve it at all energies. As the energy rises, D-scattering should become more important, producing a steady increase in δ_2 and hence a large contribution from curve (b) in Fig. 5–11. In compensation the coefficient of curve (a) must change by the right amount. This coefficient involves the factor $\sin\delta_0\sin\delta_2$, which consequently must be negative at sufficiently high energies and must decrease as the energy increases.

It was pointed out by Jastrow [19] that δ_0 would have this behavior if the nucleon force had a repulsive core of suitably small radius, surrounded by an attractive potential. For purposes of illustration, let us consider a P-wave in such a potential. The P-wave at 200 MeV senses only the potential outside approximately 0.5 fm. Hence, if the repulsive core is inside this radius, the P-wave will be scattered only by the attractive potential and will have a positive phase shift. As the energy increases and the repulsive potential begins to influence the scattering, the phase shift decreases, and as the energy increases still more, a point will be reached at which the repulsive scattering is predominant and the phase shift actually becomes negative. A very considerable energy is required before this sign change occurs for P-waves or waves of higher L. However, S-waves sense the whole potential at all energies. At low energies, the S-state wave function, which vanishes at the origin, has appreciable amplitude only at distances in the outer attractive region, and hence the S-phase shift is positive. As the energy increases, the wave function is compressed into smaller distances, the effect of the repulsive region becomes more important, and the phase shift, which has been an increasing function of energy, begins to decrease and eventually becomes negative. The energies at which the phase shift reverses its slope and at which it becomes negative are sensitive to the details of the potential shapes, but with potentials that agree with experiment the ^1S-phase shift reaches its maximum between 10 and 20 MeV and becomes negative somewhere around 200 MeV. Thus the uniform differential cross section over the whole region of 150–450 MeV may be

understood in terms of the steady changes of phase shift attributable to a potential with a repulsive core.

Other types of forces could introduce angular functions with maxima at 90° and 45°. A force of the form $V(r)\mathbf{L}\cdot\mathbf{S}$ does not mix states of different L, as does the tensor force, but it does yield different scattering for states of the same L and different J. With the phase shifts depending on both L and J, terms in $Y_L{}^1Y_{L'}^{1*}$ and $Y_L{}^2Y_{L'}^{2*}$ are introduced into $\sigma(\theta)$. Of course, the F-wave is not enhanced at lower energies as it is by the tensor force, and it is reasonable to include the P-scattering while ignoring the P-F interference. The $\mathbf{L}\cdot\mathbf{S}$ operator is zero in singlet states, and for triplet states it is $\frac{1}{2}[J(J+1)-L(L+1)-2]$. Thus the ratios of the $\mathbf{L}\cdot\mathbf{S}$ forces in the three P-states are $F(^3P_2):F(^3P_1):F(^3P_0)=1:-1:-2$. If no other forces act in the P-states, the $\mathbf{L}\cdot\mathbf{S}$ forces produce an angular distribution of the form $a+\sin^2\theta$, where the constant a is small compared to 1 and vanishes in the Born approximation† [20]. Clearly this distribution builds up the 90° cross section. However, it has not been possible to produce an isotropic $\sigma_{pp}(\theta)$ over the whole observed energy range by $\mathbf{L}\cdot\mathbf{S}$ forces alone without the introduction of a repulsive core.

In turning to the results of polarization experiments, we find that an $\mathbf{L}\cdot\mathbf{S}$ force is indicated. This statement is made in the context of an energy-independent potential defined even for very short distances of approach of two nucleons. There are serious questions as to how far this concept should be trusted. These doubts will be discussed after we have explained the results.

We have reached three important conclusions:

1. There is a large exchange force.
2. The singlet force, at least, has a repulsive core.
3. In proton-proton scattering the three P-states have different phase shifts, thus eliminating the minimum in $\sigma(\theta)$ around 45°; we have attributed this P-state splitting to a tensor force, particularly because $^3P_2$-$^3F_2$ coupling will help appreciably to make $\sigma(\theta)$ isotropic.

---

† In Born approximation, the phase shift due to a potential $V(r)$ acting in a state of angular momentum l is

$$\delta = -\left(\frac{Mk}{\hbar^2}\right)\int r^2V(r)f_l{}^2(kr)\,dr. \tag{5–39}$$

Although the applicability of this formula is restricted to certain energy regions whose precise limits are determined by l and by the nature of V, the Born approximation provides a useful guide in qualitative discussions. For n-p scattering the function f_l is the spherical Bessel function j_l; for p-p scattering it is the corresponding Coulomb function.

These conclusions have been reached without detailed analysis of the experimental data. To make further progress and, indeed, to confirm our conclusions, exact quantitative fits must be found. For example, is a tensor force in the P-state really indicated, or would the splitting due to an $\mathbf{L} \cdot \mathbf{S}$ force produce sufficient cross section at 45°? The answers to such questions require exact numerical investigation.

5-7 MORE PRECISE ANALYSIS OF EXPERIMENTAL DATA

The most instructive way of presenting the experimental data is to analyze them for the phase shifts of all possible states in a given energy range. We have mentioned that there is a vast body of experimental measurements in the range $E_{\text{lab}} = 0$–450 MeV and that inelastic effects there are small. A considerable number of data have been accumulated also for the energy range 450–750 MeV, and a phase-shift analysis has been attempted [21] after making corrections for inelastic effects. In this book, we shall discuss briefly the results for the energy range 0–450 MeV.

Phase-shift analyses can be done either for the data at a fixed energy or for the data at many different energies. In the single-energy analysis, the aim is to determine a set of phases δ for all states up to a maximum $L = L_{\max}$. For $L > L_{\max}$, the phases are assumed to be generated by the one-pion-exchange potential. The method of analysis is then to search for sets of phases up to $L_{\max}$ which minimize the least-square sum

$$M = \frac{1}{n} \sum_{i=1}^{n} \left[\frac{y_i(\delta) - y_i(\text{exp})}{e_i} \right]^2, \tag{5-40}$$

where the y_i are the n quantities observed at that particular energy, $y_i(\delta)$ is the value calculated for a specific set of phase shifts δ, $y_i(\text{exp})$ is the experimental value, and e_i is the probable error in $y_i(\text{exp})$. Such single-energy analyses have been performed at many different energies.

The alternative method is to do an energy-dependent analysis, in which the experimental data in an entire energy range are analyzed simultaneously. In this method, each phase is expanded in terms of some set of energy-dependent functions:

$$\delta(E) = \alpha\delta^{\text{OPEP}}(E) + \sum_{i=1}^{N} \beta_i f_i(E), \tag{5-41}$$

where α and β_i are adjustable parameters for states $L < L_{\max}$, and $\alpha = 1$, $\beta_i = 0$ for other states. The OPEP value constitutes the leading term, but α remains adjustable because a phase-shift analysis is a method of

presenting experimental data and should not prejudge theoretical results.† The functions $f_i(E)$ may be chosen with some guidance from theory (the Livermore group [22] does so), but what is of basic importance is that there be enough of them to permit expression 5–41 to represent any smooth function $\delta(E)$. MacGregor, Arndt, and Wright [23] obtain precision fits to 1076 items of p-p data in the range 1–450 MeV by having 26 adjustable parameters in their analysis. They search for all phase parameters up to $L = 5$ and use V_{OPEP} for the higher partial waves. A similar analysis has also been done by the same authors for 990 items of n-p data in the same energy range. Many other groups, notably those of Breit [24], Signell [25], and Kazarinov [27], as well as Hoshizaki [26] and Perring [28], have done phase-shift analyses of the N-N data.

Two main conclusions follow from these extensive analyses: (1) the $T = 1$ scattering matrix is very accurately determined up to $E_{\text{lab}} = 450$ MeV, and (2) the $T = 0$ scattering matrix is also fairly well determined up to $E_{\text{lab}} = 450$ MeV, the accuracy being good at energies between 100 and 200 MeV. Figures 5–12a and 5–12b show the phases up to $L = 2$ that have been extracted by MacGregor et al. [23]. The coupled phases are the nuclear "bar" phase shifts, as defined by Eq. 5–30. It should be noted that single-energy analyses at various energies between 25 and 330 MeV yield results in general agreement with the energy-dependent analysis. Because of deviation from charge independence, the p-p and n-p phases differ slightly. The accuracy of the analyses is such that MacGregor et al. [23] are able to give separate sets of $^1S_0$-phases for p-p and n-p scattering. In Fig. 5–12a, only the p-p $^1S_0$-phase shifts are plotted.

These studies also reveal that in this entire energy range the phases for $L = 4$ and 5 strongly resemble the phases produced by V_{OPEP} alone. Indeed, these phases can be very well fitted by taking the coupling constant g^2 in V_{OPEP} to be a free parameter. The best fit is obtained for a value of g^2 very close to the value of $g^2 = 15$ obtained from π-N scattering data, in accordance with the predictions in Section 5–3.

From Fig. 5–12, it will be seen that both the $^1S_0$- and the $^3S_1$-phases change sign at higher energies, confirming that at short distances the nuclear force is repulsive. The $^1S_0$-phase shift changes sign around $E_{\text{lab}} = 250$ MeV, while the $^3S_1$-phase shift becomes repulsive at about 370 MeV, indicating that the potential is more attractive in this state. This is also manifested in

† It is important, however, to ensure the correct low-energy behavior of these phases. For example, the parameters of the $L = 0$ phase should be adjusted to give the correct scattering length and effective range at low energies.

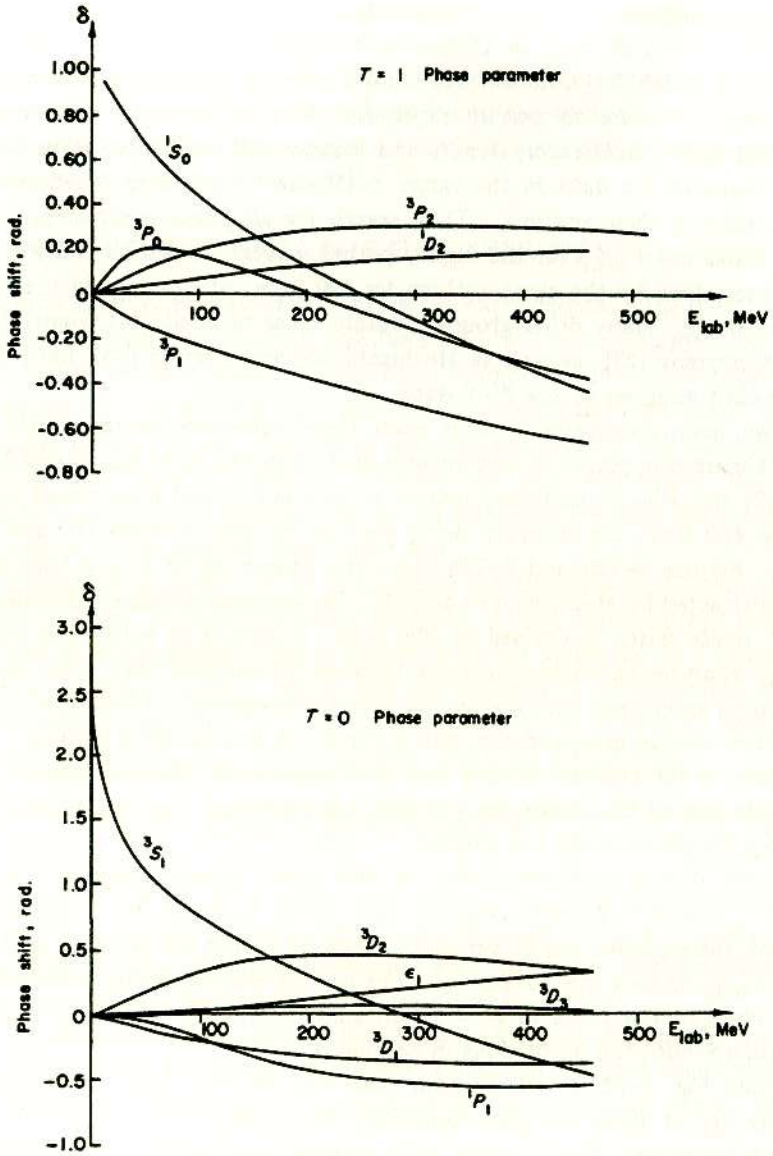

Fig. 5-12 Nuclear phase parameters for nucleon-nucleon scattering for $L \leqslant 2$. In (a) the phase shifts are for the $T = 1$ channel; in (b) the phases are the nuclear "bar" phase shifts for the $T = 0$ channel as defined in Eq. 5–30. The values are taken from the multienergy analysis of MacGregor et al. [23], and continuous curves are drawn through them. The error bars are small and are not shown.

the extreme-low-energy behavior of the phases: as $E_{\text{lab}} \to 0$, $\delta(^1S_0) \to 0$, whereas $\delta(^3S_1) \to \pi$, implying that there is a bound state in $^3S_1$.

At low energies ($E_{\text{lab}} \leqslant 20$ MeV), it will also be seen that $\delta(^3P_2) \ll |\delta(^3P_1)| < \delta(^3P_0)$. Furthermore, $\delta(^3P_2)$ is positive throughout, $\delta(^3P_1)$ is always negative, and $\delta(^3P_0)$ goes from positive to negative around 200 MeV. We have already mentioned that, for energies up to 20 MeV, the P-wave is essentially scattered by the force outside 2 fm, which is dominantly V_{OPEP}. MacGregor [29] calculated the Born approximation to the ^3P- and ^1D-phase shifts using V_{OPEP} and found that 98% of $\delta(^1D_2)$ comes from the region outside 2 fm; the corresponding figures for the three ^3P-states with $J = 0, 1$, and 2 are 70, 70, and 50%, respectively. The behavior of these phases at low energies can therefore be explained by the long-range part of V_{OPEP}.

This behavior is, of course, representative of a mixture of a fairly weak central force and a dominant tensor force. If we assume a potential $V_C + V_T S_{12}$, there are simple expressions for the uncoupled and the coupled bar phases in the Born approximation [15]. Let δ_C and δ_T denote the Born phases that would be produced by the potentials V_C and V_T, respectively. Then, since the expectation values of S_{12} in the three ^3P-states are -4, 2, and $-\frac{2}{5}$, we have

$$\delta(^3P_0) = \delta_C - 4\delta_T, \qquad \delta(^3P_1) = \delta_C + 2\delta_T, \qquad \delta(^3P_2) = \delta_C - \tfrac{2}{5}\delta_T. \tag{5–42}$$

If V_C and V_T are taken to be positive, δ_C and δ_T are negative and it follows that

$$\delta(^3P_0) > \delta(^3P_2) > \delta(^3P_1). \tag{5–43}$$

The positive signs for V_C and V_T are predicted by V_{OPEP} in the ^3P-states, since $S = 1$ and $T = 1$, with $(\boldsymbol{\sigma}_1 \cdot \boldsymbol{\sigma}_2) = (\boldsymbol{\tau}_1 \cdot \boldsymbol{\tau}_2) = 1$. We further note that $\delta(^3P_1)$ in Eq. 5–43 is always negative, whereas, so long as δ_C is sufficiently small, $\delta(^3P_0)$ and $\delta(^3P_2)$ can still be positive, in conformity with the experimental findings.

At higher energies, the three ^3P-phases are at direct variance with the behavior shown in Eq. 5–43. Although the $^3P_1$-phase shift remains negative throughout, the $^3P_0$- and $^3P_2$-phases cross over near 100 MeV; indeed, the $^3P_0$-phase shift changes from positive to negative at about 200 MeV. Such behavior cannot be explained by $V_C + V_T S_{12}$ alone, but may be reproduced by invoking a spin-orbit force $V_{LS}\mathbf{L} \cdot \mathbf{S}$, which is of short range and therefore becomes operative at higher energies. With a potential of the form $V_C + V_T S_{12} + V_{LS}\mathbf{L} \cdot \mathbf{S}$, the Born phase shifts are given by

$$\delta(^3P_0) = \delta_C - 4\delta_T - 2\delta_{LS},$$

$$\delta(^3P_1) = \delta_C + 2\delta_T - \delta_{LS},$$
$$\delta(^3P_2) = \delta_C - \tfrac{2}{5}\delta_T + \delta_{LS}. \tag{5–44}$$

We see that, if δ_{LS} is positive, corresponding to a negative V_{LS}, then, when it is sufficiently large, $\delta(^3P_0)$ may change from positive to negative, while $\delta(^3P_2)$ continues to remain positive. The effect of this spin-orbit term is apparent even around 50 MeV, when $\delta(^3P_0)$ changes its slope. Such a spin-orbit force is generated, not by the one-pion-exchange process, but only by the exchange of heavier bosons of spin 1, and is therefore largely restricted within a radius of about 0.7 fm.

Finally, a word of caution is necessary in regard to the interpretation of phase shifts extracted from multienergy analyses. Most of the experimental data are clustered about 10, 25, 50, 95, 140, 210, and 320 MeV. At each of these energies, single-energy analyses have been done, and these are model independent. Multienergy analyses restrict the phase shifts and energy to a narrow band of values, but since the data are at rather widely separated energies, this restriction may be artificial. For example, at 95 MeV, the $^3P_0$-phase shift, according to single-energy analysis, is $11.17 \pm 2.15°$, whereas multienergy analysis gives $10.30 \pm 0.23°$. Thus the error limits in multienergy analyses should not be taken literally [30].

5-8 PHENOMENOLOGICAL NUCLEON-NUCLEON POTENTIALS

We have seen how a more or less unique set of phase shifts has been extracted in the laboratory energy range 0–450 MeV to correlate a large body of elastic N-N scattering data. This knowledge, however, is insufficient to determine a two-nucleon potential uniquely. Even in the simplest case of a local central potential without a bound state, it is necessary to know the phase shifts of a given partial wave at all positive energies to determine the potential uniquely. In spite of this ambiguity, it is convenient to construct N-N potentials that can reproduce these experimental phases because in the nonrelativistic region we have a dynamical model, namely, the Schrödinger equation, which can be applied to any nuclear problem, provided that the potential is known. In atomic physics, for example, the successes of the Coulomb potential are well known. In the nuclear case, although many different potentials can be constructed that fit the experimental phase shifts equally well from 0 to 450 MeV they yield different results in a many-body problem. For two nucleons scattering in the presence of a third nucleon, the scattering need not be elastic, since some energy may be taken away by the third particle. Thus "off-the-energy-shell" matrix elements of the interaction play an important role in determining the properties (like binding energy or equilibrium density) of a many-body system. One motivation for studying nuclear matter (see Chapter 9), for example, is to try to differentiate between potentials that yield the same phase shifts up to about 400 MeV.

Fortunately, some theoretical guide lines restrict the form of the N-N potential. First, there are the invariance principles, which state that the potential should remain invariant under symmetry operations like translation of space or momentum coordinates, rotation and reflection of the space axes, and time reversal. Additionally, using charge independence, the neutrons and protons may be treated on an equal footing for each i-spin state $T = 0$ and 1, so that the nuclear potential must be symmetric with respect to the exchange of the two nucleons. Finally, since we are considering the energy range in which inelastic processes can be ignored, the potential must be unitary. These principles were exploited by Eisenbud and Wigner [31] and later generalized by Okubo and Marshak [32]. The most general functional form of the potential may be written as

$$V = V_C + V_{LS}\mathbf{L}\cdot\mathbf{S} + V_\sigma\boldsymbol{\sigma}_1\cdot\boldsymbol{\sigma}_2 + V_T S_{12} + V_{\sigma p}(\boldsymbol{\sigma}_1\cdot\mathbf{p})(\boldsymbol{\sigma}_2\cdot\mathbf{p}) + V_{\sigma L}Q_{12}, \tag{5–45}$$

where each coefficient V_i can itself be written as

$$V_i = V_i^0(r, p, L) + V_i^\tau(r, p, L)\boldsymbol{\tau}_1\cdot\boldsymbol{\tau}_2. \tag{5–46}$$

In the above equations, $\mathbf{r} = \mathbf{r}_1 - \mathbf{r}_2$, $\mathbf{p} = \frac{1}{2}(\mathbf{p}_1 - \mathbf{p}_2)$,

$$\mathbf{L}\cdot\mathbf{S} = \tfrac{1}{2}(\mathbf{r}_1 - \mathbf{r}_2)\times(\mathbf{p}_1 - \mathbf{p}_2)\cdot(\boldsymbol{\sigma}_1 + \boldsymbol{\sigma}_2),$$

and

$$Q_{12} = \tfrac{1}{2}[(\boldsymbol{\sigma}_1\cdot\mathbf{L})(\boldsymbol{\sigma}_2\cdot\mathbf{L}) + (\boldsymbol{\sigma}_2\cdot\mathbf{L})(\boldsymbol{\sigma}_1\cdot\mathbf{L})].$$

It turns out that on the energy shell the term containing $V_{\sigma p}$ can be expressed in terms of the other terms in V.

In addition to the above general principles, we have some guidance from meson theory. Early efforts to use field theory to derive the N-N interaction through meson exchanges enjoyed only limited success, since multiple pion exchanges are very important for $r < 2$ fm and are difficult to calculate unambiguously. In the next section, we shall discuss this approach in more detail. We have seen from the phase-shift analyses of higher partial waves,

however, that the tail of the N-N potential (for $r > 3$ fm) should be of one-pion-exchange character. More progress in this direction has been made with the discovery of multipion resonances, and we shall discuss these later. But even with a completely phenomenological approach, the tail of the potential should be taken as that of OPEP. We now discuss some of the recently developed phenomenological potentials.

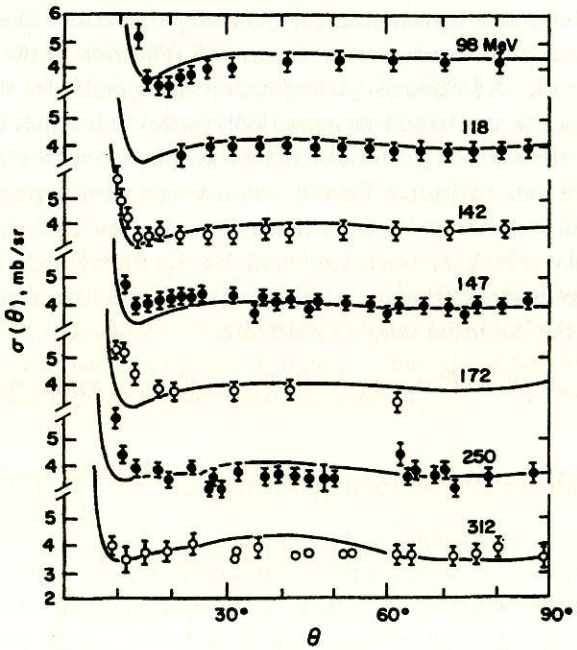

Fig. 5-13a

In Sections 5–6 and 5–7, we made analyses of the scattering data, keeping the potential model in mind. We indicated how the data demand that there be short-range repulsion, exchange force of almost Serber character, and tensor and spin-orbit components in the nucleon-nucleon potential. The earlier attempts to incorporate all these features in a phenomenological potential were due to Brueckner, Gammel, and Thaler [33] and Signell and Marshak [34]. In these attempts, the potential contained only the first four terms of Eq. 5–45, $V_{\sigma p}$ being superfluous for fitting phase shifts, and $V_{\sigma L}$

was ignored. For example, in the Brueckner-Gammel-Thaler potential, each V_i was taken to be a function of the relative distance r alone (which is a special case of Eq. 5–46), and to contain an infinite ("hard") repulsive core of 0.4 fm in each state, followed by an attractive potential of Yukawa

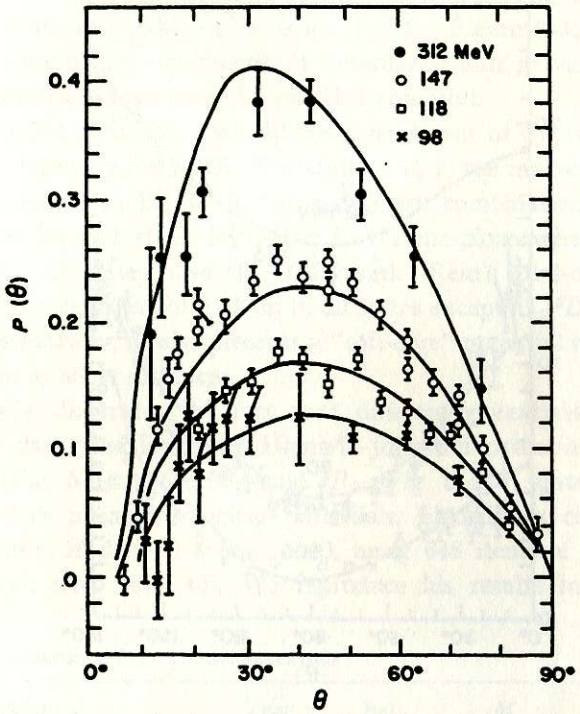

Fig. 5-13b

shape, whose range and strength were adjustable parameters for singlet-even, singlet-odd, triplet-even, and triplet-odd states. There were thus more than twenty adjustable parameters in the potential. In view of the number of data available in those days, the overall fit was reasonable. There were, however, two important shortcomings in this potential. First, it was noted that the singlet-even potential which fitted the $^1S_0$-phases yielded too large a $^1D_2$-phase shift at higher energies. It has been argued [35] that a purely local static potential cannot reproduce the experimental $^1S_0$- and

$^1D_2$-phases simultaneously. The second defect was that the tail of this potential did not correspond to one-pion-exchange form.

In later potentials given by Hamada and Johnston [36] and by the Yale group [37] both the above shortcomings were rectified. The term

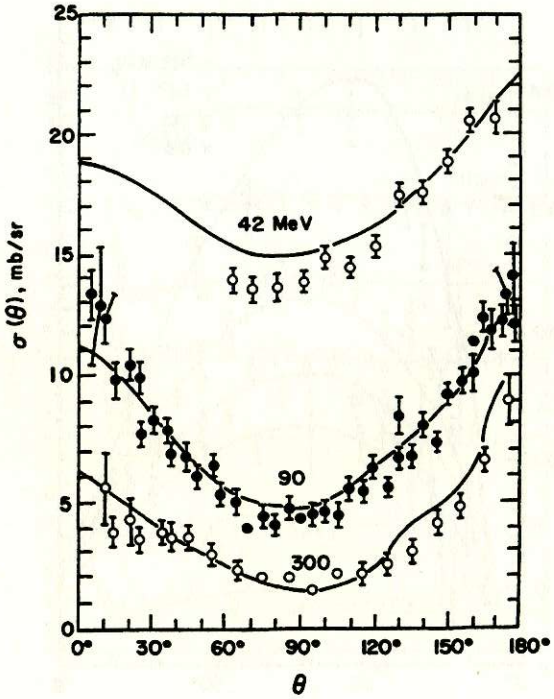

Fig. 5-13c

Fig. 5-13 Comparison of some of the experimentally measured nucleon-nucleon scattering data at various energies with the predictions of the Hamada-Johnston potential [36], shown by the solid lines. The p-p differential cross sections are shown in (a); the p-p polarization data in (b); and the n-p differential cross section in (c).

containing $V_{\sigma L}$ in Eq. 5–45 was included (in slightly different forms) in these potentials, so as to make the interaction weaker in the $^1D_2$-state than in the $^1S_0$-state. This L^2-dependent potential also helps in depressing the $^3D_2$-phases, thus making the interaction stronger in the $^3S_1$-$^3D_1$ state than in the $^3D_2$-state. In both the Yale and Hamada-Johnston (H-J) potentials,

the hard-core radius was close to 0.5 fm. The overall fit to data was greatly improved. There are minor discrepancies in the H-J potential, such as having some unphysical bound states for very high values of L, which can be removed by altering some parameters slightly [38]. Also, the H-J potential yields too large $^3F_4$-phases at higher energies, resulting in some broad bumps in the calculated p-p differential cross section, which are absent in the experimental data (see Fig. 5–13a). To obtain better agreement with the $^3F_4$-phases, the Yale group arbitrarily take $V_{LS} = 0$ for $J > 2$. Figure 5–13 presents for comparison some of the experimentally determined data at various energies and the theoretical curves given by the H-J potential.

An alternative potential, with different treatment of the repulsive core, has been developed by Reid [39]. For states $J \leqslant 2$, the mathematical form, although equivalent to Eq. 5–45, has a different combination of arbitrary functions—one for each state; for higher J's the one-pion-exchange potential may be used. All states have the OPEP tail. Reid's hard-core potential has a repulsive-core radius of 0.42 fm in all states except $^3S_1$-$^3D_1$, where it is 0.55 fm. Alternatively, he also presents a "soft-core" potential with Yukawa-type repulsion at short distances.

Figure 5–14 illustrates the fact that different potentials can fit the experimental data; the Reid and Hamada-Johnston potentials are shown for the $^1S_0$- (Fig. 5–14a), the $^3P_1$- and $^3P_0$- (Fig. 5–14b) states. For some of the hard-core phenomenological potentials, Signell has computed the least-square sum M defined in Eq. 5–40, using 648 items of 10–330 MeV p-p data taken from ref. [40]. We reproduce his results in Table 5–2:

TABLE 5-2 Goodness of Fit of Some Potentials

Potential	Year	Ref.	M	r_c, fm
Brueckner-Gammel-Thaler	1958	33	106	0.40
Hamada-Johnston	1962	36	2.98	0.4855
Yale	1962	37	3.81	0.5115
Reid hard-core	1968	39	2.72	0.423

In the notation of Eq. 5–40, $y_i(\delta)$ are the values of the observable y_i calculated from the phases generated by the chosen potential. It will be seen that the overall fits of the H-J and Yale potentials are nearly as good as the fit of the more recent Reid potential.

Figure 5–14 shows that the "soft core" of the Reid potential attains a height of more than 800 MeV for $r \sim 0.4$ fm. In this sense, the core is not

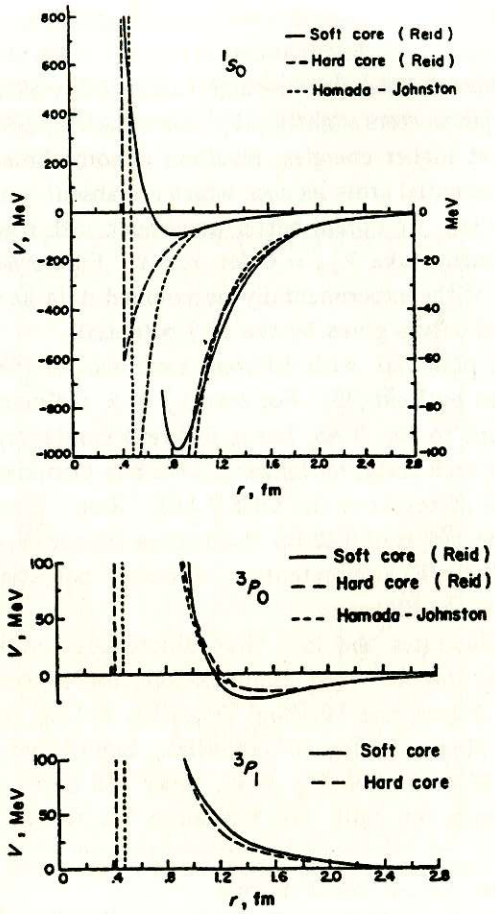

Fig. 5-14 Comparison of the Hamada-Johnston [36] and the Reid hard- and soft-core potentials [39]: (a) in the $^1S_0$-state and (b) in the $^3P_1$- and $^3P_0$-states. (After Reid [39].)

really very soft, but Sprung and Srivastava [41] have shown that it is possible to fit the $^1S_0$-phase shifts accurately with a "supersoft" repulsive core whose maximum height is only about 200 MeV, while still retaining the V_{OPEP} tail. This is made possible by spreading out the repulsive region to about 0.8 fm and at the same time reducing the height of the repulsive core. Sprung and de Tourreil [63] have also constructed supersoft potentials for the other partial waves (including the coupled channels) which fit the experimental phases accurately.

Many alternative and fruitful ways of constructing phenomenological interactions have been reported. One such approach is the so-called boundary-condition model (BCM), mainly developed by Lomon and Feshbach [42]. No attempt is made to specify the potential inside some boundary which delimits the "region of ignorance"; instead, one specifies boundary conditions (usually a separate energy-independent logarithmic derivative of the radial wave function for each partial wave at a common boundary of ~ 0.7 fm) that allow one to carry through a numerical evaluation of the wave function and hence of the phase shifts. The wave function outside the boundary is given by some potential, which may, for example, be generated by various one-boson-exchange processes.

In Section 5-3 we mentioned that the N-N potential is expected, from considerations of the meson theory, to be nonlocal especially for small internucleon distances. A simple form of nonlocality (not given by meson theory) is separable in r and r',

$$V(r, r') = g(r)g(r'), \tag{5-47}$$

where $g(r)$ is a smooth, finite-range function. Such potentials were first introduced by Yamaguchi [43] and later developed by Tabakin† [44] and Mongan [45]. The great advantage of this form is its simplicity in calculations. The two-body T-matrix, defined in the next section, can be calculated analytically for such potentials and is itself separable in r and r'. Mitra [46] has shown that the three-body problem can be solved exactly for such potentials. The form given in Eq. 5-47 is called a "rank-one" separable potential, since there is only one term on the right side. In order to fit the S-state phase shifts which change sign, one generally requires a rank-two separable potential with one repulsive and one attractive term. Separable potentials cannot have the local character of OPEP for larger distances and are therefore not very realistic. However, they may be regarded as offering one convenient way of extrapolating the off-shell behavior which is very different from the local approach.

Another class of nonlocal potentials contain momentum dependence explicitly:

$$V(r, p) = V_1(r) + \frac{p^2}{m} V_2(r) + V_2(r) \frac{p^2}{m}, \tag{5-48}$$

where p^2 is the operator $-\hbar^2\nabla^2$. This may be regarded as an expansion

† The Tabakin potential yields the value for the quadrupole moment of the deuteron as only 0.128 fm², which is far too low.

of a general nonlocal potential in a power series of p^2, with the leading terms retained. Phenomenologically, $V_1(r)$ is taken as attractive, while $V_2(r)$ is repulsive and of shorter range. Difficulties arise if $V_2(r)$ is attractive for any value of r, because then the interaction becomes more and more attractive for large p^2 and may give rise to bound states with no lower bound [47]. The form of Eq. 5–48 was suggested from a phenomenological viewpoint by Peierls [48], and a preliminary fit to experimental data was obtained by Green [49]. However, further improvements have been carried out within the framework of the one-boson-exchange model, discussed in section 5–12.

5-9 DEFINITION OF A POTENTIAL FROM MESON THEORY

We now proceed to formalize the ideas of Section 5–2 in order to define the concept of a potential arising from meson exchanges, which may be used in the Schrödinger equation. To do this, we first have to define, in terms of a two-body potential V, an energy-dependent operator T whose diagonal matrix elements at the scattering energy contain all the information about elastic scattering. The T-matrix, as it is called, can also be calculated from meson-exchange processes using field theory and hence can be used to make a connection between the potential and meson-theoretical approaches.

In relative coordinates, the Schrödinger equation can be written as ($\hbar^2/M = 1$, $E_k = k^2$)

$$(H_0 + V)|\psi_k\rangle = k^2|\psi_k\rangle,$$

where $H_0 = -\nabla^2$, and we are considering solutions in the continuum, for $E_k \geqslant 0$, which describe scattering. It is necessary to specify the boundary conditions; in particular, the form of $\langle \mathbf{r}|\psi_k\rangle$ will depend on whether we want outgoing or incoming spherical waves asymptotically. An alternative way of writing the Schrödinger equation is

$$|\psi_k\rangle = |\phi_k\rangle + G(E_k)V|\psi_k\rangle, \tag{5–49}$$

where $|\phi_k\rangle$ is just the solution of the homogeneous equation

$$(H_0 - k^2)|\phi_k\rangle = 0, \tag{5–50}$$

and $G(E_k)$ is the free Green's function, defined as

$$G(E_k) = \frac{1}{E_k - H_0 + i\varepsilon}, \tag{5–51}$$

where ε is an infinitesimal quantity which is finally put to zero. If we premultiply Eq. 5–49 by $G^{-1}(E_k) = E_k - H_0 + i\varepsilon$, it is immediately seen to be equivalent to the Schrödinger equation. The quantity $i\varepsilon$ is introduced to take care of the singularities of $G(E_k)$ in the k-space and actually incorporates the boundary condition at infinity. It can be shown (see, e.g., Gottfried [50]) that $+i\varepsilon$ gives rise to an outgoing spherical wave, while $-i\varepsilon$ corresponds to an incoming spherical wave at infinity. In Eq. 5–49, the first term on the right side, $|\phi_k\rangle$, is the incident wave, while the second term, $G(E_k)V|\psi_k\rangle$, is the scattered wave. Details of these interpretations are given by Gottfried. Equation 5–49 is often called the Lipmann-Schwinger equation.

Premultiplying Eq. 5–49 by V, we obtain

$$V|\psi_k\rangle = V|\phi_k\rangle + VG(E_k)V|\psi_k\rangle. \tag{5–52}$$

Now we define an operator $T(E_k)$, such that

$$T(E_k)|\phi_k\rangle = V|\psi_k\rangle. \tag{5–53}$$

It then follows that

$$T(E_k) = V + VG(E_k)T(E_k). \tag{5–54}$$

We can generalize Eq. 5–54 to any E, but $E = E_k = k^2$ corresponds to the physical scattering case. Matrix elements $\langle \mathbf{k}'|T(E_k)|\mathbf{k}\rangle$ with $k'^2 = k^2$ are "on the energy shell" because, for scattering involving only two bodies, the energy k^2 must be conserved. However, if three or more particles are present, part of the energy may be taken away by a third particle, and the two-body T-matrix may go "of the energy shell."† Such a situation may arise, for example, in proton-proton bremsstrahlung, $p + p \to p + p + \gamma$.

The scattering amplitude $f(\mathbf{k}', \mathbf{k})$ is defined as

$$\begin{aligned} f(\mathbf{k}', \mathbf{k}) &= -2\pi^2 \int \exp(-i\mathbf{k}' \cdot \mathbf{r}')\, V(r')\psi_k(\mathbf{r}')\, d^3r' \\ &= -2\pi^2 \langle \phi_{k'}|V|\psi_k\rangle, \end{aligned} \tag{5–55}$$

where, for elastic scattering, $k'^2 = k^2$. For this case, it is customary to use the variables k and θ, the angle between $\mathbf{k}$ and $\mathbf{k}'$, and to write $f(\mathbf{k}', \mathbf{k})$ as $f_k(\theta)$. From the definition of the T-operator, we see that ($k'^2 = k^2$)

$$f_k(\theta) = -2\pi^2 \langle \mathbf{k}'|T(E = k^2)|\mathbf{k}\rangle. \tag{5–56}$$

† More precisely, $\langle \mathbf{k}'|T(E_k)|\mathbf{k}\rangle$ with $k^2 \neq k'^2$ is termed "half off-shell," while $\langle \mathbf{k}'|T(E)|\mathbf{k}\rangle$ with $E \neq k^2 \neq k'^2$ is "completely off-shell." Using unitarity, one can express a completely off-shell matrix element in terms of half-off-shell ones. In the p-p bremsstrahlung process, half-off-shell matrix elements enter into the calculation.

All the information about elastic two-body scattering is contained in $f_k(\theta)$, that is, in the T-matrix on the energy shell. It is shown in most books of quantum mechanics (see, e.g., Gottfried [50]) that

$$f_k(\theta) = \sum_{l=0}^{\infty} \sqrt{4\pi(2l+1)}\,\frac{1}{k}\,e^{i\delta_l}\sin\delta_l Y_l^0(\theta), \tag{5–57}$$

where δ_l is the phase shift of the lth partial wave, and Y_l^0 is the standard spherical harmonic function defined in Eq. A–13. We derived the above equation for S-waves in Chapter 2 (see Eq. 2–31).

To summarize, in nonrelativistic scattering theory one defines an operator $T(E)$:

$$T(E) = V + VG(E)T(E), \tag{5–58}$$

with $G(E)$ given by Eq. 5–51, whose diagonal matrix elements on the energy shell, $\langle \mathbf{k}|T(E = k^2)|\mathbf{k}\rangle$, contain all the information about the elastic scattering of two particles. Note that, when calculating T from V by using Eq. 5–58, the intermediate states also contain only two nucleons, because the potential V causes transitions only between two-nucleon states.

From meson theory also, one can calculate the scattering amplitude, which has identical physical content but does not involve the concept of a potential. To do this, one classifies processes in which one, two, three, etc., pions are being exchanged between the two nucleons. With the pion-nucleon coupling constant denoted by g, the meson-theoretical scattering amplitude $\mathscr{T}$ can be expanded in a series

$$\mathscr{T} = g^2\mathscr{T}^{(1)} + g^4\mathscr{T}^{(2)} + \cdots, \tag{5–59}$$

where $\mathscr{T}^{(1)}$ is calculated from diagram (a) in Fig. 5–15, $\mathscr{T}^{(2)}$ from diagrams (b) and (c), and so forth. Diagrams (b) and (c) are different, although in both only two pions are exchanged, because the intermediate state of (c) contains two additional virtual pions. Using the techniques of field theory, $\mathscr{T}$ can be calculated completely relativistically. There are prescribed rules, due to Feynman, for calculating the contributions of diagrams like (a), (b), and (c) and hence $\mathscr{T}^{(1)}$, $\mathscr{T}^{(2)}$, etc. [51]. We indicate in Section 5–11 how, for example, $\mathscr{T}^{(1)}$ can be calculated.

To define a potential V, we may now demand that it should be such that the scattering amplitude T calculated from it by using Eq. 5–58 be identical to $\mathscr{T}$ for all k on the energy shell. To see this in more detail, let us expand V in a power series of g^2:

$$V = g^2V^{(1)} + g^4V^{(2)} + \cdots. \tag{5–60}$$

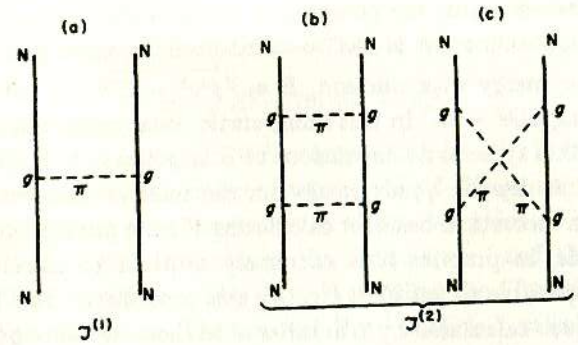

Fig. 5-15 Some meson-exchange processes contributing to the two-nucleon scattering amplitude $\mathscr{T}$. The single-pion-exchange contribution (a) is proportional to g^2 and gives $\mathscr{T}^{(1)}$; the two-pion-exchange processes (b) and (c), proportional to g^4, give $\mathscr{T}^{(2)}$.

Then, using Eq. 5–58, we obtain

$$T = g^2V^{(1)} + g^4V^{(2)} + g^4V^{(1)}GV^{(1)} + \cdots \tag{5–61}$$

$$= g^2T^{(1)} + g^4T^{(2)} + \cdots. \tag{5–62}$$

Hence

$$V^{(1)} = T^{(1)}, \tag{5–63}$$

$$V^{(2)} = T^{(2)} - V^{(1)}GV^{(1)}, \tag{5–64}$$

and so forth. Since we demand that $T^{(1)} = \mathscr{T}^{(1)}$, $T^{(2)} = \mathscr{T}^{(2)}$, etc., it follows that

$$V^{(1)} = \mathscr{T}^{(1)},$$

$$V^{(2)} = \mathscr{T}^{(2)} - V^{(1)}GV^{(1)}, \tag{5–65}$$

and so on. Knowing $\mathscr{T}^{(1)}$, $\mathscr{T}^{(2)}$, etc., from field theory, we can, in principle, calculate $V^{(1)}$, $V^{(2)}$, and the higher-order terms. Note that in calculating $\mathscr{T}^{(2)}$ all possible baryonic intermediate states should be taken; that is, the nucleon may have changed to a N^* (spin $\frac{3}{2}$, i-spin $\frac{3}{2}$) in the intermediate state. The two-pion-exchange potential (TPEP) $V^{(2)}$ will therefore depend on what intermediate states have been included in calculating $\mathscr{T}^{(2)}$.

Since the potential V is used in the Schrödinger equation, which is a nonrelativistic equation, it makes sense to take the nonrelativistic limits of the

field-theoretically calculated amplitudes $\mathscr{T}^{(1)}, \mathscr{T}^{(2)}, \ldots$. Unless some extreme approximations are made, the potential V turns out to be energy dependent. An extreme approximation is the so-called static approximation, in which the relativistic energy of a nucleon, $E = \sqrt{p^2c^2 + M^2c^4}$, is simply replaced by Mc^2, putting $p/M = 0$. In this limit, static, local potentials are obtained. Often, one makes systematic expansions of E in powers of $(p/M)^2$ and retains in V terms that depend quadratically on the relative momentum squared.

Although a theoretical basis for calculating V from multiple pion exchange has been made, in practice it is extremely difficult to calculate $V^{(2)}$ and practically impossible to get $V^{(3)}$, etc., by this procedure. The TPEP potential $V^{(2)}$ has been calculated by a number of authors, notably by Cottingham and Vinh Mau [52] and most recently by Partovi and Lomon [53]. A good discussion of TPEP can be found in a review article by Signell [30]. There is experimental evidence that multiple pions are strongly correlated, sometimes forming a metastable state with definite quantum numbers, which may be looked upon as short-lived bosons. The current trend is to replace the multiple-pion-exchange processes between two nucleons by these single boson exchanges, which are also called "resonances." This simplifies things greatly, since only terms like $\mathscr{T}^{(1)}$ have to be evaluated, and the resulting potential can be obtained directly. Before discussing the one-boson-exchange potentials (OBEP) more fully, we present some details about the resonances.

5-10 BOSON RESONANCES

First we discuss the experiments that show that multiple pions can be strongly correlated. In such cases, a two-pion or a three-pion system may be thought of as a metastable state with definite quantum numbers and be regarded as a short-lived meson in its own right. Consider the reaction of monoenergetic pions of high energy (~ 1 GeV) interacting with the protons of liquid hydrogen in a bubble chamber:

$$p + \pi^- \rightarrow \begin{matrix} \pi^- + \pi^0 + p, \\ \pi^+ + \pi^- + n. \end{matrix} \tag{5–66}$$

If the two pions in the final state formed a bound state, there would be essentially only two bodies in the final state, and each would have a definite kinetic energy. The situation is analogous to that in Section 2–6, where the final-state interaction between two neutrons was considered. If there is no real bound state of the two pions, but they are strongly correlated, this will show up as a peak when the number of events is plotted against the

kinetic energy of the third particle. Relativistically, the energy of a particle is $E^2 = (\mathbf{p})^2 + m^2$, where we have put $c = 1$; $\mathbf{p}$ is the three-momentum and m is the rest-mass of the particle. Thus

$$m^2 = E^2 - (\mathbf{p})^2 = -p_\mu{}^2, \tag{5–67}$$

where p is the four-momentum with components $(\mathbf{p}, iE)$. It is more convenient, therefore, to plot the number of events in Eq. 5–66 against $-(p_{1\mu} + p_{2\mu})^2$, where $p_{1\mu}$ and $p_{2\mu}$ are the four-momenta of the two pions. The peak in this graph will directly give the mass of the "resonance," and this is shown in Fig. 5–16. The quantity $-(p_{1\mu} + p_{2\mu})^2$ is called the "invariant mass" for reasons explained above. The mass of this "particle," called the ρ-meson, is about 765 MeV with a width Γ of about 125 MeV. This means that this compound state has a lifetime τ of the order of $\hbar/\Gamma \approx 5 \times 10^{-24}$ sec, much too short to be detected experimentally. Note that the mass of a resonance is greater than the combined mass of the two pions, whereas the mass of

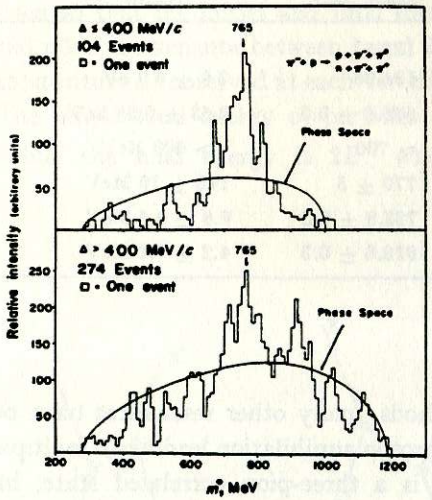

Fig. 5-16 Two-pion resonance ρ in the three-body final state in the reaction

$$\pi^- + p \rightarrow \left.\begin{matrix} p + \pi^- + \pi^0 \\ n + \pi^- + \pi^+ \end{matrix}\right\}.$$

The relative intensity of the experimental counts is plotted against the invariant mass of the two pions in the final state. The smooth curve is the phase-space prediction, normalized to the number of events plotted. The upper distribution is for the situation in which the momentum transfer to the nucleon, Δ, < 400 MeV/c, while the lower one is for $\Delta > 400$ MeV/c. The peak at 765 MeV corresponds to the ρ-mass. [After A. R. Erwin, R. March, W. D. Walter, and E. West, *Phys. Rev. Lett.* **6**, 628 (1961).]

a truly bound system is less than the sum of its constituent masses (e.g., the mass of the deuteron is less than the sum of the proton and neutron masses).

We should be able to assign definite quantum numbers to this resonance if it is to be regarded as a separate entity. The resonance is not found in the reaction $\pi^+ + p \rightarrow \pi^+ + \pi^+ + n$, hence the i-spin of the ρ-meson is 1. This i-spin of 1 is obtained by combining two pion i-spins of 1 each, and the i-spin part of the wave function is antisymmetric. Since the total wave function of two bosons must be symmetric, and the spin of each pion is zero, it follows that the ρ-meson must have odd-integral total spin, the simplest assignment being 1^-. In this particular case, more direct determination of the quantum numbers is difficult.

TABLE 5-3 Some of the Experimentally Detected Bosons That Contribute to the N-N Interaction. Parameters are taken from "Review of Particle Properties," *Rev. Mod. Phys.* **45**, 51 (1973).

Boson	Mass, MeV	Width	T	J^p
$\pi^\pm$	139.57	0	1	0^-
π^0	134.96	7.8 ± 0.9 eV		
η	548.8 ± 0.6	2.63 ± 0.58 keV	0	0^-
σ_0 [a]	≈ 700	> 600 MeV	0	0^+
ρ	770 ± 5	146 ± 10 MeV	1	1^-
ω	783.8 ± 0.3	9.8 ± 0.5 MeV	0	1^-
ϕ	1019.6 ± 0.3	4.2 ± 0.2 MeV	0	1^-

[a] Also called ε.

By the same methods, many other resonances have been detected. By studying proton-antiproton annihilation leading to multiple-pion production, the ω-meson, which is a three-pion correlated state, has been detected. Table 5-3 lists the bosons that are often used to calculate the OBEP N-N potential. It should be noted that the η-meson is stable against strong interactions and decays only by electromagnetic processes. It should be regarded, not as a multiple-pion resonance, but as a heavy, stable meson in its own right. Bosons with spin parity $(J^p) = 0^+$ are scalars, with $J^p = 0^-$ are pseudoscalars, and with $J^p = 1^-$ and 1^+ are respectively vectors and pseudovectors, because the corresponding fields transform accordingly under proper Lorentz transformation and space inversion (see Section A-4).

5-11 DERIVATION OF THE OBEP

In order to provide a more complete understanding for interested students, we give an outline of the derivation of the OBEP, using the concepts of Section 5-9. The potential will depend, of course, on the type of interaction between the meson field and the nucleons. This, in turn, depends on whether the meson field transforms as a scalar, as a pseudoscalar, or as a vector. We take the example where the exchanged boson is a pion, which has a pseudoscalar field. For simplicity, we ignore the charge of the nucleons and the pion.

Now consider Fig. 5-17, where two nucleons, 1 and 2, are scattered via the exchange of a single pion. The time scale is chosen to run upward, and there are two possible "time orderings" for the process, which are shown in Figs. 5-17a and 5-17b. We concentrate first on Fig. 5-17a. At "vertex" 1, the nucleon with momentum $\mathbf{p}$ emits a pion and goes to state $\mathbf{p}'$. At a later time, the second nucleon with momentum $-\mathbf{p}$ absorbs this virtual pion at vertex 2, itself going over to a state $-\mathbf{p}'$. For convenience, the center-of-mass frame is chosen so that the initial and final total momenta are zero. The initial and final relative momenta between 1 and 2 are $\mathbf{p}$ and $\mathbf{p}'$, respectively. Since the momentum is conserved at each vertex, the pion momentum is $\mathbf{q} = \mathbf{p} - \mathbf{p}'$. The initial total energy of particles 1 and 2 is $2E$, with $E = \sqrt{p^2 + M^2}$, while the final energy is $2E'$, where $E' = \sqrt{p'^2 + M^2}$.

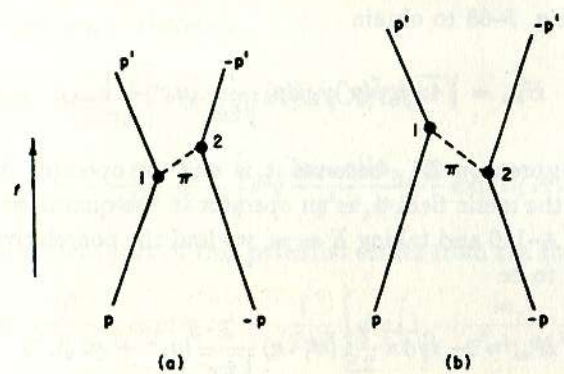

Fig. 5-17 Two-nucleon scattering via the exchange of a single pion.

For elastic scattering, $E = E'$. This is the case that we consider here, since we want to evaluate the scattering amplitude on the energy shell. As shown in Eq. A–136, the matrix element for the process at vertex 1 is

$$i\sqrt{4\pi}\, g \int \bar{\psi}(\mathbf{p}') \exp(-\, i\mathbf{p}' \cdot \mathbf{r})\, \gamma_5 \phi_\pi(\mathbf{r}) \psi(\mathbf{p}) \exp(i\mathbf{p} \cdot \mathbf{r})\, d^3r, \tag{5–68}$$

where $\psi(\mathbf{p})$ is the nucleon spinor and is defined in Eq. A–95. To proceed, we have to quantize the mesic field ϕ_π, giving it the role of creating or annihilating a pion. In this role, it acts as an operator on the meson state. We write the mesic field in the quantized form as

$$\phi_\pi(r) = \sum_{\mathbf{q}'} \frac{1}{\sqrt{2w_{q'}}} [a_{\mathbf{q}'} \exp(i\mathbf{q}' \cdot \mathbf{r}) + a_{\mathbf{q}'}{}^{+} \exp(-\, i\mathbf{q}' \cdot \mathbf{r})], \tag{5–69}$$

where $w_{q'} = \sqrt{m_\pi{}^2 + q'^2}$, and $a_{\mathbf{q}'}$ and $a_{\mathbf{q}'}^{+}$ are, respectively, the annihilation and creation operators for a meson of momentum $\mathbf{q}'$. If we denote a state with no meson present by the "vacuum" $|0\rangle$, and a state with one meson of momentum $\mathbf{q}$ by $|1_{\mathbf{q}}\rangle$, then $a_{\mathbf{q}}$ and $a_{\mathbf{q}}{}^{+}$ are defined by the equations

$$a_{\mathbf{q}}|0\rangle = 0, \tag{5–70}$$

$$a_{\mathbf{q}}{}^{+}|0\rangle = |1_{\mathbf{q}}\rangle, \tag{5–71}$$

$$a_{\mathbf{q}}|1_{\mathbf{q}}\rangle = |0\rangle. \tag{5–72}$$

Note that the initial state, with two nucleons of momenta $\mathbf{p}$ and $-\,\mathbf{p}$, is a meson vacuum $|0\rangle$, and so also is the final state. The meson field ϕ_π creates a pion at vertex 1, which in turn is annihilated at vertex 2. Let us substitute Eq. 5–69 into Eq. 5–68 to obtain

$$H_{\text{int}} = \sqrt{4\pi}\, ig\bar{\psi}(\mathbf{p}')\gamma_5\psi(\mathbf{p}) \frac{1}{\sqrt{2w_q}} (a_{\mathbf{q}}{}^{+} + a_{-\mathbf{q}}). \tag{5–73}$$

We call this expression H_{int} because it is still an operator in the meson variable, since the mesic field ϕ_π is an operator in the quantized form. Using Eqs. A–98 and A–110 and taking $E \approx m$, we find the nonrelativistic approximation of this to be

$$H_{\text{int}} = -\, i\sqrt{4\pi}\, \frac{g}{2E} (\boldsymbol{\sigma}_1 \cdot \mathbf{q}) \frac{1}{\sqrt{2w_q}} (a_{\mathbf{q}}{}^{+} + a_{-\mathbf{q}}), \tag{5–74}$$

where $\boldsymbol{\sigma}_1$ is to be understood to act on the nonrelativistic spin states of nucleon 1. Note that this is Hermitian, since $\mathbf{p}$ and $\mathbf{p}'$ should be interchanged

while taking the Hermitian adjoint. In order to reach the final state from the initial one, two operations of H_{int} are necessary; one for creating a meson and a second for annihilating it. Thus the lowest-order scattering amplitude between relative momenta $\mathbf{p}$ of the initial state and $\mathbf{p}'$ of the final state is given by second-order perturbation theory and is of the order g^2,

$$\langle \mathbf{p}'|\mathscr{T}^{(1)}|\mathbf{p}\rangle = 2\sum_n \langle 0|H_{\text{int}}|n\rangle \frac{1}{\varepsilon_i - \varepsilon_n} \langle n|H_{\text{int}}|0\rangle. \tag{5–75}$$

The factor 2 takes account of the diagram in Fig. 5–15b, which gives an identical contribution. For fixed $\mathbf{p}$ and $\mathbf{p}'$, $|n\rangle$ is just a one-meson state with fixed momentum $\mathbf{q}$, that is, $|n\rangle = |1\mathbf{q}\rangle$. The energy denominator is the difference between the initial- and the intermediate-state energies,

$$\varepsilon_i - \varepsilon_n = -\sqrt{m_\pi{}^2 + q^2} = -\, w_q. \tag{5–76}$$

Using Eqs. 5–70 to 5–73, we get

$$\langle \mathbf{p}'|\mathscr{T}^{(1)}|\mathbf{p}\rangle = -\frac{g^2}{w_q{}^2} \frac{4\pi}{4E^2} (\boldsymbol{\sigma}_1 \cdot \mathbf{q})(\boldsymbol{\sigma}_2 \cdot \mathbf{q}). \tag{5–77}$$

In the static limit, $E^{-2} = (p^2 + M^2)^{-1}$ is simply replaced by M^{-2}, assuming that $(p/M)^2 \ll 1$. According to Section 5–9, we should now equate $\langle \mathbf{p}|\mathscr{T}^{(1)}|\mathbf{p}\rangle$ to $\langle \mathbf{p}|V_{\text{OPEP}}|\mathbf{p}\rangle$, where

$$\begin{aligned} \langle \mathbf{p}'|V_{\text{OPEP}}|\mathbf{p}\rangle &= \int \exp[i(\mathbf{p}' - \mathbf{p}) \cdot \mathbf{r}]\, V_{\text{OPEP}}(r)\, d^3r \\ &= V_{\text{OPEP}}(\mathbf{q}). \end{aligned} \tag{5–78}$$

In the coordinate space, therefore,

$$\begin{aligned} V_{\text{OPEP}}(\mathbf{r}) &= \frac{1}{(2\pi)^3} \int V_{\text{OPEP}}(\mathbf{q}) \exp(i\mathbf{q} \cdot \mathbf{r})\, d^3q \\ &= -\frac{g^2}{4M^2} \frac{4\pi}{(2\pi)^3} \int d^3q \frac{(\boldsymbol{\sigma}_1 \cdot \mathbf{q})(\boldsymbol{\sigma}_2 \cdot \mathbf{q})}{q^2 + m_\pi{}^2} \exp(i\mathbf{q} \cdot \mathbf{r}). \end{aligned} \tag{5–79}$$

Note that the central part of this potential comes from the integral

$$\frac{1}{(2\pi)^3} \int d^3q \frac{q^2}{q^2 + m_\pi{}^2} \exp(i\mathbf{q} \cdot \mathbf{r}) = \frac{1}{(2\pi)^3} \int d^3q \left(1 - \frac{m_\pi{}^2}{q^2 + m_\pi{}^2}\right) \exp(i\mathbf{q} \cdot \mathbf{r})$$

and therefore contains a delta function $\delta(\mathbf{r})$ at the origin, which should be discarded. One way of doing this is to replace $(\boldsymbol{\sigma}_1 \cdot \mathbf{q})(\boldsymbol{\sigma}_2 \cdot \mathbf{q})$ by $-\,(\boldsymbol{\sigma}_1 \cdot \nabla)(\boldsymbol{\sigma}_2 \cdot \nabla)$ and bring it out of the integral. Then

$$V_{\text{OPEP}}(\mathbf{r}) = \frac{g^2}{4M^2}(\boldsymbol{\sigma}_1 \cdot \nabla)(\boldsymbol{\sigma}_2 \cdot \nabla)\frac{4\pi}{(2\pi)^3}\int d^3q\,\frac{\exp(i\mathbf{q}\cdot\mathbf{r})}{q^2 + m_\pi^2}.$$

Since

$$\frac{1}{(2\pi)^3}\int d^3q\,\frac{\exp(i\mathbf{q}\cdot\mathbf{r})}{q^2 + m_\pi^2} = \frac{1}{4\pi}\frac{\exp(-m_\pi r)}{r},$$

$$V_{\text{OPEP}}(\mathbf{r}) = \frac{q^2}{4M^2}m_\pi(\boldsymbol{\sigma}_1 \cdot \nabla)(\boldsymbol{\sigma}_2 \cdot \nabla)\left(\frac{\exp(-m_\pi r)}{m_\pi r}\right). \tag{5–80}$$

It can be shown that

$$(\boldsymbol{\sigma}_1 \cdot \nabla)(\boldsymbol{\sigma}_2 \cdot \nabla)\frac{\exp(-m_\pi r)}{m_\pi r}$$

$$= \tfrac{1}{3}m_\pi^2\left[(\boldsymbol{\sigma}_1 \cdot \boldsymbol{\sigma}_2) + S_{12}\left(1 + \frac{3}{m_\pi r} + \frac{3}{(m_\pi r)^2}\right)\right]\frac{\exp(-m_\pi r)}{m_\pi r}, \tag{5–81}$$

finally giving the form of Eq. 5–14. The extra factor of $(\boldsymbol{\tau}_1 \cdot \boldsymbol{\tau}_2)$ in Eq. 5–14 arises from i-spins of nucleons 1 and 2, which were ignored in this discussion. Since $(\boldsymbol{\sigma}_1 \cdot \boldsymbol{\sigma}_2)(\boldsymbol{\tau}_1 \cdot \boldsymbol{\tau}_2)$ is -3 for all even states, the central part of V_{OPEP} is attractive for these. We find that a strong tensor potential is naturally generated by a pseudoscalar meson exchange. We also note that, even if we did not make the static approximation in Eq. 5–77 of replacing E^{-2} by M^{-2}, the momentum dependence would be very small, of the order of $(p/M)^2$, compared with the static term.

Exchange of a scalar meson also gives rise to an attractive static central potential and, in addition, a two-body spin-orbit potential whose relative strength is proportional to m_s/M, where m_s is the mass of the scalar meson. Also, the momentum-dependent terms, which arise from expanding terms like $(E + M)/2E$, are stronger than those coming from exchange of a pseudoscalar meson.

When a vector meson is exchanged between two nucleons, the static part of the central potential is repulsive. This is analogous to the repulsive Coulomb potential, which arises from the exchange of a vector particle, the photon. It also gives rise to a spin-orbit potential, a tensor potential, and some momentum-dependent terms. The derivations of these potentials arising from scalar and vector meson exchanges are too lengthy to be given here, but they follow essentially the same lines as the pseudoscalar meson case. A detailed account can be found in Moszkowski [54].

5-12 MAIN FEATURES OF THE OBEP

We have seen that the experimental phase-shift data (for $E_{\text{lab}} < 450$ MeV) can be reproduced by various forms of phenomenological potentials. Many of these have the OPEP tail, but otherwise contain thirty or more adjustable parameters. In the past few years, however, a better understanding has been gained by appreciating the roles that the various mesons and resonances play in generating the N-N force. These are as follows:

1. The long-range part ($r > 3$ fm) of the N-N potential is given by the one-pion-exchange mechanism.

2. The attractive interaction at intermediate ranges ($0.7 < r < 2$ fm) can be simulated by the exchange of scalar mesons. Most authors introduce two scalar mesons ($J^p = 0^+$): one with $T = 0$, $m \sim 500$ MeV, and the other with $T = 1$, $m > 700$ MeV. Experimentally, at least one broad scalar resonance is seen around 700 MeV with $T = 0$. These scalar resonances may be regarded as substitutes for the two-pion-exchange contribution, which is rather difficult to calculate. The scalar meson also generates a spin-orbit term which is attractive for all states for the isoscalar ($T = 0$) case. In addition, momentum-dependent repulsive potentials are also produced.

3. The central N-N interaction is only weakly attractive in the triplet-odd states. This feature can be explained by exchange of the vector ρ-meson. The resulting potential has the characteristic $(\boldsymbol{\tau}_1 \cdot \boldsymbol{\tau}_2)(\boldsymbol{\sigma}_1 \cdot \boldsymbol{\sigma}_2)$ factor in one of the central terms, which is attractive for even-l and repulsive for odd-l states. It also produces a tensor potential of opposite sign to OPEP. This results in the tensor component of the N-N force being much weaker at intermediate ranges than that of the OPEP, bringing about better agreement with the experimental triplet-D and triplet-P phases. The spin-orbit potential generated by the ρ has a $(\boldsymbol{\tau}_1 \cdot \boldsymbol{\tau}_2)$ factor which makes it repulsive in triplet-even states and attractive in triplet-odd ones. Momentum-dependent terms of the same form as those due to the scalar meson are also produced.

4. The isoscalar vector mesons ω and ϕ contribute a very strong short-range repulsion, which is needed to fit the S-wave phases at higher energies. These mesons also give rise to an attractive spin-orbit potential in all triplet states, which adds to the scalar contribution. In triplet-even states, this nearly cancels out with the repulsive ρ-contribution, leaving only a strongly attractive spin-orbit potential in triplet-odd states. This is needed to explain the experimental splitting of the triplet P-waves above 50 MeV.

In constructing an OBEP, one generally includes all the resonances up to 1 GeV which are listed in Table 5–3 and another scalar meson, σ_1, with

$T = 1$. If all the masses and coupling constants of these bosons were known from other sources, the predictions of such a potential could be compared directly with experiment. Not much information is available, however, about the coupling constants. Before discussing this, we note that two types of coupling, direct and gradient, are possible (see Eqs. A-136 to A-139). For pseudoscalar mesons, these essentially give identical potentials in the lowest order. For each vector meson, however, there are two distinct coupling constants g_v and f_v, as given in Eqs. A-138 and A-139. In the absence of detailed knowledge about all these coupling constants, they can be taken as "search parameters" to obtain the best possible agreement between the experimental and theoretically calculated phase shifts. Additionally, the masses of σ_0 and σ_1 are taken as adjustable, since they parametrize part of the two-pion-exchange contributions. Since the ω and ϕ are so similar, their effects are often included in a single isoscalar vector meson. The tensor coupling f_v for this meson is generally taken to be zero, since this value is indicated from studies of the electromagnetic form factors of nucleons [54]. The pion-nucleon coupling constant g^2 is known to be 15.0 ± 0.3 from π-N scattering data [55] and is generally kept fixed around this value. Even when it is taken as a search parameter, its optimum value comes close to the above number, which puts the OBEP model in a favorable light. After making these simplifying assumptions, there are eight free parameters in the model: m_{σ_0}, m_{σ_1}, g_{σ_0}, g_{σ_1}, g_π, g_ω, g_ρ, and f_ρ.

The most elaborate OBEP models have been constructed by Bryan and Scott [56], Ingber [57], Ueda and Green [58], and Erkelenz, Holinde, and Bleuler [59]. These models have been successful in reproducing the N-N data up to 350-MeV laboratory energy, the fits being comparable to those of purely phenomenological potentials which use many more parameters. These potentials also fit the S-wave data and the deuteron parameters reasonably well, but there are some important discrepancies. Signell [60] and MacGregor, Arndt, and Wright [23] have extracted the (bar) mixing parameter ε_1 between the $^3S_1$- and $^3D_1$-phases from n-p scattering data by single-energy phase-shift analyses at different energies, as shown by the open circles in Fig. 5–18. This parameter† is important because it is a measure of the tensor-to-central ratio in the triplet-even $J = 1$, $T = 0$ interaction. For comparison, the

† In the Blatt-Biedenharn convention, the slope of the mixing parameter ε_1^{BB} at zero energy is directly related to the quadrupole moment Q_d of the deuteron:

$$Q_d \approx \frac{1}{\sqrt{2}} \frac{d\varepsilon_1^{BB}}{dk^2}\bigg|_{k=0},$$

where $k^2 = ME_{\text{lab}}/2\hbar^2$. See P. Signell, *Phys. Rev.* C2, 1171 (1970).

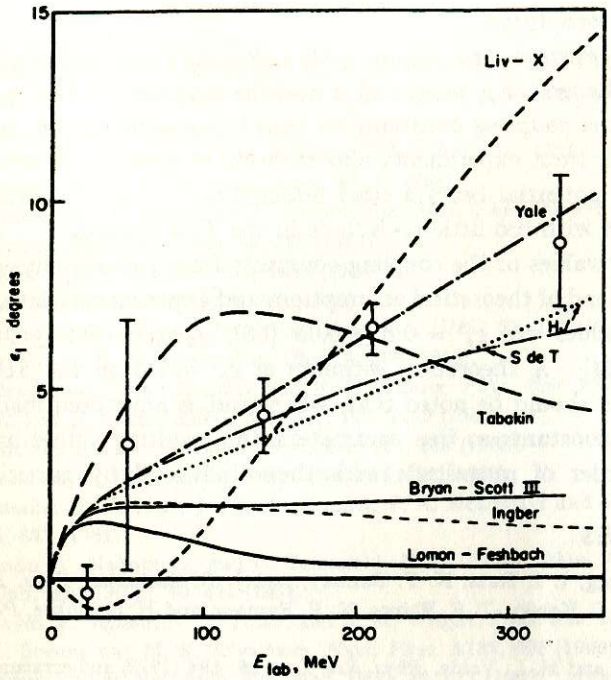

Fig. 5-18 The mixing parameter ε_1 (see Eq. 5–30 in the $T = 0$, $J = 1$ channel in n-p scattering, as extracted by Signell [60] and by MacGregor et al. [23] from single-energy analysis (shown by open circles with error bars) and from multienergy analysis (shown by the dashed curve). Predictions of the Yale [37], H-J [36], Tabakin [44], Lomon-Feshbach [42], Ingber [57], Bryan-Scott [56], and Sprung-de Tourreil [63] potentials are shown for comparison.

results of the multienergy analyses of the Livermore group [23] are also shown, along with the predictions of the different phenomenological potentials. It will be noted that the OBEP potentials generally underestimate ε_1, indicating too strong a central component relative to the tensor strength. This has serious implications in the binding-energy calculation of nuclear matter, which we shall discuss in Chapter 8. We note, however, that Grangé and Preston [64] have proposed an OBEP potential that yields ε_1 in satisfactory agreement with experiment, giving a curve slightly above that labelled S de T in Fig. 5–18.

It should be noted that in the OBEP model there is an ambiguity about how to treat the singularities at the origin in configuration space, which arise if no cutoff is introduced. Bryan and Scott, as well as Ingber, take care of this for $L > 0$ by retaining the p^2-dependent terms. For the S-wave,

either an explicit cutoff in the configuration space [56] or pionic form factors [58] must be introduced.

Recently, Partovi and Lomon [53] calculated the potential produced by single exchanges of ρ, ω, η, and π and the exchange of two pions. They did not use the coupling constants as search parameters, but chose values with guidance from experiments and theories in particle physics. Beyond 0.7 fm, their potential bears a close resemblance to the Hamada-Johnston potential, but with too little $\mathbf{L}\cdot\mathbf{S}$ force in the $T = 1$ states.

Obtaining values of the coupling constants from particle physics requires the use of a blend of theoretical assumptions and experimental data. Currently reasonable values are $g_\rho^2 = 0.6 \pm 0.05$ [55], $g_\omega^2/g_\rho^2 = 9.0 \pm 3$ [56], and $f_\rho/g_\rho = 3.7$ [54]. A theoretical estimate of g_η^2 based on the $SU(3)$ model is about 2. It should be noted that, when studies have been made treating the coupling constants as free parameters, the resulting values have agreed in general order of magnitude with those indicated by particle physics.

REFERENCES

1. J. B. Kellogg, I. I. Rabi, N. F. Ramsey, and J. R. Zacharias, *Phys. Rev.* **57**, 677 (1940); H. G. Kolsky, T. E. Phipps, N. F. Ramsey, and H. B. Silibee, *Phys. Rev.* **87**, 395 (1952).
2. R. V. Reid and M. L. Vaida, *Phys. Rev. Lett.* **29**, 494 (1972) and erratum.
3. I. Lindgren, in *Alpha-, Beta-, and Gamma-Ray Spectroscopy*, ed. K. Siegbahn, North-Holland, Amsterdam, 1966.
4. W. Rarita and J. Schwinger, *Phys. Rev.* **59**, 436, 556 (1941).
5. C. Michael and C. Wilkin, *Nucl. Phys.* **B11**, 99 (1969).
6. N. K. Glendenning and G. Kramer, *Phys. Rev.* **126**, 2159 (1962).
7. C. D. Buchanan and M. R. Yearian, *Phys. Rev. Lett.* **15**, 303 (1965).
8. J. E. Elias, J. I. Friedman, G. C. Hartmann, H. W. Kendall, P. N. Kirk, M. R. Sogard, L. P. Van Speybroeck, and J. K. de Pagter, *Phys. Rev.* **177**, 2075 (1969).
9. R. J. Adler and S. D. Drell, *Phys. Rev. Lett.* **13**, 349 (1964).
10. R. Blankenbecler and J. F. Gunion, *Phys. Rev.* **D4**, 718 (1971).
11. H. Yukawa, *Proc. Phys. Math. Soc. Japan* **17**, 48 (1935).
12. M. Matsumato and W. Watari, *Progr. Theor. Phys.* **11**, 63 (1954).
13. L. Wolfenstein, *Ann. Rev. Nucl. Sci.* **6**, 43 (1956).
14. T. V. Kanellopoulos and G. E. Brown, *Proc. Phys. Soc. (London)* **A70**, 690, 703 (1957).
15. H. P. Stapp, T. J. Ypsilantis, and N. Metropolis, *Phys. Rev.* **105**, 302 (1957).
16. O. Chamberlain, R. Donaldson, E. Segre, R. Tripp, C. Wiegand, and T. Ypsilantis, *Phys. Rev.* **95**, 850 (1954).
17. R. T. Siegel, A. J. Hartzler, and W. A. Love, *Phys. Rev.* **101**, 838 (1956).
18. W. N. Hess, *Rev. Mod. Phys.* **30**, 368 (1958).
19. R. Jastrow, *Phys. Rev.* **81**, 165 (1951).
20. K. M. Case and A. Pais, *Phys. Rev.* **80**, 203 (1950).

21. M. H. MacGregor, R. A. Arndt, and R. M. Wright, *Phys. Rev.* **169**, 1149 (1969); N. Hoshizaki, *Rev. Mod. Phys.* **39**, 700 (1967).
22. R. A. Arndt and M. H. MacGregor, *Phys. Rev.* **141**, 873 (1966).
23. M. H. MacGregor, R. A. Arndt, and R. M. Wright, *Phys. Rev.* **182**, 1714 (1969).
24. R. E. Seamon, K. A. Friedman, G. Breit, R. D. Haracz, J. M. Holt, and A. Prakash, *Phys. Rev.* **165**, 1579 (1968).
25. M. D. Miller, P. S. Signell, and N. R. Yoder, *Phys. Rev.* **176**, 1724 (1968).
26. N. Hoshizaki, *Progr. Theor. Phys. Suppl.* **42**, 1 (1968).
27. Yu M. Kazarinov, F. Lehar, and Z. Janout, *Rev. Mod. Phys.* **39**, 571 (1967).
28. J. K. Perring, *Rev. Mod. Phys.* **39**, 550 (1967).
29. M. H. MacGregor, *Phys. Rev.* **113**, 1559 (1959).
30. P. Signell, *Advan. Nucl. Phys.* **2**, 223 (1969).
31. L. Eisenbud and E. Wigner, *Proc. Natl. Acad. Sci. (U.S.)* **27**, 281 (1941).
32. S. Okubo and R. E. Marshak, *Ann. Phys.* **4**, 166 (1958).
33. K. A. Brueckner, J. A. Gammel, and R. M. Thaler, *Phys. Rev.* **109**, 1023 (1958).
34. P. Signell and R. E. Marshak, *Phys. Rev.* **109**, 1229 (1958).
35. D. A. Giltinan and R. M. Thaler, *Phys. Rev.* **131**, 805 (1963).
36. T. Hamada and I. D. Johnston, *Nucl. Phys.* **34**, 382 (1962).
37. K. E. Lassila, M. H. Hull, Jr., H. M. Ruppel, F. A. McDonald and G. Breit, *Phys. Rev.* **126**, 881 (1962).
38. T. Hamada, Y. Nakamura, and R. Tamagaki, *Progr. Theor. Phys.* **33**, 769 (1965).
39. R. V. Reid, *Ann. Phys.* **50**, 411 (1968).
40. H. P. Noyes, P. Signell, N. R. Yoder, and R. M. Wright, *Phys. Rev.* **159**, 789 (1967).
41. D. W. L. Sprung and M. K. Srivastava, *Nucl. Phys.* **A139**, 605 (1969).
42. E. L. Lomon and H. Feshbach, *Rev. Mod. Phys.* **39**, 611 (1967); *Ann. Phys. (N.Y.)* **48**, 94 (1968).
43. Y. Yamaguchi, *Phys. Rev.* **95**, 1635 (1954).
44. F. Tabakin, *Ann. Phys. (N.Y.)* **30**, 51 (1964).
45. T. R. Mongan, *Phys. Rev.* **175**, 1260 (1968); **178**, 1587 (1968).
46. A. N. Mitra, *Nucl. Phys.* **32**, 529 (1962).
47. F. Calogero and Yu A. Simonov, *Phys. Rev. Lett.* **25**, 881 (1970).
48. R. E. Peierls, in *Proceedings of the International Conference on Nuclear Structure, Kingston, Ontario*, Toronto University Press, 1960, p. 7.
49. A. M. Green, *Nucl. Phys.* **33**, 218 (1962).
50. K. Gottfried, *Quantum Mechanics*, Vol. 1, Benjamin, New York, 1966, p. 94.
51. S. S. Schweber, H. A. Bethe, and F. de Hoffman, *Mesons and Fields*, Vol. I, Row, Peterson, 1956, p. 242.
52. W. N. Cottingham and R. Vinh Mau, *Phys. Rev.* **130**, 735 (1960).
53. M. H. Partovi and E. L. Lomon, *Phys. Rev. Lett.* **22**, 438 (1969); *Phys. Rev.* **D2**, 1999 (1970).
54. S. Moszkowski, in *Les Houches Lectures on Nuclear Physics, Grenoble, 1968*, Gordon and Breach, New York, 1969.
55. V. K. Samaranayake and W. W. Woolcock, *Phys. Rev. Lett.* **15**, 936 (1965).
56. R. Bryan and B. L. Scott, *Phys. Rev.* **177**, 1435 (1969).
57. L. Ingber, *Phys. Rev.* **174**, 1250 (1968).
58. T. Ueda and A. E. S. Green, *Phys. Rev.* **174**, 1304 (1968).
59. K. Erkelenz, K. Holinde, and K. Bleuler, *Nucl. Phys.* **A139**, 308 (1969).

60. P. Signell, in *The Two-Body Force in Nuclei*, edited by S. M. Austin and G. M. Crawley, Plenum Press, New York, 1972, p. 9.
61. J. J. Sakurai, *Phys. Rev. Lett.* **17**, 1021 (1966).
62. S. C. C. Ting, in *Proceedings of the Fourth International Conference on High Energy Physics, Vienna, Austria, September 1968*, CERN Scientific Information Service, Geneva, 1968, p. 43.
63. R. de Tourreil and D. W. L. Sprung, *Nucl. Phys.* **A201**, 193 (1973).
64. P. Grangé and M. A. Preston, *Nucl. Phys.* **A204**, 1 (1973).
65. F. Villars, *Helv. Phys. Acta* **20**, 476 (1947).
66. S. M. Berman and S. D. Drell, *Phys. Rev.* **133**, B791 (1964).

PROBLEMS

5–1. Derive Eq. 5–8 from Eq. 5–7.

5–2. Show the following properties of the operator S_{12}.

(a) Applied to any singlet state, S_{12} gives 0.

(b) From parity considerations, S_{12} applied to a triplet function with $L = J \pm 1$ gives a linear combination of the triplet functions for $L = J + 1$ and $J - 1$ and, applied to a triplet function with $L = J$, reproduces the same function multiplied by a constant, that is,

$$S_{12}\mathscr{Y}^M_{J,1L} = a_{L,J+1}\mathscr{Y}^M_{J,1J+1} + a_{L,J-1}\mathscr{Y}^M_{J,1J-1} \tag{1}$$

if $L = J \pm 1$, and

$$S_{12}\mathscr{Y}^M_{J,1J} = a_{J,J}\mathscr{Y}^M_{J,1J}. \tag{2}$$

(c) The operator S_{12} commutes with J_z, and hence the coefficients $a_{L,J+1}$, $a_{L,J-1}$, and $a_{J,J}$ are independent of M.

(d) $a_{J+1,J-1} = a_{J-1,J+1}$.

(e) By considering the particular case in which $\hat{\mathbf{r}}$ is along the z-axis and $M = 1$, and using the fact that $Y_l^m(\theta = 0) = \sqrt{(2l+1)/4\pi}\,\delta_{l0}$, show that

$$a_{J,J} = \langle \mathscr{Y}^M_{J,1J} | S_{12} | \mathscr{Y}^M_{J,1J} \rangle = 2.$$

(f) Similarly, taking the special case $\hat{\mathbf{r}} = \mathbf{k}$, $M = 0$ and $M = 1$, use Eq. 1 above to find two equations between $a_{J-1,J+1}$ and $a_{J-1,J-1}$. Thus show that

$$\langle \mathscr{Y}^M_{J,1J-1} | S_{12} | \mathscr{Y}^M_{J,1J-1} \rangle = \frac{-2(J-1)}{2J+1}, \tag{3}$$

$$\langle \mathscr{Y}^M_{J,1J+1} | S_{12} | \mathscr{Y}^M_{J,1J-1} \rangle = \frac{6\sqrt{J(J+1)}}{2J+1}. \tag{4}$$

Similarly show that

$$\langle \mathscr{Y}^M_{J,1J+1} | S_{12} | \mathscr{Y}^M_{J,1J+1} \rangle = \frac{-2(J+2)}{2J+1}. \tag{5}$$

5–3. Demonstrate either directly or from the formulas in Appendix I of Case and Pais [20], that the P-wave contribution to $\sigma_{pp}(\theta)$ is

$$\begin{aligned}\pi\lambda\!\!\!^{-2}\{[\tfrac{17}{4}\sin^2\delta_2 + \tfrac{9}{4}\sin^2\delta_1 + \tfrac{1}{2}\sin^2\delta_0 \\ + \tfrac{9}{2}\cos(\delta_2-\delta_1)\sin\delta_2\sin\delta_1 + 2\cos(\delta_2-\delta_0)\sin\delta_2\sin\delta_0] \\ - \sin^2\theta[\tfrac{21}{8}\sin^2\delta_2 + \tfrac{9}{8}\sin^2\delta_1 + \tfrac{27}{4}\cos(\delta_2-\delta_1)\sin\delta_2\sin\delta_1 \\ + 3\cos(\delta_2-\delta_0)\sin\delta_2\sin\delta_0]\},\end{aligned}$$

where δ_0, δ_1, and δ_2 are the $^3P_0$-, $^3P_1$-, and $^3P_2$-phase shifts, respectively. If the phase shifts are small and the Born approximation is valid, show that the contribution from an $\mathbf{L}\cdot\mathbf{S}$ force is $9\pi\lambda\!\!\!^{-2}\delta_2^2\sin^2\theta$, where δ_2 is the part of the $^3P_2$-phase shift due to the $\mathbf{L}\cdot\mathbf{S}$ force.

5–4. (a) For the tensor operators $S_{12}(\mathbf{r})$ defined in the text, prove that

$$S_{12}^2(\mathbf{r}) = 6 + 2\boldsymbol{\sigma}_1\cdot\boldsymbol{\sigma}_2 - 2S_{12}(\mathbf{r}). \tag{1}$$

Hence show that, acting on a singlet state, S_{12}^2 gives zero, whereas for a triplet state it has a substantial central component.

(b) For plane-wave states in a volume Ω,

$$\psi_{\mathbf{k}_1}(\mathbf{r}_1) = \frac{1}{\sqrt{\Omega}}\exp(i\mathbf{k}_1\cdot\mathbf{r}_1), \tag{2}$$

prove that the matrix element of V_T defined in Eq. 5–9 is given by the expression

$$\begin{aligned}&\int \psi^*_{\mathbf{k}_1+\mathbf{q}}(\mathbf{r}_1)\psi^*_{\mathbf{k}_2-\mathbf{q}}(\mathbf{r}_2)V_T(r)S_{12}(\mathbf{r})\psi_{\mathbf{k}_1}(\mathbf{r}_1)\psi_{\mathbf{k}_2}(\mathbf{r}_2)\,d^3r_1\,d^3r_2 \\ &= -\left(\frac{4\pi}{\Omega}\right)V_T^{(2)}(q)S_{12}(\mathbf{q}),\end{aligned} \tag{3}$$

where

$$V_T^{(2)}(q) = \int_0^\infty j_2(qr)V_T(r)r^2\,dr,$$

j_2 being the spherical Bessel function of order 2, and

$$S_{12}(\mathbf{q}) = \frac{3(\boldsymbol{\sigma}_1\cdot\mathbf{q})(\boldsymbol{\sigma}_2\cdot\mathbf{q})}{q^2} - (\boldsymbol{\sigma}_1\cdot\boldsymbol{\sigma}_2).$$

Comment on the statement that nondiagonal matrix elements (3) are negligible for very small values of q if $V_T(r)$ is of short range. Taking, for simplicity, a Yukawa form for $V_T(r)$ of one-pion-exchange range, estimate the value of q at which $V_T^{(2)}(q)$ is maximum.

5–5. Using the notation of Section 5–9, we can write the Schrödinger equation for energy $E_k = k^2$ as (with kinetic-energy operators $T = H_0$)

$$(k^2 - H_0)|\psi_k\rangle = V|\psi_k\rangle.$$

In **r**-space this becomes

$$(k^2 + \nabla^2)\psi_k(\mathbf{r}) = \int \langle \mathbf{r}|V|\mathbf{r}'\rangle \psi_k(\mathbf{r}')\, d^3r',$$

and in **p**-space the same equation is

$$(k^2 - p^2)\psi_k(\mathbf{p}) = \int \langle \mathbf{p}|V|\mathbf{p}'\rangle \psi_k(\mathbf{p}')\, d^3p',$$

where we use the notation $\langle \mathbf{p}|\psi_k\rangle = \psi_k(\mathbf{p})$, etc.

(a) Consider an attractive separable potential acting in the s-state,

$$\langle \mathbf{r}|V|\mathbf{r}'\rangle = -\lambda g(r)g(r'), \tag{1}$$

where λ is a positive constant. Show that the Schrödinger equation in the **p**-space reduces to

$$(k^2 - p^2)\psi_k(\mathbf{p}) = -\lambda g(p) \int g(p')\psi_k(\mathbf{p}')\, d^3p', \tag{2}$$

where

$$g(p) = \int \langle \mathbf{p}|\mathbf{r}\rangle g(r)\, d^3r$$

$$= \frac{1}{(2\pi)^{3/2}} \int \exp(-i\mathbf{p}\cdot\mathbf{r})\, g(r)\, d^3r.$$

(b) Noting that Eq. 2 above is of algebraic nature, prove that the outgoing scattering solution is given by

$$\psi_k(\mathbf{p}) = \delta(\mathbf{p} - \mathbf{k}) - \frac{\lambda g(k)}{1 + \lambda \int d^3q[g^2(q)/(k^2 - q^2 + i\varepsilon)]} \frac{g(p)}{k^2 - p^2 + i\varepsilon}. \tag{3}$$

The scattering amplitude for elastic scattering is defined by Eq. 5–55 in the text. Using that definition and Eq. 3, show that

$$f_k = -2\pi^2\langle \mathbf{k}|V|\psi_{\mathbf{k}}\rangle = \frac{2\pi^2\lambda g^2(k)}{1 + \lambda \int d^3q[g^2(q)/(k^2 - q^2 + i\varepsilon)]}. \tag{4}$$

(c) Use Eqs. 4 and 5–57 to prove that

$$k \cot \delta = \frac{1 + \lambda I}{2\pi^2\lambda g^2(k)}, \tag{5}$$

where

$$I = P\int d^3q \frac{g^2(q)}{k^2 - q^2},$$

the symbol P indicating the principal part integral. You will have to make use of the identity

$$\int d^3q \frac{g^2(q)}{k^2 - q^2 + i\varepsilon} = P\int d^3q \frac{g^2(q)}{k^2 - q^2} - i2\pi^2 k g^2(k).$$

(d) Taking a specific example, let us put

$$V(k, k') = -\frac{\hbar^2}{M}\lambda \frac{1}{\sqrt{k^2 + \eta^2}} \cdot \frac{1}{\sqrt{k'^2 + \eta^2}} \text{ MeV fm}^3, \tag{6}$$

where we have now written $\hbar^2/M$ explicitly to clarify the units. (Note that λ has units of fm^{-1}.) Using formula 5, show that

$$k \cot \delta = \frac{(k^2 + \eta^2) - 2\pi^2\lambda\eta}{2\pi^2\lambda}. \tag{7}$$

Hence note that the effective-range formula 2–41 is exact for this potential, with scattering length a and effective range r_0 given by

$$\frac{1}{a} = \eta\left(1 - \frac{\eta}{2\pi^2\lambda}\right), \qquad r_0 = \frac{1}{\pi^2\lambda}. \tag{8}$$

Compare these results with those of Problem 2–7. Note that, since the simple Bargmann potential of Problem 2–7 also satisfies the effective-range formula exactly, it can be chosen to be "phase equivalent" to the potential of Eq. 6, that is, the two yield the same phase shift $\delta(k)$ for all positive values of k. This implies that the on-shell values of $\langle \mathbf{k}'|T(k^2)|\mathbf{k}\rangle$ with $k'^2 = k^2$ are the same for the two, but the off-shell matrix elements may be very different.

5–6. The bound-state problem with the potential given by Eq. 1 of Problem 5–5 can be solved exactly. In this case, we put $k^2 = -\alpha^2$, where the binding of the two-body system is $\hbar^2\alpha^2/M$. Then the Schrödinger equation (Eq. 2) of Problem 5–4 modifies to

$$(\alpha^2 + p^2)\psi_\alpha(\mathbf{p}) = \lambda g(p) \int g(p')\psi_\alpha(\mathbf{p}')\, d^3p'.$$

Show that the bound-state energy α^2 is determined by the equation

$$\frac{1}{\lambda} = \int d^3q \frac{g^2(q)}{\alpha^2 + q^2}.$$

Can there be more than one bound state for such a potential?

5–7. Consider a nucleon confined in a very large sphere of radius R, such that its energy eigenvalues are nearly continuous. Let the number of states of a given partial wave l with wave number lying between k and $k + dk$ be denoted by $g_l^{(0)}(k)\, dk$. Next assume the nucleon to be in the same enclosure, but in the presence of a one-body potential $U(r)$ of range $r_n \ll R$. Let the state density in k-space be now denoted by $g_l(k)$.

(a) Prove that

$$g_l(k) - g_l^{(0)}(k) = \frac{2l+1}{\pi} \cdot \frac{\partial \delta_l(k)}{\partial k}, \tag{1}$$

where $\delta_l(k)$ is the phase shift suffered by the nucleon of wave number k in the presence of potential $U(r)$.

Hint: Note that the eigenvalues k are determined in the two cases by the boundary conditions

$$kR + \frac{l\pi}{2} = \pi n \quad \text{[free nucleon]},$$

and

$$kR + \frac{l\pi}{2} + \delta_l(k) = \pi n \quad \text{[nucleon in the field of } U(r)\text{]},$$

where $n = 0, 1, 2$, etc.

(b) Formula 1 shows that, if the phase shift *rises* steeply over a narrow range of k and then flattens, it will give rise to a sharp bump in the level density with a width determined by $\partial\delta_l/\partial k$. Since a discrete bound state may be regarded as a Dirac-delta function in the level density, these sharp bumps in the continuum arising from Eq. 1 may be regarded as "resonances." Invoking the uncertainty principle, note that a particle in a resonant state in the continuum will be trapped there for a finite lifetime.

Look up the energy levels of ^{8}Be in Fig. 12 of T. Lauritsen and F. Ajzenberg-Selove, *Nucl. Phys.* **78**, 1 (1966), where the α-α scattering phase shifts for $l = 0, 2$, and 4 are also shown. Comment on the three lowest-lying levels, 0^+, 2^+, and 4^+, in the light of the above discussion.

A relevant and fascinating account of the synthesis and detection of the ^{8}Be ground state is given by H. Staub, *Adventures in Experimental Physics*, Vol. γ, 1 (1973).

(c) Show that the scattering cross section in the lth partial wave may be written as

$$\sigma_l(k) = \frac{4\pi}{k^2}(2l+1)\frac{1}{\cot^2\delta_l + 1}. \tag{2}$$

The Born approximation result given by Eq. 5–39 suggests that, for small values of k, $\sin\delta_l \propto k^{2l+1}$, a result that turns out to be correct even in exact analysis. Imagine the phase shift δ_l as a function of k to rise sharply from 0 to π in a short range of k-values and then flatten out. Sketch a plot of σ_l for this situation. Note that σ_l reaches its "unitary limit," $(2l+1)4\pi\lambda^2$, at a value of k for which $\delta_l(k) = \pi/2$.

5–8. Consider the "half-off-shell" scattering amplitude as defined in Eq. 5–55, with $k'^2 \neq k^2$,

$$\begin{aligned} f(\mathbf{k}', \mathbf{k}) &= -2\pi^2\langle \mathbf{k}'|T(E = k^2)|\mathbf{k}\rangle \\ &= -2\pi^2 \int \exp(-i\mathbf{k}'\cdot\mathbf{r})\, V(r)\psi_k(\mathbf{r})\, d^3r. \end{aligned} \tag{1}$$

Show that the S-wave contribution to Eq. 1 can be written as

$$f_0(k', k) = -8\pi^3 \int_0^\infty \frac{\sin k'r}{k'} V(r) u_k(r)\, dr, \tag{2}$$

where $(1/r)u_k(r)$ is the wave function in the S-state. Denoting the asymptotic form of $u_k(r)$ by $v_k(r)$ (see Section 2–3):

$$u_k(r) \sim v_k(r) = \frac{\exp[i\,\delta_0(k)]}{k}\sin(kr + \delta_0), \tag{3}$$

show that

$$f_0(k', k) = f_0(k, k) + (2\pi)^3(k'^2 - k^2)\int_0^\infty \frac{\sin k'r}{k'}[u_k(r) - v_k(r)]\, dr, \tag{4}$$

where $f_0(k, k) = [\exp(i\,\delta_0(k))/k]\sin\delta_0(k)$ is the on-shell scattering amplitude. Note that, for a finite-range potential $V(r)$ with range r_n, the upper limit in the integral of Eq. 4 is just r_n, since, for $r > r_n$, $u_k = v_k$.

The off-shell scattering amplitude $f_0(k', k)$ thus depends sensitively on the Fourier transform of the "wound" $[u_k(r) - v_k(r)]$, while the on-shell part $f_0(k, k)$ is completely determined by the phase shift [T. Fulton and P. Schwed, *Phys. Rev.* **115**, 973 (1959)].

Hint: Note that Eq. 2 may be rewritten as

$$f_0(k', k) = -8\pi^3 \int_0^\infty \frac{\sin k'r}{k'}\left(k^2 + \frac{d^2}{dr^2}\right)[u_k(r) - v_k(r)]\, dr.$$

Chapter 6

Nuclear Binding Energies

6-1 INTRODUCTION

Clearly, a basic property of a nucleus is its total energy or mass in its ground state. We have already remarked that the mass is near $ZM_p + NM_n$; it is its deviation from this value which is of interest. The quantity most easily measured is the mass of the neutral atom, denoted by $M(A, Z)$. We define the binding energy of a nuclide as

$$B(A, Z) = ZM_{\mathrm{H}} + NM_n - M(A, Z), \tag{6-1}$$

where M_{H} is the mass of the hydrogen atom (H^1). The binding energy consists of the binding energy of the nucleus, plus the difference between the binding energy of the electrons and that of Z hydrogen atoms. The electronic contribution is negligible for all usual purposes.†

Nuclear masses can be obtained by a number of methods. The most direct technique is mass-spectrometric determination of the mass-to-charge ratio in electric and magnetic fields. Atoms of the desired substance are ionized and introduced into the mass spectrometer, along with a comparison material of known mass and almost the same mass-to-charge ratio. Comparison materials are often various hydrocarbons, and advantage is taken of the presence of multiply charged ions. The procedure usually makes it possible

† Various other quantities contain the same information as B. One is the *mass excess* $M - A$, where M is expressed in mass units. One mass unit (= 1 u = 931.44 MeV) is one-twelfth the mass of the neutral atom ^{12}C (1 mu = 10^{-3} u). Another expression that has been used is the *packing fraction* $(A - M)/A$. The authors agree with Wapstra that the latter usage is best avoided.

to arrange a "mass doublet" between the unknown mass and a known mass. In this way, many nuclidic masses have been measured in terms of carefully determined standards [1, 2].†

An alternative direct mass measurement may occasionally be made by observing the change in the moment of inertia of a molecule when one isotope of an element is replaced by another. The mass of one of the isotopes must be known. The method is accurate if the molecular spectrum has frequencies in the microwave region; their precise values are related to the rotational energies and hence to the moments of inertia. Only a few values have been determined in this way [3].

The differences between certain nuclear masses can be obtained from the thresholds of various nuclear reactions and radioactive decays. The end-point energies of β-spectra (corrected by two electron masses in positron decay) give the mass difference between parent and daughter atoms. Of course, if the daughter nucleus is left in an excited state, the energy of the subsequent γ-decay must be included. The energy difference between an α-active nuclide (A, Z) and the daughter $(A - 4, Z - 2)$ consists of the kinetic energy of the α-particle, corrected for the recoil of the nucleus, less the binding energy of the α-particle; in this case also, we must be sure that we are dealing with the ground-state transition, or, if we are not, we must include the energy of the de-excitation γ-rays. Nuclear reactions of the types (p, n), (d, p), (n, γ), (d, α), etc., can be used to find mass differences if the energies of the incident and final particles or photons are known. A large number of such reactions have been studied sufficiently accurately to produce mass data. Useful compilations of radioactive and reaction data are published in conference reports and nuclear data tables [4, 5, 6].

By these various methods, many atomic masses have been measured in several ways with results that do not always agree. It is an extensive task to assess the reliability of the various measurements, to reconcile the discrepancies, and to obtain a best value. Wapstra and Gove [7] have prepared an extensive mass table by making a least-squares reduction of the available Q-value and mass-doublet data. The basic data are displayed in Fig. 6–1, which represents the binding energy per nucleon, B/A, plotted against A, for the most stable nuclide for each A.‡ Determination of the best mass values is a continuing process.

† In all work done before 1960 a different mass unit, denoted as amu, was used. It was equal to $\frac{1}{16}$ the mass of the ^{16}O atom.

‡ Usually there is only one β-stable nuclide for a given A, but in 58 cases there are two such nuclides.

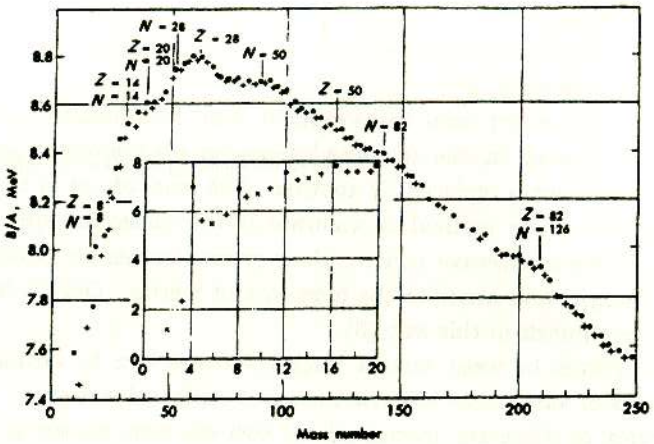

Fig. 6-1 Binding energy per nucleon of the most β-stable isobars. Each point represents an average of a few neighboring nuclides: solid circles for even-even, crosses for odd A. In the insert for low A, oblique crosses refer to odd-odd nuclides. [After Wapstra.]

The most remarkable aspect of the experimental masses revealed in Fig. 6–1 is the approximate constancy of the binding energy per nucleon. Except for the very lightest atoms ($A < 10$), B/A is never less than 7.4 MeV and never greater than 8.8 MeV. This was one of the facts realized in the early 1930's from the mass measurements of Aston [8, 9], and it led Heisenberg [10] to propose exchange forces between nucleons. If each nucleon interacted through an attractive force with all other nucleons, we would expect a potential energy proportional to the number of pairs, that is, roughly proportional to A^2. Indeed, as more particles were added and the attraction became stronger, we might expect the particles to draw closer together, so that the binding would increase faster than A^2. Then B/A would be proportional to at least A. But B/A is nearly constant, and, as more particles are added, nuclear density is also constant. In other words, nuclear forces saturate, as if each nucleon were effectively interacting with only a few others. The saturated value of B/A is reached in nuclei with about 10 or more particles.

We shall see in Chapter 8 that complete understanding of the saturation involves the precise nature of the internucleon forces, especially the contributions of the tensor force, the repulsive core, and the exchange forces, as well as the Pauli exclusion principle. However, the gross features of the variation of the binding energy with mass number A may be understood by considering the nucleus as a zero-temperature Fermi gas of uniform density contained in a volume Ω and by assuming the effective interaction between

the nucleons inside the nucleus to be reasonably smooth and its contribution estimable by a perturbation calculation. Before carrying out such a calculation, we try to justify this model of the nucleus in the following section.

6-2 FERMI GAS MODEL OF THE NUCLEUS

A nucleus is a self-bound system consisting of A fermions with a core density which is approximately uniform. In a first approximation, a nucleus can be regarded as a sphere of uniform density having an equivalent radius R (see Chapter 4). The average volume occupied by a nucleon in this picture is $(4\pi/3)r_0^3$, where $r_0 = RA^{-1/3}$ is slightly greater than 1 fm (see Table 4–1). The average distance between two nucleons then is $\sim 2r_0$, which is about 2 fm. The first question to ask is, "Why may the system be regarded as a gas and not, for example, as a solid?" The characteristic feature of a solid is that the constituent atoms in it are localized in space, so that the vibrational energy due to thermal and zero-point motion is small compared to the potential energy between the atoms. This keeps the atoms glued to fixed positions, although they can oscillate about their equilibrium positions. When the temperature is increased so that the thermal energy becomes comparable to the potential energy or larger, the solid turns to a liquid and ultimately a gas. In a nucleus, if it is to be regarded as a solid, a nucleon should be localizable within a distance $\Delta x \sim 1$ fm, since the average interparticle spacing is about 2 fm. This localization would give rise to a zero-point energy $(\hbar^2/2M)[1/(\Delta x)^2] \approx 21$ MeV, which is much larger than the potential energy of two nucleons that are 2 fm apart. This indicates that even in the absence of thermal motion the nucleons may be regarded as a Fermi gas. Had the two-nucleon force been much stronger at the internucleon distance of 2 fm, the Fermi gas picture would cease to be valid.

The next question concerns the interaction between the various nucleons in the gas. Are the nucleons in the gas strongly interacting, or can they be regarded as independent of each other in the first approximation, and the potential energy estimated using perturbation theory with an effective interaction? We saw in Chapter 5 that the interaction between two nucleons is quite strong; hence at first sight the independent-particle picture does not seem plausible. Although we shall give a detailed justification of the independent-particle picture in a later section, two salient points are worth mentioning here. First, although the two-nucleon scattering phase shifts indicate a strong short-range repulsion followed by a deep attractive tail, these could equally well be fitted at low energies by a weak attractive potential

which became still weaker as the relative momentum between the pair of nucleons increased. This would result from partial cancellation of the strong repulsive and attractive parts of the potential, leaving a rather weak effective interaction. Second, in the ground state of the Fermi gas all single-particle states up to a certain momentum k_F are fully occupied. A pair of particles of momenta $\mathbf{k}_1$ and $\mathbf{k}_2$ ($k_1, k_2 < k_F$) can only scatter, conserving momentum, to two states $\mathbf{k}_1 + \mathbf{q}$ and $\mathbf{k}_2 - \mathbf{q}$, where these momenta are greater than k_F. This cannot be real scattering, however, since the energy of the pair is not conserved. These virtual scatterings introduce only high-momentum components into the wave function (since k_F is large), modifying it at short relative distances. Since no real scattering can take place, a virtual scattering has to be followed by other energy-nonconserving scatterings to bring the pair back to the configuration in which the states $\mathbf{k}_1$ and $\mathbf{k}_2$ are occupied. Thus no phase shifts can be introduced into the pair wave function inside the nucleus, with the consequence that it "heals" to its unperturbed form in a relatively small distance compared to the interparticle distance. The short-range part of the pair wave function ($r < 1$ fm) may be distorted through the high-momentum components introduced via the virtual scatterings. It is reasonable, therefore, to make a first-order approximation that the nucleons are moving freely within the nuclear volume Ω, with the undistorted spatial wave functions of the form $(1/\sqrt{\Omega}) \exp(i\mathbf{k}_i \cdot \mathbf{r}_i)$. The total wave function of the nucleus is an antisymmetrized product of such single-particle states, taking account, of course, of the spin and i-spin parts also.

A noninteracting Fermi gas has a ground state with all single-particle levels up to the Fermi energy completely filled, and all other levels empty. This corresponds to a Fermi distribution with temperature $\theta = 0°$K. In our simple picture the single-particle levels form a continuum, whereas in a real nucleus they are discrete. A real nucleus cannot absorb an arbitrary amount of energy from an external source because of the discrete nature of its energy levels, but can go to an excited state if the energy supplied equals the gap between the ground and the excited state. Typically, this is of the order of 100 keV–1 MeV, or, in degrees Kelvin†, 10^9–10^{10} °K. Thus, if a nucleus is in a laboratory of ambient room temperature, or a furnace with ambient temperature of 10^4 °K or so, it is unable to absorb any energy and remains an isolated system of $\theta = 0°$K. If the gas model of the nucleus is taken literally, however, the nucleus can absorb any arbitrary amount of energy, since its energy levels are continuous. Is it justifiable, then, to use the zero-

† A temperature of $\theta = 1°$K corresponds to an energy $k_B\theta \approx 10^{-4}$ eV, where k_B is Boltzmann's constant.

temperature distribution for a nucleus at room or high ambient temperature? We shall see that for nuclear densities the zero-temperature Fermi distribution yields an average nucleon kinetic energy of ~ 23 MeV or about 10^{11} °K, and even if the individual nucleons are considered to be at room or furnace temperature, their thermal energies are completely negligible in comparison to the kinetic energy of the zero-temperature distribution. Thus, as long as the Fermi energy θ_F (expressed in degrees Kelvin) of the gas is very much greater than the ambient temperature θ, it is valid to use the zero-temperature distribution.

An extreme example of this is the so-called neutron star. As the name implies, it consists mainly of neutrons, and the interior temperature can be as great as 10^9 °K. Neutron stars are believed to be very dense, and the radius may be only 10 km, but the mass of the star is comparable to that of the sun. A simple calculation yields the mass density $\rho \sim 10^{15}$ g/cm^3, which is of the same order as the nuclear density. Thus θ_F for a neutron star is $\sim 10^{11}$ °K, which is much higher than the ambient temperature of 10^9 °K. It is proper, therefore, to consider the neutron star to be a zero-temperature Fermi gas.† A gas with zero-temperature characteristics is termed completely degenerate, because its behavior is very different from that of a classical gas.

It is now a simple matter to calculate the kinetic energy of a nucleon in this model. Each state of linear momentum $\mathbf{p}$ can accommodate four nucleons according to the exclusion principle when the spin-isospin degeneracy is taken into account. We assume first that the numbers of protons and neutrons in the nucleus are the same and that the volume Ω is large enough to regard the momentum states as continuous. All states up to a "Fermi momentum" p_F are filled in a zero-temperature gas, so that the total number of nucleons is A. Assuming that there is one quantum state per volume h^3 of the phase space, we obtain

$$A = \frac{4\Omega}{h^3}\int_0^{p_F} d^3p = \frac{16\pi}{3}\Omega\left(\frac{p_F}{h}\right)^3.$$

This yields a relation between $k_F = p_F/\hbar$ and the nucleon density $\rho = A/\Omega$,

$$\rho = \frac{2}{3\pi^2}k_F^3. \tag{6-2}$$

† Baym, Bethe, and Pethick [11] have estimated that the uniform neutron gas approximation for neutron stars is valid only for $\rho > 2.4 \times 10^{14}$ g/cm^3. For lesser densities, a description in terms of a lattice of neutron-rich nuclei, immersed in a neutron gas, is more appropriate.

Current data on the density of heavy nuclei indicate that $k_F = 1.36\ \text{fm}^{-1}$, but it is less for lighter nuclei. The total kinetic energy of the gas is

$$\langle T \rangle = 4\frac{\Omega}{h^3}\int_0^{p_F}\frac{p^2}{2M}d^3p = \frac{3}{5}\frac{\hbar^2 k_F^2}{2M}A, \tag{6-3}$$

which shows that the average kinetic energy of a nucleon is 60% of the value for the most energetic particle. It is also seen from Eqs. 6–2 and 6–3 that

$$\langle T \rangle = \frac{3}{5}\frac{\hbar^2}{2M}\left(\frac{3\pi^2}{2}\right)^{2/3}\rho^{2/3}A. \tag{6-4}$$

For $k_F = 1.36\ \text{fm}^{-1}$, the Fermi kinetic energy is 38 MeV and the average kinetic energy of a nucleon is about 23 MeV.

Next, we examine the potential energy of the system. For simplicity, we first take an attractive Wigner type of central two-body effective interaction, which is the same for all states, and consider only the direct term. Since there are $A(A-1)/2 \approx A^2/2$ pairs of nucleons,

$$\langle V \rangle = \frac{A^2}{2}\int\frac{\rho(\mathbf{r}_i)}{A}\frac{\rho(\mathbf{r}_j)}{A}V_W(r_{ij})\,d^3r_i\,d^3r_j, \tag{6-5}$$

where $\rho(\mathbf{r})/A$ is the probability of finding a particle at point $\mathbf{r}$. In the gas model ρ is simply A/Ω. Using this and the fact that the interaction depends only on relative coordinates, we obtain

$$\langle V \rangle = \tfrac{1}{2}\rho A\int V_W(r_{ij})\,d^3r_{ij} = A\rho\bar{V}_W, \tag{6-6}$$

where $\bar{V}_W$ is half the volume integral of the interaction and is independent of A. Combining Eqs. 6–4 and 6–6, we note that for this case the energy per nucleon as a function of density is given by

$$\frac{E}{A} = c_1\rho^{2/3} - c_2\rho, \tag{6-7}$$

where c_1 and c_2 are positive constants independent of A. The equilibrium density is obtained by minimizing the energy per particle, and we see that a purely attractive force like V_W tends to make $\rho \to \infty$, that is, the system collapses.

As we mentioned before, there are several mechanisms which prevent this collapse, depending on the details of the two-nucleon force. For simplicity, the above analysis was performed by assuming a purely attractive force. If

there is a repulsive core in the potential, the particles cannot be packed too closely together, since the repulsion starts to dominate. This has to be reflected in the formalism by noting that, although the probability of finding a particle at any given position is uniform throughout the gas, the probability of finding a second particle at $\mathbf{r}_i$ is altered when it is known that there is one at $\mathbf{r}_j$. This "correlation effect" is a function of $\mathbf{r}_{ij}$. We also know that there is a strong tensor component in the two-nucleon force. It does not contribute any binding in the first order to a spherical system, but gives attraction in the second order. Its contribution, however, does not increase linearly with ρ but flattens out with increasing density, ultimately decreasing for very large densities. This helps greatly in producing saturation.

Furthermore, the introduction of exchange forces radically alters the potential contribution. The space-exchange force, for example, is attractive in even states and repulsive in odd states. This certainly reduces the potential energy. For example, the four particles in ^{4}He are all in relative S-states, about the center and in relation to each other, but the fifth particle in ^{5}He must, by the exclusion principle, be in a central p-state, and is in a relative P-state with all the other particles. With a pure space-exchange type of force, the fifth particle would be repelled. One can estimate the effect of exchange forces rather simply in this model. A Majorana-type space-exchange force V_M is attractive for space-symmetric pairs and repulsive for antisymmetric pairs. Let ξ be the fraction of the interacting particles within the nuclear force range which form antisymmetric states in the space coordinates. Then the contribution to the potential energy from the symmetric pairs is, as derived in Eq. 6–6, given by $A\rho(1-\xi)\bar{V}_M$, and the contribution from the antisymmetric pairs is $-A\rho\xi\bar{V}_M$. The total potential-energy contribution from Wigner- and Majorana-type forces is

$$\langle V \rangle = A\rho[\bar{V}_W + (1-2\xi)\bar{V}_M]. \tag{6-8}$$

Note that ξ is a function of the nucleon density ρ, decreasing with decreasing density. This change arises because, for a fixed number of particles, the larger the nucleus, the lower are the kinetic energies, the more the relative momentum of any nucleon pair is reduced, and the greater is the increase in the corresponding de Broglie wavelength. But two particles with an antisymmetric space part of the wave function cannot occur at the same point, for in that case the wave function must vanish, and the probability of their being within a de Broglie wavelength of each other is correspondingly very small. Thus, in Eq. 6–8, $1-2\xi$ is a decreasing function of density and helps to bring about saturation.

We see from Eqs. 6–4 and 6–8 that the total energy of the gas is a linear function of the nucleon number A. Furthermore, the saturation density ρ_0, which minimizes the energy per particle, is independent of A because the constants c_1 and c_2 in Eq. 6–7, as well as others that enter with more complicated forces, are determined only by the characteristics of the force. It follows, therefore, that the binding energy per nucleon is a constant independent of A in this simple model, which is the major trend of the accumulated experimental data in Fig. 6–1.

To get a better fit to data we shall have to take account of surface effects due to the finiteness of the nuclear volume, Coulomb forces between protons, and the so-called symmetry and pairing effects. Since these make energy contributions that are not proportional to the number of particles, the binding energy per particle displays some gross A-dependence, which we shall study for each of these effects within the framework of the Fermi gas model.

In evaluating the kinetic energy $\langle T\rangle$ from Eq. 6–4, we assumed the number of momentum states between $\mathbf{p}$ and $\mathbf{p}+d\mathbf{p}$ to be $(4\Omega/h^3)\,d^3p$, which is strictly true only if the surface-to-volume ratio in configuration space is zero. More careful calculations show that this is $(4\Omega/h^3)[1-(Sh/8\Omega p)]\,d^3p$, where S is the surface area of the nucleus (see Problem 6–6). This has the effect of increasing the average kinetic energy of a nucleon by an additional term which is proportional to the surface-to-volume ratio, that is, $A^{-1/3}$. When this effect is included, the total kinetic energy $\langle T\rangle$ is increased by this surface term, which is proportional to $A^{2/3}$. Surface effects also modify the potential-energy contribution because a nucleon near the surface region will have fewer neighbors. This can be seen in the following manner. The expression $\langle V\rangle$ in Eq. 6–5 may be written as

$$\langle V\rangle = \frac{A^2}{2\Omega}\int V_W(r_{ij})\,d^3r_{ij}\,d^3R_{ij},$$

where $\mathbf{r}_{ij}=\mathbf{r}_i-\mathbf{r}_j$, and $\mathbf{R}_{ij}=(\mathbf{r}_i+\mathbf{r}_j)/2$. In writing Eq. 6–6, we assumed that the integration over d^3R_{ij} is simply Ω. But if the volume Ω is finite (i.e., a sphere of radius R_0), we must impose the conditions

$$|\mathbf{r}_i| = \left|\mathbf{R}_{ij}+\frac{\mathbf{r}_{ij}}{2}\right| < R_0 \qquad \text{and} \qquad |\mathbf{r}_j| = \left|\mathbf{R}_{ij}-\frac{\mathbf{r}_{ij}}{2}\right| < R_0,$$

which restrict the region of integration. For simplicity, if we assume V_W to be an attractive square well of range r_n, a straightforward but tedious calculation shows that Eq. 6–6 is modified to

$$\langle V\rangle = A\rho\bar{V}_W\left[1-\frac{9}{16}\frac{r_n}{R_0}+\frac{1}{32}\left(\frac{r_n}{R_0}\right)^3\right]. \tag{6–9}$$

The cubic term in the square bracket is negligible, but the linear term is significant. Assuming that $R_0 = r_0A^{1/3}$, we find for the potential energy

$$\langle V\rangle = A\rho\bar{V}_W - \tfrac{9}{16}A^{2/3}\rho\bar{V}_W\left(\frac{r_n}{r_0}\right), \tag{6–10}$$

which also shows that the potential energy is reduced by a factor proportional to $A^{2/3}$. The magnitude of the surface term depends on the surface area of the nucleus and as such is shape dependent.

Another important contribution to the nuclear energy comes from the electrostatic field between the protons, which is due to the long-range Coulomb force, and increases quadratically with Z. For a sphere of radius R_0 having constant charge density and total charge Ze, the Coulomb energy is

$$E_{Co} = \frac{3}{5}\frac{(Ze)^2}{R_0}. \tag{6–11}$$

This is a classical expression.† An accurate quantum-mechanical expression requires a good knowledge of the wave function of the protons and includes exchange contributions. In fact, information about the charge distribution and charge radii can be obtained from a knowledge of the Coulomb-energy shift of mirror nuclei and analog states. However, here we are more interested in the general trends, so we simply write, for a spherical nucleus of sharp surface,

$$E_{Co} = \frac{k_CZ^2}{A^{1/3}}, \tag{6–12}$$

where k_C is a constant.

Meyers and Swiatecki [13] have generalized this expression for the more general case of a deformed nucleus with a diffused surface. If the surface diffuseness is of the Woods-Saxon type (Eq. 4–9), they find the following expression for the Coulomb energy:

$$E_C = E_{Co}\,g(\text{shape}) - \left(\frac{\pi^2}{2}\right)\left(\frac{e^2}{r_0}\right)\left(\frac{a_0}{r_0}\right)^2\left(\frac{Z^2}{A}\right), \tag{6–13}$$

† It may be noted that in many older publications the term Z^2 in Eq. 6–11 is replaced by $Z(Z-1)$ to allow for the granularity of the charge, the argument being that no proton can interact with itself. However, Peaslee [12] has shown that quantally this is incorrect, and the direct Coulomb term should be proportional to Z^2.

where the function g(shape) depends on the deformation parameters and $a_0 = 0.546$ fm is defined in Eq. 4–9. We shall find the form of g(shape) in Chapter 12 for some simple types of deformation.

Adding these energies so far calculated, we may write the binding energy per particle of a spherical nucleus as

$$\frac{B(A)}{A} = -\frac{\langle T\rangle + \langle V\rangle + E_{Co}}{A}$$

$$= a_V - a_S A^{-1/3} - k_C(A - I_A)^2 A^{-4/3}, \qquad (6\text{–}14)$$

where a_V, a_S, and k_C are, respectively, called the volume, surface, and Coulomb coefficients and are independent of A. In the Coulomb term, we have taken the charge $Z = Z_A$, where Z_A is the atomic number of the most stable isobar of mass number A. Since very roughly $Z_A = \frac{1}{2}A$, we have expressed Z_A as

$$Z_A = \tfrac{1}{2}(A - I_A),$$

where $I_A = N - Z$ and is the neutron excess of the most stable isobar. Although we have obtained the gross A-dependence of the binding energy from the Fermi gas model, it is too much to expect that the numerical values of the various coefficients a_V, a_S, etc., will be predicted accurately. Rather, the point of view is taken that these constants are to be determined by fitting the observed masses, and for this reason the formula is called semiempirical. We shall comment on these numerical coefficients while discussing the complete mass formula, but we mention here that the predictions of these from our simple model are of the right order of magnitude.

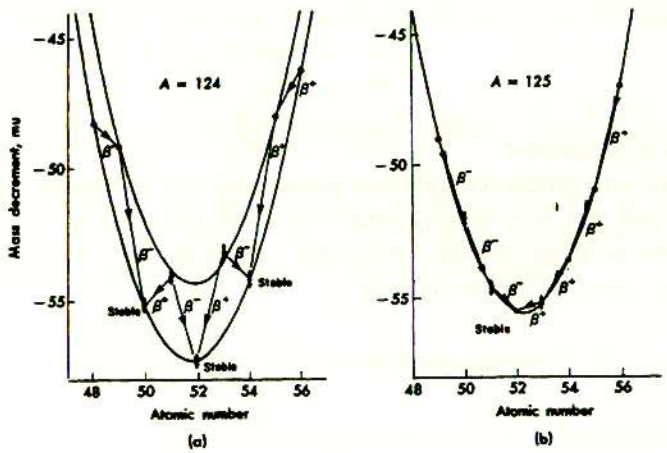

Fig. 6-2 (a) Mass excesses for $A = 124$; the lower curve is for even-even, and the upper one for odd-odd, nuclides. (b) Mass excesses for $A = 125$.

For further enlightenment, we must turn from the general trend of B/A to investigate the details in smaller regions. Let us examine the dependence of the mass decrement on Z for fixed A by studying isobars. It is observed that a plot of mass excess against Z is very accurately parabolic. For odd A, there is one parabola; for even A, the even-even and odd-odd isobars lie on different parabolas. These facts are illustrated in Fig. 6–2 for $A = 124$ and $A = 125$, where the large number of β-emitters known provide several points on each parabola. Note the following points:

1. The binding energy per particle of the most stable even-even nuclide (^{124}Te) is greater than that of the most stable odd-A nuclide (^{125}Te), which in turn is greater than that of any of the odd-odd nuclei.

2. There is only one stable odd-A nuclide, whereas there are more than one stable even-even nuclide with $A = 124$ and no stable odd-odd nuclide. This general pattern is followed throughout the periodic table. In fact, only four very light odd-odd nuclides are β-stable.

It is desirable that we understand these results as well as the parabolic shape. The Coulomb energy is parabolic in Z, but Eq. 6–14 is clearly incomplete, for if we replaced Z_A by a variable Z, then B would be a maximum for $Z = 0$. In other words, the nucleus would be all neutrons, and indeed, if Coulomb energy were the only consideration, this would be true. But the exclusion principle will allow only two neutrons and two protons in a given energy level. If we replaced the 52 protons in ^{124}Te with 52 neutrons, these could not go in the 26 low-energy levels occupied by the protons, but would have to enter the 37th to 62nd energy levels, since the first 36 levels already have their full quotas of neutrons. This change would lead to a tremendous increase in energy. At the other extreme, if there were no Coulomb energy, the exclusion principle would dictate equal numbers of neutrons and protons for stability. If we depart from $Z = N$, the Coulomb energy favors lowering Z, but the exclusion principle leads to an increase of energy. This latter energy is known as the *symmetry* energy, and the balance of Coulomb and symmetry energies determines the most stable charge for a given A.

The symmetry energy may be attributed to changes in both kinetic and potential energy. Although the kinetic-energy correction can be obtained very easily, we shall derive for it a more general expression which we can also use for the potential-energy part. Consider a nucleus with $N - Z = I$. Let the Fermi momenta for neutrons and protons be denoted by $k_F{}^N$ and $k_F{}^Z$,

respectively, and let k_F be the Fermi momentum when $N = Z = A/2$. In the gas model, the number of momentum states between $\mathbf{k}$ and $\mathbf{k} + d\mathbf{k}$ is given by $\alpha k^2\, dk$, where α is a constant. We have

$$\alpha \int_0^{k_F^N} k^2\, dk = N, \qquad \alpha \int_0^{k_F^Z} k^2\, dk = Z, \qquad \alpha \int_0^{k_F} k^2\, dk = \frac{A}{2}.$$

It then follows from these equations that

$$k_F{}^N = k_F\left(1 + \frac{I}{A}\right)^{1/3}, \qquad k_F{}^Z = k_F\left(1 - \frac{I}{A}\right)^{1/3}. \tag{6–15}$$

Expanding binomially up to the second order, we obtain

$$(k_F{}^N - k_F) = \left(\frac{1}{3}\frac{I}{A} - \frac{1}{9}\frac{I^2}{A^2}\right)k_F,$$

$$(k_F{}^Z - k_F) = \left(-\frac{1}{3}\frac{I}{A} - \frac{1}{9}\frac{I^2}{A^2}\right)k_F. \tag{6–16}$$

The total kinetic energy of the system in the gas model is given by

$$\langle T\rangle = \alpha \int_0^{k_F^N} t(k)k^2\, dk + \alpha \int_0^{k_F^Z} t(k)k^2\, dk,$$

where $t(k)$ is the one-body kinetic energy in the momentum space. We define

$$f(y) = \alpha \int_0^{y} t(k)k^2\, dk.$$

Then, making a Taylor-series expansion, we obtain

$$\begin{aligned} f(k_F{}^N) &= f(k_F) + \left.\frac{\partial f}{\partial y}\right|_{k_F}(k_F{}^N - k_F) + \frac{1}{2}\left.\frac{\partial^2 f}{\partial y^2}\right|_{k_F}(k_F{}^N - k_F)^2 + \cdots \\ &= f(k_F) + \alpha t(k_F)(k_F)^2(k_F{}^N - k_F) + \tfrac{1}{2}\alpha\left[\left.\frac{\partial t}{\partial k}\right|_{k_F}(k_F)^2 + 2k_F t(k_F)\right] \\ &\quad \cdot (k_F{}^N - k_F)^2 + \cdots, \end{aligned}$$

where the first term $f(k_F)$ is the kinetic energy when $N = A/2$, and the other terms are due to neutron excess. We can write a similar expression for $f(k_F{}^Z)$. The kinetic contribution to the symmetry energy is then

$$\begin{aligned} \langle T_{\text{sym}}\rangle &= \alpha t(k_F)(k_F)^2[(k_F{}^N - k_F) + (k_F{}^Z - k_F)] \\ &\quad + \tfrac{1}{2}\alpha\left[\left.\frac{\partial t}{\partial k}\right|_{k_F}(k_F)^2 + 2k_F t(k_F)\right][(k_F{}^N - k_F)^2 + (k_F{}^Z - k_F)^2]. \end{aligned}$$

Substituting for $(k_F{}^N - k_F)$ and $(k_F{}^Z - k_F)$ from Eq. 6–16 and noting that $\alpha = 3A/2(k_F)^3$, we immediately get

$$\langle T_{\text{sym}}\rangle = \frac{1}{6}\left.\frac{\partial t}{\partial k}\right|_{k_F} k_F \frac{I^2}{A}. \tag{6–17}$$

Note that Eq. 6–17 has been derived without specifying the form of $t(k)$. If we put $t(k) = \hbar^2k^2/2M$, we obtain

$$\langle T_{\text{sym}}\rangle = \tfrac{1}{3}t(k_F)\frac{I^2}{A}. \tag{6–18}$$

Thus the kinetic-energy symmetry term is parabolic in neutron excess, and its coefficient is one-third the kinetic Fermi energy of nuclear matter, or about 13 MeV.

The potential contribution to the symmetry energy comes from two different physical effects. One of these arises because the nucleons inside the nucleus move in an average one-body potential $U(k)$, which is itself momentum dependent, and the other because the $T = 0$ nucleon-nucleon force is more attractive than the $T = 1$ part of the interaction. As we shall see in Chapter 8, the average potential $U(k)$ is most attractive for $k = 0$, and it becomes less attractive with increasing k in an approximately quadratic way. Irrespective of its form, this gives rise to a symmetry energy that equals $\frac{1}{6}k_F(\partial U/\partial k)|_{k_F}(I^2/A)$ as before. Calculation of $U(k)$, performed in Chapter 8, indicates that this part of the symmetry-energy coefficient is repulsive and about 7 MeV in magnitude.

To calculate the i-spin part of the symmetry energy, we note that the nuclear force is more attractive for the $T = 0$ n-p (singlet) pairs than for the $T = 1$ n-p, p-p, or n-n (triplet) pairs. For a given A, the number of n-p pairs is a maximum when $N = Z$. With increasing neutron excess, the number of triplet pairs increases, with a corresponding decrease in singlet pairs. This causes a decrease in potential energy. These ideas can be formulated more precisely. In a neutron-rich nucleus, $N = \frac{1}{2}(A + I)$ and $Z = \frac{1}{2}(A - I)$. The number of triplet pairs is $\frac{1}{2}(N^2 + Z^2 + NZ)$, and the number of more attractive singlet pairs is $\frac{1}{2}NZ$. Alternatively, we can say that there are $\frac{1}{8}(3A^2 + I^2)$ triplet pairs and $\frac{1}{8}(A^2 - I^2)$ singlet pairs. If the effective Wigner-type interactions in the $T = 1$ and $T = 0$ states are denoted by V_1 and V_0, respectively, then, following Eq. 6–6, we can write for the direct contribution

$$\langle V\rangle = A\rho(\tfrac{3}{4}\bar{V}_1 + \tfrac{1}{4}\bar{V}_0) + \frac{1}{4}\frac{I^2}{A}\rho(\bar{V}_1 - \bar{V}_0), \tag{6–19}$$

where, as before, $\bar{V}_1$ is half the volume integral of the potential V_1. An estimate in regard to nuclear matter ($I = 0$) indicates that $\langle V\rangle/A \approx -40$ MeV, with the $T = 1$ and $T = 0$ parts contributing about equally, that is, $3V_{1\rho} \approx V_{0\rho} \approx -80$ MeV. This shows that the coefficient of the I^2/A term in Eq. 6–19 is about 13 MeV and is repulsive. A more accurate estimate of this term yields about 10 MeV. Thus the symmetry term in the mass formula is repulsive and is given by $a_{\text{sym}}(I^2/A)$, where

$$a_{\text{sym}} = \tfrac{1}{3}t(k_F{}^0) + \tfrac{1}{6}k\left.\frac{\partial U}{\partial k}\right|_{k=k_F} + \tfrac{1}{4}\rho(\bar{V}_1 - \bar{V}_0). \tag{6–20}$$

Each of the terms in the right-hand side of this equation is repulsive, the total being about 30 MeV. In the above analysis of the symmetry energy, we have neglected all surface effects. These reduce the repulsive contribution of the symmetry energy, this contribution being proportional to $(I^2/A)\cdot(1/A^{1/3})$.

Combining all the terms that we have derived, we may write a semi-empirical mass formula for the binding energy $B^{LD}_{\text{sph}}(A, Z)$ of a spherical nucleus with a sharp surface as

$$B^{LD}_{\text{sph}}(A, Z) = a_V A - a_S A^{2/3} - k_C Z^2 A^{-1/3} - a_{\text{sym}} I^2 A^{-1} + a_{\text{surf sym}} I^2 A^{-4/3} + \delta\, a_{\text{pair}} A^{-\varepsilon}, \tag{6–21}$$

where the last term has been added to account for the different behaviors of even-even, odd-odd, and odd-A nuclei. We have seen that, for a given A, the binding-energy-against-Z parabola for even-even nuclei shows maximum stability, the odd-odd nuclei have the least stability, and the binding energies of the odd-A nuclei are intermediate between the others. This behavior can be reproduced by taking the coefficient a_{pair} to be positive, and assuming that δ is $+1$ for even-even, 0 for odd-A, and -1 for odd-odd nuclei. The origin of this "pairing effect" lies in the special property of the nucleon-nucleon force, which gives extra binding between pairs of like nucleons in similar quantum states. This will be discussed in Chapter 8.

A formula of the type of Eq. 6–21 was first developed by Von Weizsäcker [14] and Bethe and Bacher [15], and the arguments to justify the symmetry term were given by Wigner [16]. In this simple form it neglects the correction to the Coulomb term due to the diffuseness of the surface and, more importantly, deformation and shell effects. A more general form of the mass formula for distorted nuclei has been given by Myers and Swiatecki and is written as

$$B(A, Z) = C_V A - C_S A^{2/3}\cdot f(\text{shape}) - k_C Z^2 A^{-1/3} g(\text{shape}) + \delta a_{\text{pair}} A^{-\varepsilon} + C_d\left(\frac{Z^2}{A}\right) + \delta B$$

$$= B^{LD}_{\text{dist}}(A, Z) + \delta B, \tag{6–22}$$

where

$$C_V = a_V\left[1 - \kappa\left(\frac{N-Z}{A}\right)^2\right], \qquad C_S = a_S\left[1 - \kappa\left(\frac{N-Z}{A}\right)^2\right],$$

$$C_d = \frac{\pi^2}{2}\left(\frac{a_0}{r_0}\right)^2\frac{e^2}{r_0}, \qquad k_C = \frac{3}{5}\frac{e^2}{r_0}, \qquad \varepsilon = 0.5, \tag{6–23}$$

f(shape) and g(shape) are shape-dependent functions dependent also on the deformation parameters of the nucleus, so that $f = g = 1$ for spherical shapes, and δB is the shell correction which arises due to single-particle bunching of levels and cannot be obtained from the liquid-drop part $B^{LD}_{\text{dist}}(A, Z)$. We shall discuss the forms of functions f and g for some simple types of deformation in Chapter 12. The term $C_d(Z^2/A)$ is a correction term to the Coulomb energy to account for the diffuseness of the surface (see Eq. 6–13).

The liquid-drop part of the mass formula $B^{LD}_{\text{dist}}(A, Z)$ has a smooth dependence on A if the binding energies of the most stable isobars are considered. The shell effect gives a superimposed structure on this smooth curve. By assuming a certain theoretical form (and its deformation dependence) for δB, Myers and Swiatecki [13] parametrized it in terms of three adjustable constants. The other adjustable parameters of the formula are a_V, a_S, κ, and r_0 in Eq. 6–22. The two other parameters, a_{pair} and ε, were taken to be 11 MeV and 0.5, respectively, from even-odd mass difference data and not adjusted. The seven free parameters (three for δB and a_V, a_S, κ, r_0) were determined by making a least-squares fit in a multi-dimensional space of about 1200 ground-state experimental binding energies, the deformations being obtained from the experimental quadrupole moments. The best values that Myers and Swiatecki quote are as follows:

$$a_V = 15.68 \text{ MeV}, \quad a_S = 18.56 \text{ MeV}, \quad k_C = 0.717 \text{ MeV}, \quad \kappa = 1.79$$
$$\text{(fixed parameters are } a_{\text{pair}} = 11 \text{ MeV}, \quad \varepsilon = 0.5). \tag{6–24}$$

These values imply $r_0 = 1.2049$ fm, $a_{\text{sym}} = 28.06$ MeV, and $a_{\text{surf sym}} = 33.22$ MeV.

We do not discuss here the form of δB and the associated three parameters taken by Myers and Swiatecki, but it should be realized that the numerical values of the parameters in expression 6–24 are somewhat dependent on the

form of δB that is chosen. The importance of the shell effect will be briefly discussed in the next section, and its actual evaluation will be made in Chapter 12.

The above mass formula can be used to find the Z-value of the most stable nucleus for a given A. For simplicity, neglecting the surface-symmetry term in Eq. 6–21, and setting $\partial B/\partial Z|_A = 0$, we find the condition

$$Z = \frac{A/2}{1 + (k_C/2a_{\text{sym}})A^{2/3}}, \tag{6–25}$$

which shows that for light nuclei the most stable nucleus has $Z = A/2$, while for heavier nuclei, $Z < N$.

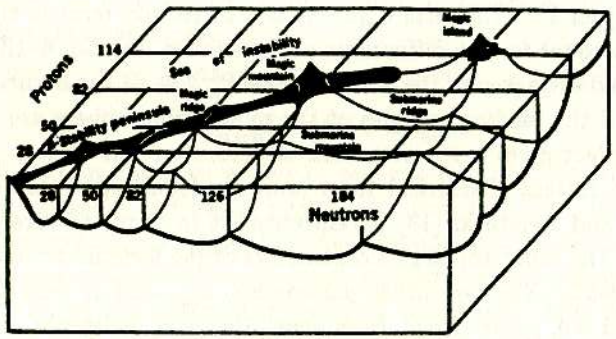

Fig. 6-3 Nuclear stability is illustrated in a scheme that shows a peninsula of known elements and an island of predicted stability (nuclei around $Z = 114$ and $N = 184$) in a sea of instability. Grid lines show magic numbers of protons and neutrons giving rise to exceptional stability. Magic regions of the mainland peninsula are represented by mountains or ridges. [After S. G. Thompson and C. F. Tsang, *Science* 178, 1047 (1972).]

Using the mass formula, one can also investigate the conditions for spontaneous β-emission, α-decay, or nucleon emission. Figure 6–3 shows a schematic peninsula of stability where elements are known, and a predicted island of stability in the superheavy region which is yet to be found. "Magic" numbers, arising out of shell structure, result in extra stability and are shown schematically as mountains or ridges in this diagram.

6-3 SHELL EFFECTS AND REFINEMENTS IN THE MASS FORMULA

The semiempirical mass formula 6–21 is able to reproduce the main trend in the variation of binding energy of nuclei with mass number A and charge Z. That the finer details are not fitted, however, can be seen clearly when we plot the difference $(M_{\text{exp}} - M_{LD})$ versus the neutron number N. Here M_{exp} is the experimental mass of a given nucleus, and M_{LD} is the spherical liquid-drop value given by Eq. 6–21 and the Myers-Swiatecki parameters (6–24). We should mention here that the mass formula derived in Section 6–2 is often called the liquid-drop mass formula because a charged spherical liquid drop has surface tension and Coulomb terms similar to what we have obtained.

The liquid-drop analogy can be extended to calculate the kinetic energy of oscillations of the nucleus about its spherical shape (see Section 9–2). Figure 6–4 shows a plot of $(M_{\text{exp}} - M_{LD})$ against N. This quantity is also called the experimental shell effect. It will be seen that the deviations are particularly large for $N = 2$, 8, 20, 28, 50, 82, and 126. Similar large discrepancies show up when the plot is made against proton number Z. Many other nuclear properties show peculiarities at these "magic" numbers. Although the mean deviation over the periodic table is about 3 MeV, in the vicinity of the magic numbers the difference can be as large as 10 MeV. We should not be surprised at this because our derivation did not take account of the "shell effects": the single-particle levels in a real nucleus are discrete with large energy gaps between major shells, while we assumed a smooth, continuous distribution of levels. The local maxima in the binding energies of the heavier nuclei are associated with the filling up of these shells. In Chapter 12 on fission, after we have discussed the shell structure more fully, we shall explain how the semiempirical mass formula can be corrected for these shell effects. Furthermore, corrections have to be applied for deformed nuclei—apart from introducing obvious corrections in the Coulomb energy, deforma-

Fig. 6-4 "Experimental" shell correction $(M_{\text{exp}} - M_{LD})$, plotted against the neutron number N. Here M_{exp} is the experimental mass of a nuclide (in MeV), while M_{LD} is the mass predicted by the spherical liquid-drop formula 6–21. [After Myers and Swiatecki [13].] ▶

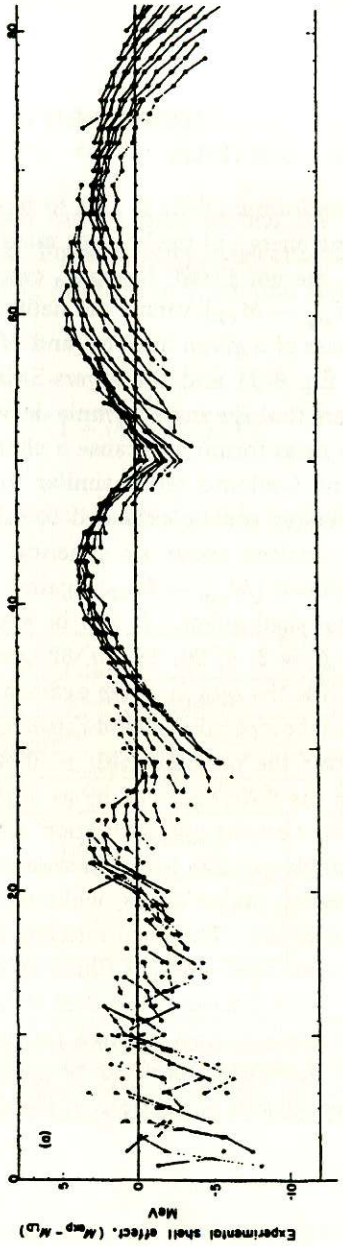

Fig. 6-4 "Experimental" shell correction ($M_{\text{exp}} - M_{LD}$), plotted against the neutron number N. Here M_{exp} is the experimental mass of a nuclide (in MeV), while M_{LD} is the mass predicted by the spherical liquid-drop formula 6–21. [After Myers and Swiatecki [13].]

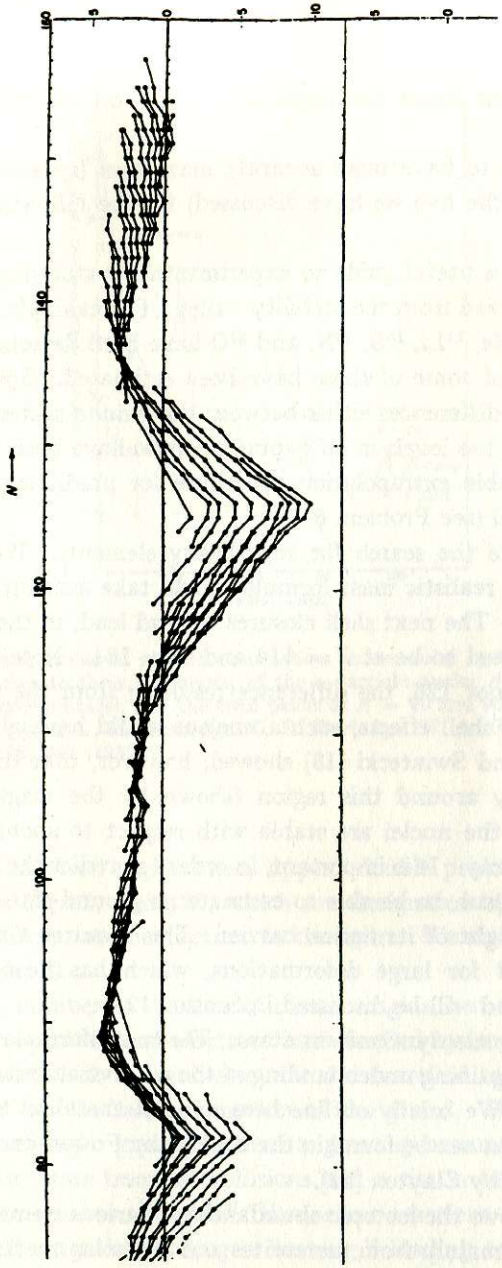

Fig. 6-4 (continued)

tion of the nuclear shape has important effects on the density of single-particle levels.

It is desirable to have more accurate mass laws (necessarily with more parameters than the five we have discussed) for the following applications:

1. To provide a useful guide to experimentalists studying the properties of nuclei far removed from the stability valley. For example, light, neutron-rich nuclei like ^{8}He, ^{11}Li, ^{15}B, ^{19}N, and ^{21}O have been detected [17], and the binding energies of some of these have been estimated. Specific equations relating the mass differences either between the ground states of neighboring nuclei or between the levels in an i-spin multiplet have been developed [18]; these give a reliable extrapolation procedure for predicting the masses of these exotic nuclei (see Problem 6–7).

2. To facilitate the search for superheavy elements. We have already mentioned that a realistic mass formula should take account of shell effects and deformation. The next shell closures beyond lead, in the single-particle model, are predicted to be at $Z = 114$ and $N = 184$. Note that the magic number for Z is not 126, the difference resulting from the Coulomb force. In the absence of shell effects, such a nucleus would have almost no fission barrier. Myers and Swiatecki [13] showed, however, that there may be an island of stability around this region (shown by the magic mountain in Fig. 6–3), where the nuclei are stable with respect to spontaneous fission, α-decay, and β-decay. It is important, in order to predict the lifetime of such a superheavy nucleus, to be able to estimate its ground-state mass and also the shape and height of its fission barrier. This requires a reliable method of calculating δB for large deformations, which has been developed by Strutinsky [19] and will be discussed in Section 12–4.

3. To study nucleosynthesis in stars. The mass formula has played an important role in gaining understanding of the relative abundance of elements in the universe. We briefly outline here some of the ideas on this subject; further information can be found in the booklet by Fowler and Stephens [20], and in the article by Clayton [21].

Figure 6–5 shows the isotopic abundances of various elements in our solar system, obtained mainly from meteorites and the solar spectrum. The data from stellar sources give a similar abundance curve, although there are some differences. The main feature is that 93% of all atoms are hydrogen, followed by about 7% of ^{4}He. All the heavier elements add up to give about 0.1% of the total atoms. Among the heavier elements, there is an overabundance of α-particle nuclei with $A = 16, 20, \ldots, 40$ and also a pronounced peak for

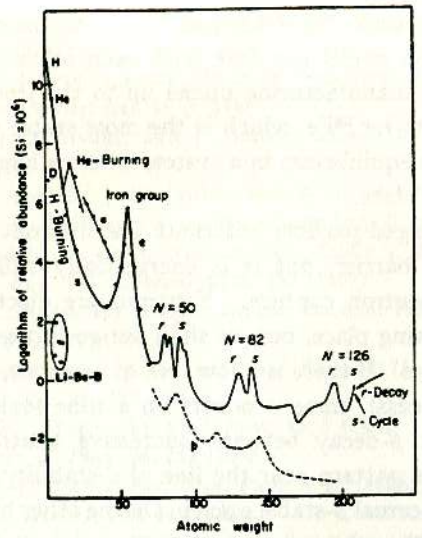

Fig. 6-5 Schematic curve of atomic abundances in our solar system. Note the overabundances, relative to their neighbors, of the α-particle nuclei $A = 16, 20, \ldots, 40$; the peak at the iron group nuclei, and the twin peaks at $A = 80$ and 90, at 130 and 138, and at 194 and 208. [After E. M. Burbidge, G. R. Burbidge, W. A. Fowler, and F. Hoyle, *Rev. Mod. Phys.* **29**, 547 (1957).]

^{56}Fe. Beyond the iron region there appear double peaks for neutron shell closure at $N = 50$, 82, and 126, which are designated by r (rapid neutron capture) and s (slow neutron capture) in the figure. We shall presently discuss these in some detail.

There are a number of theories of cosmic origins, but all of them include a stage in which protons and electrons have formed hydrogen atoms that are distributed throughout the universe. In this rarefied medium, pockets of gas are formed by the random motion of the atoms. If the local density becomes large enough, gravity causes a growing accumulation of matter, resulting in ever more frequent collisions and a rise in temperature. When the temperature reaches about 10^{7} °K, nuclear reactions start and a star is born. The first stage is "hydrogen burning," leading to the formation of helium and the release of more energy. This is the longest stage in the life of a star, occupying about 99% of its lifetime. When the hydrogen is largely depleted, the star core contracts and its temperature keeps rising. At about 10^{8} °K "helium burning" takes place, with three He nuclei fusing via a series of nuclear reactions to yield ^{12}C, thus releasing more energy. Further α-

particle additions produce ^{16}O, ^{20}Ne, and ^{24}Mg. As the temperature rises to $6 \cdot 10^8$ °K, the carbon nuclei can fuse with each other and with helium to form heavier nuclei, manufacturing nuclei up to the iron region. The peak in this region appears for ^{56}Fe, which is the most stable nucleus, and results from an approach to equilibrium in a system where a large variety of nuclear reactions are taking place.

Above iron, charged-particle reactions are improbable because of the increasing Coulomb barrier, but it is energetically still favorable to form heavier nuclei by neutron capture. Neutrons are ejected in many of the nuclear reactions taking place, but we shall not go further into the details of the source of neutrons. If there is a low flux of neutrons, the capture process is called slow (*s*-process), since it occurs on a time scale of 10–1000 years, sufficient to permit β-decay between successive neutron captures. This results in a synthesis pattern near the line of β-stability, and the *s*-peaks in Fig. 6–5 are for the normal β-stable nuclei. On the other hand, a large neutron flux may be available to the iron group elements for capture on a very short time scale, ~ 0.01–10 s, so that neutron-rich isotopes are generated. The three *r*-peaks in the figure are thought to represent neutron-rich nuclei like $^{80}_{30}Zn_{50}$, $^{130}_{48}Cd_{82}$, and $^{195}_{69}Tm_{126}$, respectively. In the *r*-process synthesis, the formation of neutron-excess nuclei is limited by (γ, n) reactions and by β^--decays. One assumes dynamic equilibrium between (n, γ) and (γ, n) processes, and the slow β^--decay causes a leakage from the equilibrium. A detailed knowledge of the energetics (i.e., the mass law) is required to calculate the track of the *r*-process. In fact, Seeger [22] has shown that both shell effects and deformation energies must be included in the mass formula to obtain the best agreement with experimental data.

In order to examine the predictions of the above theories in a quantitative way, it is necessary, among other things, to have values for the masses of many nuclear species. Many of these are experimentally known, but for the unstable exotic species no longer found on earth, or even readily formed in laboratory reactions, one is forced to rely on a mass formula.

REFERENCES

1. R. C. Barber, R. L. Bishop, L. A. Cambey, H. E. Duckworth, J. D. Macdougall, W. McLatchie, J. H. Ormrod, and P. van Rookhuyzen, in *Nuclidic Masses*, edited by W. H. Johnson, Jr., Springer-Verlag, Berlin, 1964, p. 393.
2. Accounts of mass-spectroscopic measurements of several groups are reported in *Proceedings of the Third International Conference on Atomic Masses, Winnipeg, Manitoba*, edited by R. C. Barber, University of Manitoba Press, 1967, pp. 673–830.

3. S. Geschwind, *Encyclopedia of Physics*, edited by S. Flügge, Vol. 38/1, Springer-Verlag, Berlin, 1958, p. 38.
4. N. C. Rasmussen, V. J. Orphan, and Y. Hukai, in *Proceedings of the Third International Conference on Atomic Masses* (ref. 2), p. 278.
5. V. E. Viola, Jr., J. A. Swant, and J. Graber, *Atomic Data and Nuclear Data Tables* **13**, 35 (1974).
6. G. Murray, J. M. Freeman, J. G. Jenkin, and W. E. Burcham, in *Proceedings of the Third International Conference on Atomic Masses* (ref. 2), p. 545.
7. A. H. Wapstra and N. B. Gove, *Nuclear Data Tables* **9**, 267 (1971).
8. F. W. Aston, *Proc. Roy. Soc. (London)* **A115**, 487 (1927).
9. F. W. Aston, *Mass Spectra and Isotopes*, Arnold, London, 1933.
10. W. Heisenberg, *Z. Phys.* **77**, 1 (1932).
11. G. Baym, H. A. Bethe, and C. J. Pethick, *Nucl. Phys.* **A175**, 225 (1971).
12. D. C. Peaslee, *Phys. Rev.* **95**, 717 (1954).
13. W. D. Myers and W. J. Swiatecki, *Nucl. Phys.* **81**, 1 (1966).
14. C. F. von Weizsäcker, *Z. Phys.* **96**, 431 (1935).
15. H. A. Bethe and R. F. Bacher, *Rev. Mod. Phys.* **8**, 82 (1936).
16. E. P. Wigner, *Phys. Rev.* **51**, 106, 947 (1937).
17. A. M. Poskanzer, S. W. Cosper, E. K. Hyde, and J. Cerny, *Phys. Rev. Lett.* **17**, 1271 (1966).
18. G. T. Garvey, W. J. Gerace, R. L. Jaffe, I. Talmi, and I. Kelson, *Rev. Mod. Phys.* **41**, S1 (1969).
19. V. M. Strutinsky, *Nucl. Phys.* **A95**, 420 (1967); **A122**, 1 (1968).
20. W. A. Fowler and W. E. Stephens, *Resource Letter* OE-1 on "Origin of Elements," American Institute of Physics. This booklet also contains a reprint of the classic paper (often referred to in literature as B²FH) by E. M. Burbidge, G. R. Burbidge, W. A. Fowler, and F. Hoyle, *Rev. Mod. Phys.* **29**, 547 (1957).
21. D. Clayton, *Physics Today*, May 1969, p. 28.
22. P. A. Seeger, *Ark. Fysik* **36**, 495 (1966).

PROBLEMS

6–1. α-Particles from radon have an energy of 5.486 MeV. By how much do the masses of radon and radium differ?

6–2. When $M(A, Z)$ is greater than $M(A-4, Z-2) + M(4, 2)$, the nucleus (A, Z) is unstable against α-emission. Compute the kinetic energy of the emitted α-particle as a function of A, for the range of A for which the energy is positive, on the basis of mass formula 6–21, with the parameters given by Eq. 6–24. Use the most stable charge Z_A for Z. Compare the energies obtained with known α-energies. What are the two lightest naturally occurring α-emitters known? Justify the general lack of known α-emitters for A less than 200, in view of the wide range of A for which the kinetic energy available is positive.

6–3. Using the semiempirical mass formula, discuss the energy parabolas for the ground states of nuclei with $A = 110$, and determine an experimental value for the separation of the parabolas.

6–4. Show, ignoring surface effects, that the states of a Fermi gas in a spherical enclosure of radius R with energy less than $\hbar^2k^2/2M$ number $(2/9\pi)(kR)^3$.

6–5. Consider a very large number N of noninteracting fermions enclosed in a large volume Ω, and let the surface-to-volume ratio of the enclosure be small enough for surface effects to be negligible. Let the density of the fermions be large enough that the kinetic energy of a particle greatly exceeds its rest mass, so that the particle energy in a state $\mathbf{p}$ is simply $\varepsilon_p = pc$.

(a) Assuming that only two fermions can be accommodated in a given state $\mathbf{p}$, show that the Fermi energy ε_F is given by

$$\varepsilon_F = cp_F = (3\pi^2)^{1/3}\hbar c\rho^{1/3}, \tag{1}$$

where $\rho = N/\Omega$.

(b) Consider a neutron star core with $\rho > 10^{17}$ g/cm^3. For such densities, the neutrons are in the extreme relativistic limit, and the above model may be used. In such a gas, a certain fraction of protons, electrons, and other heavier particles will be present. Consider only the protons and electrons, appearing from the reaction

$$n \to p + e^- + \bar{\nu},$$

where the neutrinos escape without interaction. Noting that for the equilibrium condition the Fermi energies must match, that is,

$$\varepsilon_F(n) = \varepsilon_F(p) + \varepsilon_F(e),$$

use Eq. 1 and the fact that the gas is neutral to prove that the proton-to-neutron ratio is $N_p/N_n = \frac{1}{8}$.

6–6. *Surface effects in density of states.* (a) Consider a particle of mass m in an enclosure of volume Ω. Define the number of single-particle states available to the particle between energies ε and $\varepsilon + d\varepsilon$ as $g(\varepsilon)\,d\varepsilon$. Note that the classical partition function at temperature T is given by ($\beta = 1/k_BT$; k_B is the Boltzmann constant)

$$Z_{\text{cl}}(\beta) = \frac{1}{h^3}\int \exp(-\beta p^2/2m)\,d^3p\,d^3r$$

$$= \frac{\Omega}{h^3}(2\pi m)^{3/2}\cdot\frac{1}{\beta^{3/2}}. \tag{1}$$

Alternatively, by writing

$$Z(\beta) = \int_0^\infty g(\varepsilon)\exp(-\beta\varepsilon)\,d\varepsilon, \tag{2}$$

we see that $Z(\beta)$ in general is the Laplace transform of the density of states $g(\varepsilon)$, and the latter can be recovered from $Z(\beta)$ by taking its inverse Laplace transform. Using the classical expression for $Z(\beta)$ given in Eq. 1, and looking up a table of Laplace transforms (e.g., in M. Abramowitz and I. A. Stegun, *Handbook of Mathematical Functions*, Dover Publications, New York), show that the classical density of states is

$$g_{\text{cl}}(\varepsilon) = \frac{\Omega}{4\pi^2}\left(\frac{2m}{\hbar^2}\right)^{3/2}\sqrt{\varepsilon}. \tag{3}$$

(b) In order to take the surface effects into account, we must recognize that at any finite temperature T the particle has an uncertainty in configuration space characterized by its de Broglie wavelength $\lambda\!\!\!^{-}_d$:

$$\lambda\!\!\!^{-}_d = \frac{\hbar}{p}. \tag{4}$$

In Eq. 4, replace p by its average value $\bar{p}$ at a given temperature T, and, taking Boltzmann weighting, show that

$$\bar{p} = 2\left(\frac{2m}{\pi}\right)^{1/2}\frac{1}{\beta^{1/2}},$$

and hence

$$\lambda\!\!\!^{-}_d = \frac{h}{4\sqrt{2\pi m}}\cdot\beta^{1/2}. \tag{5}$$

We now associate a finite radius $\lambda\!\!\!^{-}_d$ with the particle, and modify Eq. 1 to exclude a volume $S\lambda\!\!\!^{-}_d$ from Ω (S is the surface area of the enclosure) to obtain

$$Z_{\text{semicl}}(\beta) = \frac{\Omega - S\lambda\!\!\!^{-}_d}{h^3}(2\pi m)^{3/2}\cdot\frac{1}{\beta^{3/2}}. \tag{6}$$

Taking the Laplace inverse of Eq. 6, show that the surface-corrected density of states is

$$g_{\text{semicl}}(\varepsilon) = \frac{\Omega}{4\pi^2}\left(\frac{2m}{\hbar^2}\right)^{3/2}\sqrt{\varepsilon} - \frac{S}{16\pi}\left(\frac{2m}{\hbar^2}\right), \tag{7}$$

which is dependent on the shape of the enclosure.

6–7. *Garvey-Kelson mass formula.* (a) Although the overall behavior of the binding energy $B(A, Z)$ is well reproduced by the semiempirical mass formula, the local fluctuations in the experimental values due to shell effects make this expression less useful for precise predictions of the bindings of the more exotic nuclides. These local fluctuations can be canceled, however, by constructing mass relations involving adjacent nuclides, such that the n-n, n-p, and p-p bonds cancel off separately. Consider, for example, the simple mass relation

$$M(N, Z) + M(N+1, Z+1) = M(N, Z+1) + M(N+1, Z), \tag{1a}$$

which can be graphically represented by

$$\begin{array}{c|c|c|}
Z+1 & - & + \\
\hline
Z & + & - \\
\hline
 & N & N+1
\end{array}, \qquad (1b)$$

where each square represents a nuclide with a given N, Z.

Show that the number of n-n and p-p bonds separately and exactly cancel out in Eq. 1, although this is not true for the n-p bonds. Also note that expression 1 is exactly satisfied if the local behavior of the mass can be represented by

$$M(N, Z) = f_1(N) + f_2(Z),$$

where f_1 and f_2 are arbitrary functions.

(b) Since n-p bonds are also important in determining the mass of a nuclide, it is necessary to modify the four-term formula 1 so that these too are canceled. The two six-term formulas which are next in simplicity can be easily constructed graphically by superimposing two square structures corner to corner:

$$\begin{array}{c|c|c|c|}
Z+2 & & + & - \\
\hline
Z+1 & - & + & + \\
\hline
Z & + & - & \\
\hline
 & N & N+1 & N+2
\end{array} \quad \text{and} \quad \begin{array}{c|c|c|c|}
Z+2 & + & - & \\
\hline
Z+1 & - & + & + \\
\hline
Z & & + & - \\
\hline
 & N & N+1 & N+2
\end{array}$$

(2) (3)

Formulas 2 and 3, which are known as the Garvey-Kelson mass formulas [18], can be easily written down algebraically.

Show that formula 2 is satisfied exactly if

$$M(A, Z) = f_1(Z) + f_2(N) + f_3(I), \qquad (2')$$

while formula 3 is true if

$$M(A, Z) = g_1(Z) + g_2(N) + g_3(A), \qquad (3')$$

where the f_i's and g_i's are unspecified arbitrary functions, and $I = N - Z$. Equations 2 and 3 have been tested, with certain restrictions, throughout the periodic table and are accurate to within 200 keV. They are very useful, therefore, in predicting the unknown mass of a nuclide if the masses of the other five members of the difference equation are experimentally known.

(c) The Kelson-Garvey approach may also be applied to elementary particles. The semistable baryons with spin-parity $\frac{1}{2}^+$ may be grouped in a

multiplet; these are (n, p, Λ, Σ^+, Σ^0, Σ^-, Ξ^0, and Ξ^-). Individual members of the multiplet may be specified by i-spin T, its third component T_3, and an additional quantum number S called "strangeness"; the nucleons have $S = 0$, the Λ and Σ's have $S = -1$, and the Ξ's have $S = -2$.

Draw a two-dimensional plot with S as the x-axis and charge C as the y-axis, and place the members of the $\frac{1}{2}^+$ multiplets in the appropriate places. Assume the mass dependence of a baryon to be given by a formula analogous to expression 2′, that is,

$$M(C, S) = f_1(C) + f_2(S) + f_3(S - C).$$

Hence derive the mass formula

$$M(\Xi^-) + M(\Sigma^+) + M(n) = M(\Xi^0) + M(\Sigma^-) + M(p). \qquad (4)$$

Look up the masses of the above baryons in the most recent Review of Particle Properties [e. g. *Phys. Lett.* **50B**, 1 (1974)] and confirm that formula 4 is obeyed with high accuracy. This formula, which relates to electromagnetic mass splittings, can also be derived from the SU_3 classification of particles; see, for example, the article on unitary symmetry by P. T. Mathews in *High Energy Physics*, Vol. 1, Academic Press, New York, 1967, p. 392.

6–8. The interaction of a Λ-particle with a nucleon is of a short-range, attractive nature (see Chapter 2). Note that a free Λ has a lifetime of 2.5×10^{-10} s.

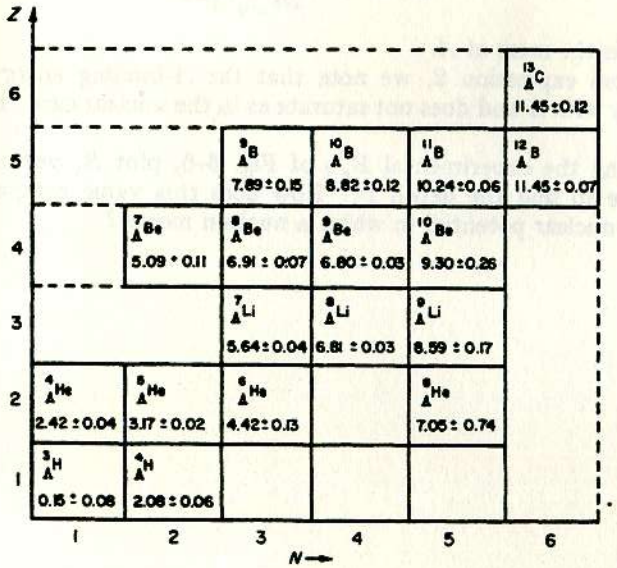

Fig. 6-6 Separation energies of the Λ-particle in light hypernuclei (all energies in MeV).

and decays by the weak interaction

$$\Lambda \rightarrow p + \pi^-$$

with a release of energy $Q = 37.7$ MeV. Because of the attractive interaction of a Λ with nucleons, it can form a bound state in a nucleus, although this interaction is too weak to form a two-body Λ-N bound pair. A nucleus containing a Λ-particle is called a hypernucleus and typically has a lifetime of the order of 10^{-10} s. The separation energy of a Λ-particle in a hypernucleus is denoted by B_Λ, and Fig. 6–6 is a chart of the experimentally known B_Λ's. Although heavier hypernuclei certainly exist, they are very hard to identify experimentally. In Fig. 6–6, the notation is standard: for example, ${}^5_\Lambda$He denotes that there are five baryons (four nucleons + one Λ) in the system, and that the Λ is trapped in a He nucleus.

(a) In a simple model, the Λ-particle moves in an average potential $U_\Lambda(r_\Lambda)$ which is generated by the two-body Λ-nucleon interaction:

$$U_\Lambda(r_\Lambda) = \int \rho(\mathbf{r}) V(|\mathbf{r} - \mathbf{r}_\Lambda|)\, d^3r, \tag{1}$$

where $\rho(\mathbf{r})$ is the nuclear density. As the nucleon number A is increased, explain why you expect the depth of U_Λ to remain the same, but its radius R to increase as $A^{1/3}$. Assuming, for simplicity, that U_Λ is a square well of depth D and radius $R = r_0 A^{1/3}$, show that

$$B_\Lambda \approx D - \frac{\pi^2\hbar^2}{2m_\Lambda r_0^2 A^{2/3}}, \tag{2}$$

where m_Λ is the mass of Λ.

(b) From expression 2, we note that the Λ-binding energy B_Λ varies continually with A and does not saturate as in the nuclear case. Explain why this is so.

(c) Using the experimental B_Λ's of Fig. 6–6, plot B_Λ versus $A^{-2/3}$ and extrapolate to find the depth D. How does this value compare with the analogous nuclear potential in which a nucleon moves?

Part II

Nuclear Models